



Universität für Bodenkultur Wien

Department of Applied Genetics and Cell Biology

Head of Department: Joseph Strauss

---

# RECOMBINANT ZEIN PROTEIN BODIES FOR THE ENCAPSULATION OF THERAPEUTIC PROTEINS

---

Thesis prepared for the degree of

**Doctor of Philosophy**

Under the supervision of

**Eva Stöger**

Submitted by

**Marc Tschofen**

Vienna, March 2020

## Acknowledgements

Firstly, I would like to express my sincere gratitude to my supervisor and mentor Prof. Eva Stöger for her guidance throughout this journey. You began to shape my scientific career long before I started as a PhD candidate. You never failed to lend an open ear and you always provided valuable advice, scientific and personal. I could not have wished for a better supervisor than you were.

The same goes for the members of the Stöger lab, Elsa, Stani, Julia, Ulli, Eszter, Maria, Lukas, and Jenny. You were always available for fruitful discussions and just brightened everyday life in the lab. Especially Stani and Jenny made working late hours enjoyable and fun. Jenny contributed significantly to the success of this project.

I am also thankful for having been part of the BioToP PhD program. Besides the excellent scientific education, I do not want to miss the social network and support offered by the people of BioToP. Christa and Grete helped to navigate the bureaucracy and became friends along the way. BioToP also provided funding and offered the opportunity to gain experience abroad. In this regard, I want to acknowledge the people who hosted me abroad, Jihong Liu Clarke at NIBIO Norway, Erling Olaf Koppang at NMBU Norway, Sylvain Marcel at iBio CDMO, Maria Esteve-Gassent at Texas A&M, as well as Karen MacDonald and Somen Nandi at UC Davis. I am also thanking the people of the Grillari lab, the Swoboda lab, and the lab of Alessandro Vitale as well as Daniel Maresch for their collaboration. Last but not least, I greatly appreciate the effort of my examiners Reingard Grabherr and Stefan Schillberg.

Finally, I want to thank my friends and family who always supported me. Without your encouragement during the ups and downs, I would not be where I am or who I am.

## Abstract

Oral administration is the preferred route of drug delivery for any pharmaceutical due to its patient compliance. Oral vaccines have the added benefit of being able to induce mucosal immunity. Something that needle-injected vaccines cannot. Mucosal immunity is particularly important because mucosal layers commonly constitute the point of entry for pathogens. However, vaccines face major challenges during oral delivery. Oral vaccines need to survive degradation in the stomach, they need to penetrate the mucus, cross the epithelium and elicit an immune response. Encapsulation of vaccines into particles can help in regard to all of these aspects. One way to encapsulate vaccines is expression as a fusion protein with zein; the major storage protein of maize.

The adjuvant effect of zein has been demonstrated before and one possible explanation for this effect is the increased cellular uptake facilitated by zein. This thesis aimed to investigate the uptake efficiency of zein protein bodies (PBs) into *in vitro* cells of the human intestine. Fluorescent zein PBs were recombinantly produced by transient expression in *Nicotiana benthamiana*. A new process was developed that enabled the scalable enrichment of PBs. They were analyzed for nicotine content and particles were quantified by flow cytometry. Upon administration, human intestinal cells endocytosed zein PBs at a higher amount and a higher rate compared to fluorescent polystyrene beads. Additionally, only PBs triggered those cells to release GM-CSF and IL-6. Two cytokines that are known to recruit antigen presenting cells and elicit a higher immune response overall. Consequently, the endocytosis of PBs was demonstrated in dendritic-like cells as well.

Finally, the zein-mediated encapsulation tool itself was improved. So far, recombinant zein PBs that were intended as a drug delivery vehicle only encapsulated one single component. Through the coexpression of various zeins, it was possible to generate multicomponent PBs. Various combinations are now available that induce the formation of particles that consist of two to four components. The architecture of these PBs can either be a core-shell structure or homogeneously mixed. In the future, this will enable modifications to the particle characteristics such as stability, mucus penetration, cellular uptake, and release of active compound.

Keywords: Zein, encapsulation, oral vaccine, drug delivery, molecular farming

## Kurzfassung

Die orale Verabreichung ist aufgrund der Akzeptanz durch Patienten der bevorzugte Verabreichungsweg für jedes Arzneimittel. Orale Impfstoffe haben den zusätzlichen Vorteil, dass sie eine Schleimhautimmunität auslösen können. Etwas, das mittels Injektion verabreichte Impfstoffe nicht können. Schleimhautimmunität ist besonders wichtig, da Schleimhautschichten häufig die Eintrittsstelle für Krankheitserreger darstellen. Impfstoffe stehen jedoch vor großen Herausforderungen bei der oralen Verabreichung. Orale Impfstoffe müssen den Abbau im Magen überleben, die mukosale Schicht durchdringen, das Epithel überwinden und eine Immunantwort auslösen. Die Einkapselung von Impfstoffen in Partikel kann in Bezug auf all diese Aspekte hilfreich sein.

Ein Weg, Impfstoffe einzukapseln, ist die Expression als Fusionsprotein mit Zein; das wichtigste Speicherprotein von Mais. Die adjuvante Wirkung von Zein wurde zuvor bereits gezeigt, und eine mögliche Erklärung für diesen Effekt ist die durch Zein unterstützte zelluläre Aufnahme. Ziel dieser Arbeit war es, die Aufnahmeeffizienz von Zein protein bodies (PBs) in Zellen des menschlichen Darms *in vitro* zu untersuchen. Fluoreszierende Zein-PBs wurden durch transiente Expression in *Nicotiana benthamiana* rekombinant hergestellt. Es wurde ein neues, skalierbares Verfahren entwickelt, das die Anreicherung von PBs ermöglicht. Diese wurden auf Nikotingehalt analysiert und die Partikel wurden durch Durchflusszytometrie quantifiziert. Bei der Verabreichung haben humane Darmzellen Zein-PBs in einer höheren Menge und in einer höheren Rate aufgenommen als fluoreszierende Polystyrolkugeln. Zusätzlich wurde durch PBs die Freisetzung von GM-CSF und IL-6 ausgelöst. Diese zwei Zytokine können antigenpräsentierende Zellen rekrutieren und insgesamt eine höhere Immunantwort auslösen. Folglich wurde die Endozytose von PBs auch in dendritischen Zellen nachgewiesen.

Schließlich wurde die Zein-vermittelte Einkapselung selbst verbessert. Bisher bestanden rekombinante Zein-PBs, die als Vehikel zur Arzneimittelaufnahme gedacht waren, nur aus einer einzigen Komponente. Durch die Koexpression verschiedener Zeine konnten PBs mit mehreren Komponenten erzeugt werden. Mittlerweile sind verschiedene Kombinationen verfügbar, die die Bildung von Partikeln aus zwei bis vier Komponenten induzieren. Die Architektur dieser PBs kann entweder eine Core-Shell-Struktur sein oder die Komponenten können homogen gemischt sein. Dies soll zukünftig Modifikationen der Partikeleigenschaften wie Stabilität, Schleimhautpenetration, zelluläre Aufnahme und Wirkstofffreisetzung ermöglichen.

## Contents

|       |  |    |
|-------|--|----|
| 1     | Introduction   | 7  |
| 1.1   | An unmet need for oral vaccines  | 7  |
| 1.2   | Drug delivery by micro- and nanocarriers   | 8  |
| 1.3   | Zeins self-assemble into stable particles  | 11 |
| 2     | Objectives   | 17 |
| 3     | Material and Methods   | 18 |
| 3.1   | Molecular cloning  | 18 |
| 3.2   | Phylogenic analysis  | 19 |
| 3.3   | Plants and Agrobacteria  | 19 |
| 3.4   | Protein body size determination  | 19 |
| 3.5   | Processing of plant material for uptake studies  | 20 |
| 3.6   | Flow cytometry of protein bodies   | 20 |
| 3.7   | Mammalian cell culture   | 21 |
| 3.8   | PB uptake and flow cytometry of HCE cells  | 21 |
| 3.9   | Microscopy of mammalian cells  | 22 |
| 3.10  | Analysis of nicotine content in PB preparations  | 22 |
| 3.11  | Microscopy of multicomponent PBs in leaves of <i>Nicotiana benthamiana</i>                         | 23 |
| 4     | Results and Discussion   | 24 |
| 4.1   | Endocytosis of zein protein bodies into mammalian epithelial and immune cells                      | 24 |
| 4.1.1 | Optimized processing enables scalable enrichment of gz93-EGFP PBs                                  | 25 |
| 4.1.2 | gz93-EGFP PBs are endocytosed by human colon epithelial cells and stimulate cytokine release       | 29 |
| 4.1.3 | PBs are taken up by immune cells   | 32 |
| 4.2   | Generation of recombinant multicomponent zein PBs  | 34 |
| 4.2.1 | Coexpression of gamma zein and alpha zein  | 34 |
| 4.2.2 | Native UTRs do not improve the incorporation of alpha into gamma zein PBs in <i>N. benthamiana</i> | 36 |
| 4.2.3 | Other zeins form protein bodies as well  | 41 |
| 4.2.4 | Multicomponent PBs by coexpression of zeins  | 45 |
| 5     | Summary and Conclusion   | 67 |
| 6     | Outlook  | 68 |
| 7     | Zusammenfassung und Schlussfolgerung   | 69 |
| 8     | References   | 70 |
| 9     | List of Tables   | 80 |
| 10    | List of Figures  | 81 |
| 11    | Abbreviations  | 86 |
| 12    | Appendix   | 88 |



# 1 Introduction

Vaccines save an estimated 2-3 million lives every year through the prevention of infections and they are one of the most significant inventions in modern medicine. They are the second most important option to prevent infection-related mortality after clean drinking water (Baschieri, 2012; WHO, 2018a). Not only can vaccines target a multitude of pathogens but they are also a very cost-effective method to fight diseases because vaccination is a prophylactic health care measure with some vaccines providing life-long protection (Landsverk et al., 2017). On top of that, herd-immunity also protects the part of the population that did not receive vaccination. Through vaccines, incidences of devastating infections that once caused a great number of deaths like smallpox, diphtheria, pertussis, tetanus, poliomyelitis, measles, rubella, mumps, or *Haemophilus influenzae*, were all reduced by 98-100% (Rappuoli et al., 2002). The benefits of vaccination reach far beyond avoidance of suffering and death into socio-economic aspects. Estimates are that every \$1 spent on measles-mumps-rubella vaccine (MMR-V) saves \$16.34 in direct costs of treatment (Centers for Disease Control and Prevention, 1999). Then again, on a global level, infectious and parasitic diseases still rank to be the third most common cause of death (14.9%) after cardiovascular diseases (31.4%) and malignant neoplasms (15.8%). In low-income countries however, infectious diseases are at 37.2% still the most frequent cause of death (WHO, 2018b).

## 1.1 An unmet need for oral vaccines

Vaccines work most efficiently when they can block the entry of pathogens or eliminate them locally before they spread (Kozlowski, 2012). Most pathogens invade the host's body through mucosal surfaces and the release of immune effectors to this point of entry is therefore crucial as a first line of defense. A key molecule that resides at mucosal barriers is secretory immunoglobulin A (sIgA). The immune system is triggered to release antigen-specific sIgA to mucosal surfaces when the initial immunization occurred at a mucosal site. This is in contrast to injected vaccines that usually are not able to stimulate sIgA secretion. Mucosal vaccines are therefore a particularly valuable tool because they are designed to target mucus layers such as gastrointestinal, respiratory, or urogenital epithelia. Immunization at these barriers generally causes a wider humoral as well as cellular immune response at mucosal and systemic sites (Vela Ramirez et al., 2017). Besides the immunological aspects, mucosal vaccines offer other benefits over injected vaccines as well. They are, for example, easier and safer to administer. Nasal, sublingual, oral, vaginal, or rectal administration does not necessitate syringe-mediated application and can therefore be carried out through self-administration. This omits the need for trained personnel which is sometimes a limiting factor for vaccination campaigns in low-income countries. It also eliminates the risk of infections caused by improper injection or waste

disposal, a risk that concerns patients as well as healthcare workers. Not surprisingly, the patient compliance for oral drugs is much higher for being pain-free. A fact that should be considered in the overall acceptance of vaccines. Additionally, vaccine preparations for injection need to be in aqueous form whereas mucosal vaccines can be of the solid-dose format such as capsules or tablets. As a consequence, mucosal vaccines are better suited to withstand higher temperatures and do not require a cold-chain which is an important aspect to manage the logistics of the “last mile”; especially in low- to middle-income countries (New, 2019). Oral drugs also do not require aseptic conditions. That makes the conditions of the production process less demanding and cheaper overall.

Although there is a general agreement for the need of oral vaccines, their development has its own challenges that need to be overcome. Whatever form of vaccine is delivered orally, whether it is a live-attenuated, inactivated, or a subunit vaccine, they all need to face the harsh conditions of the gastrointestinal (GI) tract. Low pH and digestive enzymes are two factors that are difficult to overcome particularly for proteins and peptides. Even if degradation of the vaccine is prevented and it arrives at the immune inductive tissue, recognition of the vaccine is not guaranteed. Due to these facts, oral vaccines are usually administered at a higher dose than parenteral ones. However, if the immunogenicity is low and the dosage is too high, an antigen might cause oral tolerance instead of immunity (Mestecky et al., 2007). In this case, the immune system recognizes an antigen as non-pathogenic and does not react when challenged with the pathogen the vaccine was intended to protect from. Encapsulation of vaccines into micro- or nanocarriers is able to help overcome some of the challenges met by oral vaccines.

## **1.2 Drug delivery by micro- and nanocarriers**

Encapsulation strategies can be based on natural polymeric material such as particle-forming proteins and chitosan or synthetic such as poly(lactic-co-glycolic) acid (PLGA), but they can also be lipid-based vehicles such as liposomes, bilosomes, or ISCOMs (Immune-stimulating complexes) (Vela Ramirez et al., 2017). All of these delivery strategies are increasingly investigated by academia and industry because they can be a solution to the challenges faced by orally administered vaccines. These challenges are mainly the resistance of the antigen against digestive enzymes and acidic pH in the GI tract, low uptake rates as well as low immunogenicity or induction of tolerance (Reinholz et al., 2018). Protein- and peptide-therapeutics are particularly susceptible to the degradation machinery of the mammalian digestive tract. One aspect of the chemical barrier is the highly acidic environment of the stomach (pH 1-3). The low pH denatures the tertiary structure of many proteins and as a result the denatured protein is more accessible to hydrolytic exo- and endopeptidases such as pepsin, trypsin, or carboxypeptidase (Renukuntla et al., 2013; Van de Graaff, 1986). However,

the challenge is not only the very low pH of the stomach but the wide range of pH along the GI tract. Although it starts off low at pH 1-3 in the stomach, it increases to pH 6.0–6.5 in the duodenum and pH 5.5–7.0 in the colon (Pawar et al., 2014). Therefore, fortifying drugs against the acidic environment of the stomach might not be sufficient if the target tissue is located later in the gut. The synthetic polymer PLGA can already serve as an encapsulation vehicle on its own but one study developed the concept further. PLGA particles containing HIV Env protein were additionally coated with the methacrylate-based polymer Eudragit FS30D. This coating only dissolves at pH >7.0 which protected the vaccine from degradation in the stomach and from being released in the small intestine. Thereby it was successfully released in the large intestine. Delivery to this part of the GI tract was more capable of inducing a robust cellular and humoral immune response at vaginal and rectal mucosa than vaccines delivered to the small intestine (Zhu et al., 2012). Genitorectal immunity set aside, the small intestine is generally more relevant for the recognition of antigens from the intestinal lumen than the large intestine. Once the encapsulated vaccine exits the stomach, it needs to cross two barriers before it can reach the underlying immune effector cells. These barriers are the mucus and the epithelium. The mucus layer is an adhesive and viscoelastic gel comprised primarily of a mesh of mucins with a varying thickness of 123-480  $\mu\text{m}$  (Ensign et al., 2012). Mucoadhesion and mucus-penetration are two engineering strategies that can be applied to increase the number of particles that overcome this first barrier. Mucoadhesion is generally achieved by a positively charged and hydrophobic surface; characteristics that are commonly provided by natural polymers such as chitosan (Wu et al., 2018). Although mucoadhesive particles have generated impressive results that even reached commercialization (Guada et al., 2016; Nagarwal et al., 2011), the fast mucus turnover time of 50-270 minutes constitutes an additional challenge (Lehr et al., 1991). Mucus-penetration on the other hand, tries to avoid tight interaction of particles with the mucin matrix. The characteristics necessary for this are a hydrophilic and an overall neutral surface charge; two criteria that are commonly met by viruses (Wu et al., 2018). When the microcarriers have made it through the mucus and onto the layer of epithelial cells, they need to pass this final barrier by either para- or transcellular transport (Reinholz et al., 2018). Microcarriers offer the added benefit that the uptake of antigens in particulate form is generally more efficient by up to 30-fold compared to soluble antigens (Gregory et al., 2013). This can be improved even further by functionalizing the particle's surface such that it binds certain markers of cells in the intestinal wall. The two cell types that are most relevant for antigen uptake from the intestinal lumen are M cells and absorptive epithelial cells (or enterocytes). The main function of M cells is the non-degenerative transcytosis of antigens from the lumen towards dendritic cells and macrophages in the underlying tissue (Pridgen et al., 2015). Therefore, M cell-specific targeting is a particularly promising strategy to enhance the efficacy of mucosal vaccines. Additionally, these cells are covered by a much thinner

mucus layer than other cells of the intestine (Jang et al., 2004). Numerous M cell-ligands such as Ulex europaeus 1, Galectin-9, or antibodies that target M cell-receptors resulted in increased delivery of antigens (Clark et al., 2001; Foster et al., 1998; Hase et al., 2009; Kyd and Cripps, 2008; Nochi et al., 2007). However, M cells can only be found in Peyer's Patches; a part of the gut-associated lymphoid tissue. As a result, M cells occur in a much lower number than enterocytes. Only 1 in 10 million epithelial cells is a M cell (Kim et al., 2012). Due to their innate function, most work has focused on M cells to achieve enhanced uptake of particulate vaccines. Enterocytes on the contrary are the most common cell type in the absorptive surface area of the intestine. Studies have shown that enterocytes are also capable of transcytosing macromolecules and bacteria across the epithelial barrier (Devriendt et al., 2012; Neal et al., 2006). This transcytosis can further be improved by conjugating particles to lectins or bacterial adhesins. For instance, nanoparticles modified with a tomato-lectin were endocytosed more

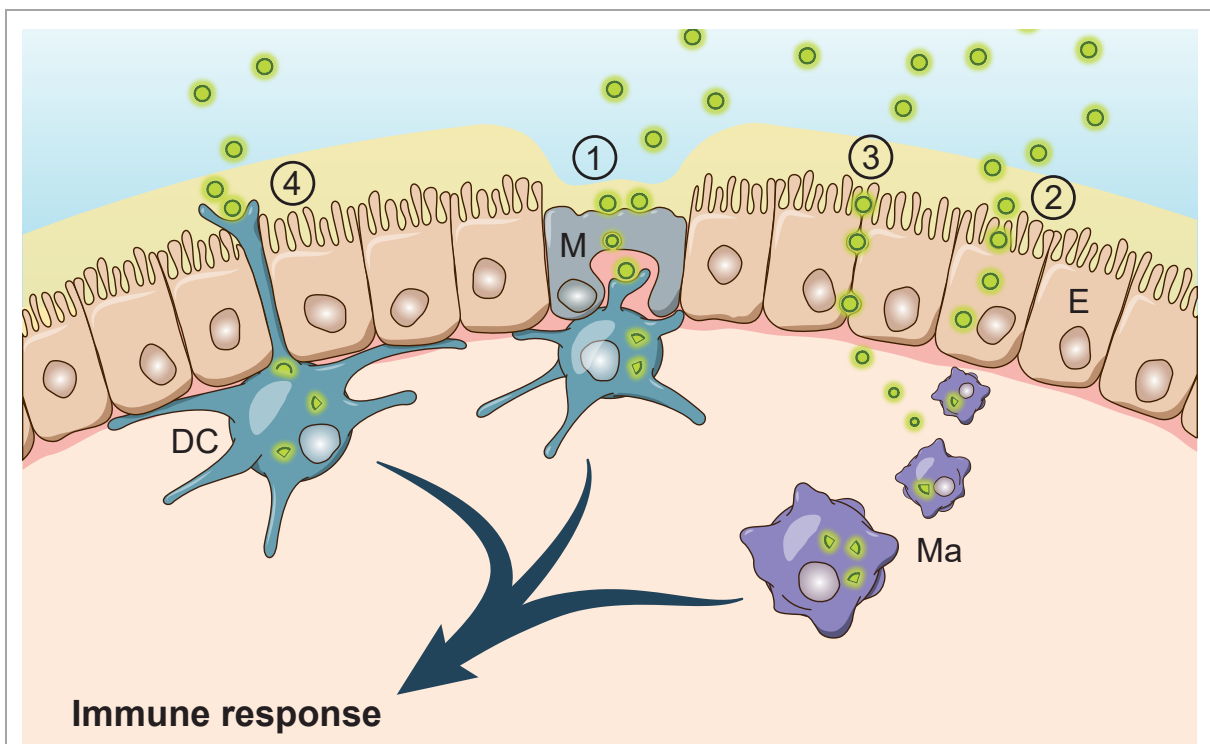


**Figure 1: Schematic drawing of the four routes by which particle drugs, in this case protein bodies (PB), can travel across the epithelium. (1) Particles can be transcytosed by M cells (M) that reside in Payer's patches. Reduced thickness of mucus and tight interaction of M cells and dendritic cells (DC) make this route highly favorable. (2) Transcytosis of particles through enterocytes (E) was also described. The benefit of this route is the abundance of enterocytes in the intestine. (3) Particles can also travel across the epithelium through tight junctions between epithelial cells. (4) DCs also use these tight junctions to reach their dendrites into the lumen of the intestine to probe for antigens. On the basolateral side of the epithelium, APCs such as DCs and macrophages (Ma) trigger the cascade that ultimately results in the immune response.**

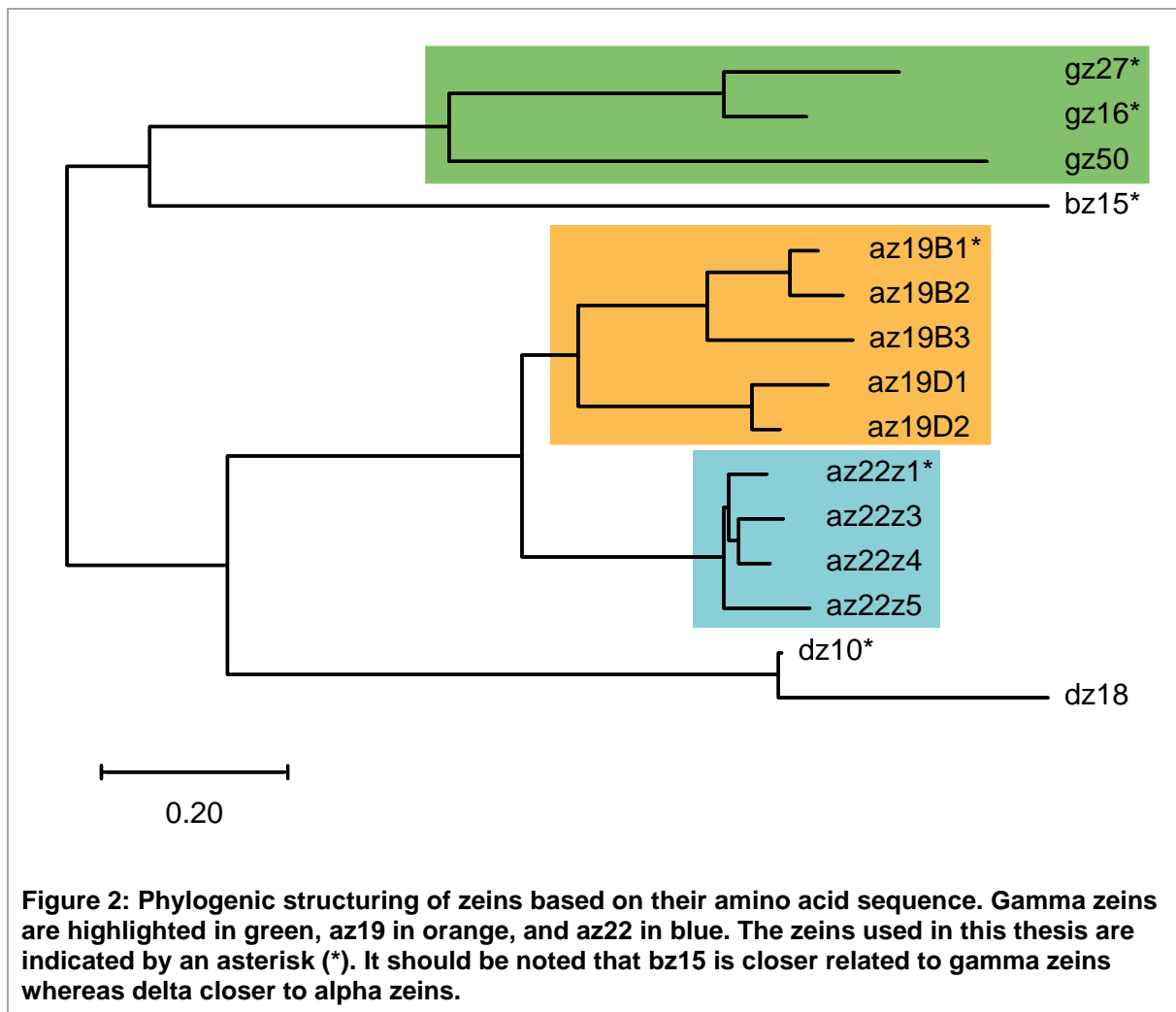
efficiently by rat enterocytes *in vivo* than unmodified ones (Carreno-Gómez et al., 1999; Hussain et al., 1997). Similarly, wheat germ agglutinin and concanavalin A led to more nanoparticles being transcytosed across monolayers of Caco-2 cells *in vitro* (Chen et al., 1996; Russell-Jones et al., 1999). Regarding bacterial adhesins, many studies focused on F4 fimbriae originating from enterotoxigenic *Escherichia coli*. F4 fimbriae target aminopeptidase N on porcine enterocytes. Conjugation of antigens to F4 fimbriae resulted in a rapid and strong sIgA and IgG response in piglets (Melkebeek et al., 2012; Tiels et al., 2008). Microcarriers can not only travel across the epithelium by means of transcytosis through enterocytes or M cells, they can also find their way through tight junctions in between those cells (Sonaje et al., 2012). Regardless of the route, the ultimate goal for particle vaccines are antigen-presenting cells (APCs) on the basal side of epithelial cells. APCs such as macrophages and dendritic cells then trigger the cascade that finally results in the immune response against the encapsulated antigen. Additionally to the aforementioned routes, dendritic cells can extend their dendrites through the tight junctions between epithelial cells to probe for antigens and endocytose them directly from the intestinal lumen; a process also known as periscoping (Figure 1) (Gewirtz and Madara, 2001; Rescigno et al., 2001). Further down the immunological signaling cascade, B cells are activated and stimulated by the crosslinking of B cell-receptors and the antigen. This crosslinking is more efficiently achieved by antigens that are displayed on the surface of a particle – as opposed to soluble antigens – because there they are present at a higher density and in a structurally ordered fashion (López-Sagasetta et al., 2016). Although this principle is also utilized by attenuated or inactivated vaccines, the same was accomplished quite early by subunit vaccines as well. The hepatitis B virus antigen forms spherical particles when expressed recombinantly and in 1981 these particles became the first subunit vaccine, the first recombinantly produced vaccine, and the first to prevent cancer (Hilleman, 2000; Valenzuela et al., 1982). It is also a prominent example of a vaccine particle that is formed by protein self-assembly.

### **1.3 Zeins self-assemble into stable particles**

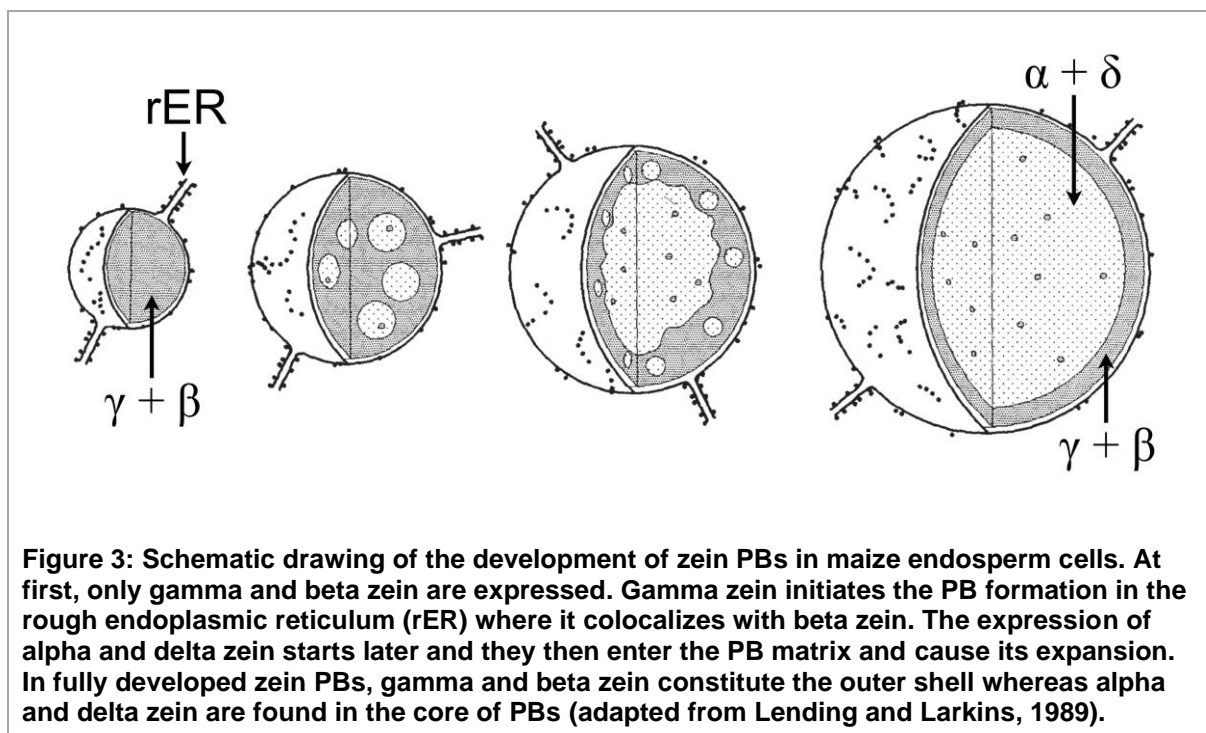
Many naturally occurring proteins self-assemble into large structures in the nm and  $\mu\text{m}$  size range. These proteins can arrange into specific shapes such as fibers, tubes, and hollow or solid spheres (Mandal et al., 2014). The formation of large protein structures is mostly driven by weak noncovalent interactions such as Van der Waals forces, electrostatic energy, and hydrophobic interaction (Domingo-Espín et al., 2011). Large proteins have evolved for several reasons. Either their morphological function demands a certain layout like is the case

| <b>Table 1: List of zeins in developing maize endosperm (adapted from Woo et al., 2001)</b> |                                   |                |                 |               |
|---|-----------------------------------|----------------|-----------------|---------------|
| Name (Abbreviation)   | Percent in Endosperm cDNA Library | Amino Acids    | MW (calculated) | MW (SDS-PAGE) |
| 27 kDa gamma zein (gz27)  | 5.4                               | 204            | 21,822          | 27 kDa        |
| 16 kDa gamma zein (gz16)  | 2.9                               | 163            | 17,663          | 16 kDa        |
| 50 kDa gamma zein (gz50)  | 1.5                               | 278            | 32,882          | 50 kDa        |
| 15 kDa beta zein (bz15)   | 4.7                               | 160            | 17,458          | 15 kDa        |
| 18 kDa delta zein (dz18)  | 1.0                               | 190            | 21,220          | 18 kDa        |
| 10 kDa delta zein (dz19)  | 0.5                               | 129            | 14,431          | 10 kDa        |
| 19 kDa alpha zein (az19D1)  | 1.2                               | 222            | 24,818          | 19 kDa        |
| 19 kDa alpha zein (az19D2)  | 1.0                               | 220            | 24,706          | 19 kDa        |
| 19 kDa alpha zein (az19B1)  | 15.9                              | 213            | 23,359          | 19 kDa        |
| 19 kDa alpha zein (az19B2)  | 0.1                               | 246            | 27,128          | 22 kDa        |
| 19 kDa alpha zein (az19B3)  | 5.7                               | 219            | 24,087          | 19 kDa        |
| 19 kDa alpha zein (az19B4)  | 0.06                              | In-frame stop  | NA              | NA            |
| 19 kDa alpha zein (az19B5)  | 0.05                              | Truncated cDNA | NA              | NA            |
| 22 kDa alpha zein (az22z1)  | 4.9                               | 242            | 26,359          | 22 kDa        |
| 22 kDa alpha zein (az22z3)  | 0.5                               | 245            | 26,751          | 22 kDa        |
| 22 kDa alpha zein (az22z4)  | 0.5                               | 246            | 26,923          | 22 kDa        |
| 22 kDa alpha zein (az22z5)  | 0.1                               | 245            | 26,701          | 22 kDa        |

for viral capsids or they have a cooperative function such as the structural protein collagen. The formation of large protein complexes is also a way to reduce their surface area. This means that less of the protein is exposed to the solvent which can be energetically favorable. The reduced surface area also results in increased stability against degradation and this stability is further supported by their extensive internal organization (Goodsell and Olson, 2000). Preventing premature degradation is particularly important for seed storage proteins (SSPs). The purpose of SSPs is to provide nitrogen for the germinating seedling after extended times of storage. Some do that so efficiently that they are able to germinate after 2000 years in a non-frozen state (Sallon et al., 2008). Historically, SSPs are grouped into four classes that are distinguished by their solubility. Albumins are soluble in water, globulins in salt solutions, prolamins in alcohol dilutions, and glutelins in acidic or alkaline solutions. However, each class has subgroups that again have specific solubility characteristics. Cereals mainly store their proteins as prolamins and in maize these prolamins are called zeins (Krishnan and Coe, 2001). The zeins themselves are grouped into alpha, beta, gamma, and delta zeins based on differences in solubility. Individual members are then further specified by their molecular weight and some of them are present in multiple copies in the maize genome (Woo et al., 2001). An overview of this is provided in Table 1 and the phylogenetic tree in Figure 2 shows their evolutionary distance. The deposition of zeins happens in a temporally coordinated fashion in the endoplasmic reticulum of developing endosperm cells. This deposition results in the formation of large spherical structures called protein bodies (PBs).



In fully developed PBs, the zeins are distinctly localized and their spatial organization manifests in a layered core-shell structure (Guo et al., 2013; Lending and Larkins, 1989). Gamma and beta zeins are the first to be expressed during seed maturation. Both are rich in cysteines and they are cross-linked by disulfide bonds. Of these, gz27 is thought to be essential for the induction of PB formation (Geli et al., 1994). At later stages, alpha and delta zeins are expressed and they then penetrate the PB matrix to accumulate in their core whereas gamma and beta zeins form the outer shell (Figure 3). This accumulation of alpha and delta zeins drives the expansion of PBs with fully developed PBs having diameters of 1 to 2  $\mu\text{m}$ . The localization of alpha and delta zeins in the core of PBs seems a logical consequence due to their higher hydrophobicity compared to gamma and beta (Herman, 1999). However, hydrophobicity is not the only driver determining the structure of PBs. Interactions between zeins seem to be specific even though the exact mechanism has not yet been identified (Bagga et al., 1997; Coleman et al., 1996). Yeast two-hybrid experiments identified that gamma zeins strongly interact with each other and with beta zein while az19 and az22 only weakly interact with each other but prefer to do so with delta zein (Kim et al., 2002). This grouping of zeins is also seen by their evolutionary distance based on protein sequence homology (Figure 2). The



same yeast two-hybrid study also found that *gz16* and *bz15* are the only ones that are able to interact with the alpha/delta zein group. Besides protein interactions, asymmetric targeting of zein mRNAs to subdomains of the endoplasmic reticulum is essential for the correct arrangement of PBs (Washida et al., 2004, 2009).

The self-assembling capability of zeins has attracted a lot of attention from researchers investigating the encapsulation and delivery of therapeutic agents. The number of articles published annually on zein has increased from an average 41 between 1990 and 2000 to north of 260 in 2019 (“zein” in title, abstract, and keywords on Scopus). Most of these studies use commercially available zein to encapsulate the therapeutic agents. Commercial zein is extracted from corn products or coproducts using aqueous alcohols. Classically, zein is extracted with 88% (w/w) 2-propanol with 0.25% NaOH from corn gluten meal; a protein-rich coproduct of the wet-milling process (Anderson and Lamsa, 2011). It was determined that the zein that is available on the market consists almost exclusively of alpha zein (Wilson, 1988). For the preparation of loaded microcarriers, zein and the active component can be linked by a multitude of *in vitro* methods. These include chemical crosslinking, emulsification/solvent evaporation, emulsification/precipitation/gelation, spray drying, supercritical anti-solvent technique and phase separation (Zhang et al., 2016). Many benefits have been demonstrated for such loaded zein microcarriers. They can be used to delay the release of the active compound (Hurtado-López and Murdan, 2006), to improve its stability (Lee et al., 2013), to target specific organs such as the liver (Lai and Guo, 2011), and to improve bioavailability after oral administration (Ahmed et al., 2015; Hashem et al., 2015; Luo et al., 2013). Besides these advantageous characteristics, another reason why zein has gained so much attention is because it was approved as “generally recognized as safe” by the U.S. Food and Drug

Administration in 1985 (Zhang et al., 2015). Although extracted alpha zein has been used to encapsulate proteins *in vitro* (Lee et al., 2016), the majority of studies focused on other non-proteinaceous products such as alpha-tocopherol (Luo et al., 2011), curcumin (Gomez-Estaca et al., 2012), ketoprofen (Jiang et al., 2012), and procyanidins (Zou et al., 2012) because of their hydrophobicity. Another way of encapsulating proteins into zein PBs is *in vivo* by heterologous expression of zein as a fusion with the protein of interest. As mentioned earlier, it was shown that amongst all zeins gz27 is the most relevant for the induction of PB formation. Its capability to do so derives from structural features within its amino acid sequence. gz27 is divided into three domains: the N-terminal part hosts eight repeats of the hexapeptide PPPVHL, a linker-region with alternating P-X, and a C-terminal region that is homologous to 2S albumins and is rich in cysteines (Geli et al., 1994; Llop-Tous et al., 2010; Mainieri et al., 2014; Prat et al., 1985). It was later determined that out of the 204 amino acids of gz27 (without the signal peptide) only the N-terminal 93 amino acids are required for the formation of PBs. These 93 amino acids of gz27 only include the (PPPVHL)<sub>8</sub> and the P-X domain. This sequence will be called gz93 from here on. The (PPPVHL)<sub>8</sub> domain forms a left-handed amphipathic polyproline II helix that facilitates the oligomerization by hydrophobic interactions that are then stabilized by intermolecular disulfide-bridges (Llop-Tous et al., 2010). In this regard, Cys<sup>7</sup> and Cys<sup>9</sup>, that proceed the (PPPVHL)<sub>8</sub> domain, are more important than Cys<sup>64</sup>, Cys<sup>82</sup>, Cys<sup>84</sup>, and Cys<sup>92</sup> that follow. The capability to form PBs is therefore an intrinsic feature of gz93 and is not dependent on other factors provided by the maize endosperm, where gz93 derives from. gz93 also induces PB formation when other proteins are fused to its C-terminus. This is very well documented for fluorescent marker proteins (Llop-Tous et al., 2010) but also for proteins of interest such as enzymes (Llop-Tous et al., 2011) or antigens (Hofbauer et al., 2016; van Zyl et al., 2017). gz93 fusion proteins have been recombinantly expressed in numerous eukaryotic hosts. PB formation of gz93 fusions has been demonstrated in human HEK293T cells, monkey kidney cells Cos1, Chinese hamster ovary cells, filamentous fungi *Trichoderma reesei*, Sf9 insect cells, and plants such as *Arabidopsis thaliana*, *Medicago sativa* (alfalfa), or *Nicotiana* spp. (Alvarez et al., 2010; Torrent et al., 2009). Examples of therapeutic proteins that were fused to gz93 include antigens of viruses such as influenza (Hofbauer et al., 2016), bluetongue (van Zyl et al., 2017), *Yersinia pestis* (Alvarez et al., 2010), and human papillomavirus (Whitehead et al., 2014), or they were hormonal proteins such as calcitonin, epidermal growth factor, and human growth hormone (Torrent et al., 2009). Because of this versatility, gz93 was patented under the name Zera® by the Spanish company ERA Biotech SL., which is now called Zip Solutions SL (Ludevid et al., 2006). The expression of recombinant proteins as gz93-induced PBs also helps to improve yields by proposedly preventing degradation of the protein of interest (Alvarez et al., 2010). For gz27, it has indeed been demonstrated that it can withstand digestion by pepsin in simulated gastric fluid (Krishnan et al., 2010). A feature that

is also true for rice prolamins and that is a crucial prerequisite for the oral administration of vaccines (Takaiwa et al., 2015). Administration of viral antigens encapsulated into PBs of gz93 can also be immunogenically favorable. gz93 displayed adjuvant effects when the ectodomain of hemagglutinin subtype 5 of the influenza virus was fused to gz93 and injected subcutaneously into mice. gz93-H5 PBs were able to induce a similar immune response as soluble H5 administered alongside Freund's adjuvant, whereas soluble H5 without an adjuvant failed to induce a response. It is important to note that in the same study it was not possible to detect a significant immunological reaction against gz93 (Hofbauer et al., 2016). The adjuvant effect might be explained by an increased cellular uptake rate of antigen. The (PPPVHL)<sub>8</sub> domain of gz93 closely resembles the sequence of a cell-penetrating peptide (PPPVRL)<sub>3</sub> called sweet arrow peptide (Pujals and Giralt, 2008). The amphipathic nature of this domain may facilitate the interaction with membranes and therefore the endocytosis of gz93 PBs. As described earlier, efficient endocytosis of oral vaccines is crucial to ensure their transfer across the gut epithelium. The cellular uptake of gz93 PBs shall be investigated in this thesis. Additionally, the concept of encapsulation into zein PBs shall be developed further. Formation of multicomponent PBs promises to enable adjustments of particle stability, release of active compound, and cellular uptake.

## 2 Objectives

One objective of this thesis is to further our knowledge about the applicability of zein particles as microcarriers for oral vaccines. The efficacy of oral vaccines strongly depends on the bioavailability of the antigen. The endocytosis of loaded particles by cells of the intestinal epithelium is therefore a crucial parameter. A high uptake rate means higher efficacy which translates to a lower dose that in turn leads to a wider therapeutic window and less side effects. The endocytosis of fluorescent gz93 PBs shall therefore be investigated in cultured human colonic epithelial cells. This shall be analyzed qualitatively by confocal imaging and quantitatively by comparing flow cytometry data of cells treated with PBs versus cells treated with synthetic beads. Furthermore, it shall be investigated whether the endocytosis of PBs is able to trigger epithelial cells to release cytokines that are involved in the recruitment of APCs. If so, uptake of PBs by APCs shall be investigated as well. Since these studies will require relatively large amounts of PBs, a scalable, filtration-based method for the enrichment of PBs shall be developed.

Another objective is to further advance the zein-based encapsulation system. As of now, all biomedical applications of gz93 revolved around generating PBs that consisted of only one bioactive agent. By creating PBs with two or more components, it should be possible to add more functionality to the system. The presence of additional zeins in recombinant PBs might help to control their stability and the release kinetics of therapeutic proteins. If these multi-zein PBs arrange into a core-shell structure like they do in maize, the outer shell could be modified for enhanced endocytosis in the target organism. The second part of this thesis therefore aims to create recombinant PBs that consist of multiple components and the highly ordered structure of PBs in maize served as a model. As a prerequisite, it will be systematically analyzed whether zeins other than gz27/gz93 are able to form PB-like structures as fusion proteins in *Nicotiana benthamiana*. Zeins with different fluorescent markers shall then be coexpressed to investigate their capability to form multicomponent PBs. Since it has been demonstrated that mRNA-targeting influences the structural organization of zein PBs, experiments shall elucidate whether the inclusion of mRNA zip codes has beneficial effects on the formation of multi-zein bodies.

## 3 Material and Methods

### 3.1 Molecular cloning

Constructs were designed *in silico* with the software SnapGene and fully or partially synthesized by GeneCust Europe. Constructs az19-mCherry, gz27-EGFP, gz93-EGFP were delivered in a pBluescriptIISK+ background and transferred into the binary pTRA vector (Maclean et al., 2007) by *SmaI/XbaI*-mediated restriction cloning. For constructs az22-mCitrine-FLAG, gz16-mKO2-cMyc, bz15-mTagBFP2-VSV, dz10-V5, and az19-mCherry-HA the pTRA backbone was provided to GeneCust Europe and final constructs were delivered in this destination vector. Recombination of *BamHI/XbaI*-digested DNA fragments generated constructs gz27-mCherry-HA, gz27-mTagBFP2-VSV, gz93-mCherry-HA, gz93-mTagBFP2-VSV, az19-EGFP, az19-mKO2-cMyc, az22-EGFP, az22-mCherry-HA, az22-mTagBFP2-VSV, gz16-EGFP, gz16-mCherry-HA, gz16-mTagBFP2-VSV, bz15-EGFP, bz15-mCherry-HA, dz10-EGFP, dz10-mCherry-HA, and dz10-mKO2-cMyc. Native zein 5'- and/or 3'-UTRs were also synthesized by GeneCust Europe and inserted into az19-mCherry, gz27-EGFP, and gz93-EGFP by *XhoI/KpnI* and *HindIII/SmaI*-mediated restriction cloning, respectively, to produce constructs 53U-az19-mCherry, 53U-gz27-EGFP, 53U-gz93-EGFP, 5U-az19-mCherry, 5U-gz27-EGFP, 5U-gz93-EGFP, 3U-az19-mCherry, 3U-gz27-EGFP, 3U-gz93-EGFP. Primers 5'-GATACAGTCTCAGAAGACCAGAG-3', 5'-GGAACTACTCACACATTATTCTGGAG-3', 5'-CCTTGCTCACCATCGCCGTAGCAGCACTTGCAG-3', 5'-GTGCTGCTACGGCGATGGTGAGCAAGGGCGAGGAG-3' were used in overlap-extension PCRs to combine fragments and introduce restriction sites *XhoI* and *SmaI* during the generation of constructs 53U-mCherry, 5U-mCherry, 3U-mCherry and mCherry (no zein, no zein UTR).

All zeins include their native signal peptide and neither zeins nor fluorescent proteins were codon optimized for the expression in *Nicotiana benthamiana*. All constructs were designed with a (GGGS)<sub>2</sub> linker between zein and the fluorescent protein. Constructs that contain a C-terminal peptide tag have their tag attached by a G<sub>3</sub> linker after the fluorescent protein. Constructs that do not contain native zein UTRs instead harbor a UTR from tobacco etch virus (TEV) for increased mRNA stability. The pTRA vector is a derivative of pPAM (GenBank accession number AY027531) and contains the 35S promoter with duplicated transcriptional enhancer and the 35S terminator both originating from Cauliflower mosaic virus (CaMV) as well as matrix attachment regions of tobacco Rb7 up- and downstream of the promoter and terminator, respectively (Halweg et al., 2005; Maclean et al., 2007; Rademacher et al., 2002; Sack et al., 2007).

GenBank accession numbers for each zein are az19 (AF371269), gz27 (AF371261), gz93 (N-terminal 93 amino acids of AF371261), gz16 (AF371262), bz15 (AF371264), dz10 (AF371266), and az22 (AF371274). Amino acid sequences can also be found in the appendix.

### **3.2 Phylogenetic analysis**

15 zein amino acid sequences were aligned with ClustalW in MEGA X (Kumar et al., 2018; Larkin et al., 2007). The evolutionary history was inferred using the Neighbor-Joining method (Saitou and Nei, 1987). The optimal tree with the sum of branch length = 5.31566557 is shown. The tree is drawn to scale, with branch lengths in the same units as those of the evolutionary distances used to infer the phylogenetic tree. The evolutionary distances were computed using the Poisson correction method (Zuckermandl and Pauling, 1965) and are in the units of the number of amino acid substitutions per site. All ambiguous positions were removed for each sequence pair (pairwise deletion option). There was a total of 312 positions in the final dataset.

### **3.3 Plants and Agrobacteria**

*Nicotiana benthamiana* plants grew on soil in a chamber with a 16 h photoperiod at 70% relative humidity and day/night temperatures of 26°C and 16°C, respectively. pTRA constructs were transferred into chemically competent *Agrobacterium tumefaciens* GV3101 containing the helper plasmid pMP90RK (Koncz and Schell, 1986). Cultures of *Agrobacterium* strains were inoculated from glycerol cryo-stocks and cultivated in YEB medium containing 25 mg/l kanamycin, 25 mg/l rifampicin, and 50 mg/l carbenicillin. Cultures were incubated at 28°C while shaking at 200 rpm. Prior to infiltration, the cultures were pelleted and washed twice with infiltration medium (10 mM MES pH 5.6, 10 mM MgCl<sub>2</sub>, 100 µM acetosyringone) and adjusted with infiltration medium to specific optical densities at 600 nm wavelength (OD<sub>600</sub> of 0.2 if not stated otherwise). Infiltration of *Nicotiana benthamiana* leaves was performed manually with 1 ml syringes. Leaves were harvested 8 days post infiltration (dpi) to produce PBs for uptake assays whereas smaller samples for size determination were harvested at 4 and 12 dpi as well.

### **3.4 Protein body size determination**

The diameter of gz93-EGFP PBs was determined at 4, 8, and 12 dpi by analyzing maximum projected Z-stacks of CSLM pictures. For each sample, a 5 x 5 mm section was excised from agroinfiltrated leaves of *Nicotiana benthamiana* and mounted on a glass slide with tap water as immersion medium. The samples were observed under a Leica SP5 Confocal Laser Scanning Microscope (CLSM) using a 63x water immersion objective (NA 1.20). Argon

laser power was set to 16% and the 488 nm laser line was set to 2% output for the excitation of EGFP. Forty-eight pictures along the z-axes were recorded at a resolution of 1024 x 1024 px for each picture with a step size of 1.1  $\mu\text{m}$  (bidirectional scanning at 400 Hz, 2x line averaging). Maximum projections of z-stacks were exported from Leica Software and analyzed using Adobe Photoshop. 832, 986, and 821 individual protein bodies from at least three samples per time point were measured for 4, 8, and 12 dpi, respectively. Statistical significance between time points was determined by one-way ANOVA with post-hoc Tukey's test.

### **3.5 Processing of plant material for uptake studies**

*Nicotiana benthamiana* leaf material expressing gz93-EGFP or gz93-mTagBFP2 was harvested at 8 dpi and stored at  $-20^{\circ}\text{C}$  until processing. Leaf material, 200 g, were homogenized in a Waring-type blender with the addition of 800 ml PBS extraction buffer (137 mM NaCl, 2.7 mM KCl, 10 mM  $\text{Na}_2\text{HPO}_4$ , 1.8 mM  $\text{KH}_2\text{PO}_4$ , pH 7.4) supplemented with 2% Triton X-100. The extract was further homogenized with a disperser (IKA ULTRA-TURRAX® S 25 N - 10 G) and then repeatedly pelleted by centrifugation at 15000 rcf for 30 min at  $4^{\circ}\text{C}$ . The supernatants were discarded, and the pellets were washed twice with PBS extraction buffer including 2% Triton X-100 and twice with PBS lacking Triton X-100. The resulting suspension was then filtered through a 180  $\mu\text{m}$  nylon mesh filter utilizing a vacuum-assisted bottle-top filter holder. Small amounts of antifoam Y-30 were added when necessary. This was then subjected to the first tangential flow filtration (TFF) using a nylon filter cloth with a 10  $\mu\text{m}$  cutoff. Since TFF systems with this pore rating were not available, we built a prototype TFF filter holder that can be equipped with any cloth or membrane. This filter holder provided a surface area of 96  $\text{cm}^2$  and was operated by a peristaltic pump. gz93-EGFP PBs passed through the 10  $\mu\text{m}$  filter and the permeate is washed and concentrated using a second TFF with a 0.65  $\mu\text{m}$  cutoff (SpectrumLabs; C02-E65U-07-N). Once some of the permeate has passed the first filter, both systems can be operated simultaneously. The concentrated retentate is subjected to low speed density centrifugation over a cushion of 40% CsCl (1.4225  $\text{g}/\text{cm}^3$ ) at 4800 rcf for 30 min at  $20^{\circ}\text{C}$ . The top layer was collected and washed twice with five sample volumes PBS, in order to remove CsCl, by pelleting at 21000 rcf for 5 min at  $20^{\circ}\text{C}$ .

### **3.6 Flow cytometry of protein bodies**

Processed samples of gz93-EGFP PBs were measured in a V-bottom 96-well plate and data was collected for 10000 events using a flow cytometer (CytoFlex S, Beckman Coulter). EGFP signal was excited at 488 nm and emission was measured at 525 nm. Forward scatter, side scatter, and EGFP gain were set to 40, 24 and 50, respectively. In order to show the

reproducibility of the method three independent measurements, each including 5 replicates, were performed. Flow cytometer data was analyzed with CytExpert 2.3 (Beckman Coulter).

### **3.7 Mammalian cell culture**

Human colonic epithelial cells (HCEC-1CT, CkHT-039-0229, Evercyte GmbH, Vienna) were routinely grown at 37°C under a humidified atmosphere of 7% CO<sub>2</sub> in DMEM:199 (4:1/Biochrome, Germany) supplemented with 2% cosmic calf serum (HyClone, Logan, UT), EGF (25 ng/mL), hydrocortisone (1 g/mL), insulin (10 g/mL), transferrin (2 g/mL) and sodium selenite (5 nM) (all from Sigma Aldrich GmbH, St Louis, MO). Differentiation of cells towards colonic epithelial cells (Roig et al., 2010a) was induced by culturing cells for 48 hours in DMEM:199 (4:1) supplemented with 0.1% cosmic calf serum, EGF (1.25 ng/ml), hydrocortisone (1 µg/ml), insulin (10 µg/ml), transferrin (2 µg/ml), sodium selenite (5 nM) and GSK-2 inhibitor IX (5 µm, Merck, Germany).

U937 cells (ATCC CRL 1593) were cultivated in RPMI 1640 (Biochrome, Germany) containing 10 % heat inactivated fetal calf serum and 4 mM L-Glutamine (Sigma Aldrich GmbH, St Louis, MO). Differentiation of cells towards macrophage-like cells was induced by culturing  $7 \times 10^5$  cells/ml cells in medium containing 100 nM phorbol 12-myristate 13-acetate (PMA) for 24 hours (Mendoza-Coronel and Castañón-Arreola, 2016). Medium was changed to routine medium and cells were cultivated for further 48 hours until cells attached to the surface showing the development of dendritic-like morphology.

### **3.8 PB uptake and flow cytometry of HCE cells**

For uptake studies, the medium was supplemented with 100 units/ml of penicillin, and 100 µg/ml of streptomycin (Sigma Aldrich GmbH St Louis, MO) and  $2 \times 10^4$  cells/cm<sup>2</sup> were seeded and differentiated for 48 hours until confluence was reached. Based on the results from the quantification of PBs using a flow cytometer, cells were incubated with 150 gz93-EGFP PBs/cell at 37°C (n = 3) for 2, 6, 12, 18 and 24 hours. Prior to cell detachment using 0.1%/0.02% Trypsin/EDTA for 5 minutes, cells were washed thoroughly with PBS to remove remaining particles. The uptake of fluorescent particles into the cells was analyzed in a flow cytometer (CytoFlex S, Beckman Coulter). Yellow-green labelled 1 µm polystyrene microspheres (F13081, Thermo Fisher Scientific, Waltham, MA) were used for comparison. As a negative control, cells were kept for 6 hours at 4°C to prevent active particle uptake. The negative control was carried out with 150 gz93-EGFP PBs or polystyrene microspheres (PS beads) per cell, respectively, and the signal obtained was subsequently subtracted from the fluorescent signal obtained from cells incubated at 37°C.

The supernatant of cells was collected after 24 hours of incubation either with or without gz93-EGFP PBs or PS beads, centrifuged for 15 minutes with 500 rcf at 4°C and stored at -80°C until analysis of cytokine content. Cytokines interleukin-6 and granulocyte macrophage colony stimulating factor (GM-CSF) secreted into the media by HCEC-1CT cells were measured using the MILLIPLEX® MAP Human Cytokine/Chemokine panel (Hcytomag-60-K, Merck Millipore, Burlington, MA). As a positive control, cells were incubated for 24 hours with 200 ng/ml TNF $\alpha$  (Sigma Aldrich GmbH St Louis, MO) to induce cytokine secretion. Statistical significance was determined by ordinary one-way ANOVA with Sidak's multiple comparisons test.

### **3.9 Microscopy of mammalian cells**

HCE cells were seeded in 8-well micro-slides (Cat#80826, ibidi, Gräfelfing, Germany) and differentiated after a cell number of  $3 \times 10^4$  cells/cm<sup>2</sup> was reached. After incubation with gz93-EGFP PBs for 4 hours, cells were washed 3 times with PBS. In order to visualize the cell nuclei, cells were stained for 5 minutes with 2  $\mu$ g/ml Hoechst 33342 (H1399, Thermo Fisher Scientific). Additionally, cells were incubated for 5 minutes at 37°C with 5  $\mu$ g/ml of the lipophilic cell membrane dye FM4-64 (T13320, Thermo Fisher Scientific). Cellular uptake of PBs into HCEC-1CT was confirmed by confocal light scanning microscopy (CLSM) using a Leica TCS SP8 with a 63x water immersion objective (NA 1.20) (Leica Microsystems, Wetzlar, Germany; lasers: diode 405 nm, white light laser 488 nm, 565 nm; detectors: HyD 432 – 472 nm, PMT 503 – 515 nm). Z-stacks were generated with a step size of 0.7  $\mu$ m.

U937 cells were incubated for 2 hours with gz93-EGFP and gz93-mTagBFP2 PBs at 37°C. Lysosomes of cells were loaded by pulsing cells with 0.1 mg/ml Alexa Fluor 647–dextran for 4.5 hours, and then cells were chased for 2 hours. Cellular uptake of PBs into U937 cells was confirmed by CLSM as described for HCE cells.

### **3.10 Analysis of nicotine content in PB preparations**

Nicotine extraction was performed as described (Moghbel et al., 2015). PBs derived from 50 mg of leaves (FW) were extracted for 2 h in 1 ml extraction solution (40% aqueous methanol containing 0.1% 1N hydrochloric acid). The supernatant was collected, and the pellet was re-extracted twice. The supernatants were combined and evaporated to dryness (Savant Speed Vac SC-110 with cooling unit RVT-100, Savant instruments, Holbrook). For comparison, 50 mg of leaves of *Nicotiana benthamiana* were ground and extracted according to the same protocol. A nicotine standard (Merck, N0267) was used for quantification. For HPLC-ESI-MS/MS measurements, the sample was dissolved in 12  $\mu$ L of 80 mM ammonium formate buffer (pH 3.0) and 5  $\mu$ L were loaded on a BioBasic C18 column (BioBasic-18, 150 x 0.32 mm, 5  $\mu$ m,

Thermo Scientific) using a Dionex Ultimate 3000 system directly linked to a QTOF instrument (maXis 4G ETD, Bruker). A gradient from 99.0% to 6.2% of solvent A and 1.0% to 93.8% of solvent B (solvent A: 80 mM ammonium formate buffer at pH 3.0, B: 80% acetonitrile and 20% A) was applied over a 10 min interval at a flow rate of 6  $\mu$ L/min. The mass spectrometer was equipped with the standard ESI source and measurements were performed in positive ion, DDA mode (= switching to MSMS mode for eluting peaks). MS-scans were recorded (range: 100-1500 m/z) and the 4 highest peaks were selected for fragmentation. Instrument calibration was performed using an ESI calibration mixture (Agilent).

### **3.11 Microscopy of multicomponent PBs in leaves of *Nicotiana benthamiana***

To investigating the formation of multicomponent zein PBs in *Nicotiana benthamiana*, fluorescent zein proteins were expressed on their own or in combination. The generation of plasmids was described in section 3.1 and the infiltration process was described in section 3.3. Leaf sections with a size of 5 x 5 mm were excised from the plants and mounted on a glass slide with tap water as the immersion medium. The samples were analyzed with a Leica SP8 confocal laser scanning microscope using a 63x objective with a numerical aperture of 1.2 and a refraction index of 1.33. The power of the white light laser was always set to 70% whereas the intensity of individual laser lines, gain, and digital magnification were changed according to necessity. Images were acquired at either 512 x 512 or 1024 x 1024 pixels with line averaging between 2 and 8 (no frame averaging).

Sample preparation for transmission electron microscopy was performed as follows. Infiltrated leaves of *Nicotiana benthamiana* were cut into squares of 1 mm<sup>3</sup> fixed overnight at 4°C in 2% paraformaldehyde + 2.5% glutaraldehyde in 0.1 M cacodylate buffer pH 7.4. The samples were washed with 0.1 M cacodylate buffer pH 7.4 and fixed again further fixed with 1% OsO<sub>4</sub> + 0.8% KFeCN for 3 h at room temperature. Samples were washed with ddH<sub>2</sub>O, and again transferred to 2% uranyl acetate in ddH<sub>2</sub>O for overnight incubation at 4°C. After another washing step with ddH<sub>2</sub>O, the samples were sequentially dehydrated with increasing concentrations of acetone at 4°C and later sequentially embedded into Spurr's resin by immersions in increasing concentrations of resin (in acetone). Ultra-thin sections were viewed with a JEOL 200CX transmission electron microscope.

## 4 Results and Discussion

### 4.1 Endocytosis of zein protein bodies into mammalian epithelial and immune cells

It was reported previously that zein PBs can have an adjuvant effect when administered by injection. For example, fusion of a human papillomavirus (HPV) antigen to gz93 enhanced the immune responses in mice (Whitehead et al., 2014). Similarly, when the influenza antigen H5 was fused to gz93, the resulting PBs were able to elicit a strong immune response that was on par with soluble H5 plus Freund's complete adjuvant, whereas soluble H5 without adjuvant failed to induce an immune response (Hofbauer et al., 2016). Particulate formulations of antigens generally show this immunostimulatory effect and one possible explanation is that upon internalization of a single particle many copies of the antigen enter the cell whereas a much higher dose must be administered to achieve comparable local concentrations surrounding the cell (Colino et al., 2009; Snapper, 2018). Alternatively, the enhanced immune response may also be due to superior antigen display and stability or other immunostimulatory signals (Smith et al., 2013). Additionally, gz93 harbors eight repeats of a proline-rich domain (VHLPPP)<sub>8</sub> that closely resembles the sweet arrow peptide (VRLPPP)<sub>3</sub> which is known to have cell penetrating capabilities (Sánchez-Navarro et al., 2017).

The following part focuses on the potential of PBs for oral application. It investigates the internalization efficiency of zein PBs into cells of the mucosal lining, comparing the uptake of fluorescent gz93 PBs and fluorescent poly-styrene beads of similar size. This demonstrated efficient PB internalization into intestinal epithelial cells as well as APCs. Furthermore, it was analyzed whether the epithelial cells secrete cytokines that are known to recruit APCs.

As a prerequisite, it was necessary to ensure sufficient production of gz93 PBs. Although transient expression in plants can be cost-effective, the industrial downstream processes for the purification of biopharmaceuticals may account for approximately 70-80% of the total manufacturing costs regardless of the expression host (Schillberg et al., 2019). In the case of gz93 for oral delivery, the complexity of the downstream process was therefore reduced by the development of a filtration-based enrichment strategy.

#### 4.1.1 Optimized processing enables scalable enrichment of gz93-EGFP PBs

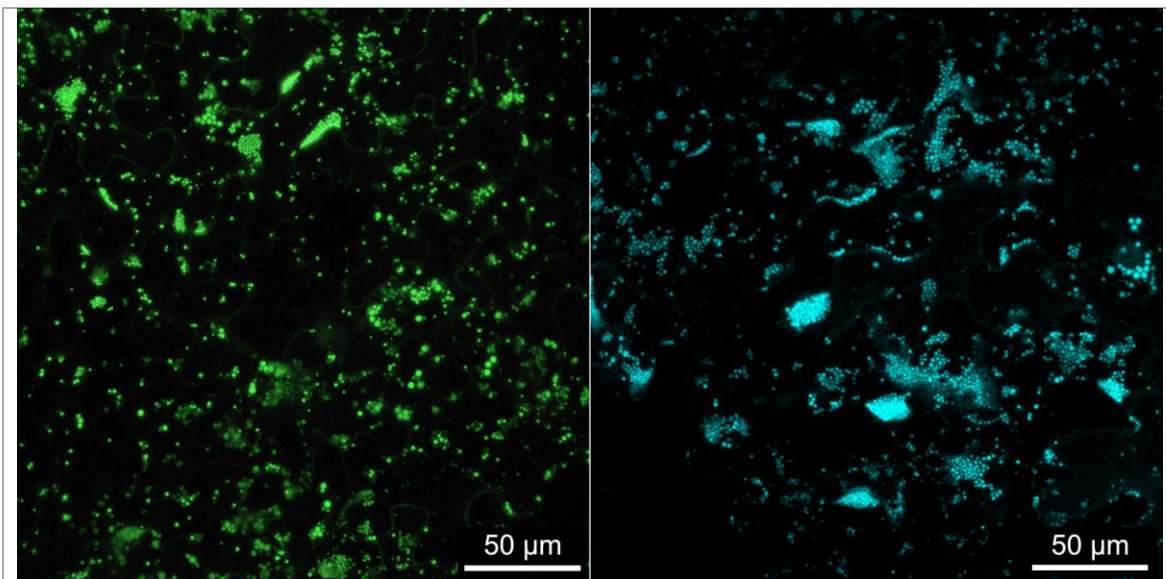
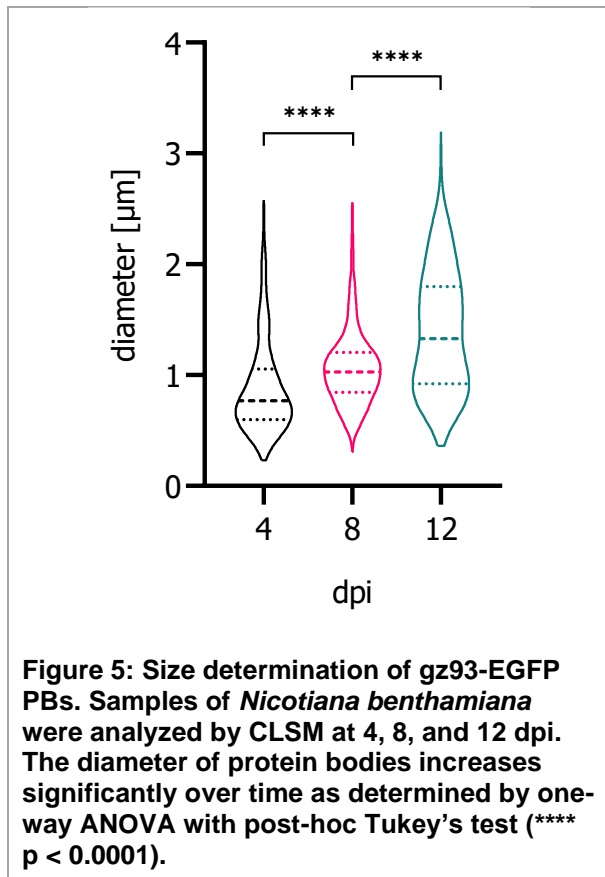


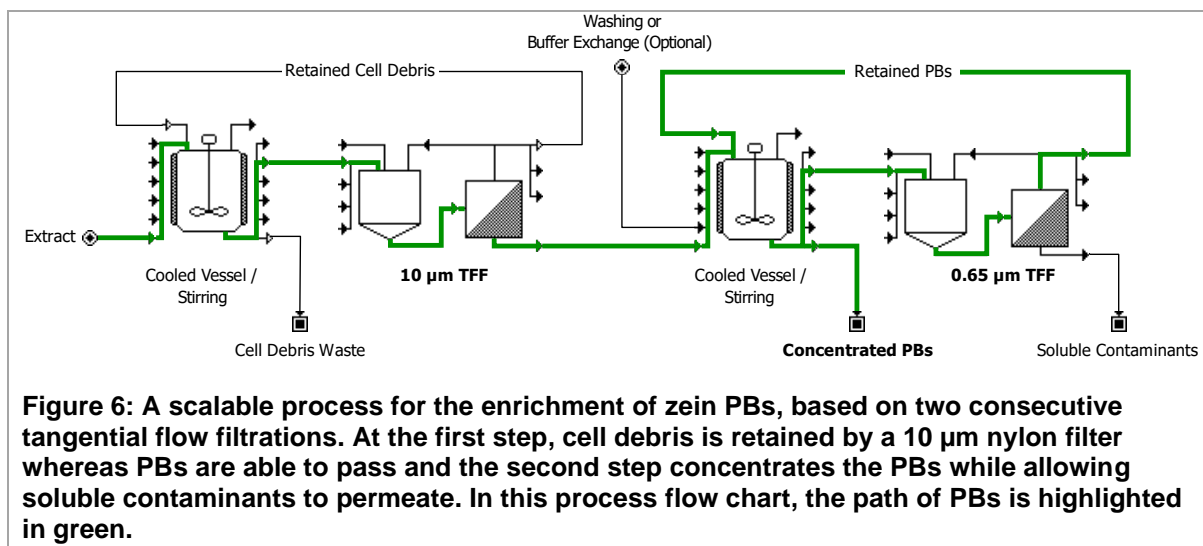
**Figure 4:** Leaf cells of *Nicotiana benthamiana* are expressing (A) gz93-EGFP or (B) gz93-mTagBFP2 PBs at 8 dpi. Z-stacks of 48 CSLM pictures were displayed as maximum projections and the median diameter of 986 individual PBs was determined to be 1.03  $\mu\text{m}$  ( $\text{SD}\pm 0.34$ ). Scale bars represent 25  $\mu\text{m}$  or 50  $\mu\text{m}$ , respectively.

To recombinantly produce fluorescent PBs, EGFP was fused to the C-terminal end of gz93 connected by a flexible (GGGGS)<sub>2</sub>-linker (gz93-EGFP). In another construct, EGFP was replaced by mTagBFP2; a fluorescent protein that is more stable in acidic conditions than EGFP. The gz93-EGFP plasmid was transferred to leaves of *Nicotiana benthamiana* by agroinfiltration and the formation of spherical PBs was confirmed by CLSM (Figure 4). The size distribution of PBs was analyzed at 4, 8, and 12 dpi and median diameters of 0.77 ( $\text{SD}\pm 0.43$ ), 1.03 ( $\text{SD}\pm 0.34$ ), and 1.33 ( $\text{SD}\pm 0.55$ )  $\mu\text{m}$  were determined, respectively (Figure 5). This indicates that gz93-EGFP particles keep increasing in size during accumulation of protein. PBs at 8 dpi with a median diameter of 1.03  $\mu\text{m}$  were chosen for cellular uptake studies.

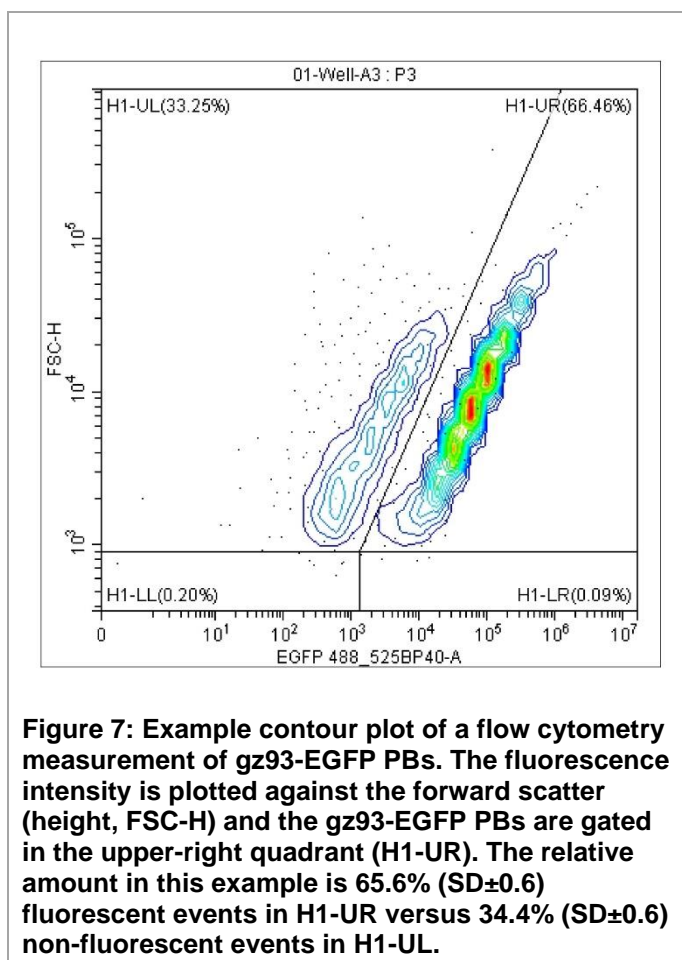


Particulate vaccine strategies have been reported to be effective at lower antigen doses compared to soluble formulations (De Smet et al., 2014). However, oral vaccines generally require a higher dose of antigen to induce an immune response when compared to traditional parenteral immunizations (Pavot et al., 2012). This presents a challenge in the development of oral vaccine applications and the corresponding production platforms need to be highly scalable. Even though plant-based production systems are very flexible with respect to upstream production, the downstream processing procedure often includes limiting bottlenecks. To obtain sufficient amounts of PBs, a new downstream procedure for the enrichment of

zein protein bodies was developed. It is based on a combination of filtration steps (Figure 6) and is therefore more scalable than previously described processes based on ultracentrifugation (Hofbauer et al., 2016; Joseph et al., 2012; van Zyl et al., 2017; Whitehead et al., 2014). The procedure comprised initial washing steps with buffer containing Triton X-100 to solubilize membranes and to remove soluble host proteins and other compounds from the insoluble fraction. This was followed by coarse straining through a 180 µm mesh and two subsequent tangential flow filtrations with pore sizes of 10 and 0.65 µm, respectively. The first TFF retained large cell debris whereas gz93-EGFP PBs pass through the filter. The second TFF step was carried out to remove additional soluble host proteins and particles that are smaller than gz93-EGFP PBs. Through this procedure, it was possible to reduce the sample volume and concentrate it by a factor of 100. As a result, much more of the sample could be subjected to centrifugation over a cushion of 40% CsCl (1.4225 g/cm<sup>3</sup>) that allowed to separate particles with a higher density than gz93-EGFP PBs (e.g. starch granules). In addition, this step was performed at only 4800 rcf, and this enabled more sample to be processed compared to procedures where centrifugation is done at ultrahigh speeds (> 50000 rcf).



The resulting preparations of gz93-EGFP PBs were evaluated by flow cytometry. This method allowed to identify two populations of particles with distinct fluorescence properties (Figure 7). In agreement with inspection by confocal microscopy, we concluded that the population of fluorescent particles represents gz93-EGFP PBs. The mean concentration of fluorescent particles ( $n = 3$ ) was  $3.18E+06$  events/ $\mu\text{l}$  ( $SD \pm 13,2\%$ ) corresponding to  $5.12E+07$  gz93-EGFP PBs/g fresh weight of leaves.



For this study, the PBs were recovered by a newly established enrichment process based on two tangential flow filtration steps and low-speed centrifugation. This procedure can easily be adapted to kg amounts of leaf material without the need to invest in expensive large equipment for continuous ultracentrifugation. It was also demonstrated that fluorescent zein PBs can be analyzed and quantified by flow cytometry. It is likely that the procedure can also be adapted for non-fluorescent particles by using antigen-specific antibodies with fluorescent labels, thereby providing a general procedure for quality control of particulate formulations. It is important

to note that oral vaccine formulations do not require the extensive purification and sterile conditions necessary for injected formulations. The downstream processing reported for plant-made oral vaccines ranges from simple homogenization to minimal processing and partial purification (Chan and Daniell, 2015; Loza-Rubio et al., 2012; Merlin et al., 2017; Pniewski et al., 2018). The presence of plant-derived contaminants such as cell wall debris or starch particles, which cannot be completely removed by filtration and density centrifugation steps are therefore unlikely to constitute a regulatory problem. On the contrary, biocompatible plant constituents such as starch microparticles have even been studied as vaccine adjuvants (Rydell and Sjöholm, 2004; Stertman et al., 2006).

The nicotine levels of *Nicotiana benthamiana* leaves and of the gz93-EGFP PB preparation were determined by HPLC-ESI-MS/MS. The nicotine content from 1 g of leaf material was 47501 ng (SD±20258), whereas the residual nicotine content in a PB sample derived from 1 g of leaves was 3.89 ng (SD±0.2). This demonstrates that during the downstream procedure, nicotine was depleted by a factor of 1.22E+04. The residual amount of nicotine is comparable to the nicotine content found in some vegetables. For example, levels of nicotine in edible parts of tomato and eggplant are 3–7 ng/g (Moldoveanu et al., 2016), and average nicotine exposure from consumption of vegetables is approximately 1000 ng/day (Andersson et al., 2003).

#### 4.1.2 gz93-EGFP PBs are endocytosed by human colon epithelial cells and stimulate cytokine release

The human colon epithelial cell line HCEC-1CT (immortalized by hTERT and CDK4) was used to demonstrate endocytosis of zein PBs into cells of the intestinal barrier. This cell line maintains expression of cell type specific markers and functions of colon epithelial cells (Roig et al., 2010b). The uptake of gz93-EGFP PBs into HCEC-1CT cells was demonstrated by CLSM and quantified by flow cytometry. CLSM images showed that cells are able to internalize gz93-EGFP PBs within 4 hours of incubation (Figure 8 A-D). The cellular internalization was confirmed by providing optical sections (xy-) with xz- and yz-projections (Figure 8 E), which allowed a clear differentiation between extra- and intracellular PBs. Furthermore, the internalization is proven by the overlay of the green signal, originating from the gz93-EGFP PB, and the red signal emitted by FM4-64, reported to stain endocytic membranes (Hansen et al., 2009).

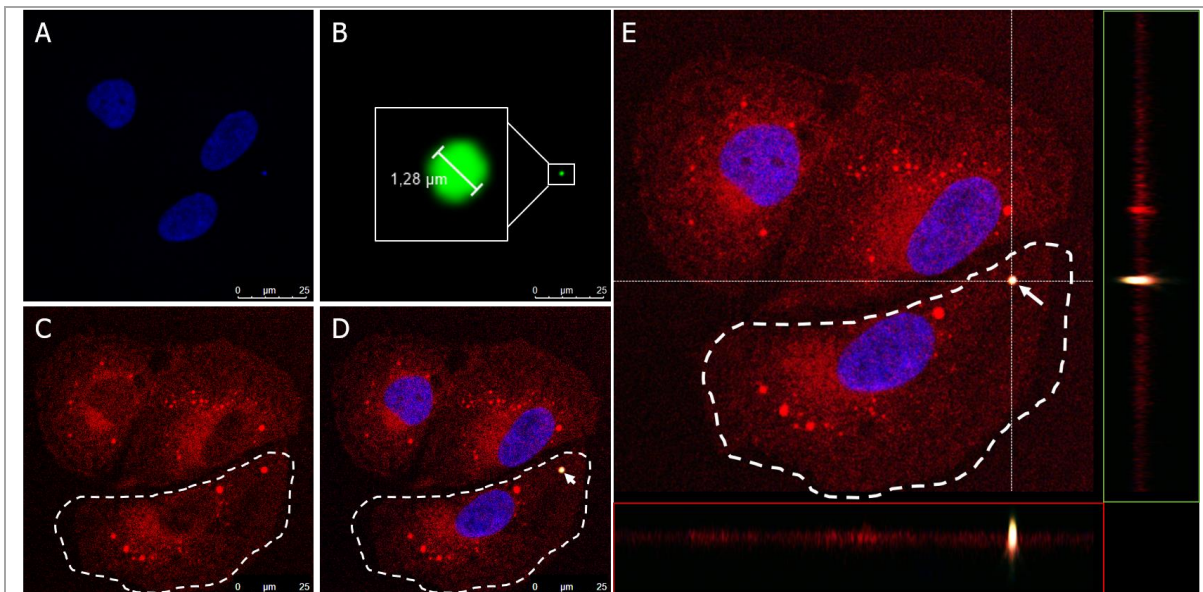
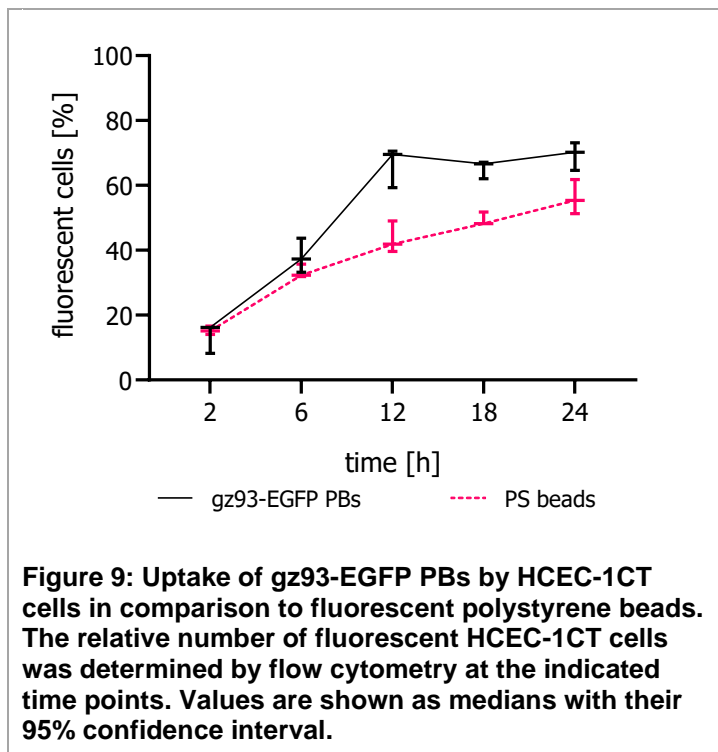


**Figure 8: HCEC-1CT cells have internalized gz93-EGFP PBs after 4 hours of incubation. The cell nucleus was stained with Hoechst 33342, displayed in blue (A), gz93-EGFP PBs emit green fluorescence (B) and the cell membrane and intracellular structures were stained in red with FM4-64 (C). When all channels are merged (D) an orange signal results from the overlay of the green and red fluorescence that indicates the internalization of gz93-EGFP PB into HCEC-1CT cells. The cell was imaged in 32 sections (with a step size of 0.7  $\mu\text{m}$ ), and the cell is shown in the XY-axis at  $z = 11$ . YZ- (E, green panel) and XZ-projections (E, red panel) clearly confirm the internalization of the analyzed PB (arrow). The bar represents 25  $\mu\text{m}$ .**

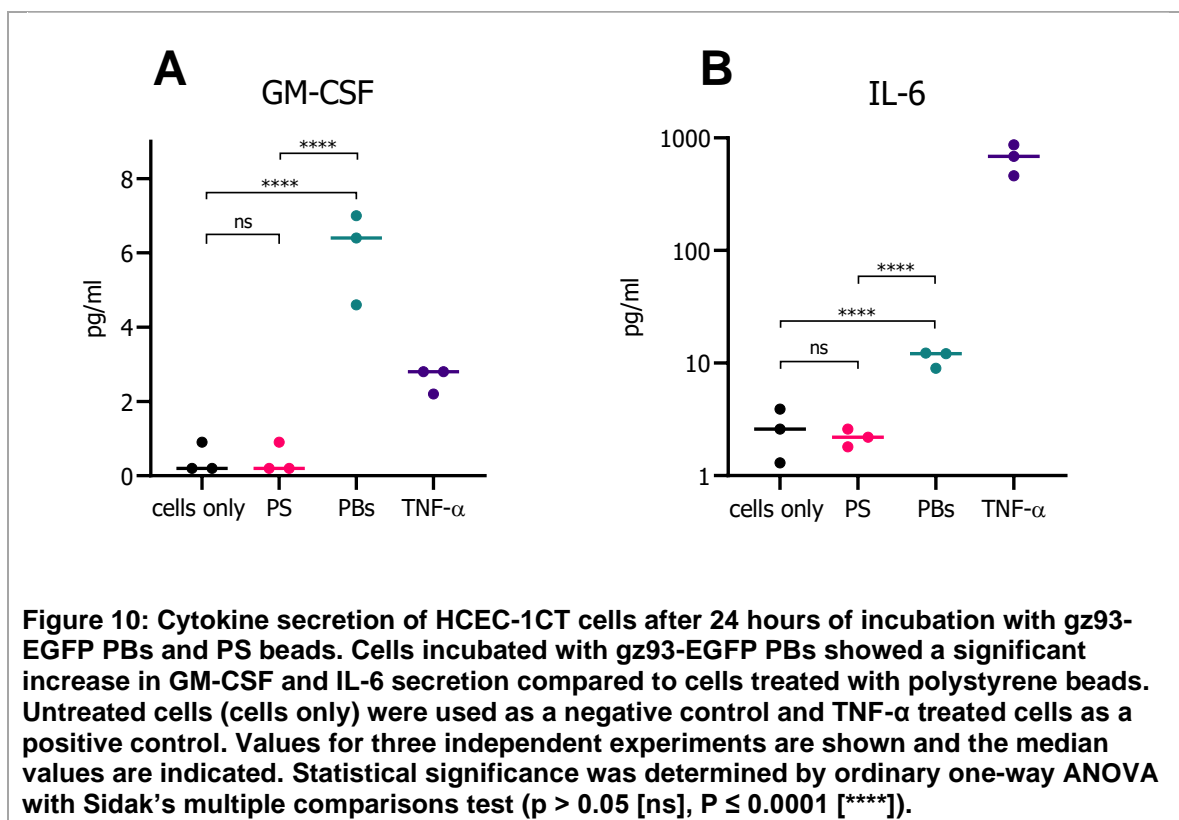
A second experiment was carried out to quantitatively assess the uptake of PBs by flow cytometry and to compare the uptake efficiencies of PBs versus PS beads. Based on the quantification of fluorescent events per  $\mu\text{l}$ , 150 gz93-EGFP PBs or PS beads per cell were added to *in vitro* cultures of HCEC-1CT cells and incubated for 2, 6, 12, 18, and 24 hours. Endocytosis of gz93-EGFP PBs occurred faster than that of PS beads as indicated by a sharper increasing curve for the PBs, reaching a plateau after 12 hours (Figure 9). Mean values after 12 hours reached 66.5% (SD $\pm$ 6.2) and 43.5% (SD $\pm$ 4.9) for gz93-EGFP PBs and



PS beads, respectively. The difference of 22.9% (SD± 4.6) was significant in the Student's t-test ( $p < 0.01$ ). Also, after exposure for 18 h and 24 h, the overall number of fluorescent cells incubated with PS beads remained below the levels obtained with gz93-EGFP PBs (t-test;  $p < 0.05$ ).

Having confirmed that human colon epithelial cells are able to endocytose gz93-EGFP PBs, we investigated whether endocytosis might lead to the secretion of cytokines that can activate the

immune system. Amongst others, the cytokine GM-CSF is known to have an activating effect on APCs such as macrophages and dendritic cells (Hamilton, 2002). We thus collected the culture medium supernatants from the uptake assays ( $n = 3$ ) and subjected them to Luminex assays. Secretion of GM-CSF was only elevated upon administration of 150 gz93-EGFP PBs per cell, but not after treatment with the same amount of PS beads (Figure 10 A). IL-6 levels



were also significantly increased upon incubation with gz93-EGFP PBs as compared to the same dose of PS beads (Figure 10 B).

These results indicate that the PBs are internalized more efficiently into intestinal epithelial cells than synthetic polystyrene beads. After 12 hours of incubation, the proportion of cells that had taken up fluorescent PBs reached 66.5% (SD±6.2). In contrast, after 12 hours of incubation with PS beads, only 43.5% (± 4.9) of cells had internalized PS particles, and the number of fluorescent cells only reached 56.1% (± 5.3) after 24 hours. This enhanced uptake efficiency of PBs might be due to the amphipathic proline-rich repeat found in the N-terminal sequence of gamma zein. It favors interaction with membranes (Kogan et al., 2004) and is assumed to have cell-penetrating effects that could promote the cellular uptake (Fernández-Carneado et al., 2004).

In addition to the uptake of fluorescent PBs, the data demonstrates an immunostimulatory effect on the cells resulting in an increased secretion of chemoattractant molecules such as GM-CSF. GM-CSF is involved in the differentiation of granulocytes and macrophages as well as in the activation and proliferation of neutrophils, macrophages, and dendritic cells (Hamilton, 2002). With respect to mucosal immunization, the presence of GM-CSF was shown to increase antigen-specific antibody production (Okada et al., 1997). GM-CSF also promotes IL-6 secretion (Evans et al., 1998) and accordingly IL-6 levels were also elevated when cells were subjected to PBs. Both chemokines play a pivotal role in the initiation of a humoral response to antigenic proteins (Tada et al., 2018), and IL-6 has been explored as a molecular adjuvant for mucosal vaccines (Rath et al., 2013; Su et al., 2008; Thompson and Staats, 2011). The observed cytokine release indicates the PB formulation's potential to enhance immunity and to exert an adjuvant effect which supports the findings of Whitehead et al. (2014) and Hofbauer et al. (2016).

### 4.1.3 PBs are taken up by immune cells

The uptake of fluorescent PBs was also investigated in human immune cells using the myelomonocytic cell line U937. Cells were first matured and differentiated as indicated by decreased cell proliferation and attachment to the well surface. Two hours after gz93-EGFP PBs were added, most of the cells had taken up multiple particles (Figure 11 A+B). In order to obtain information about the localization of the internalized PBs, the endosomal compartments of those cells were visualized with Dextran Alexa Fluor 647 which is known to localize in late endosomes after endocytosis (Johnson et al., 2016). Since EGFP fluorescence is not stable in the acidic environment of late endosomes, EGFP was replaced by mTagBFP2 on gz93. mTagBFP2 is a blue fluorescent protein variant with a pKa of  $2.7 \pm 0.2$  and therefore much more stable under acidic conditions (Subach et al., 2011). gz93-mTagBFP2 PBs were produced and recovered in the exact same manner as described for the gz93-EGFP PBs and had a similar appearance and size (Figure 4 B). The gz93-mTagBFP2 PBs colocalized with

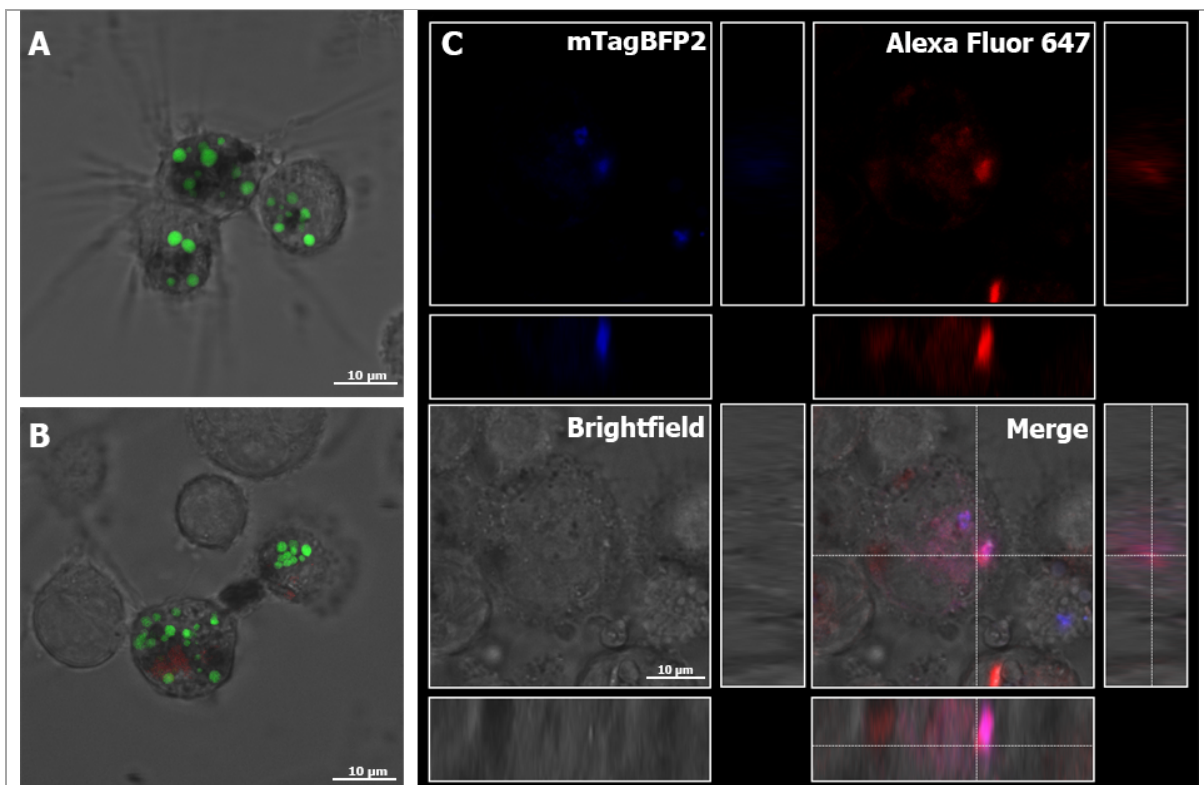


**Figure 11: The uptake of gz93-EGFP and gz93-mTagBFP2 PBs into U937 cells was confirmed by CLSM. Upon PMA treatment, cells attached to the vessel surface and exhibited morphological changes such as the growth of dendrite-like structures (A). Endosomal compartments were loaded and visualized with Alexa Fluor 647-dextran (red, B). Colocalization of blue fluorescent gz93-mTagBFP2 PBs with endosomal compartments (red) results in a purple signal (C, merge).**

compartments stained with Dextran Alexa Fluor 647 (Figure 11 C). It is therefore likely that the PBs are transported to the late endosomes, where usually antigen processing takes place.

Besides antigen uptake via intestinal epithelial cells, dendritic cells can capture antigens directly from the intestinal lumen by extending dendrites through the epithelium (Rescigno et

al., 2001). Since GM-CSF is known to recruit dendritic cells to the subepithelial layer (Egea et al., 2010), it is feasible that its secretion would lead to an increased number of dendrites reaching through tight junctions. Therefore, the uptake of PBs into APCs was investigated using the monocytic model cell line U937 (Altaf and Revell, 2013). APCs have the ability to internalize particles of various sizes with high efficiency. CLSM images confirmed the uptake of multiple PBs per cell. By using blue fluorescent PBs and visualizing the endosomal compartments with Dextran Alexa Fluor 647 it was possible to obtain information about the subcellular localization of the internalized particles. Indeed, several particles colocalized with fluorescently labelled endosomal organelles, indicating that PBs might be processed within the endolysosomal system. From there, peptides can be loaded onto Major Histocompatibility Complex (MHC) class II molecules, which is the prerequisite for a successful immune response (Blum et al., 2013; Roche and Furuta, 2015).

The presented results demonstrate the feasibility of orally administering gz93-encapsulated vaccines. The enhanced endocytosis of gz93 PBs seen in cells *in vitro* is likely to occur *in vivo* as well. The increased bioavailability might also explain the elevated immune response reported in other studies (Hofbauer et al., 2016; Whitehead et al., 2014). Additional aspects need to be investigated in order to further advance the zein PB system. These aspects include the specific resistance to degradation of processed PBs and their interaction with the mucus layer. We chose to improve the encapsulation tool by generating multicomponent PBs. This promises to enable controlling key parameters of particle vaccines.

## 4.2 Generation of recombinant multicomponent zein PBs

So far, the encapsulation of therapeutic proteins by zeins was only mediated by gz93 (Hofbauer et al., 2016; Torrent et al., 2009; van Zyl et al., 2017; Whitehead et al., 2014). This generated PBs that consisted exclusively of the single component that is the fusion between gz93 and the therapeutic protein. Inspired by the core-shell structure of zein PBs found in maize, the following part aims to create a system that allows the recombinant production of multicomponent particles. By including more than one component, it might be possible to control particle parameters like resistance to degradation, mucus penetration, cellular uptake, and release of active compound. In order to develop this next generation of PBs, specific interactions between zeins are considered, as well as targeting of mRNA to subdomains of the endoplasmic reticulum.

### 4.2.1 Coexpression of gamma zein and alpha zein

Initial coexpression experiments were carried out with az19 in combination with either gz27 or gz93. These zeins were chosen as potential interaction partners because gz93 is a well characterized tool for recombinant PB generation and az19 the most abundant zein the core of native zein PBs in maize. As described in the introduction, gz93 comprises the N-terminal part of gz27. Although gz93 can fulfill key functions of gz27 such as induction of PB formation and provision of stability, gz27 was included in this study as well, due to the hypothesis that the C-terminal part of gz27 might be required for protein-protein interactions with az19. This part is missing from gz93. az19 was chosen as a candidate because the localization pattern of zeins in maize PBs shows that the majority of their core comprises alpha zein (Lending and Larkins, 1989). Alpha zein az19B1 in particular, has by far the highest transcript level in maize endosperm (Woo et al., 2001). Therefore, this specific zein was chosen as a candidate to test whether coexpression alongside PB-inducing gz27 or gz93 would yield core-shell structured PBs.

Individual transient expression of gz27 in *Nicotiana benthamiana* induced the formation of spherical PBs with an average diameter of 1  $\mu\text{m}$ . Individually expressed, az19 on the other hand formed much smaller PBs that clustered together and appeared as a granular mass. When the two were expressed together, az19 surrounded gz27 PBs and it even seemed that they tightly interacted in areas where az19 formed cap-like structures on the surface of gz27 PBs, but it did not integrate into its core (Figure 12 A). Even though it appeared as if these az19 cap-like structures were in direct contact with gz27 PBs, they still might have been separated by a membrane due to differential localization. This question was answered by subjecting the sample to transmission electron microscopy. In Figure 13, gz27 again appeared as large spherical PBs as was previously seen in confocal images. When az19 was separated

from gz27 by an ER-membrane, it also formed round PBs; although much smaller than gz27. In contrast to that, when az19 formed cap-like structures on gz27 PBs, these cap-structures were slightly larger than spherical az19 PBs and no membrane separated the two zeins. Therefore, other factors must have prevented az19 from entering the core of gz27 PBs.

When gz93 was expressed with az19, gz93 also formed spherical PBs that were surrounded by az19 but some gz93 PBs had a hollow core. In the overlay of both pictures it can clearly be seen that these cores were filled with az19. Nevertheless, a large portion of gz93 PBs did not integrate az19 and the majority of az19 remained on the outside of gz93 (Figure 12 B). Overall, the incorporation rate of az19 into gz93 was very heterogeneous throughout the sample, such that in some cells no az19 was found inside gz93 although the cell was expressing both zeins.

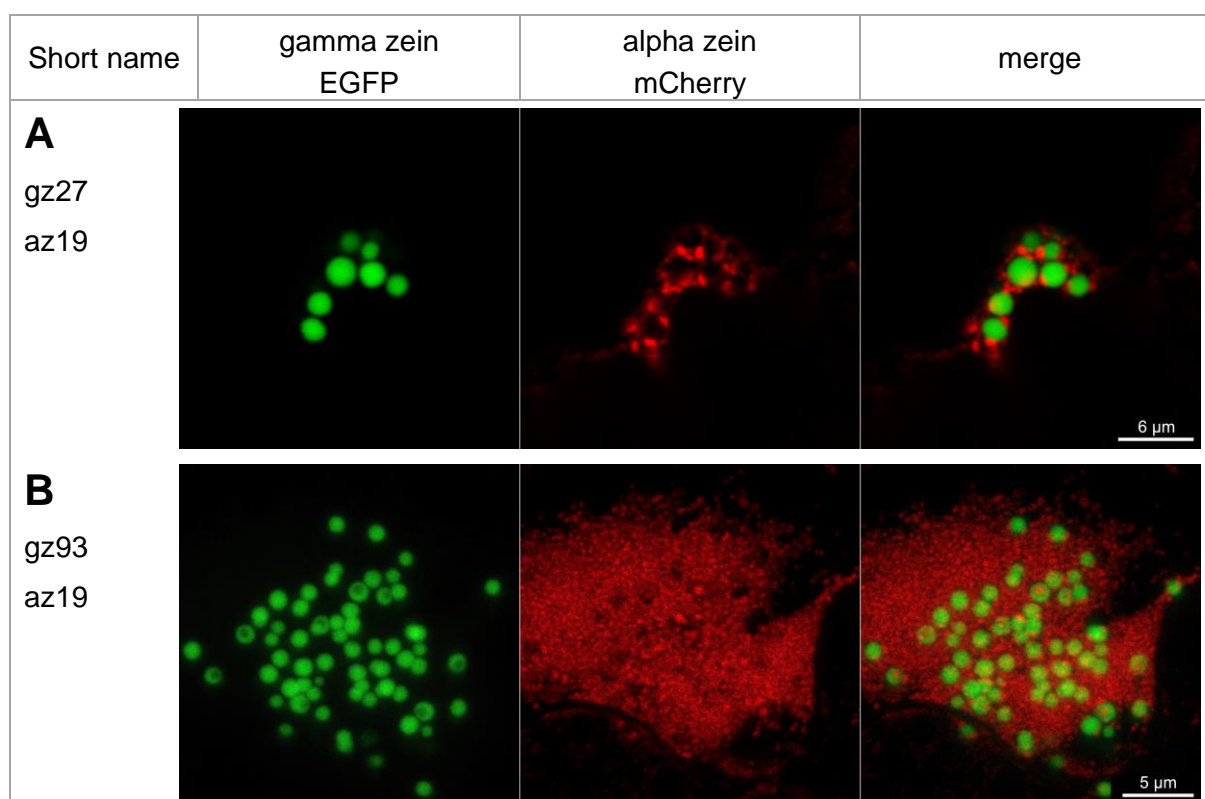


**Figure 12: Coexpression of az19 alongside gz27 (A) or gz93 (B).** Gamma zein variants were fused to EGFP and are displayed in green in the left column whereas az19 was fused to mCherry and is displayed in red in the center column. Both channels are merged in the column on the right. In (A) gz27 and az19 seem to be tightly interacting where az19 formed some sorts of caps on the gz27 PBs but they did not enter the gz27 PB's core. In the green channel of row (B), hollow gz93 can be seen and the merged picture clearly indicates that these were filled with az19. However, the majority of az19 remained on the outside of gz93 PBs. The confocal micrographs in the bottom row (B) are maximum projections of a Z-stack. These samples were analyzed at 10 dpi. Scale bars are only displayed in merged pictures but apply to all pictures of the same row.

In an attempt to improve the rate of incorporation of az19 into gz93 (or gz27), coexpression experiments were conducted where the *Agrobacteria* for alpha and gamma zeins were infiltrated sequentially, several days apart. It can be argued that the expression of various zeins in maize might be temporally orchestrated and that one is expressed before the other. However, neither the prior infiltration of alpha zein, nor of gamma zein, made a difference regarding the number of gz93 PBs that carried az19. In the case of gz27, still no incorporation of az19 was detected (not shown).

An important factor for correct zein PB assembly in maize is mRNA-targeting which is often mediated by untranslated regions (UTRs). Although the formation of core-shell structured PBs was successful without this tool, in order to further improve the incorporation efficiency of az19 into gz27, their native zein UTRs were included in the following experiments.

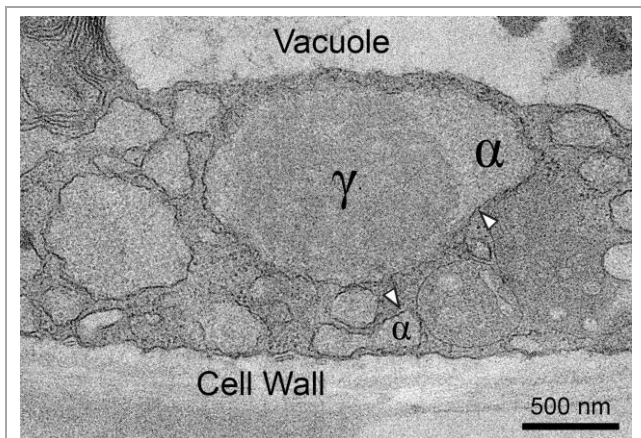


**Figure 13: Transmission electron micrograph of cap-like az19 structures on gz27 PBs. The larger gz27 PB appears darker due to its higher density and can be recognized as almost perfectly round. Some of az19 was found as much smaller, also spherical PBs or as cap-like structures on gz27. Although an ER-membrane surrounded az19 PBs that were separated from gz27, no ER-membrane was detected between az19 cap-like structures and gz27. Membranes were visualized by uranyl acetate staining. A scale bar is located in the bottom right corner.**

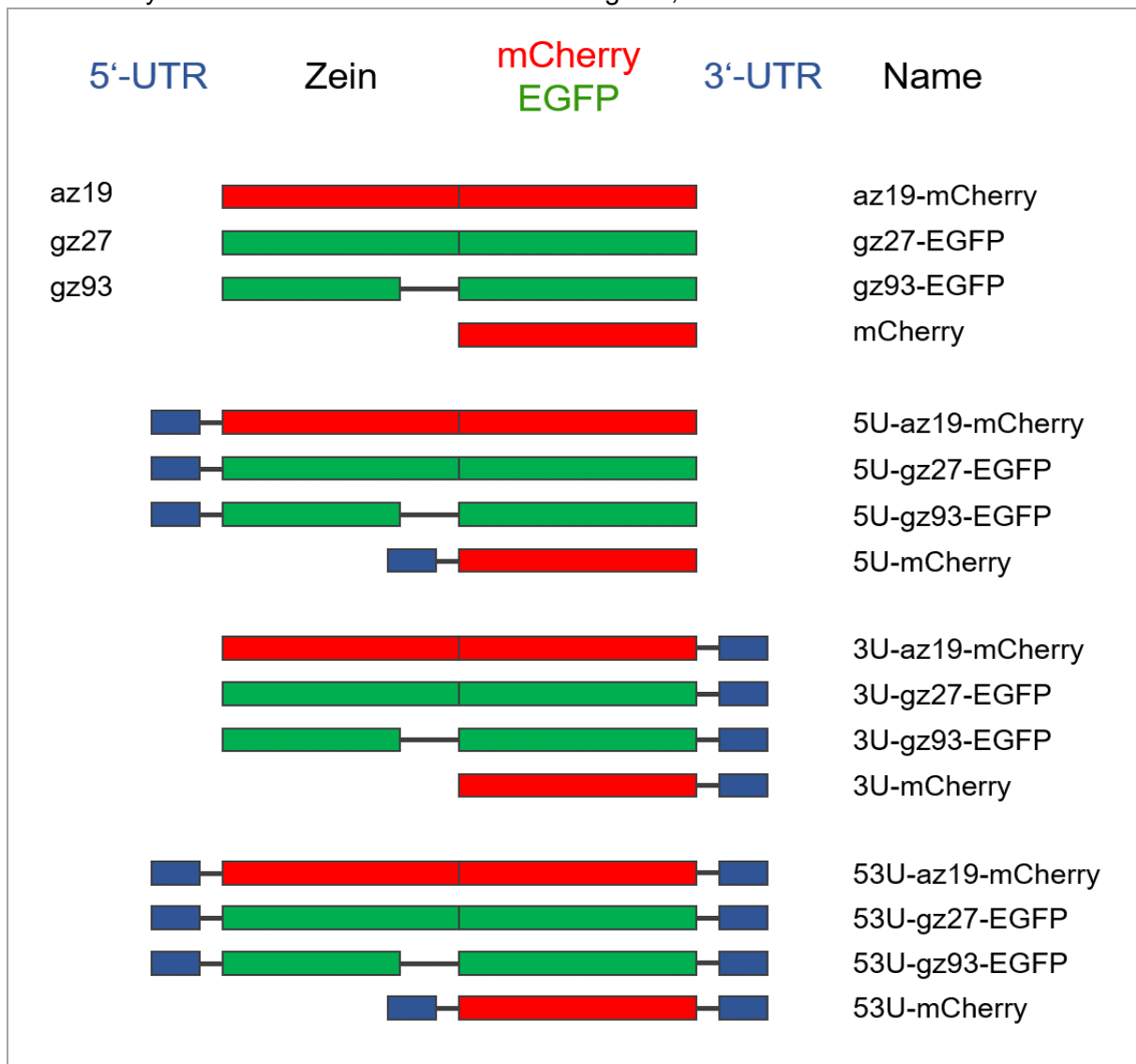
#### **4.2.2 Native UTRs do not improve the incorporation of alpha into gamma zein PBs in *N. benthamiana***

Members of the zein family as well as other prolamins in rice (*Oryza sativa*) contain mRNA-targeting signals that are also known as zip codes (Tian and Okita, 2014). mRNA-targeting is a conserved phenomenon that is able to increase the local concentration of specific proteins in certain regions of the cell (Buxbaum et al., 2015). This can facilitate the interaction of proteins that are supposed to do so or it can prevent undesirable protein-protein interactions by spatial separation (Weatheritt et al., 2014). Zip codes are commonly found in the 3'-UTR of mRNAs but in some cases they are located in the 5'-UTRs or in the coding region (Herve et al., 2004). Specific RNA-binding proteins recognize these elements based on their sequence and/or structural motif and they form a complex with motor proteins that are able to transport the mRNA along microtubules or actin filaments towards their destination (Buxbaum et al., 2015; Yang et al., 2014).

Although one study claimed that protein interactions are the sole driver of PB formation (Kim et al., 2002), others demonstrated that zein mRNAs are asymmetrically localized at a specific

subdomain of the ER called the PB-ER (Washida et al., 2004) and that deleting the zip code from delta zein mistargets its mRNA to the cisternal ER instead (Washida et al., 2009). The latter study has narrowed down the positions of four zip codes in delta zein; three being in the coding sequence and one in the 3'-UTR. Two of those four zip codes are required and sufficient to correctly target the delta zein's mRNA to the PB-ER. Although Washida et al. (2004) demonstrated the involvement of mRNA-targeting for gz27, az22, dz10 and bz15, so far delta zein is the only one for which the approximate position of its zip codes was determined.

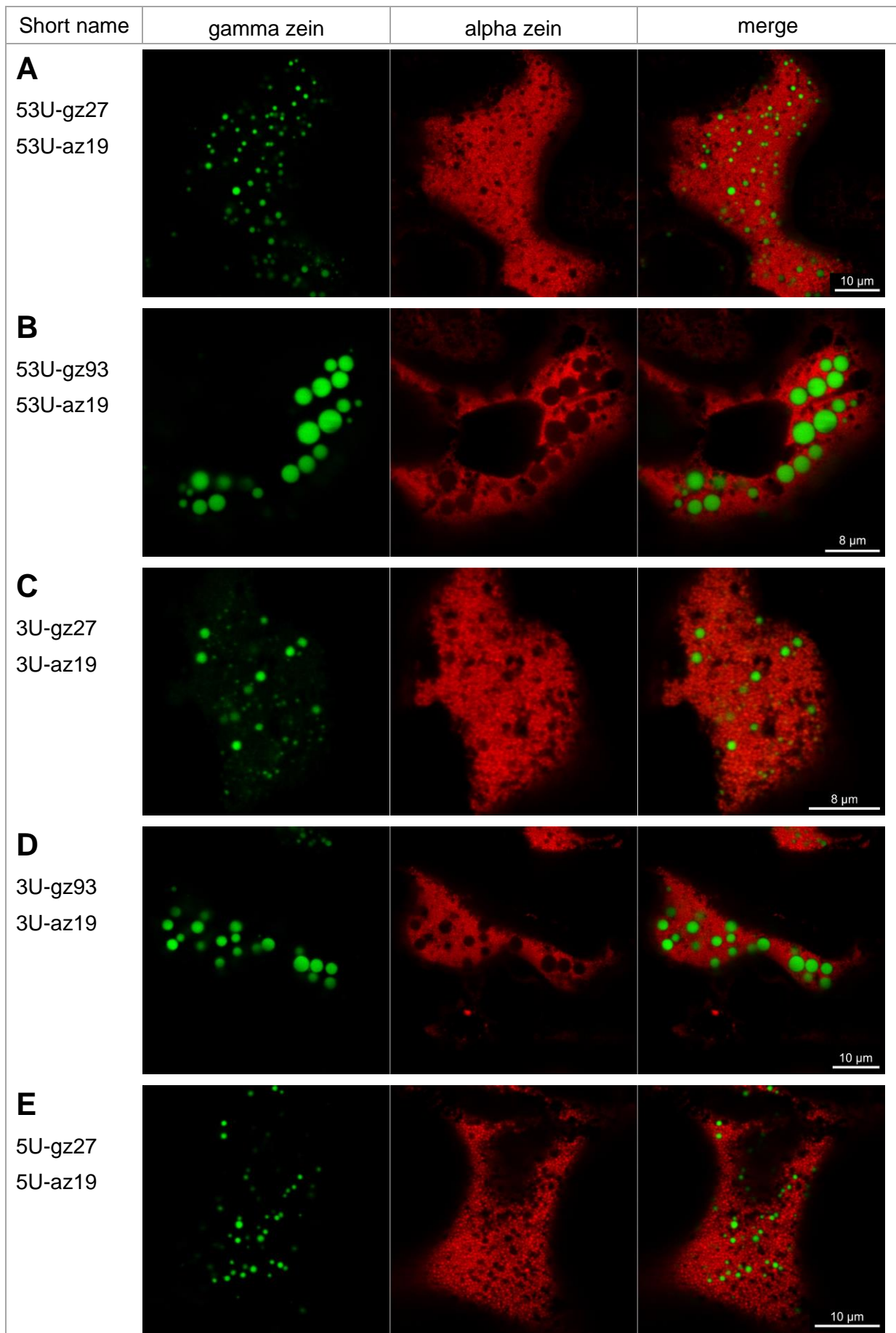
Nevertheless, in order to rule out that inefficient integration of az19 into gamma zein PBs is caused by the absence of mRNA localization signals, native 5'- and/or 3'-UTRs of az19 and



**Figure 14: Schematic representation of constructs that combine az19, gz27, gz93 and soluble mCherry with their native 5'- and/or 3'-UTRs. az19 UTRs are used in the case of soluble mCherry. UTRs are displayed in blue as small boxes flanking the proteins on the left and right for 5' and 3'-UTRs, respectively. Zeins az19, gz27, and gz93 are always located at the N-terminus (left side of fusion protein in this representation) while the fluorescent proteins EGFP and mCherry are located at the C-terminus (right side of fusion protein in this representation). The full name of each construct is displayed for reference as well. In constructs where no zein 5'-UTR is indicated, an arbitrary 5'-UTR of tobacco etch virus was used as a control.**

gz27 were added to their transcript sequences and tested in coexpression experiments that analyzed combinations thereof. Furthermore, 5'- and/or 3'-UTRs of az19 were added to the coding sequence of mCherry to determine whether they are sufficient to change the destination of a soluble protein. A schematic representation of all constructs created for this set of experiments is displayed in Figure 14.

Since the positions of mRNA zip codes on az19 and gz27 are so far unknown and in order to assure that any potential mRNA zip code would be present, the plasmid constructs of az19, gz27, and gz93 were extended to include their native 5'- and 3'-UTR. However, the coexpression of construct 53U-az19 with either 53U-gz27 or 53U-gz93 did not yield any incorporations (Figure 15 A+B). Therefore, including native 5'- and 3'-UTRs in the respective plasmids did not improve the incorporation rate of az19 into gamma zein PBs in *Nicotiana benthamiana*. To assess their individual effects, constructs were generated where the aforementioned zein transcripts include only their native 3'-UTR. In this setting, again, no incorporations were observed (Figure 15 C+D). In contrast, when only native 5'-UTRs were used, construct 5U-az19 was able to generate inclusions in PBs from 5U-gz93 to a similar extent as constructs without the native zein UTR (Figure 15 F), but not more than that (Chapter 4.2.1). Also comparable to earlier experiments without native zein UTRs, PBs of the 5U-gz27 construct failed to incorporate alpha zein from 5U-az19 plasmids (Figure 15 E). When expressed in *Nicotiana benthamiana*, the presence of native zein UTRs had no positive effect on the incorporation of az19 into gamma zein variants. The UTRs did not alter the localization of soluble mCherry when coexpressed with gz93 (Figure 15 G+H). Regardless of the presence or absence of UTRs, some mCherry signal was emitted from areas where gz93 PBs are located. It is likely that the high abundance of mCherry molecules due to overexpression might lead to unspecific entrapment into the PB matrix.



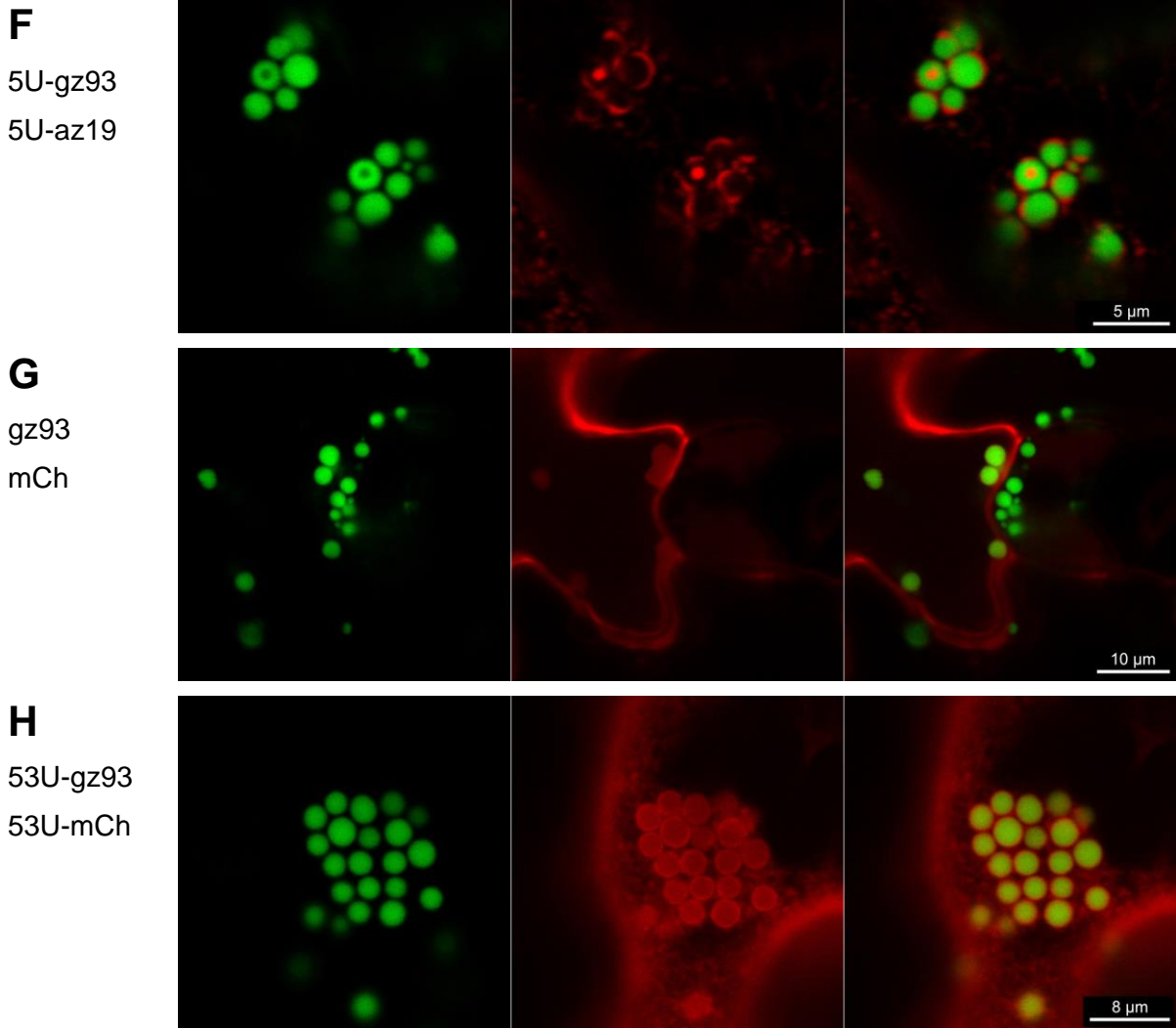


**Figure 15: Evaluation of localization effects of native zein UTRs on incorporation efficiency of az19 into gamma zein PBs. Constructs of az19, gz27, and gz93 were extended to include their native 5'- and/or 3'-UTRs (UTRs of az19 were used on soluble mCherry) and tested in coexpression experiments. Gamma zein variants (gz27 and gz93) were fused to EGFP and are displayed in green in the left column. az19 were fused to mCherry and are displayed in red in the center column whereas the merge of both channels can be found in the column on the right side. Scale bars are only displayed in merged pictures but apply to all pictures of the same row.**

Possible reasons why including native zein UTRs had little to no effect on az19 encapsulation into gamma zein PBs are, for one, that asymmetric mRNA localization has not been demonstrated for az19 in maize, and secondly it is likely that the specific RNA-binding proteins that recognize zip codes of zeins in maize are not present in leafy tissue of *Nicotiana benthamiana*. An interesting question that is outside the scope of this thesis is whether az19 UTRs would be able to change the destination of a soluble protein in maize endosperm cells. This was observed in maize with gz27. In this case, mRNA-targeting was used successfully as a tool to change the default secretory pathway of a recombinant protein. When expression of  $\alpha$ -L-iduronidase in maize endosperm was regulated by the gamma zein-derived promoter, 5'-

UTR, signal peptide and the 3'-UTR terminator, these elements were sufficient to integrate the enzyme into the matrix of the PBs and hence it was retained in the ER (He et al., 2012). This is therefore another tool to yield proteins with oligomannosidic glycosylation which does not require alterations to the amino acid sequence such as the addition of a KDEL-tag.

Coexpression of gz93 and az19, regardless of the presence of UTRs, was able to create PBs with a core-shell structure in *Nicotiana benthamiana*. However, throughout multiple experiments it became apparent that whenever az19 formed inclusions in gz93 PBs, the total amount of az19 within that particular cell was very low. Therefore, it can be speculated that the efficiency of az19 incorporation into gz93 is based on a certain stoichiometric ratio. Since the goal of this study is to generate multicomponent PBs where the protein in the inner core carries an antigen for vaccination, producing less of it would ultimately lead to major drawbacks during manufacturing. Yield is a key parameter in recombinant protein production. Plus, the idea of PBs with more than two layers seemed appealing. Through the inclusion of multiple components, it might be able to control and fine-tune particle characteristics relevant for oral delivery. Therefore, further zeins were evaluated for their behavior in the formation of recombinant PBs.

#### 4.2.3 Other zeins form protein bodies as well

Attempted mRNA targeting did not enhance the incorporation rate of alpha into recombinant gamma zein PBs in *Nicotiana benthamiana*. In a heterologous expression setting, however, protein-protein interaction between different classes of zeins might be sufficient to generate layered multicomponent PBs. Selected zeins were therefore evaluated as interaction partners. Besides the zeins gz27, gz93, and az19 that were introduced earlier, 16 kDa gamma zein (gz16), 15 kDa beta zein (bz15), 10 kDa delta zein (dz10), and 22 kDa alpha zein (az22) were used as candidates for these studies. Each zein was fused to a different fluorescent protein but in order to obtain a more versatile toolbox, each zein was combined with at least three fluorescent proteins (Table 2). Each zein was first tested individually for its ability to form PB-like aggregates.

**Table 2: List of fluorescent zein variants**

| <b>Zeins</b>  | <b>Fluorescent protein</b>              |
|---|---|
| GeneBank<br>Accession Number                                    |   |
| <b>gz27</b><br>AF371261   | mTagBFP2<br>EGFP<br>mCherry             |
| <b>gz93</b><br>AF371261   | mTagBFP2<br>EGFP<br>mCherry             |
| <b>az19</b><br>AF371269   | EGFP<br>mKO2<br>mCherry                 |
| <b>gz16</b><br>AF371262   | mTagBFP2<br>EGFP<br>mKO2<br>mCherry     |
| <b>bz15</b><br>AF371264   | mTagBFP2<br>EGFP<br>mCherry             |
| <b>dz10</b><br>AF371266   | EGFP<br>mKO2<br>mCherry                 |
| <b>az22</b><br>AF371274   | mTagBFP2<br>EGFP<br>mCitrine<br>mCherry |
| Amino acid sequences for each part can be found in the appendix |   |

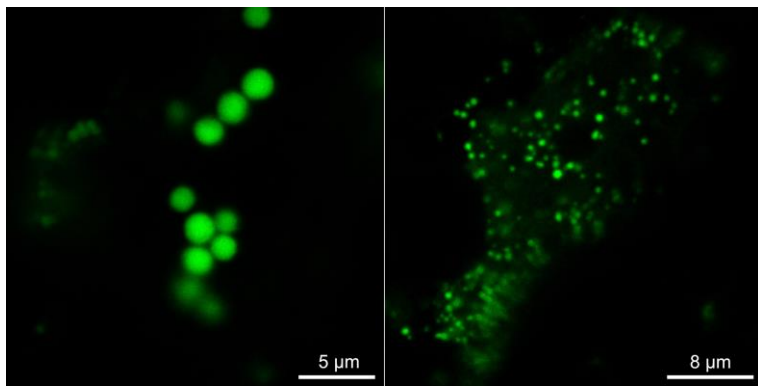


**Figure 16: gz27 PBs have a wider size distribution in *Nicotiana benthamiana* with larger ones being approximately 1-2 µm or smaller ones at 200 nm.**

As has been described earlier (Chapter 4.2.1), gz27 induces the formation of PBs in maize and was also able to do so in *Nicotiana benthamiana* when fused to EGFP. gz27 PBs can be as big as 1-2 µm in diameter but they often stayed relatively small in the 200 nm range (Figure 16). gz93 on the other hand formed large PBs in

the 1-2 µm range much more consistently (Figure 17). Since gz93 comprises the N-terminal 93 amino acids of gz27 and these seem to be more relevant for PB formation than the C-terminal part of gz27 (Llop-Tous et al., 2010), it can be argued that extending the N-terminal 93 amino acids of gamma zein by either EGFP or its native C-terminus still allows large PBs to form, whereas the presence of the full 27 kDa gamma zein plus EGFP is too much. Diametric PB growth might be sterically hindered in this case. Another possibility is that the C-terminus is relevant for the packing of gamma zein and its absence causes gz93 PBs to have a reduced density and therefore they appear larger. Altered PB densities can also affect the ability to interact with other zeins and ultimately determine whether other zeins are able to form inclusions in gamma zein PBs. The specific densities of gz27 and gz93 were not determined in this study. Lastly, different amounts of expressed protein might cause the PB sizes of gz27 and gz93 to deviate. However,

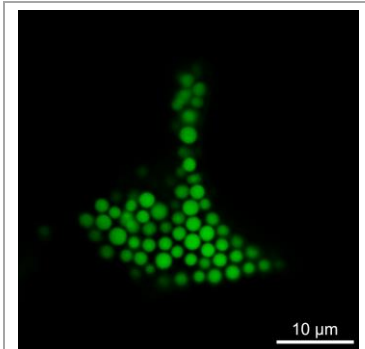


**Figure 17: gz93 formed large PBs > 1 µm much more consistently than gz27.**

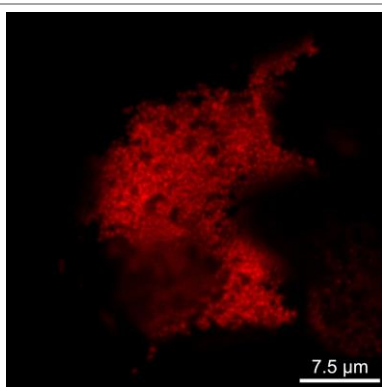


**Figure 18: az19 always appears as clusters of small (~100 nm) PBs.**

determining the expression level of zeins for leaf sections did not seem useful in this case. This is because there seemed to be a relatively high heterogeneity in expression levels between cells of the same leaf section. Since the protein amount of a leaf section is an average between cells, analyzing this average would not help to explain the different appearance of PBs between neighboring cells.

As seen in coexpression experiments with gz27 and gz93, az19 formed very small PBs in the range of 100 nm. They clustered together and appeared as large granular structures (Figure 18). Other zeins such as gz16, bz15,

dz10, and az22 often displayed the same behavior but each of these other zeins also occasionally occurred as larger aggregates above 1  $\mu\text{m}$  in diameter, whereas az19 only formed small PBs below 300 nm. gz16 mostly formed small PBs that closely resembled az19 but within these clusters also larger aggregates developed with a size of approximately 2  $\mu\text{m}$  (Figure 19). Surprisingly, gz16 also localized in what appeared to be the nucleus but it is more likely that these gz16 PBs resided in the nuclear envelope reflecting the connection between the ER and the nuclear envelope. At this site, only larger variants of gz16 PBs were seen. In rare cases, gz16 massively dilated the ER by assembling into loosely packed aggregates of 10  $\mu\text{m}$  diameter on average, similar to those described in transgenic *Arabidopsis thaliana* (Mainieri et al., 2018). The behavior of individually expressed gz16 is particularly interesting because gz16 is a derivative of gz27 where deletion events eliminated the N-terminal Pro-rich repeats and some Cys-residues. Both elements are key factors for the formation of PBs. Therefore, gz16 can be seen as the C-terminal counterpart of gz93, both derived from gz27. It has been speculated that gz16 acts as a bridge that mediates the interaction of gz27, which is located on the outside of PBs, with other zeins located towards the inside of PBs in maize (Mainieri et al., 2018). If so, gz16 should be relevant for the recombinant generation of multicomponent PBs.

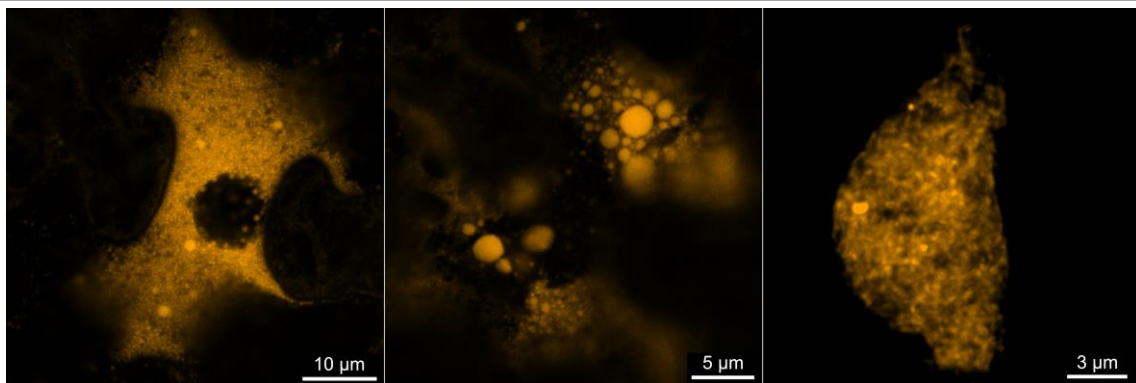


**Figure 19: gz16 either forms small PBs in the 100 nm range or large, loosely packed aggregates that can be around 10  $\mu\text{m}$  in diameter.**

bz15 is another zein that is expected to play a pivotal role in the interaction of various zeins. Early localization studies in maize endosperm showed that bz15 and gz27 are the zeins that are expressed first during the temporal development of PBs. They colocalize early on and comprise the nascent PBs. After alpha zein has entered the PB matrix to fill a large portion of the PB's core, bz15 and gz27 are still colocalized at the periphery of the PBs (Lending and Larkins, 1989). The individual expression of bz15 in *Nicotiana benthamiana* yielded PBs that similar in appearance to az19; large clusters of small PBs in the 100 nm range. However, sometimes larger, irregularly shaped aggregates were intermixed in those clusters (Figure 20). dz10 produced PBs that were either small such as az19 or in the gamma zein range of 1-2  $\mu\text{m}$

(Figure 21). Interestingly, it has been demonstrated that dz10 is able to interact with bz15 (Bagga et al., 1997) even though these two zeins are not localized together in maize PBs. There, dz10 enters the core of PBs while bz15 remains in the periphery (Lending and Larkins, 1989).

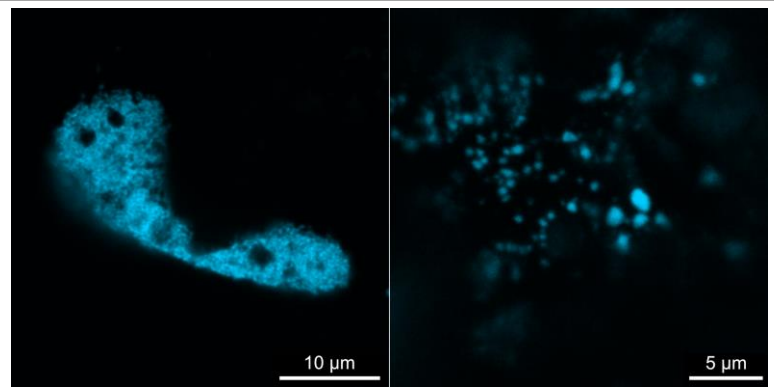


**Figure 20: bz15 sometimes aggregates into larger particles above 1 µm but mostly it behaves like az19.**

dz10 also seems to be relevant for the interactions of zeins with the binding luminal protein BiP (Randall et al., 2005). BiP is a chaperone believed to play a role in the PB assembly in the ER (Vitale and Ceriotti, 2004). dz10 is therefore a promising candidate for the generation of multicomponent PBs as well.

Of all the zeins chosen for this study, az22 displayed the widest variability in terms of PB shape and size besides gz16. In some instances, az22 made small PBs like az19 but more often it created larger structures (Figure 22). In the size range of 2-10 µm they displayed an irregular shape but beyond 10 µm they were smooth and mostly oval. In theory, az22 also seems like a promising candidate for multicomponent PBs because in native zein PBs az22 is found at the interface between the outer gz27/bz15 shell and the core comprised by az19 (Holding et al., 2007).

All zeins selected for this study were successfully expressed and visualized in *Nicotiana benthamiana*. All zeins formed some sort of recombinant PB, particle, aggregate or granular structure. Individual expression of zeins provides an insight into their intrinsic capability to form polymeric structures. This will act as the basis in detecting aberrant behavior during coexpression with other zeins. Additionally, since it has been established that not only gz27-based sequences form PBs, other zeins might be utilized to encapsulate therapeutic proteins as well. Certain zeins might have beneficial characteristics in terms of stability, size, mucoadhesion, or induction of immune response. Determining these characteristics for each zein was beyond the scope of this thesis but might be the focus of future studies.

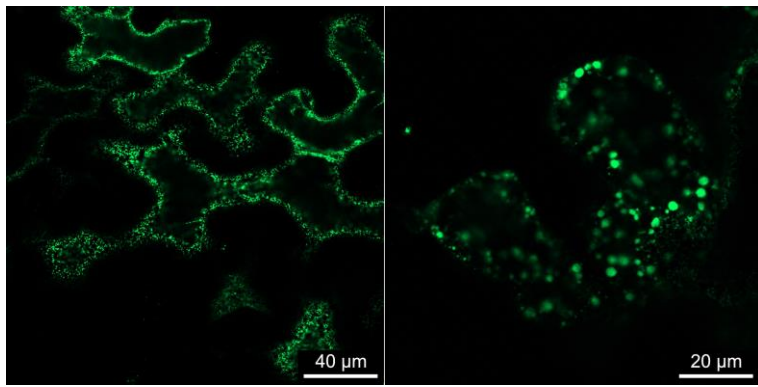


**Figure 21: dz10 PBs tend to be variable in size as well. Frequently, they are below 1 µm but can also be above.**

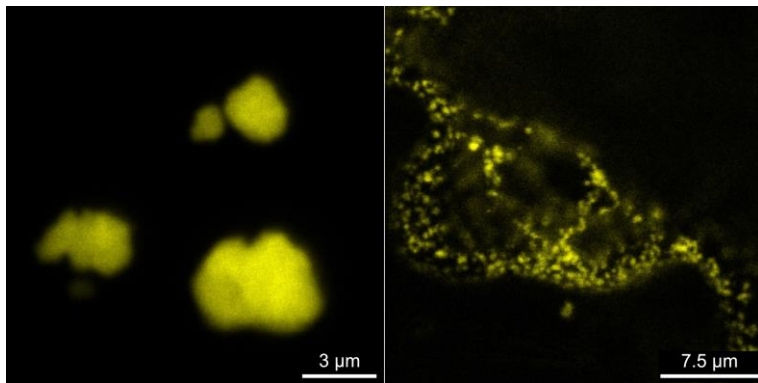


**Figure 22: az22 often crates irregularly shaped aggregates well above 2 µm but it can also appear as small granular structures.**

#### 4.2.4 Multicomponent PBs by coexpression of zeins

Initially, gz27 and az19 were chosen as candidates to test their ability to assemble into particles in a layered fashion. The choice of these zeins was based on the assumption that gz27 is the key player for the induction of PB formation and that az19 constitutes the major part of a PB's core (Lending and Larkins, 1989; Woo et al., 2001). As has been described in an earlier chapter (4.2.1), az19 never incorporated into gz27 PBs under any circumstances. Sequentially infiltrating gamma zein first and alpha zein later or in reverse order did not cause any improvement and neither did the inclusion of native UTRs for potential mRNA-targeting. As a consequence, all zeins selected for this project were expressed on their own and in combinations of two, plus almost all possible combinations of three that involve gz27 or gz93 were carried out as well. An overview of this is given in Table 3 and Table 4.

**Table 3: List of combinations of two zeins coexpressed**

|      | az19        | az22            | dz10            | bz15        | gz16            |
|------|-------------|-----------------|-----------------|-------------|-----------------|
| gz27 | Figure 12 A | Figure 23 A + B | Figure 32 A     | Figure 25 A | Figure 26 A + B |
| gz93 | Figure 12 B | Figure 23 C + D | Figure 32 B     | Figure 25 B | Figure 26 C + D |
| gz16 | Figure 28 C | Figure 28 A + B | Figure 29 A + B | Figure 28 D |                 |
| bz15 | Figure 25 C | x               | x               |             |                 |
| dz10 | Figure 29 C | Figure 29 D     |                 |             |                 |
| az22 | Figure 34 B |                 |                 |             |                 |

az22 for example was described to be sequestered by gz27 when coexpressed in *Nicotiana tabacum* seeds (Coleman et al., 1996). The authors of this study found az22 inside of gz27 PBs as less-electron-dense locules. Since they could not detect az22 in the absence of gz27, they speculated that gz27 protects az22 from proteolytic degradation. In this thesis however, az22 was detectable when expressed on its own in leaves of *Nicotiana benthamiana*. When az22 was coexpressed with gz27, small aggregates of az22 seemed intermixed into or onto gz27 PBs on some occasions (Figure 23 A). These confocal images might reflect what Coleman et al. (1996) observed with transmission electron microscopy but this type of incorporation is far from the distinct core-shell structure that zein PBs exhibit natively in maize or what can be achieved by coexpressing other zeins (see below). In most cases, gz27 and az22 were located separately and displayed a similar behavior as with individual expression. gz27 formed perfectly round PBs with a smooth internal matrix whereas az22 aggregated irregularly and appeared granular. These az22 aggregates sometimes surrounded gz27 PBs and seemed closely attached but did not penetrate the matrix of gz27 (Figure 23 B). Interestingly, the coexpression of az22 with gz93 however did yield big inclusions of az22 in gz93 PBs in some cases (Figure 23 C+D). The same discrepancy between gz27 and gz93 was observed when they were expressed alongside az19. az19 also only formed inclusions in

**Table 4: List of combinations of three zeins coexpressed**

|             | az19        | az22        | dz10        | bz15        |
|-------------|-------------|-------------|-------------|-------------|
| gz27 + gz16 | Figure 27 C | Figure 27 B | Figure 32 C | Figure 31 C |
| gz27 + bz15 | Figure 24 C | x           | Figure 31 A |             |
| gz27 + dz10 | Figure 30 A | Figure 30 B |             |             |
| gz27 + az22 | x           |             |             |             |
|             | az19        | az22        | dz10        | bz15        |
| gz93 + gz16 | Figure 27 D | Figure 27 A | Figure 32 D | Figure 31 D |
| gz93 + bz15 | Figure 24 B | Figure 24 A | Figure 31 B |             |
| gz93 + dz10 | Figure 30 D | Figure 30 C |             |             |
| gz93 + az22 | Figure 34 A |             |             |             |

gz93 but not in gz27. As has been discussed in the case of az19, gz93 and gz27 might have different densities that allow or restrict interactions with other zeins. Extending the complete sequence of gz27 with EGFP might cause steric hindrance and therefore block off elements that are important in the interaction with az22.

Coleman et al. (1996) argued that bz15 might be a necessary partner in the interaction of gz27 with az22. In the developing endosperm of maize, gz27 and bz15 are the first zeins to be expressed. bz15 gets linked to gz27 by disulfide bridges during these early stages of PB formation and the two make up the PB shell later when alpha and delta zeins have entered the PB's core. The authors therefore state that the hydrophobic characteristics of bz15 may be a bridging element between gamma and alpha zein and that az22 assembly occurs on the surface of the gz27/bz15 complex. Coexpression experiments of gz93, bz15, and az22 indeed revealed that in this combination many PBs displayed a distinct core-shell structure (Figure 24 A). Although gz93 made up the outer shell and az22 the inner core of the PBs as expected, bz15 surprisingly colocalized with az22 on the inside. Based on the knowledge about the structure of PBs in maize, bz15 was expected to localize with gz93 in the outer shell (Lending and Larkins, 1989). At this point, the only apparent explanation for this differential localization of bz15 is time-coordinated expression. If bz15 really is a bridging element between gamma and alpha zein that is able to interact with both, the fact that in maize gz27 and bz15 are expressed before az22 is likely to place them together whereas the interaction of az22 with bz15 at later time points may allow az22 to enter the PB's matrix. During transient expression in *Nicotiana benthamiana*, however, the expression of all three zeins is initiated at the same time. This seems to enable different localization patterns because the time factor is eliminated and effects are mostly based on variations in interaction strength. However, bz15 also did not colocalize with gamma zein when expressed in dual combinations with either gz27 or gz93 (Figure 25 A+B). Regardless of the exact mechanism, the simultaneous expression of gz93, bz15, and az22 allows the generation of PBs with a distinct core-shell structure in the leafy tissue of a plant that is very well adopted by the biotech industry. This combination of zeins a promising candidate for the oral codelivery of multiple active compounds. Whether the individual zeins have effects on particle attributes such as stability, mucoadhesion, or release, will be determined in a later project.

The quest for further core-shell-inducing combinations was continued because various zeins might provide different effects to the final multicomponent PB. Next, it was also tested whether bz15 can facilitate the incorporation of az19 into gamma zein PBs. In gz93 PBs, bz15 and az19 did colocalize in the core of gz93 but these inclusions were much smaller than bz15 plus az22 and the main portion of the two proteins was located outside of the gz93 PBs (Figure 24 B). The localization pattern was somewhat surprising when gz27 was used instead of gz93. bz15 remained outside, but closely attached to the gz27 PB and the az19 signal homogenously

coincided with bz15 and all of the gz27 matrix (Figure 24 C). In no other combination of zeins was az19 homogenously mixed into the matrix of gamma zein PBs. The interaction of az19 with bz15, however, was also detected when the two were coexpressed in the absence of a third zein (Figure 25 C).

Delta zeins are interesting candidates for the generation of layered PBs as well because they colocalize in the core of maize PBs alongside alpha zeins (Esen and Stetler, 1992). Delta zeins are methionine-rich proteins that received some attention for improving the sulfur amino acid content of transgenic animal feed (Bagga et al., 1997; Kim and Krishnan, 2019). Coexpression of dz10 together with gz27 yielded PBs that had the shape and size of gz27 but were homogenously emitting signal from both gz27 and dz10 (Figure 32 A). The two proteins were therefore evenly intermixed and did not display any form of layering. Nevertheless, this form of multicomponent PB can be just as useful as layered core-shell PBs, depending on the features provided by dz10. The coexpression of dz10 with gz93, however, did cause dz10 to localize on the inside of gz93 PBs as a distinct core (Figure 32 B). The absence of gz27's C-terminal part on gz93 therefore seems to influence the internal organization of zein PBs. Whether homogenously mixed or core-shell zein PBs are more useful for drug delivery purposes is a question that needs to be answered in the future.

In native zein PBs from maize, gz16 is located at the interface between the outer gamma/beta-shell and the inner alpha/delta-core (Yao et al., 2016). It is hypothesized that gz16 has some involvement in the expansion of PBs during their development when the core is filled with alpha zeins (Guo et al., 2013). Data from yeast two-hybrid experiments suggest that gz16 interacts with all other members of the zein family (Kim et al., 2002, 2006). This makes gz16 a promising candidate for the recombinant production of layered PBs. Similar to dz10, the coexpression of gz16 with gz27 generated PBs in which both zeins homogenously mixed. The fluorescent signal emitted from these PBs originated from gz27 and gz16 with no detectable structural features. When gz16 was expressed on its own, the resulting PBs were often smaller than the typical gz27 size of 1  $\mu\text{m}$ . The amount of gz16 seemed to affect the size of PBs when it colocalized with gz27. When neighboring cells expressed different ratios of gz27 to gz16 – as apparent by differential fluorescent intensity – the PBs that had a higher content of gz16 appeared smaller, whereas lower amounts of gz16 generated PBs that were more similar in size to gz27 (Figure 26 A). Occasionally, gz16 also assembled into very large aggregates (above 10  $\mu\text{m}$ ) that are loosely packed as was seen with single expression of gz16 but in the case of coexpression these large aggregates emitted signal for both gz16 and gz27 (Figure 26 B). As with other coexpression partners, gz93 again yielded a very different picture than gz27. gz16 was able to create cavities in gz93 PBs and the nature of these cavities varied. In some instances, it was only one center cavity that resembled a core-shell structure (Figure 26 C) whereas in other cases gz93 PBs had many holes of various sizes throughout the entire

PB (Figure 26 D). The distribution of gz16 within these PBs also varied to a certain extent. Some gz16 always colocalized with gz93, but the core would only be filled by gz16 if no other zein was present. When gz93 and gz16 were the only interactions partners, the fluorescent signal from gz16 was stronger in the core and weaker in the gz93 shell. However, when a third zein integrated into the PB, gz16 was only detectable in the shell alongside gz93 while leaving the core to be filled by the third zein.

When az22 was coexpressed with gz93 and gz16, the cavity created by gz16 were filled with az22 (Figure 27 A). In those instances, some gz16 signal came from the outer gz93 layer whereas it seemed that most of it located at the interface between gz93 and az22. This is in accordance with observations from wild-type PBs in maize (Guo et al., 2013; Yao et al., 2016). Not only does this corroborate the crucial role of gz16 in the structural assembly of zein PBs, but it also enables the generation of ectopically engineered PBs with distinct layering. The combination of gz16 and az22 with full size gz27 was also able to produce PBs with cavities filled by az22, although this was a rare event (Figure 27 B). Here, gz16 did not accumulate at the interface but colocalized in a more homogenous manner with gz27. When az22 was substituted by az19, gz16 could not facilitate the incorporation of az19 neither when combined with gz27 nor with gz93 (Figure 27 C+D). It can thus be hypothesized that az19 is lacking certain features that allow reliable protein interactions with gamma zeins. It will be evaluated later in this thesis whether az22 is able to mediate between gamma zeins and az19. Experiments with az19 again confirmed that gz16 causes cavities exclusively in gz93 but not in gz27. If gz27 and gz93 were left aside and only gz16 was expressed with alpha zeins, the preference for interaction was not that clear. gz16 and az22 formed individual PBs that were relatively small (below 0.5  $\mu\text{m}$ ) and these intermixed but did not localize in the same PBs (Figure 28 A). gz16 and az22 solely appeared together when they formed large (above 3  $\mu\text{m}$ ) aggregates (Figure 28 B). In the case of az19 however, it was very difficult to distinguish whether its signal originates from PBs that harbor both az19 and gz16, or if PBs containing only one of the components each were mixed and in close proximity (Figure 28 C). The situation was much clearer when bz15 was expressed alongside gz16. Even though the PBs had a submicron size, it was evident that the PBs emitted signal for both zeins (Figure 28 D). Colocalization of dz10 and gz16 had an interesting effect. Individually, they formed rather small PBs, but when colocalized, the resulting PBs had a larger diameter than their individual components (Figure 29 A). This might indicate an involvement of dz10 in the gz16-driven expansion of zein PBs. In some cases, dz10 and gz16 formed very large (above 10  $\mu\text{m}$ ) aggregates of irregular and somewhat loose structure (Figure 29 B). The capability of dz10 to interact with alpha zein might be relevant for such a role. When dz10 was coexpressed with either az19 or az22, the resulting PBs remained small and seemed to contain both zeins, respectively (Figure 29 C+D). When dz10 was combined with these alpha zeins in the

presence of gamma zein, neither az19 nor az22 integrated into gz27 PBs (Figure 30 A+B) although they did so when coexpressed with gz93 (Figure 30 C+D). In all these incorporation events dz10, colocalized with the alpha zeins in the core of the PBs. This is in accordance with maize-derived PBs where dz10 is found in the core along with alpha zeins and it again supports the idea that dz10 plays a role in the structuring of zein PBs besides gz16. Consequently, it was tested how gamma zein PBs would behave in the presence of both dz10 and gz16. In the case of gz27, all three zeins again homogeneously colocalized in PBs without any detectable layered structure (Figure 32 C). This was not the case when gz93 was used instead of gz27. The gz93 PBs were generally larger and gz16 colocalized with gz93 which created many small holes that were filled with dz10 (Figure 32 D). Again, the generation of structured PBs was more successful with gz93 than with gz27. The distinct localization of each zein also resembled the situation in native maize PBs where gz16 is more closely associated with gz27, whereas dz10 can be found in the core.

It was demonstrated earlier that bz15 had a substantial impact on the integration of alpha zeins into gz93 PBs (Figure 24 A+B). Therefore, its effect on gamma zein PBs in the presence of dz10 or gz16 was evaluated as well. Combining gz27, bz15, and dz10 led to the formation of PBs with a core-shell structure in which the bz15 signal was stronger in the gz27 shell whereas the dz10 signal was stronger inside the core (Figure 31 A). This pattern again coincides with what would be expected from maize PBs. The situation was opposite when gz93 was substituted for gz27. In this case, bz15 did not colocalize with gz93 in the shell of the PB but it was found in the core together with dz10 (Figure 31 B). This seemed to influence the size of the inclusion since it was bigger than in gz27. Combining bz15 with gz16 and gz27 gave rise to small PBs that emitted signal for all three zeins with no evident internal structure (Figure 31 C). bz15, gz16, and gz93 however, produced large PBs with large and small inclusions (Figure 31 D). These zeins organized into structured PBs most consistently among all combinations. gz93 provided the outer framework whereas the signal from gz16 came from this outer layer as well as from the core (with the signal from the core being slightly stronger). bz15 however, exclusively resided in the internal part of the PB. In native maize PBs, bz15 localizes with gz27 in the shell and gz16 is found at the interface towards the core. Due to the lack of temporally coordinated expression in this recombinant setup, bz15 and gz16 might be competing for the interaction with gamma zein solely based on their affinity towards it.

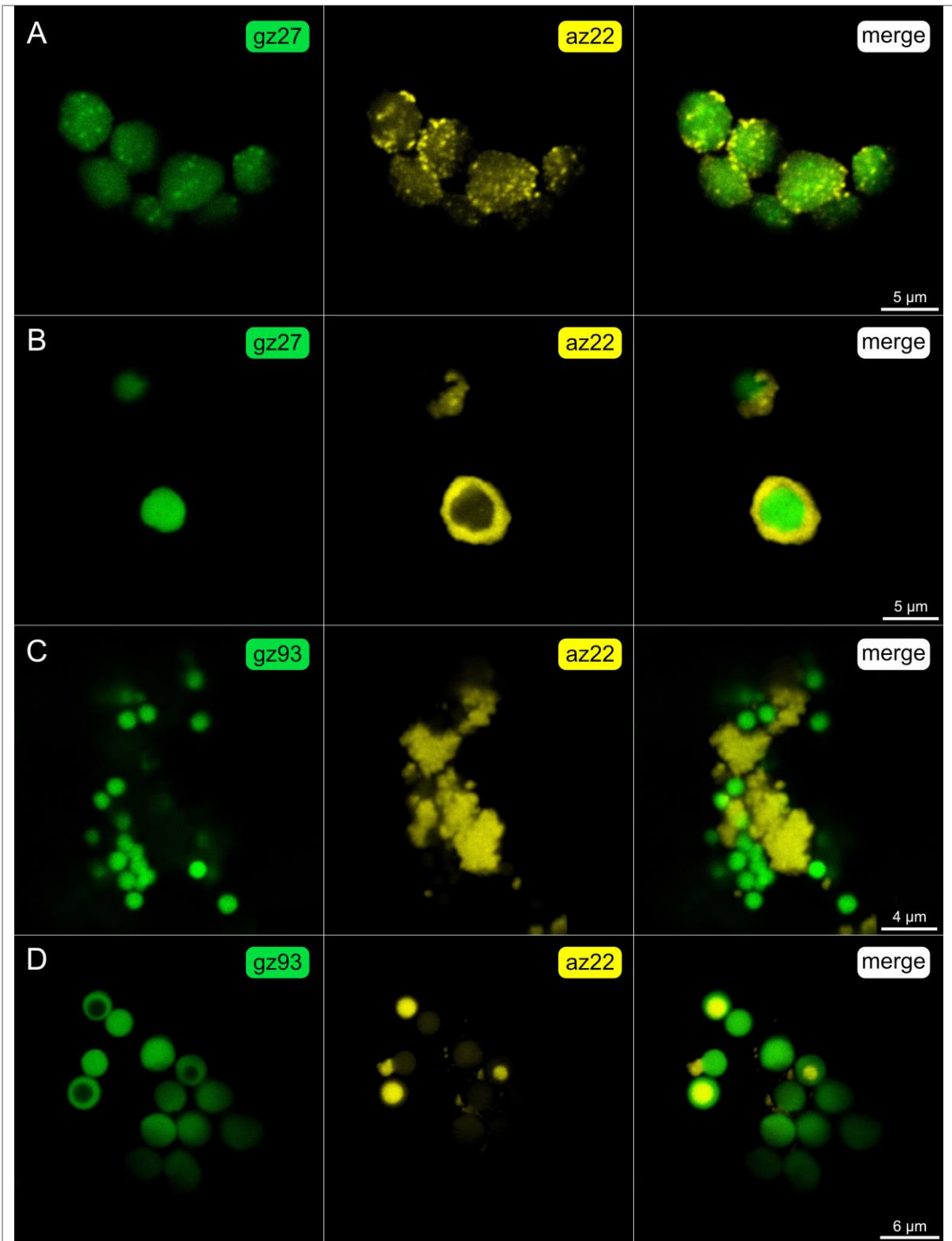


**Figure 23: Coexpression of az22 with either gz27 or gz93. The coexpression of gz27 and az22 caused small granules of az22 to intermix into or onto gz27 PBs (A). In other instances, az22 organized into larger structures that were able to surround gz27 PBs (B). In combination with gz93, az22 also sometimes appeared as large granular structures outside of gz93 (C), but in other cases az22 was found inside of gz93 PBs as large cores (D).**

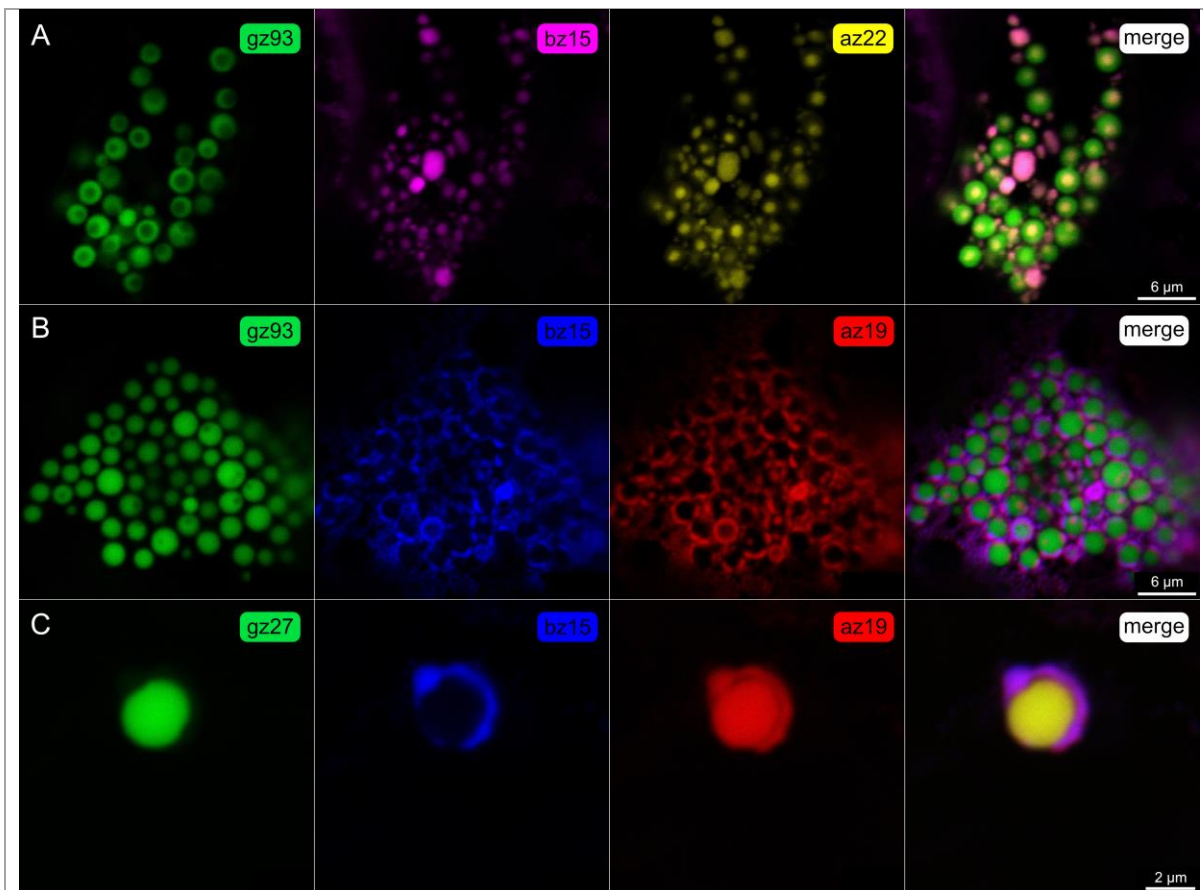


**Figure 24: Coexpression of gamma zeins along bz15 and alpha zeins. bz15 reliably colocalized with az22 in gz93 PBs and the incorporations were relatively big (A). When az22 was substituted by az19, fewer and smaller incorporations occurred (B). bz15 also remained on the outside when express along with gz27. az19 was also found together with bz15 on the outside but surprisingly, az19 was also found homogenously mixed with gz27 (C). Something that has not been seen in other coexpression experiments so far. Overall, this set of experiments showed that bz15 prefers to colocalize with alpha zein over gamma zeins. This is in contrast to what would be expected from what is observed in maize.**

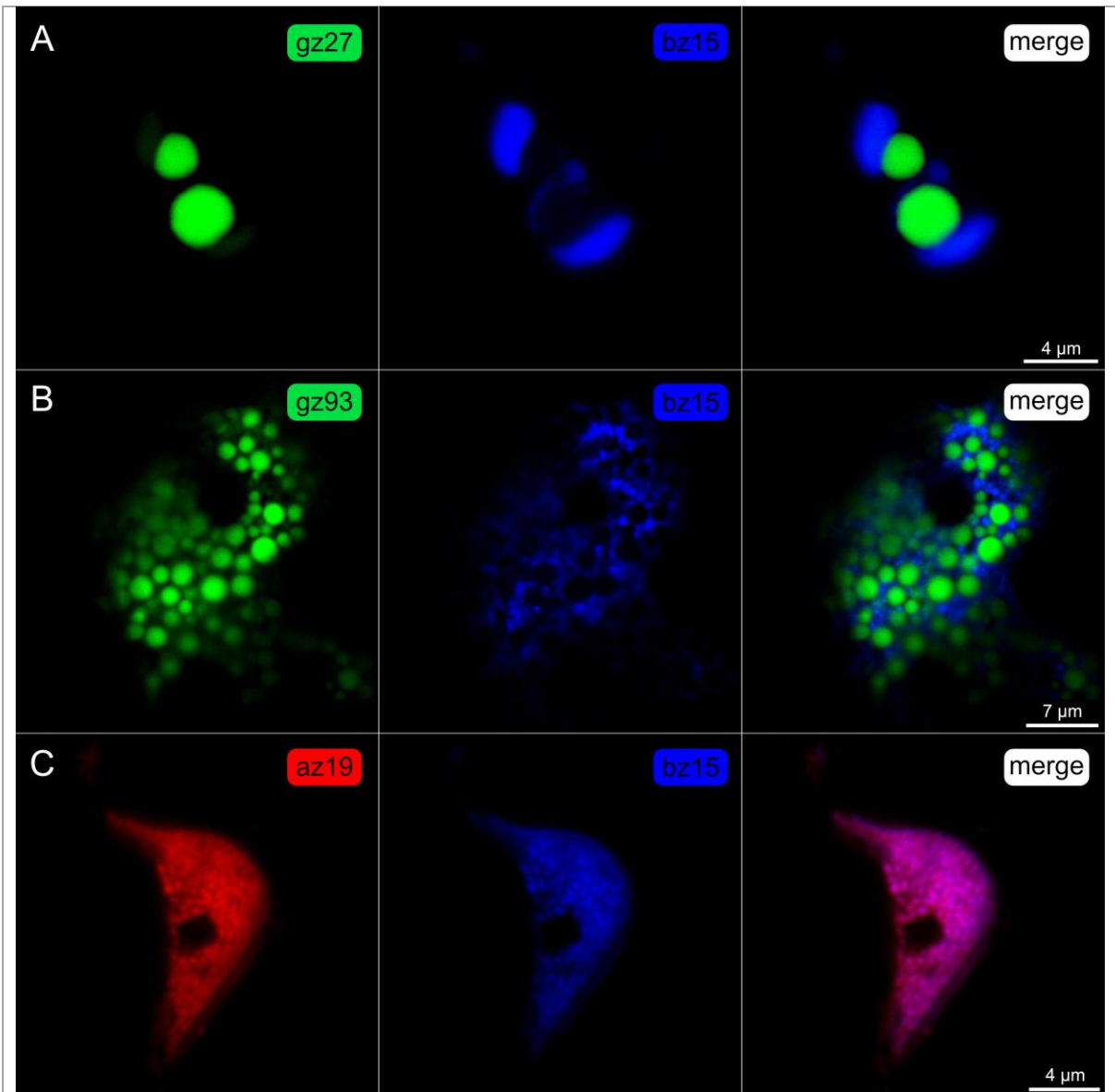


**Figure 25: Coexpression of gamma zeins with bz15 and az19 with bz15. Unexpectedly, neither gz27 (A) nor gz93 (B) colocalized with bz15 even though gz27 and bz15 together form the shell in maize PBs. az19 and bz15 however, colocalized (C) as they did when expressed in combinations of three with either gz27 or gz93 (Figure 24 B+C).**

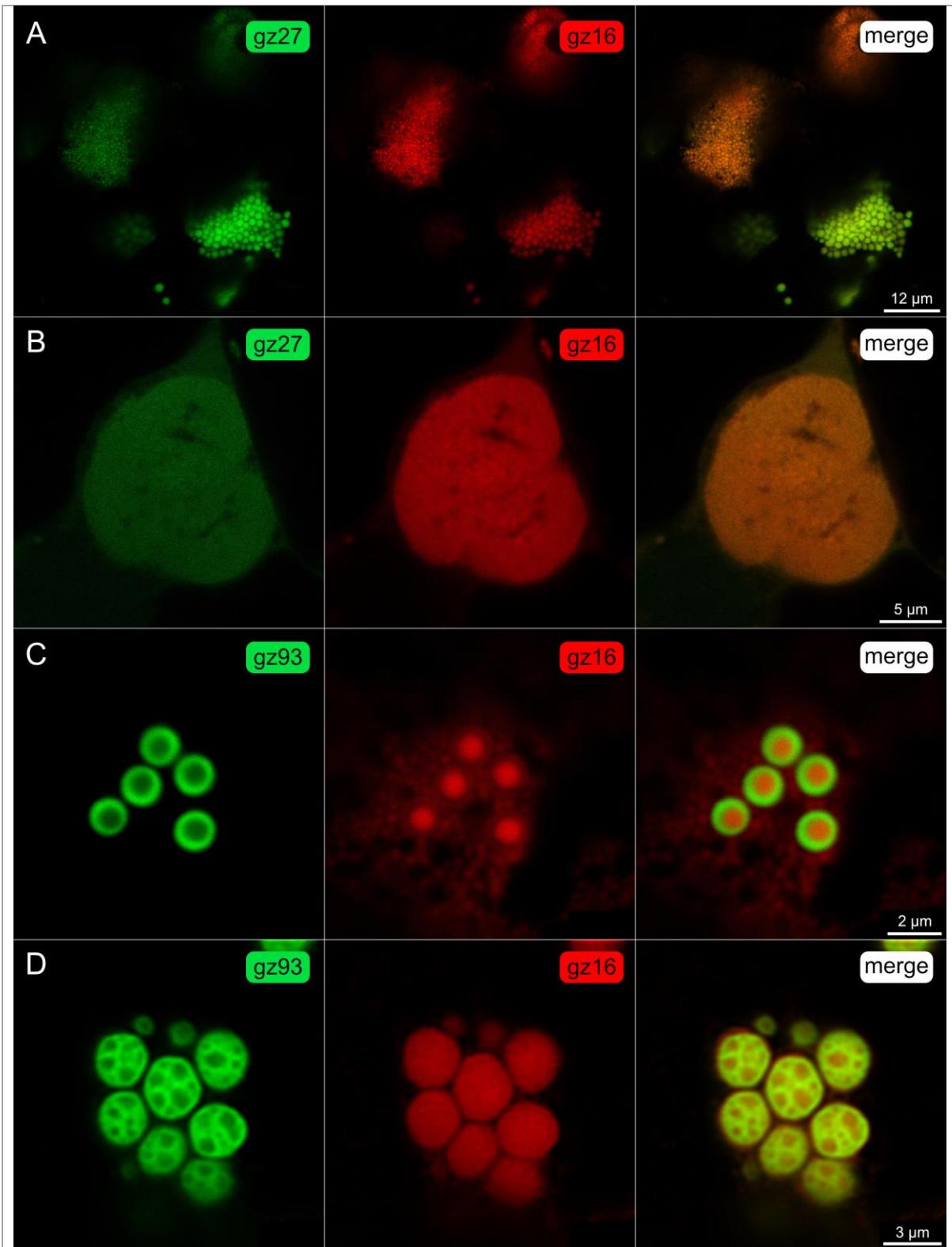


**Figure 26: Coexpression of gz27 or gz93 together with gz16. gz16 homogenously colocalized into PBs of varying size (A). When neighboring cells expressed different ratios of gz27 and gz16, the diameter was affected. More gz16 meant smaller PBs and less led them to be bigger. Sometimes these two zeins would generate very large aggregates which resembled the ones seen with individual expression of gz16 (B). gz16 also interacted with gz93 where it was able to create various kinds of holes. In some cases, there would be only one center core made up by gz16 (C) but in other instances multiple holes occurred in the same PB (D).**

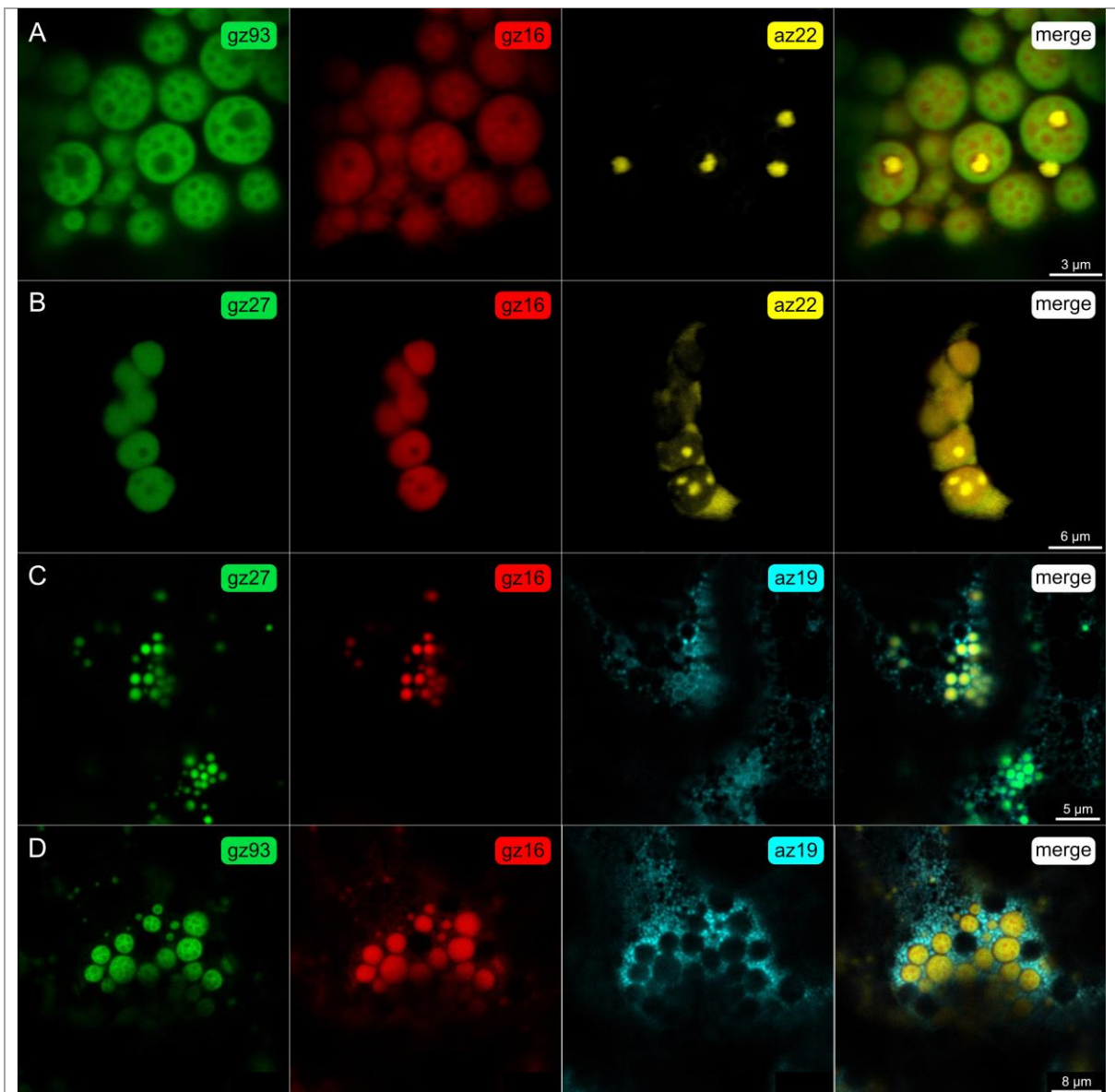


**Figure 27: Coexpression of gamma and alpha zeins. As previously seen, gz16 created holes in gz93 PBs. In the presence of az22, these holes were filled by az22 whereas the concentrations of gz16 seemed to be higher in the interface between gz93 and az22 (A). In very rare cases, these gz16-induced holes also occurred in gz27 PBs where they were filled by az22 as well (B). When az19 was substituted for az22, az19 always remained outside of the PBs (C + D). These two combinations again confirmed that the hole-generating effect of gz16 works mainly on gz93 (D) but not gz27 (C).**

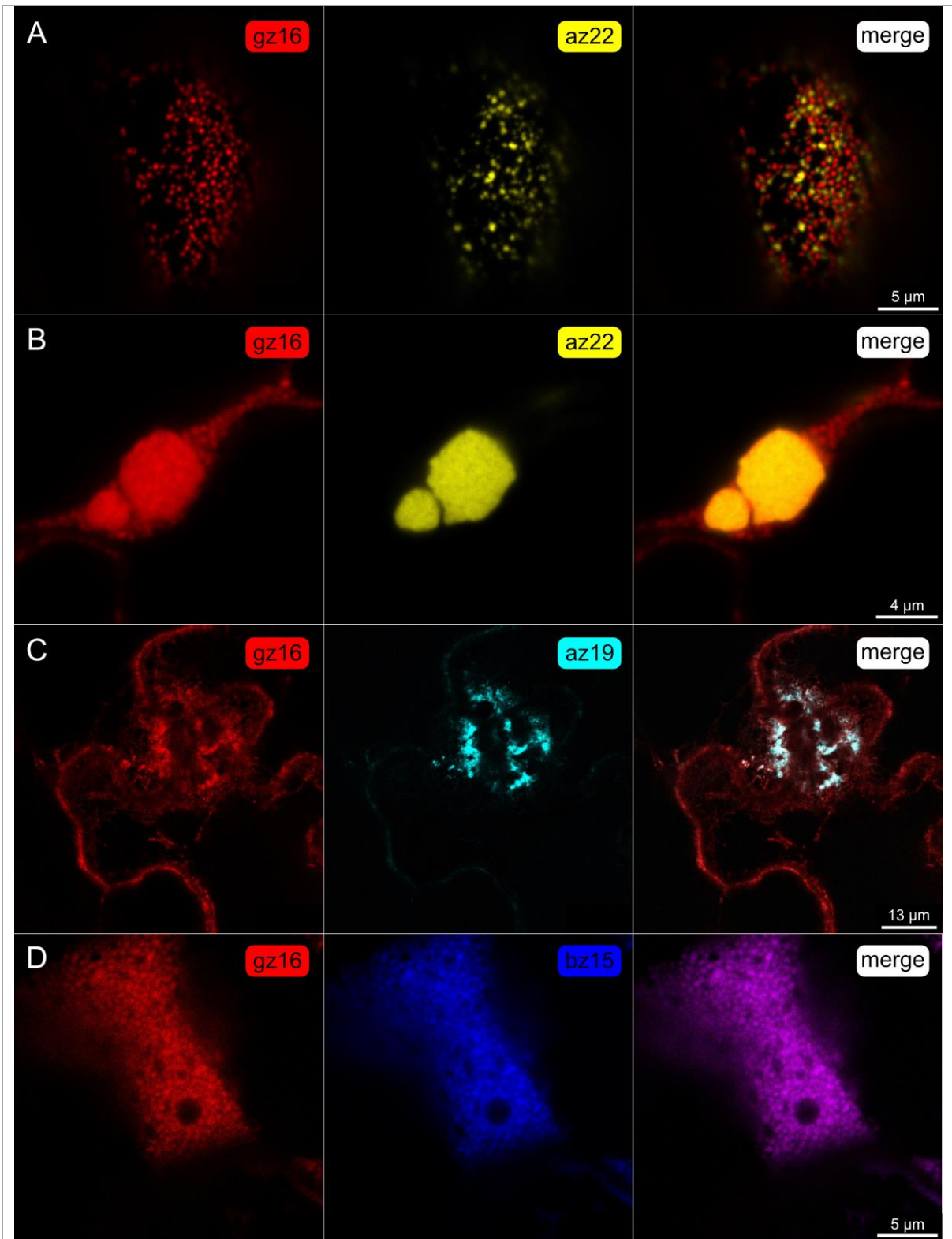


**Figure 28: Coexpression of gz16 with other zeins. When gz16 and az22 formed small PBs (< 0.5  $\mu\text{m}$ ), the PBs intermixed but the two zeins did not localize in the same PBs (A). Colocalization of gz16 and az22 only occurred when they created large (> 1  $\mu\text{m}$ ) aggregates (B). In the case of az19, both zeins remained small and it is therefore difficult to assess whether individual PBs intermixed or if they colocalized (C). For the combination of bz15 with gz16 however, it was clear that these small PBs contained both zeins (D).**

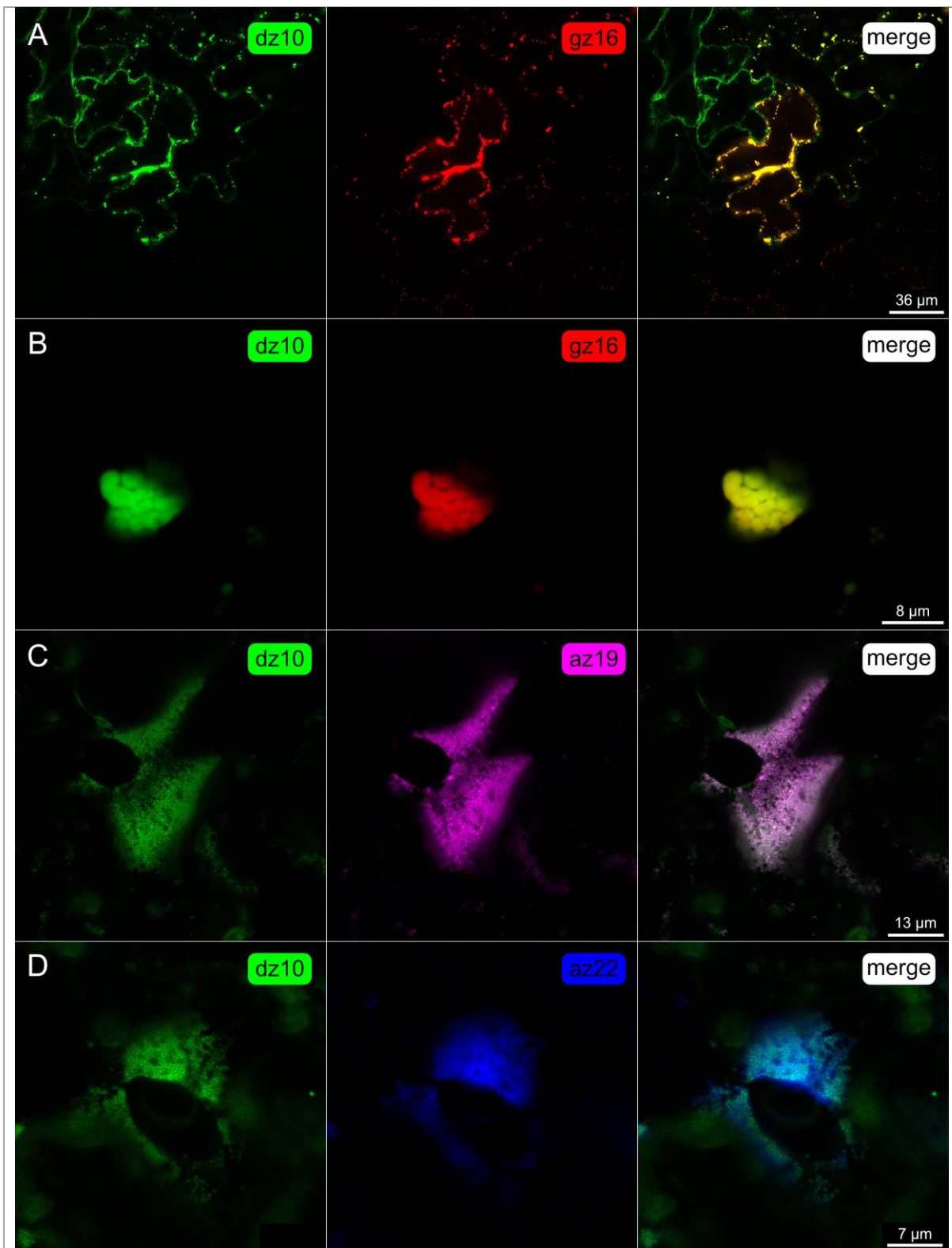


**Figure 29: Coexpression of dz10 together with other zeins. In panel (A) it can be seen that the cell in the top left corner only expressed dz10 whereas the cell at the bottom only expressed gz16. In both cases the PBs were rather small. However, in the cell that expressed both zeins, the PBs are larger than when they are individually expressed. In some cases, the generated larger aggregates that emitted signal for both zeins (B). When dz10 was coexpressed with az22 (C) or az19 (D), the PBs remained small but seemed to localize together (technical imperfection due to moving sample in row D).**

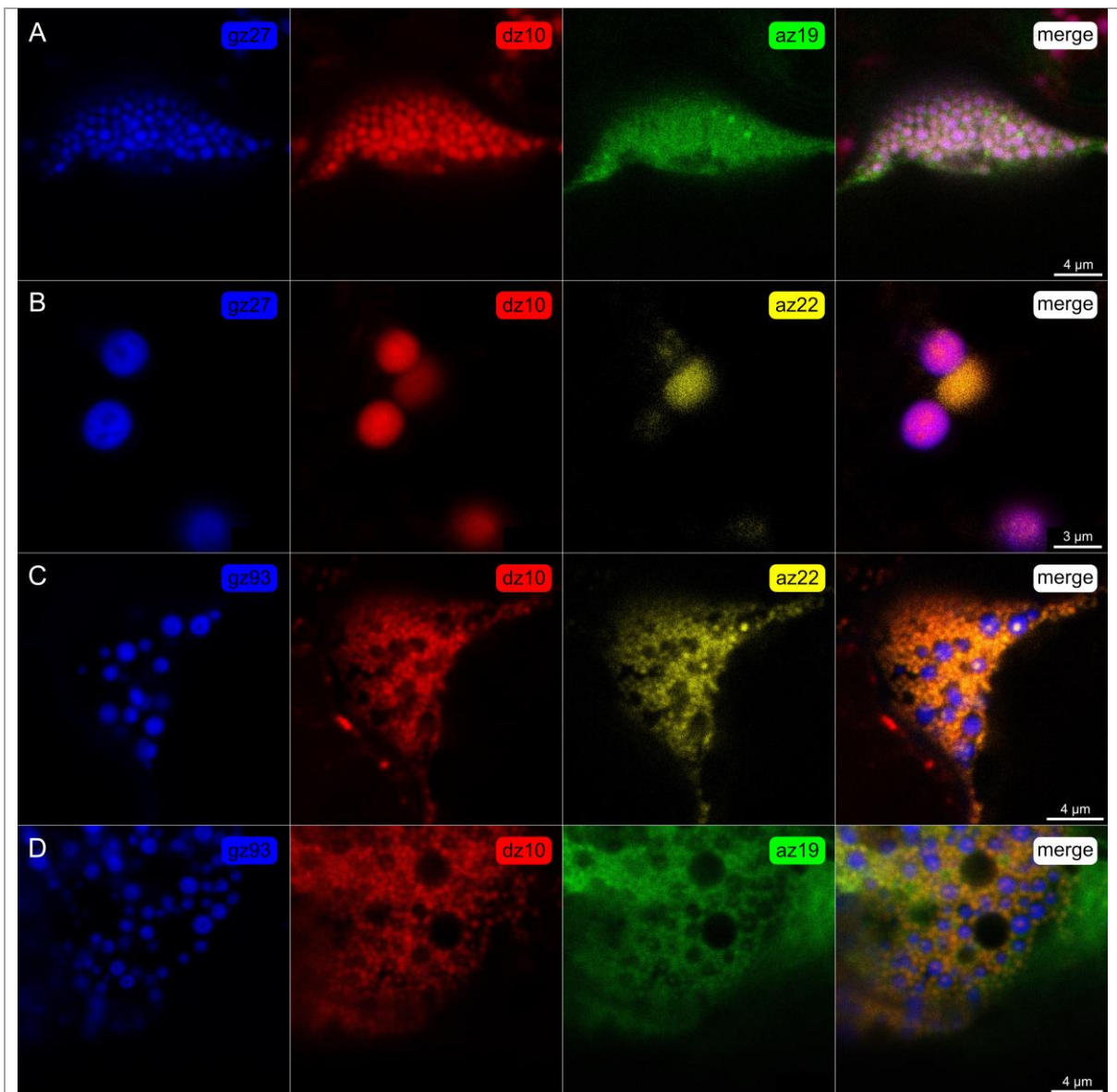


**Figure 30: The effect of dz10 on the incorporation of alpha zeins into gamma zeins. dz10 was not able to facilitate the incorporation of az19 (A) or az22 (B) into PBs of gz27. However, both az22 (C) and az19 (D) integrated into PBs of gz93. These inclusions contained dz10 alongside the respective alpha zein. Unfortunately, large proportions of alpha zein remained on the outside surrounding the gz93 PBs.**

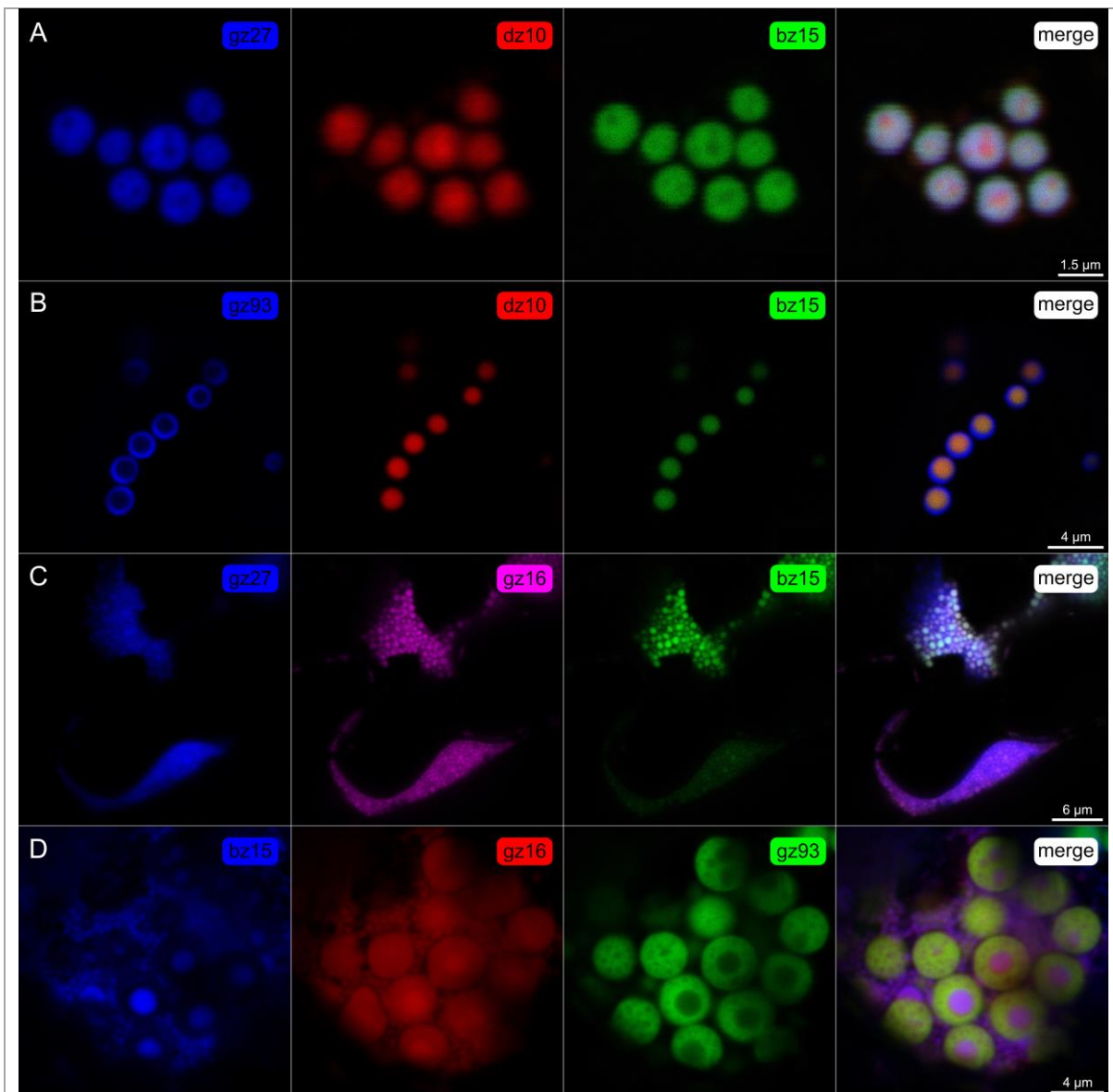


**Figure 31: Coexpressions investigating the effects of bz15 and on gamma zein PBs in the presence of a third zein. Combining gz27 with bz15 and dz10 yields structured PBs with an organization similar to native PBs. gz27 and bz15 colocalized in the shell whereas dz10 mostly resided in the core (A). This organization was turned around in the case of gz93. bz15 was found in the core along with dz10 and only gz93 comprised the shell (B). bz15 and gz16 together with gz27 created PBs that homogeneously emitted signal for all three zeins (C). Coexpression of bz16 and gz16 with gz93, however, produced layered PBs very reliably (D). A similar effect of gz16 was seen in other combinations as well. In this case, gz16 again caused small and big holes in gz93 PBs that were filled by both gz16 and bz15. Some of the gz16 signal, however, also came from the gz93 shell.**

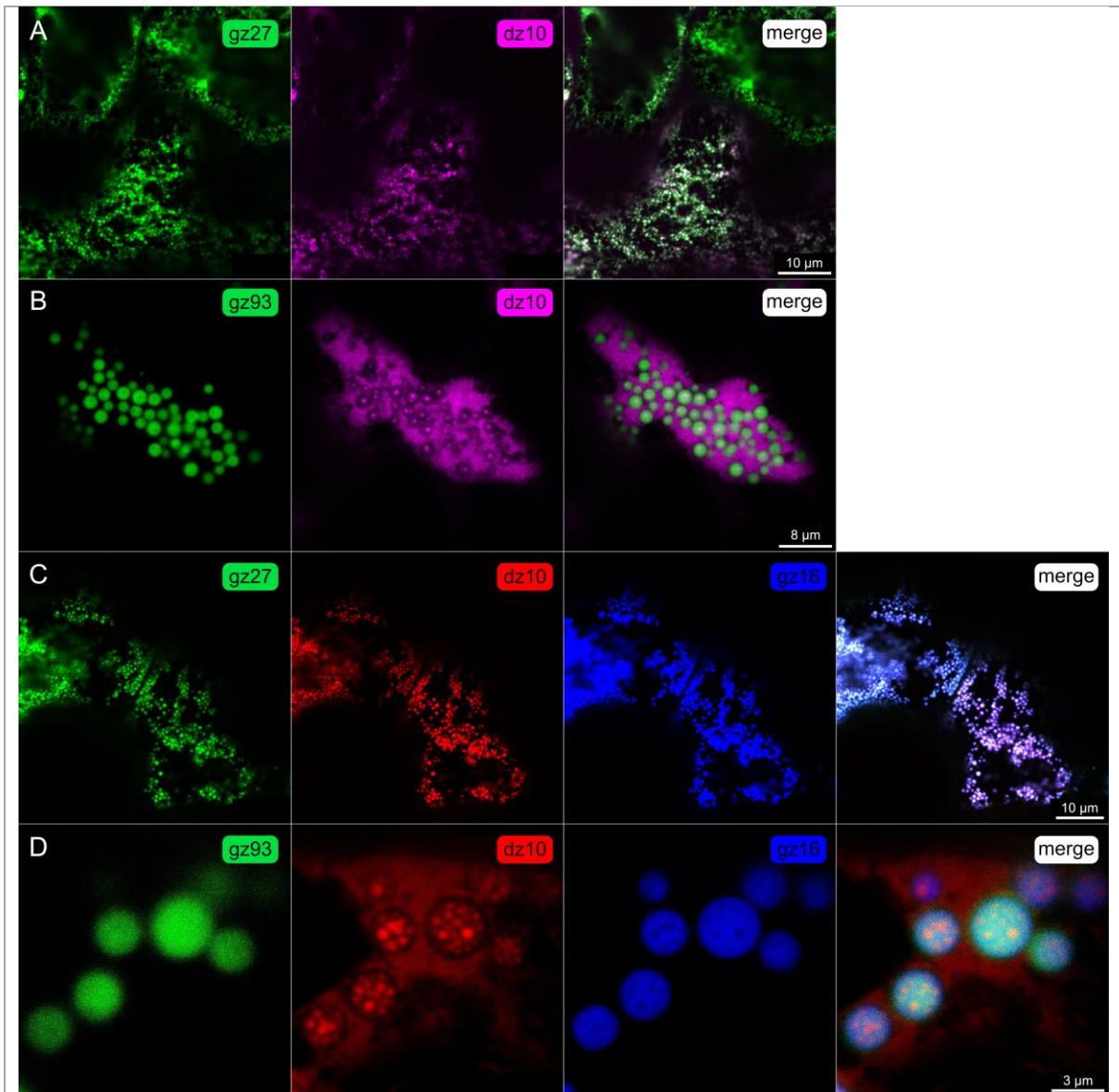


**Figure 32: Coexpression of gamma zeins and dz10. gz27 and dz10 homogeneously colocalized in PBs without visible structuring (A). Together with gz93, however, dz10 entered the PBs and was found as small cores inside of gz93 (B). The addition of gz16 to those combinations painted as very similar picture. gz27 + dz10 + gz16 formed PBs with all components homogeneously mixed (C) whereas dz10 appeared as core-structures in a matrix provided by colocalized gz93 and gz16 (D).**

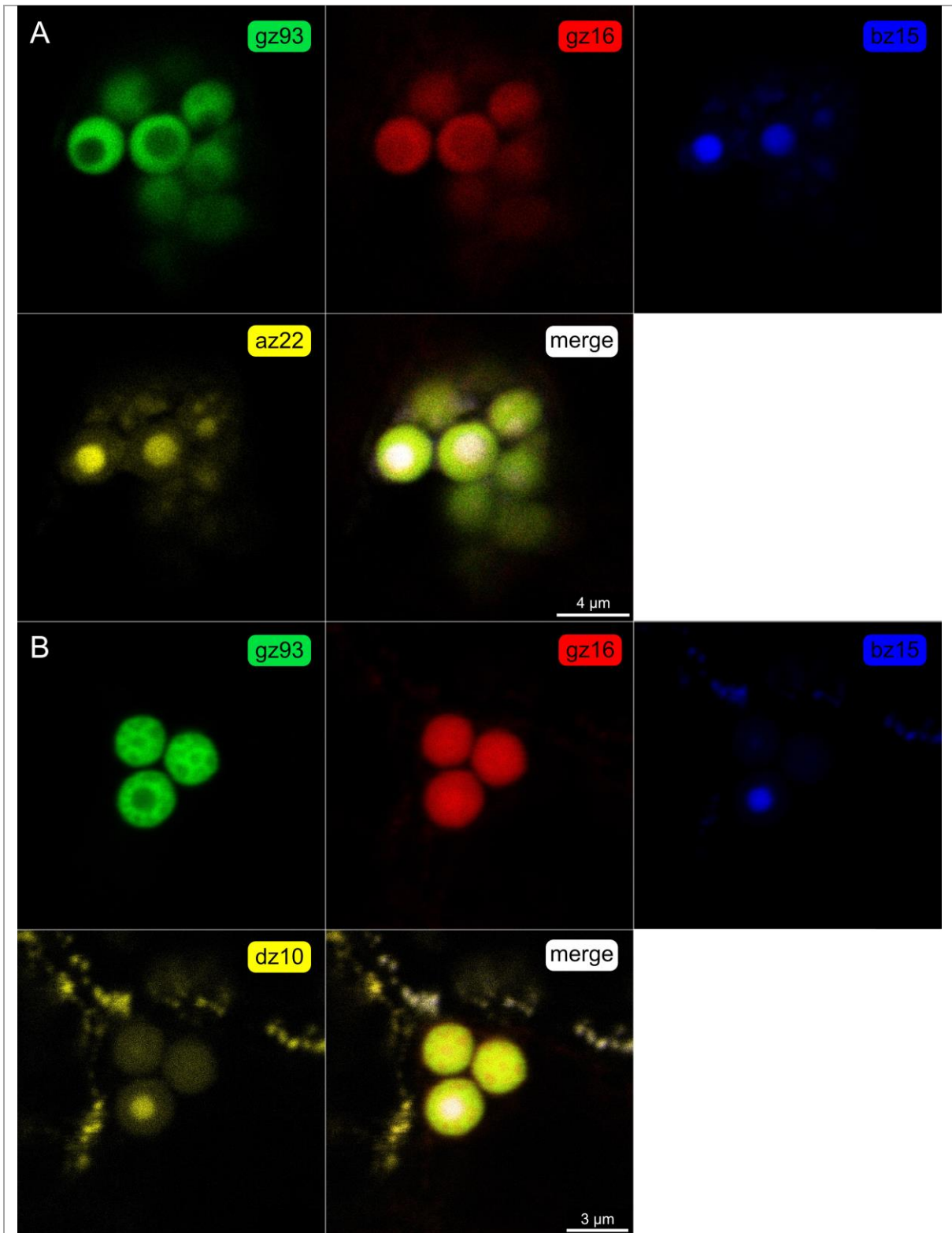


**Figure 33: Coexpression of four zeins. When gz93 and gz16 are expressed alongside bz15 and az22, gz93 provides the shell of the PBs, gz16 is mostly found in the shell as well although some gz16 signal is also emitted from the core, but bz15 and az22 are the main constituents of the core in this combination (A). The PBs had a similar appearance when dz10 was used instead of az22. Again, gz93 provided the shell, the signal from gz16 was a bit more diffuse in this case, but bz15 and dz10 were mainly found in the core of the PBs (B).**

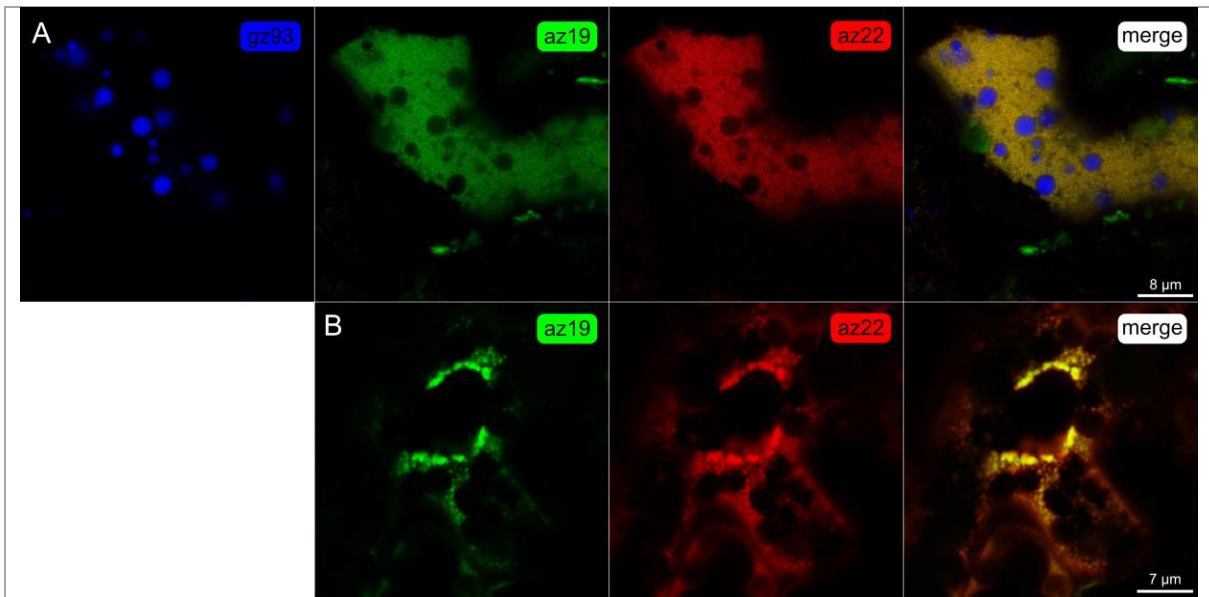
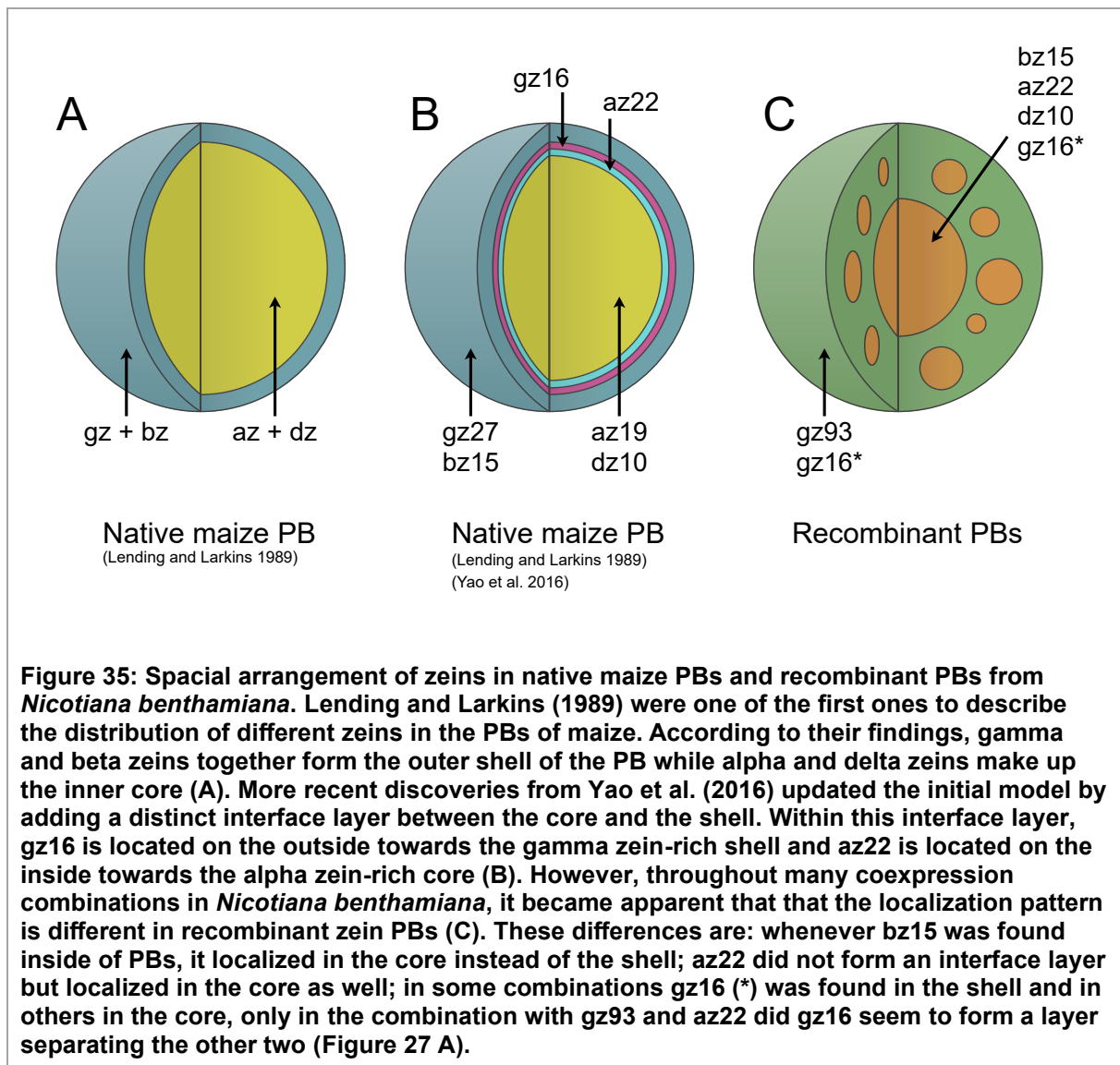


**Figure 34: Coexpression of az19 and az22. Both alpha zeins colocalized into small PBs but failed to integrate into gz93 PBs (A). This colocalization of alpha zeins was also reproduced in the absence of gz93 (B).**

Finally, two promising combinations of four zeins were selected for coexpression experiments as well. gz93 + gz16 + bz15 with either az22 or dz10 (Figure 33 A+B). In both cases gz93 provided the outer framework of the PBs and gz16 would colocalize with the outer layer whereas some of it was found in the inner core as well. bz15 on the other hand exclusively resided in the core along with az22 in the former and with dz10 in the latter combination. This again highlights the crucial role of gz16 or bz15 in addition to gz93 in the generation of recombinant PBs with multiple layers and components.

Throughout all these coexpression experiments it became apparent that at least one of either gz16, bz15, or dz10 is required to achieve a reliable incorporation of alpha zein in transiently produced gamma zein bodies. While the coexpression of az22 did not mediate the incorporation of az19 into gz93 PBs (Figure 34 A) this setup showed that az19 and az22 interacted and formed PBs that contained both alpha zeins. The same could also be reproduced in the absence of gz93 (Figure 34 B). This possibly means that az22 is indeed required to mediate the integration of az19 but that at least one of the other zeins mentioned above is required as well. This is also in accordance to more recent findings in zein PBs from maize. While Lending and Larkins (1989) initially published a model that placed all alpha zeins in the core and all gamma zeins in the shell (Figure 35 A), Yao et al. (2016) later updated that model and described that gz16 and az22 are localized at an interface layer between the shell and the core (Figure 35 B). Relative to each other, gz16 is facing outwards and az22 is facing inwards. Therefore, a bridging function of gz16 and az22 is very conceivable. In recombinant PBs, a similarly crucial role was observed for gz16 but not for az22. gz16 was most successful in integrating into gz93 PBs and caused cavities in them. In the presence of other zeins, gz16 colocalized with gz93 in the shell and the other zeins occupied the core while in the absence of other zeins, gz16 filled the cavities in gz93 PBs. In general, recombinant PBs displayed a slightly different layout than what would be expected from maize PBs. The central core was frequently smaller than in maize PBs and very often multiple cavities occurred in a single PB (Figure 35 C).



Overall, it was possible to recombinantly produce multicomponent PBs by transient coexpression of zeins in *Nicotiana benthamiana*. The design was based on the model of naturally occurring zein PBs in maize. However, the mechanism of PB formation in maize is not fully understood yet. It was therefore not clear whether the expression of two or more zeins is sufficient to induce their colocalization into the same particles. Protein-protein interactions are an important factor for the structural organization of PBs in maize (Kim et al., 2002), but other mechanisms are essential as well. Altered mRNA-targeting, for example, can disrupt the localization pattern of zeins in maize PBs (Washida et al., 2009). In *Nicotiana benthamiana*, however, including UTRs that commonly harbor mRNA-targeting zip codes did not affect the colocalization of az19 with gz27 or gz93. It had already been demonstrated that the formation of PBs triggered by gz93 is independent of host factors (Torrent et al., 2009), but the potential to organize into layered PBs in a heterologous expression system was not investigated in detail. The ability to produce recombinant multicomponent PBs opens the possibility to

functionalize and fine-tune characteristics of particle therapeutics. Additional components may be used to influence the stability of PBs and the release kinetics of active compound. In this study, all zeins were used as fusion proteins where the zein sequences were extended by fluorescent proteins. Since the presence of a fusion partner did not prevent the formation of multicomponent PBs, this enables further functionalization. The fusion partners can be chosen based on their effect on aspects such as stability or they can help to increase the affinity towards cells of the target organism in order to aid in endocytosis. However, it might very well be that certain fusion proteins have deleterious effects on PB formation. Therefore, specific fusion candidates need to be evaluated on a case-by-case basis. A more general challenge is heterogeneity. The coexpression experiments in this study were carried out as coinfiltrations of different *Agrobacteria* clones. As a consequence, the PB populations were sometimes heterogeneous between cells of an infiltrated leaf. A setup that successfully generated layered PBs in one cell did not necessarily work in all neighboring cells. Therefore, the colocalization results presented here need to be understood as the most common appearance based on observation. The non-uniform behavior also prevented reliable characterization of PBs. Any analytical data from a mix of PBs is not representative of either state (i.e. different expression levels between different cells). The reason for the heterogeneity of the multicomponent PBs may result from a difference in protein ratio or from slight temporal differences in the onset of expression. A possible solution is to include the necessary expression cassettes on a single plasmid which allows the infiltration of a single *Agrobacterium* clone and thereby omit the uncertainty of uneven distribution of different bacteria in the leaf. For this study, however, the versatility of individual plasmids was crucial because of the large combinatorial approach (36 plasmids) that also tested sequential infiltration. Alternatively, if the imbalanced ratio is caused by gene-silencing effects, the choice of promoters and/or inclusion of gene-silencing suppressors might eliminate heterogeneity. The present work helps to identify the most promising combinations of zeins that can be further characterized and fine-tuned.

For the PB-based vaccine system, there are no conceivable limitations on the choice of target since oral vaccines are not only able to induce mucosal but also systemic immunity. Regarding the administration, oral delivery is undoubtedly the preferred method for reasons that were elaborated in the introduction (1.1). Industrial production of PB-vaccines can be realized by processes similar to the one presented in this study. Follow-up results, which are not included in this thesis, indicate that processing of multicomponent PBs did not cause disruption of their internal structure and that they can withstand harsh treatments such as high-speed homogenization. This is a crucial prerequisite for the applicability of such a product. Manufacturing of pharmaceutical proteins in *Nicotiana benthamiana* is the best established recombinant production system in plant biotechnology with some facilities being able to produce 0.5 kg of antibody on a weekly basis (Holtz et al., 2015). The processing of PBs from

*Nicotiana benthamiana* leaves presented here is scalable and cheaper than chromatography-based workflows. Albeit PB-preparations are not pure, removal of nicotine was demonstrated and should therefore be of no concern for oral application. Since, the formation of PBs is host independent, PBs might as well be produced in other plants such as stable transgenic soybeans. The processing from edible plants could be reduced even further. For example, milled flour could be used to determine batch-to-batch variation of vaccine content and diluted according to the desired dosage which is then fed to animals directly.

Regardless whether vaccines are intended for veterinary use or application in humans, they should be cheap to produce, easy to store and transport, safe to administer, and effectively induce their intended immune response. Zein PBs seem to have a positive effect on these aspects and by advancing the PB system, this thesis contributed to a strategy that may help overcome some of the challenges faced by oral vaccines.

## 5 Summary and Conclusion

In this study, fluorescent PBs were recombinantly produced by transient expression in *Nicotiana benthamiana*. Their size was evaluated at various time points and a filtration-based process was developed to enable scalable enrichment of PBs. These PBs were analyzed for nicotine content to ensure the removal of toxic compounds from the formulation. The PBs were further analyzed and quantified by flow cytometry and then used to investigate their endocytotic uptake in cultures of human intestinal cells. When compared to fluorescent polystyrene beads, zein PBs were taken up in a higher amount and at a faster rate. Furthermore, only the endocytosis of PBs triggered the cells to release GM-CSF and IL-6. Two cytokines that are known to recruit APCs such as dendritic cells and that are known to promote a higher immune response overall. Consequently, the endocytosis of zein PBs by dendritic-like cells was shown as well. The results that were presented here offer an explanation for understanding how PBs elicit the adjuvant effect reported by earlier studies. Development of a scalable downstream process and employing flow cytometry for characterization and quantification may facilitate implementation of PB production on a larger scale.

Having established some aspects of PB bioavailability, the next goal was to advance the encapsulation system by finding means to create multicomponent PBs. For initial coexpression experiments, gz27/gz93 and az19 were selected due to their localization in the shell and core of native PBs, respectively. Since the incorporation of az19 into gamma zein PBs was inefficient, mRNA-targeting was evaluated by including their native UTRs. This again did not result in the reliable formation of multicomponent PBs and therefore other zeins were added in subsequent experiments. Through the systematic combination of zeins, it was possible to identify multiple combinations that resulted in either homogeneously colocalized zein PBs or in PBs that had a distinct core-shell structure. Being able to produce PBs that consist of more than one component promises to enable fine-tuning of particle characteristics such as stability, mucus penetration, release of active compound, and cellular uptake.

## 6 Outlook

The generation of multicomponent PBs was successful with more than one combination of zeins. The appearance of the resulting PBs was therefore diverse. Some colocalized homogeneously whereas others displayed a core-shell structure with either one large core or multiple smaller inclusions. It remains to be seen which sort of multicomponent PBs offer more benefits for drug delivery purposes. Particle stability, for example, is a key feature for oral drug delivery. In future studies, the stability of each individual zein needs to be determined and consequently it shall be analyzed how they influence each other when combined homogeneously or in a core-shell structure. Additional aspects such as release of therapeutic protein and mucus penetration can be investigated. Even though the results of this thesis demonstrated the efficient uptake of zein PBs by mammalian cells, the uptake may be further enhanced by modifications of the particles' surface. The processing of PBs might be further optimized as well. Optimization can aim in two different directions. The aim can either be to improve the purity of the resulting formulation or to further simplify the process to make it even more cost-effective. Purity will be a necessity for the reliable characterization of particle attributes whereas cost reduction is desired for the commercial application. The least amount of processing will be required when the PB-encapsulated vaccine is produced in edible parts of plants. It is conceivable that from such a source, milling or homogenization are sufficient. These steps can't be omitted though because concentration and dosage of active compound need to be controlled. If the source is fresh plant tissue, some sort of drying process will be necessary to extend the shelf-life of the product. However, this step is not needed when the PBs are expressed in seeds that dry on the plant. Therefore, the generation of PBs in seeds of stable transgenic plants could be pursued or different drying techniques could be evaluated for their effect on PBs. Ultimately, the efficacy of PB-encapsulated vaccines needs to be tested *in vivo* by oral administration. A prerequisite will be that the antigen does not have deleterious effects on PB formation. Veterinary vaccines may benefit a lot from the zein PB system because they need to be even more economically competitive than human vaccines.

## 7 Zusammenfassung und Schlussfolgerung

In dieser Studie wurden fluoreszierende PBs durch transiente Expression in *Nicotiana benthamiana* rekombinant hergestellt. Ihre Größe wurde zu verschiedenen Zeitpunkten ermittelt und ein auf Filtration basierendes Verfahren wurde entwickelt, um eine skalierbare Anreicherung von PBs zu ermöglichen. Diese PBs wurden auf ihren Nikotingehalt analysiert, um die genügende Reduktion toxischer Verbindungen aus dem Produkt sicherzustellen. Die PBs wurden mittels Durchflusszytometrie quantifiziert und dann verwendet, um die Effizienz ihrer endozytotischen Aufnahme in Kulturen menschlicher Darmzellen zu untersuchen. Im Vergleich zu fluoreszierenden Polystyrolkugeln wurden Zein-PBs in einer höheren Menge und mit einer schnelleren Rate aufgenommen. Darüber hinaus löste nur die Aufnahme von PBs die Freisetzung von GM-CSF und IL-6 durch die Zellen aus. Zwei Zytokine, von denen bekannt ist, dass sie APCs wie dendritische Zellen rekrutieren und insgesamt zu einer höheren Immunantwort führen. Folglich wurde auch die Endozytose von Zein-PBs durch dendritische Zellen gezeigt. Die hier vorgestellten Ergebnisse bieten eine mögliche Erklärung dafür wie PBs den in früheren Studien berichteten Adjuvans-Effekt hervorrufen. Die Entwicklung eines skalierbaren Downstream-Prozesses und die Verwendung der Durchflusszytometrie zur Charakterisierung und Quantifizierung können die Umsetzung der PB-Produktion in größerem Maßstab erleichtern.

Nachdem einige Aspekte der Bioverfügbarkeit von PB ermittelt worden waren, bestand das nächste Ziel darin, das Einkapselungssystem zu verbessern, indem Mehrkomponenten-PBs erzeugt werden sollten. Für anfängliche Koexpressionsexperimente wurden gz27/gz93 und az19 aufgrund ihrer Lokalisierung in der Hülle bzw. im Kern nativer PBs ausgewählt. Da der Einbau von az19 in gamma-Zein-PBs ineffizient war, wurde potenzielles mRNA-Targeting unter Einbeziehung ihrer nativen UTRs eingesetzt. Dies führte wiederum nicht zu einer zuverlässigen Bildung von Mehrkomponenten-PBs, weshalb in nachfolgenden Experimenten zusätzliche Zeine verwendet wurden. Durch die systematische Kombination von Zeinen konnten mehrere Kombinationen identifiziert werden, bei denen die Komponenten entweder homogen gemischt vorlagen oder eine Core-Shell-Struktur ergaben. Die Herstellung von PBs, die aus mehr als einer Komponente bestehen, verspricht die Möglichkeit einer Feinabstimmung der Partikeleigenschaften wie Stabilität, Schleimpenetration, Wirkstofffreisetzung und Zellaufnahme zu ermöglichen.

## 8 References

- Ahmed, O. A. A., Hosny, K. M., Al-Sawahli, M. M., and Fahmy, U. A. (2015). Optimization of caseinate-coated simvastatin-zein nanoparticles: Improved bioavailability and modified release characteristics. *Drug Des. Devel. Ther.* 9, 655–662. doi:10.2147/DDDT.S76194.
- Altaf, H., and Revell, P. A. (2013). Evidence for active antigen presentation by monocyte/macrophages in response to stimulation with particles: the expression of NFκB transcription factors and costimulatory molecules. *Inflammopharmacology* 21, 279–90. doi:10.1007/s10787-013-0170-z.
- Alvarez, M. L., Topal, E., Martin, F., and Cardineau, G. A. (2010). Higher accumulation of F1-V fusion recombinant protein in plants after induction of protein body formation. *Plant Mol. Biol.* 72, 75–89. doi:10.1007/s11103-009-9552-4.
- Anderson, T. J., and Lamsa, B. P. (2011). Zein extraction from corn, corn products, and coproducts and modifications for various applications: A review. *Cereal Chem.* 88, 159–173. doi:10.1094/CCHEM-06-10-0091.
- Andersson, C., Wennström, P., and Gry, J. (2003). *Nicotine alkaloids in Solanaceous food plants*. Copenhagen: Nordic Council of Ministers.
- Bagga, S., Adams, H. P., Rodriguez, F. D., Kemp, J. D., Sengupta-Gopalan, C., Rodrigues, F. D., et al. (1997). Coexpression of the maize delta-zein and beta-zein genes results in stable accumulation of delta-zein in endoplasmic reticulum-derived protein bodies formed by beta-zein. *Plant Cell* 9, 1683–96. doi:10.1105/tpc.9.9.1683.
- Baschieri, S. (2012). *Innovation in Vaccinology - From Design, Through to Delivery and Testing.*, ed. S. Baschieri Heidelberg Dordrecht London New York: Springer Verlag doi:10.1007/978-94-007-4543-8.
- Blum, J. S., Wearsch, P. A., and Cresswell, P. (2013). Pathways of Antigen Processing. *Annu. Rev. Immunol.* 31, 443–473. doi:10.1146/annurev-immunol-032712-095910.
- Buxbaum, A. R., Haimovich, G., and Singer, R. H. (2015). In the right place at the right time: visualizing and understanding mRNA localization. *Nat. Rev. Mol. Cell Biol.* 16, 95–109. doi:10.1038/nrm3918.
- Carreno-Gómez, B., Woodley, J. F., and Florence, A. T. (1999). Studies on the uptake of tomato lectin nanoparticles in everted gut sacs. *Int. J. Pharm.* 183, 7–11. doi:10.1016/S0378-5173(99)00050-2.
- Centers for Disease Control and Prevention (1999). An ounce of prevention... What are the returns? doi:10.1001/jama.281.17.1582.
- Chan, H.-T., and Daniell, H. (2015). Plant-made oral vaccines against human infectious diseases-Are we there yet? *Plant Biotechnol. J.* 13, 1056–1070. doi:10.1111/pbi.12471.
- Chen, H., Torchilin, V., and Langer, R. (1996). Lectin-bearing polymerized liposomes as potential oral vaccine carriers. *Pharm. Res.* 13, 1378–1383. doi:10.1023/A:1016030202104.
- Clark, A. M., Blair, H., Liang, L., Brey, R. N., Brayden, D., and Hirst, B. H. (2001). Targeting polymerised liposome vaccine carriers to intestinal M cells. *Vaccine* 20, 208–217. doi:10.1016/S0264-410X(01)00258-4.
- Coleman, C. E., Herman, E. M., Takasaki, K., and Larkins, B. A. (1996). The maize gamma-zein sequesters alpha-zein and stabilizes its accumulation in protein bodies of transgenic tobacco endosperm. *Plant Cell* 8, 2335–2345. doi:10.1105/tpc.8.12.2335.
- Colino, J., Chattopadhyay, G., Sen, G., Chen, Q., Lees, A., Canaday, D. H., et al. (2009). Parameters Underlying Distinct T Cell-Dependent Polysaccharide-Specific IgG Responses to an Intact Gram-Positive Bacterium versus a Soluble Conjugate Vaccine.

- J. Immunol.* 183, 1551–1559. doi:10.4049/jimmunol.0900238.
- De Smet, R., Allais, L., and Cuvelier, C. A. (2014). Recent advances in oral vaccine development: Yeast-derived  $\beta$ -glucan particles. *Hum. Vaccines Immunother.* 10, 1309–1318. doi:10.4161/hv.28166.
- Devriendt, B., De Geest, B. G., Goddeeris, B. M., and Cox, E. (2012). Crossing the barrier: Targeting epithelial receptors for enhanced oral vaccine delivery. *J. Control. Release* 160, 431–439. doi:10.1016/j.jconrel.2012.02.006.
- Domingo-Espín, J., Unzueta, U., Saccardo, P., Rodríguez-Carmona, E., Corchero, J. L., Vázquez, E., et al. (2011). “Engineered Biological Entities for Drug Delivery and Gene Therapy,” in *Progress in Molecular Biology and Translational Science* (Elsevier B.V.), 247–298. doi:10.1016/B978-0-12-416020-0.00006-1.
- Egea, L., Hirata, Y., and Kagnoff, M. F. (2010). GM-CSF: A role in immune and inflammatory reactions in the intestine. *Expert Rev. Gastroenterol. Hepatol.* 4, 723–731. doi:10.1586/egh.10.73.
- Ensign, L. M., Cone, R., and Hanes, J. (2012). Oral drug delivery with polymeric nanoparticles: The gastrointestinal mucus barriers. *Adv. Drug Deliv. Rev.* 64, 557–570. doi:10.1016/j.addr.2011.12.009.
- Esen, A., and Stetler, D. A. (1992). Immunocytochemical Localization of delta-zein in the Protein Bodies of Maize Endosperm Cells. *Am. J. Bot.* 79, 243–248. doi:10.1002/j.1537-2197.1992.tb14544.x.
- Evans, R., Shultz, L. D., Dranoff, G., Fuller, J. A., and Kamdar, S. J. (1998). CSF-1 regulation of Il6 gene expression by murine macrophages: A pivotal role for GM-CSF. *J. Leukoc. Biol.* 64, 810–816. doi:10.1002/jlb.64.6.810.
- Fernández-Carneado, J., Kogan, M. J., Castel, S., and Giralt, E. (2004). Potential peptide carriers: Amphipathic proline-rich peptides derived from the N-terminal domain of  $\gamma$ -zein. *Angew. Chemie - Int. Ed.* 43, 1811–1814. doi:10.1002/anie.200352540.
- Foster, N., Clark, A. M., Jepson, M. A., and Hirst, B. H. (1998). *Ulex europaeus* 1 lectin targets microspheres to mouse Peyer’s patch M-cells in vivo. *Vaccine* 16, 536–541. doi:10.1016/S0264-410X(97)00222-3.
- Geli, M. I., Torrent, M., and Ludevid, D. (1994). Two Structural Domains Mediate Two Sequential Events in gamma-Zein Targeting: Protein Endoplasmic Reticulum Retention and Protein Body Formation. *Plant Cell* 6, 1911–1922. doi:10.1105/tpc.6.12.1911.
- Gewirtz, A. T., and Madara, J. L. (2001). Periscope, up! Monitoring microbes in the intestine. *Nat. Immunol.* 2, 288–290. doi:10.1038/86292.
- Gomez-Estaca, J., Balaguer, M. P., Gavara, R., and Hernandez-Munoz, P. (2012). Formation of zein nanoparticles by electrohydrodynamic atomization: Effect of the main processing variables and suitability for encapsulating the food coloring and active ingredient curcumin. *Food Hydrocoll.* 28, 82–91. doi:10.1016/j.foodhyd.2011.11.013.
- Goodsell, D. S., and Olson, A. J. (2000). Structural Symmetry and Protein Function. *Annu. Rev. Biophys. Biomol. Struct.* 29, 105–153. doi:10.1146/annurev.biophys.29.1.105.
- Gregory, A. E., Titball, R., and Williamson, D. (2013). Vaccine delivery using nanoparticles. *Front. Cell. Infect. Microbiol.* 3, 1–13. doi:10.3389/fcimb.2013.00013.
- Guada, M., Beloqui, A., Kumar, M. N. V. R., Préat, V., Dios-Viéitez, M. del C., and Blanco-Prieto, M. J. (2016). Reformulating cyclosporine A (CsA): More than just a life cycle management strategy. *J. Control. Release* 225, 269–282. doi:10.1016/j.jconrel.2016.01.056.
- Guo, X., Yuan, L., Chen, H., Sato, S. J., Clemente, T. E., and Holding, D. R. (2013). Nonredundant Function of Zeins and Their Correct Stoichiometric Ratio Drive Protein

- Body Formation in Maize Endosperm. *Plant Physiol.* 162, 1359–1369. doi:10.1104/pp.113.218941.
- Halweg, C., Thompson, W. F., and Spiker, S. (2005). The Rb7 Matrix Attachment Region Increases the Likelihood and Magnitude of Transgene Expression in Tobacco Cells: A Flow Cytometric Study. *Plant Cell* 17, 418–429. doi:10.1105/tpc.104.028100.
- Hamilton, J. A. (2002). GM-CSF in inflammation and autoimmunity. *Trends Immunol.* 23, 403–408. doi:10.1016/S1471-4906(02)02260-3.
- Hansen, G. H., Rasmussen, K., Niels-Christiansen, L. L., and Danielsen, E. M. (2009). Endocytic trafficking from the small intestinal brush border probed with FM dye. *Am. J. Physiol. - Gastrointest. Liver Physiol.* 297. doi:10.1152/ajpgi.00192.2009.
- Hase, K., Kawano, K., Nochi, T., Pontes, G. S., Fukuda, S., Ebisawa, M., et al. (2009). Uptake through glycoprotein 2 of FimH+ bacteria by M cells initiates mucosal immune response. *Nature* 462, 226–230. doi:10.1038/nature08529.
- Hashem, F. M., Al-Sawahli, M. M., Nasr, M., and Ahmed, O. A. A. (2015). Optimized zein nanospheres for improved oral bioavailability of atorvastatin. *Int. J. Nanomedicine* 10, 4059–4069. doi:10.2147/IJN.S83906.
- He, X., Haselhorst, T., Von Itzstein, M., Kolarich, D., Packer, N. H., Gloster, T. M., et al. (2012). Production of  $\alpha$ -L-iduronidase in maize for the potential treatment of a human lysosomal storage disease. *Nat. Commun.* 3. doi:10.1038/ncomms2070.
- Herman, E. M. (1999). Protein Storage Bodies and Vacuoles. *PLANT CELL ONLINE* 11, 601–614. doi:10.1105/tpc.11.4.601.
- Herve, C., Mickleburgh, I., and Hesketh, J. (2004). Zipcodes and postage stamps: mRNA localisation signals and their trans-acting binding proteins. *Briefings Funct. Genomics Proteomics* 3, 240–256. doi:10.1093/bfpg/3.3.240.
- Hilleman, M. R. (2000). Vaccines in historic evolution and perspective: a narrative of vaccine discoveries. *Vaccine* 18, 1436–1447. doi:10.1016/S0264-410X(99)00434-X.
- Hofbauer, A., Melnik, S., Tschofen, M., Arcalis, E., Phan, H. T., Gresch, U., et al. (2016). The Encapsulation of Hemagglutinin in Protein Bodies Achieves a Stronger Immune Response in Mice than the Soluble Antigen. *Front. Plant Sci.* 7. doi:10.3389/fpls.2016.00142.
- Holding, D. R., Otegui, M. S., Li, B., Meeley, R. B., Dam, T., Hunter, B. G., et al. (2007). The Maize Floury1 Gene Encodes a Novel Endoplasmic Reticulum Protein Involved in Zein Protein Body Formation. *Plant Cell Online* 19, 2569–2582. doi:10.1105/tpc.107.053538.
- Holtz, B. R., Berquist, B. R., Bennett, L. D., Kommineni, V. J. M., Muniguntti, R. K., White, E. L., et al. (2015). Commercial-scale biotherapeutics manufacturing facility for plant-made pharmaceuticals. *Plant Biotechnol. J.* 13, 1180–1190. doi:10.1111/pbi.12469.
- Hurtado-López, P., and Murdan, S. (2006). Zein microspheres as drug/antigen carriers: A study of their degradation and erosion, in the presence and absence of enzymes. *J. Microencapsul.* 23, 303–314. doi:10.1080/02652040500444149.
- Hussain, N., Jani, P. U., and Florence, A. T. (1997). Enhanced oral uptake of tomato Lectin-Conjugated nanoparticles in the rat. *Pharm. Res.* 14, 613–618. doi:10.1023/A:1012153011884.
- Jang, M. H., Kweon, M.-N., Iwatani, K., Yamamoto, M., Terahara, K., Sasakawa, C., et al. (2004). Intestinal villous M cells: An antigen entry site in the mucosal epithelium. *Proc. Natl. Acad. Sci.* 101, 6110–6115. doi:10.1073/pnas.0400969101.
- Jiang, Y. N., Mo, H. Y., and Yu, D. G. (2012). Electrospun drug-loaded core-sheath PVP/zein nanofibers for biphasic drug release. *Int. J. Pharm.* 438, 232–239. doi:10.1016/j.ijpharm.2012.08.053.

- Johnson, D. E., Ostrowski, P., Jaumouillé, V., and Grinstein, S. (2016). The position of lysosomes within the cell determines their luminal pH. *J. Cell Biol.* 212, 677–692. doi:10.1083/jcb.201507112.
- Joseph, M., Ludevid, M. D., Torrent, M., Rofidal, V., Tauzin, M., Rossignol, M., et al. (2012). Proteomic characterisation of endoplasmic reticulum-derived protein bodies in tobacco leaves. *BMC Plant Biol.* 12, 36. doi:10.1186/1471-2229-12-36.
- Kim, C. S., Gibbon, B. C., Gillikin, J. W., Larkins, B. A., Boston, R. S., and Jung, R. (2006). The maize Mucronate mutation is a deletion in the 16-kDa gamma-zein gene that induces the unfolded protein response. *Plant J.* 48, 440–451. doi:10.1111/j.1365-313X.2006.02884.x.
- Kim, C. S., Woo Ym, Y., Clore, A. M., Burnett, R. J., Carneiro, N. P., and Larkins, B. A. (2002). Zein protein interactions, rather than the asymmetric distribution of zein mRNAs on endoplasmic reticulum membranes, influence protein body formation in maize endosperm. *Plant Cell* 14, 655–72. doi:10.1105/tpc.010431.
- Kim, S.-H., Lee, K.-Y., and Jang, Y.-S. (2012). Mucosal Immune System and M Cell-targeting Strategies for Oral Mucosal Vaccination. *Immune Netw.* 12, 165. doi:10.4110/in.2012.12.5.165.
- Kim, W.-S., and Krishnan, H. B. (2019). Impact of co-expression of maize 11 and 18 kDa  $\delta$ -zeins and 27 kDa  $\gamma$ -zein in transgenic soybeans on protein body structure and sulfur amino acid content. *Plant Sci.* 280, 340–347. doi:10.1016/j.plantsci.2018.12.016.
- Kogan, M. J., López, O., Cocera, M., López-Iglesias, C., De la Maza, A., and Giralt, E. (2004). Exploring the interaction of the surfactant N-terminal domain of  $\gamma$ -Zein with soybean phosphatidylcholine liposomes. *Biopolymers* 73, 258–268. doi:10.1002/bip.10578.
- Koncz, C., and Schell, J. (1986). The promoter of TL-DNA gene 5 controls the tissue-specific expression of chimaeric genes carried by a novel type of Agrobacterium binary vector. *MGG Mol. Gen. Genet.* 204, 383–396. doi:10.1007/BF00331014.
- Kozlowski, P. (2012). *Mucosal Vaccines - Modern Concepts, Strategies, and Challenges.* , ed. P. Kozlowski Heidelberg Dordrecht London New York: Springer Verlag doi:10.1007/978-3-642-23693-8.
- Krishnan, H. B., and Coe, E. H. (2001). “Seed Storage Proteins,” in *Encyclopedia of Genetics*, eds. S. Brenner and J. H. Miller (Elsevier), 1782–1787. doi:10.1006/rwgn.2001.1714.
- Krishnan, H. B., Kerley, M. S., Allee, G. L., Jang, S., Kim, W. S., and Fu, C. J. (2010). Maize 27 kDa  $\gamma$ -Zein is a potential allergen for early weaned pigs. *J. Agric. Food Chem.* 58, 7323–7328. doi:10.1021/jf100927u.
- Kumar, S., Stecher, G., Li, M., Knyaz, C., and Tamura, K. (2018). MEGA X: Molecular Evolutionary Genetics Analysis across Computing Platforms. *Mol. Biol. Evol.* 35, 1547–1549. doi:10.1093/molbev/msy096.
- Kyd, J. M., and Cripps, A. W. (2008). Functional differences between M cells and enterocytes in sampling luminal antigens. *Vaccine* 26, 6221–6224. doi:10.1016/j.vaccine.2008.09.061.
- Lai, L. F., and Guo, H. X. (2011). Preparation of new 5-fluorouracil-loaded zein nanoparticles for liver targeting. *Int. J. Pharm.* 404, 317–323. doi:10.1016/j.ijpharm.2010.11.025.
- Landsverk, O. J. B., Snir, O., Casado, R. B., Richter, L., Mold, J. E., Réu, P., et al. (2017). Antibody-secreting plasma cells persist for decades in human intestine. *J. Exp. Med.* 214, 309–317. doi:10.1084/jem.20161590.
- Larkin, M. A., Blackshields, G., Brown, N. P., Chenna, R., McGettigan, P. A., McWilliam, H., et al. (2007). Clustal W and Clustal X version 2.0. *Bioinformatics* 23, 2947–2948.

- doi:10.1093/bioinformatics/btm404.
- Lee, S., Alwahab, N. S. A., and Moazzam, Z. M. (2013). Zein-based oral drug delivery system targeting activated macrophages. *Int. J. Pharm.* 454, 388–393. doi:10.1016/j.ijpharm.2013.07.026.
- Lee, S., Kim, Y.-C., and Park, J.-H. (2016). Zein-alginate based oral drug delivery systems: Protection and release of therapeutic proteins. *Int. J. Pharm.* 515, 300–306. doi:10.1016/j.ijpharm.2016.10.023.
- Lehr, C.-M., Poelma, F. G. J., Junginger, H. E., and Tukker, J. J. (1991). An estimate of turnover time of intestinal mucus gel layer in the rat in situ loop. *Int. J. Pharm.* 70, 235–240. doi:10.1016/0378-5173(91)90287-X.
- Lending, C. R., and Larkins, B. A. (1989). Changes in the zein composition of protein bodies during maize endosperm development. *Plant Cell* 1, 1011–1023. doi:10.1105/tpc.1.10.1011.
- Llop-Tous, I., Madurga, S., Giralt, E., Marzabal, P., Torrent, M., and Ludevid, M. D. (2010). Relevant Elements of a Maize  $\gamma$ -Zein Domain Involved in Protein Body Biogenesis. *J. Biol. Chem.* 285, 35633–35644. doi:10.1074/jbc.M110.116285.
- Llop-Tous, I., Ortiz, M., Torrent, M., and Ludevid, M. D. (2011). The Expression of a Xylanase Targeted to ER-Protein Bodies Provides a Simple Strategy to Produce Active Insoluble Enzyme Polymers in Tobacco Plants. *PLoS One* 6, e19474. doi:10.1371/journal.pone.0019474.
- López-Sagasetta, J., Malito, E., Rappuoli, R., and Bottomley, M. J. (2016). Self-assembling protein nanoparticles in the design of vaccines. *Comput. Struct. Biotechnol. J.* 14, 58–68. doi:10.1016/j.csbj.2015.11.001.
- Loza-Rubio, E., Rojas-Anaya, E., López, J., Olivera-Flores, M. T., Gómez-Lim, M., and Tapia-Pérez, G. (2012). Induction of a protective immune response to rabies virus in sheep after oral immunization with transgenic maize, expressing the rabies virus glycoprotein. *Vaccine* 30, 5551–5556. doi:10.1016/j.vaccine.2012.06.039.
- Ludevid, M. D., Bastida, M., Llompарт, B., Marzábal, P., and Torrent, M. (2006). Protein Isolation and Purification. International Patent Number WO2006056484.
- Luo, Y., Teng, Z., Wang, T. T. Y., and Wang, Q. (2013). Cellular uptake and transport of zein nanoparticles: Effects of sodium caseinate. *J. Agric. Food Chem.* 61, 7621–7629. doi:10.1021/jf402198r.
- Luo, Y., Zhang, B., Whent, M., Yu, L. L., and Wang, Q. (2011). Preparation and characterization of zein/chitosan complex for encapsulation of  $\alpha$ -tocopherol, and its in vitro controlled release study. *Colloids Surfaces B Biointerfaces* 85, 145–152. doi:10.1016/j.colsurfb.2011.02.020.
- Macleán, J., Koekemoer, M., Olivier, A. J., Stewart, D., Hitzeroth, I. I., Rademacher, T., et al. (2007). Optimization of human papillomavirus type 16 (HPV-16) L1 expression in plants: comparison of the suitability of different HPV-16 L1 gene variants and different cell-compartment localization. *J. Gen. Virol.* 88, 1460–1469. doi:10.1099/vir.0.82718-0.
- Mainieri, D., Marrano, C. A., Prinsi, B., Maffi, D., Tschofen, M., Espen, L., et al. (2018). Maize 16-kD  $\gamma$ -zein forms very unusual disulfide-bonded polymers in the endoplasmic reticulum: implications for prolamin evolution. *J. Exp. Bot.* doi:10.1093/jxb/ery287.
- Mainieri, D., Morandini, F., Maitrejean, M., Sacconi, A., Pedrazzini, E., and Alessandro, V. (2014). Protein body formation in the endoplasmic reticulum as an evolution of storage protein sorting to vacuoles: insights from maize  $\hat{1}^3$ -zein. *Front. Plant Sci.* 5, 1–11. doi:10.3389/fpls.2014.00331.
- Mandal, D., Nasrolahi Shirazi, A., and Parang, K. (2014). Self-assembly of peptides to nanostructures. *Org. Biomol. Chem.* 12, 3544–3561. doi:10.1039/C4OB00447G.

- Melkebeek, V., Rasschaert, K., Bellot, P., Tilleman, K., Favoreel, H., Deforce, D., et al. (2012). Targeting aminopeptidase N, a newly identified receptor for F4ac fimbriae, enhances the intestinal mucosal immune response. *Mucosal Immunol.* 5, 635–645. doi:10.1038/mi.2012.37.
- Mendoza-Coronel, E., and Castañón-Arreola, M. (2016). Comparative evaluation of in vitro human macrophage models for mycobacterial infection study. *Pathog. Dis.* 74, ftw052. doi:10.1093/femspd/ftw052.
- Merlin, M., Pezzotti, M., and Avesani, L. (2017). Edible plants for oral delivery of biopharmaceuticals. *Br. J. Clin. Pharmacol.* 83, 71–81. doi:10.1111/bcp.12949.
- Mestecky, J., Russell, M. W., and Elson, C. O. (2007). Perspectives on Mucosal Vaccines: Is Mucosal Tolerance a Barrier? *J. Immunol.* 179, 5633–5638. doi:10.4049/jimmunol.179.9.5633.
- Moghbel, N., Ryu, B., and Steadman, K. J. (2015). A reversed-phase HPLC-UV method developed and validated for simultaneous quantification of six alkaloids from *Nicotiana* spp. *J. Chromatogr. B* 997, 142–145. doi:10.1016/j.jchromb.2015.06.006.
- Moldoveanu, S. C., Scott, W. A., and Lawson, D. M. (2016). Nicotine Analysis in Several Non-Tobacco Plant Materials. *Beiträge zur Tab. Int. to Tob. Res.* 27, 54–59. doi:10.1515/cttr-2016-0008.
- Nagarwal, R. C., Kumar, R., Dhanawat, M., Das, N., and Pandit, J. K. (2011). Nanocrystal Technology in the Delivery of Poorly Soluble Drugs: An Overview. *Curr. Drug Deliv.* 8, 398–406. doi:10.2174/156720111795767988.
- Neal, M. D., Leaphart, C., Levy, R., Prince, J., Billiar, T. R., Watkins, S., et al. (2006). Enterocyte TLR4 Mediates Phagocytosis and Translocation of Bacteria Across the Intestinal Barrier. *J. Immunol.* 176, 3070–3079. doi:10.4049/jimmunol.176.5.3070.
- New, R. R. C. (2019). Formulation technologies for oral vaccines. *Clin. Exp. Immunol.* preprint, cei.13352. doi:10.1111/cei.13352.
- Nochi, T., Yuki, Y., Matsumura, A., Mejima, M., Terahara, K., Kim, D.-Y., et al. (2007). A novel M cell-specific carbohydrate-targeted mucosal vaccine effectively induces antigen-specific immune responses. *J. Exp. Med.* 204, 2789–2796. doi:10.1084/jem.20070607.
- Okada, E., Sasaki, S., Ishii, N., Aoki, I., Yasuda, T., Nishioka, K., et al. (1997). Intranasal immunization of a DNA vaccine with IL-12- and granulocyte-macrophage colony-stimulating factor (GM-CSF)-expressing plasmids in liposomes induces strong mucosal and cell-mediated immune responses against HIV-1 antigens. *J. Immunol.* 159, 3638–47. Available at: <http://www.ncbi.nlm.nih.gov/pubmed/9317164> [Accessed September 27, 2019].
- Pavot, V., Rochereau, N., Genin, C., Verrier, B., and Paul, S. (2012). New insights in mucosal vaccine development. *Vaccine* 30, 142–154. doi:10.1016/j.vaccine.2011.11.003.
- Pawar, V. K., Meher, J. G., Singh, Y., Chaurasia, M., Surendar Reddy, B., and Chourasia, M. K. (2014). Targeting of gastrointestinal tract for amended delivery of protein/peptide therapeutics: Strategies and industrial perspectives. *J. Control. Release* 196, 168–183. doi:10.1016/j.jconrel.2014.09.031.
- Pniewski, T., Milczarek, M., Wojas-Turek, J., Pajtasz-Piasecka, E., Wietrzyk, J., and Czyż, M. (2018). Plant lyophilisate carrying S-HBsAg as an oral booster vaccine against HBV. *Vaccine* 36, 6070–6076. doi:10.1016/j.vaccine.2018.09.006.
- Prat, S., Cortadas, J., Puigdomènech, P., and Palau, J. (1985). Nucleic acid (cDNA) and amino acid sequences of the maize endosperm protein glutelin-2. *Nucleic Acids Res.* 13, 1493–1504. doi:10.1093/nar/13.5.1493.

- Pridgen, E. M., Alexis, F., and Farokhzad, O. C. (2015). Polymeric nanoparticle drug delivery technologies for oral delivery applications. *Expert Opin. Drug Deliv.* 12, 1459–1473. doi:10.1517/17425247.2015.1018175.
- Pujals, S., and Giralt, E. (2008). Proline-rich, amphipathic cell-penetrating peptides. *Adv. Drug Deliv. Rev.* 60, 473–484. doi:10.1016/j.addr.2007.09.012.
- Rademacher, T., Häusler, R. E., Hirsch, H.-J., Zhang, L., Lipka, V., Weier, D., et al. (2002). An engineered phosphoenolpyruvate carboxylase redirects carbon and nitrogen flow in transgenic potato plants. *Plant J.* 32, 25–39. doi:10.1046/j.1365-313X.2002.01397.x.
- Randall, J. J., Sutton, D. W., Hanson, S. F., and Kemp, J. D. (2005). BiP and zein binding domains within the delta zein protein. *Planta* 221, 656–666. doi:10.1007/s00425-005-1482-z.
- Rappuoli, R., Miller, H., and Falkow, S. (2002). The Intangible Value of Vaccination. *Science* (80- ). 297, 937–939. doi:10.1126/science.1075173.
- Rath, T., Kuo, T. T., Baker, K., Qiao, S. W., Kobayashi, K., Yoshida, M., et al. (2013). The immunologic functions of the neonatal FC receptor for IGG. *J. Clin. Immunol.* 33, 9–17. doi:10.1007/s10875-012-9768-y.
- Reinholz, J., Landfester, K., and Mailänder, V. (2018). The challenges of oral drug delivery via nanocarriers. *Drug Deliv.* 25, 1694–1705. doi:10.1080/10717544.2018.1501119.
- Renukuntla, J., Vadlapudi, A. D., Patel, A., Boddu, S. H. S., and Mitra, A. K. (2013). Approaches for enhancing oral bioavailability of peptides and proteins. *Int. J. Pharm.* 447, 75–93. doi:10.1016/j.ijpharm.2013.02.030.
- Rescigno, M., Urbano, M., Valzasina, B., Francolini, M., Rotta, G., Bonasio, R., et al. (2001). Dendritic cells express tight junction proteins and penetrate gut epithelial monolayers to sample bacteria. *Nat. Immunol.* 2, 361–367. doi:10.1038/86373.
- Roche, P. A., and Furuta, K. (2015). The ins and outs of MHC class II-mediated antigen processing and presentation. *Nat. Rev. Immunol.* 15, 203–216. doi:10.1038/nri3818.
- Roig, A. I., Eskiocak, U., Hight, S. K., Kim, S. B., Delgado, O., Souza, R. F., et al. (2010a). Immortalized Epithelial Cells Derived From Human Colon Biopsies Express Stem Cell Markers and Differentiate In Vitro. *Gastroenterology* 138, 1012–1021. doi:10.1053/j.gastro.2009.11.052.
- Roig, A. I., Eskiocak, U., Hight, S. K., Kim, S. B., Delgado, O., Souza, R. F., et al. (2010b). Immortalized Epithelial Cells Derived From Human Colon Biopsies Express Stem Cell Markers and Differentiate In Vitro. *Gastroenterology* 138, 1012-1021.e5. doi:10.1053/j.gastro.2009.11.052.
- Russell-Jones, G. ., Veitch, H., and Arthur, L. (1999). Lectin-mediated transport of nanoparticles across Caco-2 and OK cells. *Int. J. Pharm.* 190, 165–174. doi:10.1016/S0378-5173(99)00254-9.
- Rydell, N., and Sjöholm, I. (2004). Oral vaccination against diphtheria using polyacryl starch microparticles as adjuvant. *Vaccine* 22, 1265–1274. doi:10.1016/j.vaccine.2003.09.034.
- Sack, M., Paetz, A., Kunert, R., Bomble, M., Hesse, F., Stiegler, G., et al. (2007). Functional analysis of the broadly neutralizing human anti-HIV-1 antibody 2F5 produced in transgenic BY-2 suspension cultures. *FASEB J.* 21, 1655–1664. doi:10.1096/fj.06-5863com.
- Saitou, N., and Nei, M. (1987). The neighbor-joining method: a new method for reconstructing phylogenetic trees. *Mol. Biol. Evol.* 4, 406–25. doi:10.1093/oxfordjournals.molbev.a040454.
- Sallon, S., Solowey, E., Cohen, Y., Korchinsky, R., Egli, M., Woodhatch, I., et al. (2008). Germination, Genetics, and Growth of an Ancient Date Seed. *Science* (80- ). 320,

- 1464–1464. doi:10.1126/science.1153600.
- Sánchez-Navarro, M., Teixidó, M., and Giralt, E. (2017). Jumping Hurdles: Peptides Able to Overcome Biological Barriers. *Acc. Chem. Res.* 50, 1847–1854. doi:10.1021/acs.accounts.7b00204.
- Schillberg, S., Raven, N., Spiegel, H., Rasche, S., and Buntru, M. (2019). Critical Analysis of the Commercial Potential of Plants for the Production of Recombinant Proteins. *Front. Plant Sci.* 10. doi:10.3389/fpls.2019.00720.
- Smith, D. M., Simon, J. K., and Baker, J. R. (2013). Applications of nanotechnology for immunology. *Nat. Rev. Immunol.* 13, 592–605. doi:10.1038/nri3488.
- Snapper, C. M. (2018). Distinct immunologic properties of soluble versus particulate antigens. *Front. Immunol.* 9. doi:10.3389/fimmu.2018.00598.
- Sonaje, K., Chuang, E.-Y., Lin, K.-J., Yen, T.-C., Su, F.-Y., Tseng, M. T., et al. (2012). Opening of Epithelial Tight Junctions and Enhancement of Paracellular Permeation by Chitosan: Microscopic, Ultrastructural, and Computed-Tomographic Observations. *Mol. Pharm.* 9, 1271–1279. doi:10.1021/mp200572t.
- Stertman, L., Lundgren, E., and Sjöholm, I. (2006). Starch microparticles as a vaccine adjuvant: Only uptake in Peyer's patches decides the profile of the immune response. *Vaccine* 24, 3661–3668. doi:10.1016/j.vaccine.2005.10.059.
- Su, B., Wang, J., Wang, X., Jin, H., Zhao, G., Ding, Z., et al. (2008). The effects of IL-6 and TNF- $\alpha$  as molecular adjuvants on immune responses to FMDV and maturation of dendritic cells by DNA vaccination. *Vaccine* 26, 5111–5122. doi:10.1016/j.vaccine.2008.03.089.
- Subach, O. M., Cranfill, P. J., Davidson, M. W., and Verkhusha, V. V. (2011). An Enhanced Monomeric Blue Fluorescent Protein with the High Chemical Stability of the Chromophore. *PLoS One* 6, e28674. doi:10.1371/journal.pone.0028674.
- Tada, R., Hidaka, A., Kiyono, H., Kunisawa, J., and Aramaki, Y. (2018). Intranasal administration of cationic liposomes enhanced granulocyte-macrophage colony-stimulating factor expression and this expression is dispensable for mucosal adjuvant activity. *BMC Res. Notes* 11, 1–8. doi:10.1186/s13104-018-3591-3.
- Takaiwa, F., Wakasa, Y., Takagi, H., and Hiroi, T. (2015). Rice seed for delivery of vaccines to gut mucosal immune tissues. *Plant Biotechnol. J.* 13, 1041–1055. doi:10.1111/pbi.12423.
- Thompson, A. L., and Staats, H. F. (2011). Cytokines: The Future of Intranasal Vaccine Adjuvants. *Clin. Dev. Immunol.* 2011, 1–17. doi:10.1155/2011/289597.
- Tian, L., and Okita, T. W. (2014). mRNA-based protein targeting to the endoplasmic reticulum and chloroplasts in plant cells. *Curr. Opin. Plant Biol.* 22, 77–85. doi:10.1016/j.pbi.2014.09.007.
- Tiels, P., Verdonck, F., Coddens, A., Goddeeris, B., and Cox, E. (2008). The excretion of F18+E. coli is reduced after oral immunisation of pigs with a FedF and F4 fimbriae conjugate. *Vaccine* 26, 2154–2163. doi:10.1016/j.vaccine.2008.01.054.
- Torrent, M., Llompart, B., Lasserre-Ramassamy, S., Llop-Tous, I., Bastida, M., Marzabal, P., et al. (2009). Eukaryotic protein production in designed storage organelles. *BMC Biol.* 7. doi:10.1186/1741-7007-7-5.
- Valenzuela, P., Medina, A., Rutter, W. J., Ammerer, G., and Hall, B. D. (1982). Synthesis and assembly of hepatitis B virus surface antigen particles in yeast. *Nature* 298, 347–350. doi:10.1038/298347a0.
- Van de Graaff, K. M. (1986). Anatomy and physiology of the gastrointestinal tract. *Pediatr. Infect. Dis.* 5, 11–16.

- van Zyl, A. R., Meyers, A. E., and Rybicki, E. P. (2017). Development of plant-produced protein body vaccine candidates for bluetongue virus. *BMC Biotechnol.* 17, 47. doi:10.1186/s12896-017-0370-5.
- Vela Ramirez, J. E., Sharpe, L. A., and Peppas, N. A. (2017). Current state and challenges in developing oral vaccines. *Adv. Drug Deliv. Rev.* 114, 116–131. doi:10.1016/j.addr.2017.04.008.
- Vitale, A., and Ceriotti, A. (2004). Protein Quality Control Mechanisms and Protein Storage in the Endoplasmic Reticulum. A Conflict of Interests? *Plant Physiol.* 136, 3420–3426. doi:10.1104/pp.104.050351.
- Washida, H., Sugino, A., Kaneko, S., Crofts, N., Sakulsingharoj, C., Kim, D., et al. (2009). Identification of cis -localization elements of the maize 10-kDa  $\delta$ -zein and their use in targeting RNAs to specific cortical endoplasmic reticulum subdomains. *Plant J.* 60, 146–155. doi:10.1111/j.1365-313X.2009.03944.x.
- Washida, H., Sugino, A., Messing, J., Esen, A., and Okita, T. W. (2004). Asymmetric Localization of Seed Storage Protein RNAs to Distinct Subdomains of the Endoplasmic Reticulum in Developing Maize Endosperm Cells. *Plant Cell Physiol.* 45, 1830–1837. doi:10.1093/pcp/pch210.
- Weatheritt, R. J., Gibson, T. J., and Babu, M. M. (2014). Asymmetric mRNA localization contributes to fidelity and sensitivity of spatially localized systems. *Nat. Struct. Mol. Biol.* 21, 833–839. doi:10.1038/nsmb.2876.
- Whitehead, M., Öhlschläger, P., Almajhdi, F. N., Alloza, L., Marzábal, P., Meyers, A. E., et al. (2014). Human papillomavirus (HPV) type 16 E7 protein bodies cause tumour regression in mice. *BMC Cancer* 14. doi:10.1186/1471-2407-14-367.
- WHO (2018a). 2018 Assessment Report of the Global Vaccine Action Plan. World Health Organization. Strategic Advisory Group of Experts on Immunization. Geneva. Available at: <http://apps.who.int/>.
- WHO (2018b). Global Health Estimates 2016: Deaths by Cause, Age, Sex by Country and by Region, 2000-2016. World Health Organization. Geneva. Available at: <http://apps.who.int/>.
- Wilson, C. M. (1988). Electrophoretic Analyses of Various Commercial and Laboratory-Prepared Zeins. *Cereal Chem.* 65, 72–73. Available at: <https://www.cerealsgrains.org/publications/cc/backissues/1988/Documents/CC1988a16.html>.
- Woo, Y. M., Hu, D. W., Larkins, B. A., and Jung, R. (2001). Genomics analysis of genes expressed in maize endosperm identifies novel seed proteins and clarifies patterns of zein gene expression. *Plant Cell* 13, 2297–317. doi:Doi 10.2307/3871509.
- Wu, L., Shan, W., Zhang, Z., and Huang, Y. (2018). Engineering nanomaterials to overcome the mucosal barrier by modulating surface properties. *Adv. Drug Deliv. Rev.* 124, 150–163. doi:10.1016/j.addr.2017.10.001.
- Yang, Y., Crofts, A. J., Crofts, N., and Okita, T. W. (2014). Multiple RNA Binding Protein Complexes Interact with the Rice Prolamine RNA Cis-Localization Zipcode Sequences. *Plant Physiol.* 164, 1271–1282. doi:10.1104/pp.113.234187.
- Yao, D., Qi, W., Li, X., Yang, Q., Yan, S., Ling, H., et al. (2016). Maize opaque10 Encodes a Cereal-Specific Protein That Is Essential for the Proper Distribution of Zeins in Endosperm Protein Bodies. *PLoS Genet.* 12, e1006270. doi:10.1371/journal.pgen.1006270.
- Zhang, Y., Cui, L., Che, X., Zhang, H., Shi, N., Li, C., et al. (2015). Zein-based films and their usage for controlled delivery: Origin, classes and current landscape. *J. Control. Release* 206, 206–219. doi:10.1016/j.jconrel.2015.03.030.

- Zhang, Y., Cui, L., Li, F., Shi, N., Li, C., Yu, X., et al. (2016). Design, fabrication and biomedical applications of zein-based nano/micro-carrier systems. *Int. J. Pharm.* 513, 191–210. doi:10.1016/j.ijpharm.2016.09.023.
- Zhu, Q., Talton, J., Zhang, G., Cunningham, T., Wang, Z., Waters, R. C., et al. (2012). Large intestine-targeted, nanoparticle-releasing oral vaccine to control genitorectal viral infection. *Nat. Med.* 18, 1291–1296. doi:10.1038/nm.2866.
- Zou, T., Li, Z., Percival, S. S., Bonard, S., and Gu, L. (2012). Fabrication, characterization, and cytotoxicity evaluation of cranberry procyanidins-zein nanoparticles. *Food Hydrocoll.* 27, 293–300. doi:10.1016/j.foodhyd.2011.10.002.
- Zuckerkindl, E., and Pauling, L. (1965). "Evolutionary Divergence and Convergence in Proteins," in *Evolving Genes and Proteins* doi:10.1016/b978-1-4832-2734-4.50017-6.

## 9 List of Tables

|  |    |
|--|----|
| Table 1: List of zeins in developing maize endosperm (adapted from Woo et al., 2001) ..... | 12 |
| Table 2: List of fluorescent zein variants.....  | 41 |
| Table 3: List of combinations of two zeins coexpressed .....                               | 46 |
| Table 4: List of combinations of three zeins coexpressed.....                              | 46 |

## 10 List of Figures

- Figure 1: Schematic drawing of the four routes by which particle drugs, in this case protein bodies (PB), can travel across the epithelium. (1) Particles can be transcytosed by M cells (M) that reside in Payer's patches. Reduced thickness of mucus and tight interaction of M cells and dendritic cells (DC) make this route highly favorable. (2) Transcytosis of particles through enterocytes (E) was also described. The benefit of this route is the abundance of enterocytes in the intestine. (3) Particles can also travel across the epithelium through tight junctions between epithelial cells. (4) DCs also use these tight junctions to reach their dendrites into the lumen of the intestine to probe for antigens. On the basolateral side of the epithelium, APCs such as DCs and macrophages (Ma) trigger the cascade that ultimately results in the immune response. 10
- Figure 2: Phylogenic structuring of zeins based on their amino acid sequence. Gamma zeins are highlighted in green, az19 in orange, and az22 in blue. The zeins used in this thesis are indicated by an asterisk (\*). It should be noted that bz15 is closer related to gamma zeins whereas delta closer to alpha zeins. .... 13
- Figure 3: Schematic drawing of the development of zein PBs in maize endosperm cells. At first, only gamma and beta zein are expressed. Gamma zein initiates the PB formation in the rough endoplasmic reticulum (rER) where it colocalizes with beta zein. The expression of alpha and delta zein starts later and they then enter the PB matrix and cause its expansion. In fully developed zein PBs, gamma and beta zein constitute the outer shell whereas alpha and delta zein are found in the core of PBs (adapted from Lending and Larkins, 1989). .... 14
- Figure 4: Leaf cells of *Nicotiana benthamiana* are expressing (A) gz93-EGFP or (B) gz93-mTagBFP2 PBs at 8 dpi. Z-stacks of 48 CSLM pictures were displayed as maximum projections and the median diameter of 986 individual PBs was determined to be 1.03  $\mu\text{m}$  ( $\text{SD}\pm 0.34$ ). Scale bars represent 25  $\mu\text{m}$  or 50  $\mu\text{m}$ , respectively. .... 25
- Figure 5: Size determination of gz93-EGFP PBs. Samples of *Nicotiana benthamiana* were analyzed by CLSM at 4, 8, and 12 dpi. The diameter of protein bodies increases significantly over time as determined by one-way ANOVA with post-hoc Tukey's test (\*\*\*\*  $p < 0.0001$ ). .... 26
- Figure 6: A scalable process for the enrichment of zein PBs, based on two consecutive tangential flow filtrations. At the first step, cell debris is retained by a 10  $\mu\text{m}$  nylon filter whereas PBs are able to pass and the second step concentrates the PBs while allowing soluble contaminants to permeate. In this process flow chart, the path of PBs is highlighted in green. .... 27
- Figure 7: Example contour plot of a flow cytometry measurement of gz93-EGFP PBs. The fluorescence intensity is plotted against the forward scatter (height, FSC-H) and the gz93-EGFP PBs are gated in the upper-right quadrant (H1-UR). The relative amount in this example is 65.6% ( $\text{SD}\pm 0.6$ ) fluorescent events in H1-UR versus 34.4% ( $\text{SD}\pm 0.6$ ) non-fluorescent events in H1-UL. .... 27
- Figure 8: HCEC-1CT cells have internalized gz93-EGFP PBs after 4 hours of incubation. The cell nucleus was stained with Hoechst 33342, displayed in blue (A), gz93-EGFP PBs emit green fluorescence (B) and the cell membrane and intracellular structures were stained in red with FM4-64 (C). When all channels are merged (D) an orange signal results from the overlay of the green and red fluorescence that indicates the internalization of gz93-EGFP PB into HCEC-1CT cells. The cell was imaged in 32 sections (with a step size of 0.7  $\mu\text{m}$ ), and the cell is shown in the XY-axis at  $z = 11$ . YZ- (E, green panel) and XZ-projections (E, red panel) clearly confirm the internalization of the analyzed PB (arrow). The bar represents 25  $\mu\text{m}$ . .... 29
- Figure 9: Uptake of gz93-EGFP PBs by HCEC-1CT cells in comparison to fluorescent polystyrene beads. The relative number of fluorescent HCEC-1CT cells was determined

by flow cytometry at the indicated time points. Values are shown as medians with their 95% confidence interval. ....30

Figure 10: Cytokine secretion of HCEC-1CT cells after 24 hours of incubation with gz93-EGFP PBs and PS beads. Cells incubated with gz93-EGFP PBs showed a significant increase in GM-CSF and IL-6 secretion compared to cells treated with polystyrene beads. Untreated cells (cells only) were used as a negative control and TNF- $\alpha$  treated cells as a positive control. Values for three independent experiments are shown and the median values are indicated. Statistical significance was determined by ordinary one-way ANOVA with Sidak's multiple comparisons test ( $p > 0.05$  [ns],  $P \leq 0.0001$  [\*\*\*\*])....30

Figure 11: The uptake of gz93-EGFP and gz93-mTagBFP2 PBs into U937 cells was confirmed by CLSM. Upon PMA treatment, cells attached to the vessel surface and exhibited morphological changes such as the growth of dendrite-like structures (A). Endosomal compartments were loaded and visualized with Alexa Fluor 647-dextran (red, B). Colocalization of blue fluorescent gz93-mTagBFP2 PBs with endosomal compartments (red) results in a purple signal (C, merge). ....32

Figure 12: Coexpression of az19 alongside gz27 (A) or gz93 (B). Gamma zein variants were fused to EGFP and are displayed in green in the left column whereas az19 was fused to mCherry and is displayed in red in the center column. Both channels are merged in the column on the right. In (A) gz27 and az19 seem to be tightly interacting where az19 formed some sorts of caps on the gz27 PBs but they did not enter the gz27 PB's core. In the green channel of row (B), hollow gz93 can be seen and the merged picture clearly indicates that these were filled with az19. However, the majority of az19 remained on the outside of gz93 PBs. The confocal micrographs in the bottom row (B) are maximum projections of a Z-stack. These samples were analyzed at 10 dpi. Scale bars are only displayed in merged pictures but apply to all pictures of the same row. ....35

Figure 13: Transmission electron micrograph of cap-like az19 structures on gz27 PBs. The larger gz27 PB appears darker due to its higher density and can be recognized as almost perfectly round. Some of az19 was found as much smaller, also spherical PBs or as cap-like structures on gz27. Although an ER-membrane surrounded az19 PBs that were separated from gz27, no ER-membrane was detected between az19 cap-like structures and gz27. Membranes were visualized by uranyl acetate staining. A scale bar is located in the bottom right corner. ....36

Figure 14: Schematic representation of constructs that combine az19, gz27, gz93 and soluble mCherry with their native 5'- and/or 3'-UTRs. az19 UTRs are used in the case of soluble mCherry. UTRs are displayed in blue as small boxes flanking the proteins on the left and right for 5' and 3'-UTRs, respectively. Zeins az19, gz27, and gz93 are always located at the N-terminus (left side of fusion protein in this representation) while the fluorescent proteins EGFP and mCherry are located at the C-terminus (right side of fusion protein in this representation). The full name of each construct is displayed for reference as well. In constructs where no zein 5'-UTR is indicated, an arbitrary 5'-UTR of tobacco etch virus was used as a control. ....37

Figure 15: Evaluation of localization effects of native zein UTRs on incorporation efficiency of az19 into gamma zein PBs. Constructs of az19, gz27, and gz93 were extended to include their native 5'- and/or 3'-UTRs (UTRs of az19 were used on soluble mCherry) and tested in coexpression experiments. Gamma zein variants (gz27 and gz93) were fused to EGFP and are displayed in green in the left column. az19 were fused to mCherry and are displayed in red in the center column whereas the merge of both channels can be found in the column on the right side. Scale bars are only displayed in merged pictures but apply to all pictures of the same row. ....40

Figure 16: gz27 PBs have a wider size distribution in *Nicotiana benthamiana* with larger ones being approximately 1-2  $\mu\text{m}$  or smaller ones at 200 nm. ....42

Figure 17: gz93 formed large PBs  $> 1 \mu\text{m}$  much more consistently than gz27. ....42

|  |    |
|--|----|
| Figure 18: az19 always appears as clusters of small (~100 nm) PBs. ....  | 42 |
| Figure 19: gz16 either forms small PBs in the 100 nm range or large, loosely packed aggregates that can be around 10 µm in diameter. ....  | 43 |
| Figure 20: bz15 sometimes aggregates into larger particles above 1 µm but mostly it behaves like az19.....   | 44 |
| Figure 21: dz10 PBs tend to be variable in size as well. Frequently, they are below 1 µm but can also be above. ....   | 45 |
| Figure 22: az22 often crates irregularly shaped aggregates well above 2 µm but it can also appear as small granular structures.....  | 45 |
| Figure 23: Coexpression of az22 with either gz27 or gz93. The coexpression of gz27 and az22 caused small granules of az22 to intermix into or onto gz27 PBs (A). In other instances, az22 organized into larger structures that were able to surround gz27 PBs (B). In combination with gz93, az22 also sometimes appeared as large granular structures outside of gz93 (C), but in other cases az22 was found inside of gz93 PBs as large cores (D). ....   | 51 |
| Figure 24: Coexpression of gamma zeins along bz15 and alpha zeins. bz15 reliably colocalized with az22 in gz93 PBs and the incorporations were relatively big (A). When az22 was substituted by az19, fewer and smaller incorporations occurred (B). bz15 also remained on the outside when express along with gz27. az19 was also found together with bz15 on the outside but surprisingly, az19 was also found homogenously mixed with gz27 (C). Something that has not been seen in other coexpression experiments so far. Overall, this set of experiments showed that bz15 prefers to colocalize with alpha zein over gamma zeins. This is in contrast to what would be expected from what is observed in maize. .... | 52 |
| Figure 25: Coexpression of gamma zeins with bz15 and az19 with bz15. Unexpectedly, neither gz27 (A) nor gz93 (B) colocalized with bz15 even though gz27 and bz15 together form the shell in maize PBs. az19 and bz15 however, colocalized (C) as they did when expressed in combinations of three with either gz27 or gz93 (Figure 24 B+C). ....   | 53 |
| Figure 26: Coexpression of gz27 or gz93 together with gz16. gz16 homogenously colocalized into PBs of varying size (A). When neighboring cells expressed different ratios of gz27 and gz16, the diameter was affected. More gz16 meant smaller PBs and less led them to be bigger. Sometimes these two zeins would generate very large aggregates which resembled the ones seen with individual expression of gz16 (B). gz16 also interacted with gz93 where it was able to create various kinds of holes. In some cases, there would be only one center core made up by gz16 (C) but in other instances multiple holes occurred in the same PB (D). ....  | 54 |
| Figure 27: Coexpression of gamma and alpha zeins. As previously seen, gz16 created holes in gz93 PBs. In the presence of az22, these holes were filled by az22 whereas the concentrations of gz16 seemed to be higher in the interface between gz93 and az22 (A). In very rare cases, these gz16-induced holes also occurred in gz27 PBs where they were filled by az22 as well (B). When az19 was substituted for az22, az19 always remained outside of the PBs (C + D). These two combinations again confirmed that the hole-generating effect of gz16 works mainly on gz93 (D) but not gz27 (C). ....   | 55 |
| Figure 28: Coexpression of gz16 with other zeins. When gz16 and az22 formed small PBs (< 0.5 µm), the PBs intermixed but the two zeins did not localize in the same PBs (A). Colocalization of gz16 and az22 only occurred when they created large (> 1 µm) aggregates (B). In the case of az19, both zeins remained small and it is therefore difficult to assess whether individual PBs intermixed or if they colocalized (C). For the combination of bz15 with gz16 however, it was clear that these small PBs contained both zeins (D). ....   | 56 |

- Figure 29: Coexpression of dz10 together with other zeins. In panel (A) it can be seen that the cell in the top left corner only expressed dz10 whereas the cell at the bottom only expressed gz16. In both cases the PBs were rather small. However, in the cell that expressed both zeins, the PBs are larger than when they are individually expressed. In some cases, the generated larger aggregates that emitted signal for both zeins (B). When dz10 was coexpressed with az22 (C) or az19 (D), the PBs remained small but seemed to localize together (technical imperfection due to moving sample in row D)...57
- Figure 30: The effect of dz10 on the incorporation of alpha zeins into gamma zeins. dz10 was not able to facilitate the incorporation of az19 (A) or az22 (B) into PBs of gz27. However, both az22 (C) and az19 (D) integrated into PBs of gz93. These inclusions contained dz10 alongside the respective alpha zein. Unfortunately, large proportions of alpha zein remained on the outside surrounding the gz93 PBs. ....58
- Figure 31: Coexpressions investigating the effects of bz15 and on gamma zein PBs in the presence of a third zein. Combining gz27 with bz15 and dz10 yields structured PBs with an organization similar to native PBs. gz27 and bz15 colocalized in the shell whereas dz10 mostly resided in the core (A). This organization was turned around in the case of gz93. bz15 was found in the core along with dz10 and only gz93 comprised the shell (B). bz15 and gz16 together with gz27 created PBs that homogeneously emitted signal for all three zeins (C). Coexpression of bz16 and gz16 with gz93, however, produced layered PBs very reliably (D). A similar effect of gz16 was seen in other combinations as well. In this case, gz16 again caused small and big holes in gz93 PBs that were filled by both gz16 and bz15. Some of the gz16 signal, however, also came from the gz93 shell.....59
- Figure 32: Coexpression of gamma zeins and dz10. gz27 and dz10 homogeneously colocalized in PBs without visible structuring (A). Together with gz93, however, dz10 entered the PBs and was found as small cores inside of gz93 (B). The addition of gz16 to those combinations painted a very similar picture. gz27 + dz10 + gz16 formed PBs with all components homogeneously mixed (C) whereas dz10 appeared as core-structures in a matrix provided by colocalized gz93 and gz16 (D). ....60
- Figure 33: Coexpression of four zeins. When gz93 and gz16 are expressed alongside bz15 and az22, gz93 provides the shell of the PBs, gz16 is mostly found in the shell as well although some gz16 signal is also emitted from the core, but bz15 and az22 are the main constituents of the core in this combination (A). The PBs had a similar appearance when dz10 was used instead of az22. Again, gz93 provided the shell, the signal from gz16 was a bit more diffuse in this case, but bz15 and dz10 were mainly found in the core of the PBs (B). ....61
- Figure 34: Coexpression of az19 and az22. Both alpha zeins colocalized into small PBs but failed to integrate into gz93 PBs (A). This colocalization of alpha zeins was also reproduced in the absence of gz93 (B). ....62
- Figure 35: Spatial arrangement of zeins in native maize PBs and recombinant PBs from *Nicotiana benthamiana*. Lending and Larkins (1989) were one of the first ones to describe the distribution of different zeins in the PBs of maize. According to their findings, gamma and beta zeins together form the outer shell of the PB while alpha and delta zeins make up the inner core (A). More recent discoveries from Yao et al. (2016) updated the initial model by adding a distinct interface layer between the core and the shell. Within this interface layer, gz16 is located on the outside towards the gamma zein-rich shell and az22 is located on the inside towards the alpha zein-rich core (B). However, throughout many coexpression combinations in *Nicotiana benthamiana*, it became apparent that the localization pattern is different in recombinant zein PBs (C). These differences are: whenever bz15 was found inside of PBs, it localized in the core instead of the shell; az22 did not form an interface layer but localized in the core as well; in some combinations gz16 (\*) was found in the shell and in others in the core, only in the combination with gz93 and az22 did gz16 seem to form a layer separating the other two (Figure 27 A). ....64



## 11 Abbreviations

|        |  |
|--------|--|
| ANOVA  | Analysis of variance                                 |
| APC    | Antigen-presenting cell                              |
| BiP    | Binding immunoglobulin protein                       |
| CaMV   | Cauliflower mosaic virus                             |
| CLSM   | Confocal light scanning microscope                   |
| DC     | Dendritic cell                                       |
| dpi    | Days post infiltration                               |
| EGF    | Epidermal growth factor                              |
| EGFP   | Enhanced green fluorescent protein                   |
| ER     | Endoplasmic reticulum                                |
| FW     | Fresh weight   |
| GI     | gastro-intestinal                                    |
| GM-CSF | Granulocyte and macrophage colony stimulating factor |
| HCEC   | Human colonic epithelial cells                       |
| HIV    | Human immunodeficiency virus                         |
| HPV    | Human papillomavirus                                 |
| IgG    | Immunoglobulin G                                     |
| IL-6   | Interleukin 6  |
| ISCOMs | Immune-stimulating complexes                         |
| MES    | 2-(N-morpholino)ethanesulfonic acid                  |
| MHC    | Major Histocompatibility Complex                     |
| mKO2   | Monomeric Kusabira Orange 2                          |
| MMR-V  | measles-mumps-rubella vaccine                        |
| NA     | Numerical aperture                                   |
| OD     | Optical density                                      |
| PB     | Protein body   |
| PBs    | Protein bodies                                       |

|               |                                 |
|---------------|---------------------------------|
| PLGA          | Poly(lactic-co-glycolic)acid    |
| PMA           | Phorbol 12-myristate 13-acetate |
| PMT           | Photomultiplier tube            |
| PS            | Polystyrene                     |
| rpm           | rotations per minute            |
| SD            | Standard deviation              |
| slgA          | Secretory immunoglobulin A      |
| spp           | species pluralis                |
| SSPs          | Seed storage proteins           |
| TEV           | Tobacco etch virus              |
| TFF           | Tangential flow filtration      |
| TNF- $\alpha$ | Tumor necrosis factor alpha     |
| UTR           | Untranslated region             |
| WHO           | World Health Organization       |
| YEB           | Yeast extract broth             |

## 12 Appendix

### Amino acid sequences

#### az19

MAAKIFCLLMLLGLSASAATATIFPQCSQAPIASLLPPYLSPA VSSVCENPILQPYRIQQAI AAG  
ILPLSPLFLQQSSALLLQQLPLVHLLAQNIRAQQLQQLVL ANLAAYSQQQQFLPFNQLAALNSA  
SYLQQQLPFSQLSAAYPQQFLPFNQLTALNSPAYLQQQQLLPFSQLAGVSPATFLTQPQL  
LPFYQHAAPNAGTLLLQQLLPFNQLALTNPATAFYQQPIIGGALF

#### gz27

MRVLLVALALLALAASATSTHTSGGCGCQPPPPVHLPPP VHLPPP VHLPPP VHLPPP VHLPP  
PVHLPPP VHVPPP VHLPPP CHYPTQPPRPQHPQHPHPCPCQQPHSPCQLQGTGCVGS  
TPILGQCVEFLRHQCSPTATPYCSPQCQLRQCCQQLRQVEPQHRYQAIFGLVLQSILQQ  
QPQSGQVAGLLAAQIAQQLTAMCGLQQPTPCPYAAAGGVPH

#### gz93

MRVLLVALALLALAASATSTHTSGGCGCQPPPPVHLPPP VHLPPP VHLPPP VHLPPP VHLPP  
PVHLPPP VHVPPP VHLPPP CHYPTQPPRPQHPQHPHPCPCQQPHSPCQ

#### az22

MATKILALLALLALLVSATNAFIIPQCSLAPSASIPQFLPPVTSMGFEHPAVQAYRLQLALAAS  
ALQQPIAQLQQQSLAHLTLQTIATQQQQQQFLPSLSHLAVVNPVTYLQQQLLASNPLALANV  
AAYQQQQQLQQFMPVLSQLAMVNPVAVYLQLSSSPLAVGNAPTYLQQQLLQQIVPALTQLA  
VANPAAYLQQLLPFNQLAVSNSAAYLQQRQQLLNPLAVANPLVATFLQQQQQLLPYNQFSL  
MNPALQQPIVGGAI

#### gz16

MKVLIVALALLALAASAASSTSGGCGCQTTPFHLPPPFYMP PPFYLPQQQPQPWQYPTQP  
PQLSPCQQFGSCGVGSPFLGQCVEFLRHQCSPAATPYGSPQCQALQQQCCHQIRQV  
EPLHRYQATYGVVLQSFLQQQPQGELAALMAAQVAQQLTAMCGLQLQQPGPCPCNAAAG  
GVYY

#### bz15

MKMOVIVLVCLALSAASASAMQMPCPCAGLQGLYGAGAGLTTMMGAGGLYPYAEYLRQPQ  
CSPLAAAPYYAGCGQPSAMFQPLRQQCCQQMRMMDVQSVAAQLQMMMQLERAAAAS  
SSLYEPALMQQQQLLAAQGLNPMAMMMMAQNMPAMGGLYQYQLPSYRTNPCGVSAIIPP  
YY

#### dz10

MAAKMLALFALLALCASATSATHIPGHLPPVMPLGTMNPCMQYCM MQGLASLMACPSLM  
LQQLLALPLQTMPVMMPQMTPNMMSPLMMPSMMSPMVLP SMMSQMMMPQCHCDAVS  
QIMLQQQLPFMFNPMAMTIPPMFLQQPFVGA

## **EGFP**

MVSKGEELFTGVVPILVELDGDVNGHKFSVSGEGEGDATYGKLTCLKFICTTGKLPVPWPTLV  
TTLTYGVQCFSRYPDHMKQHDFFKSAMPEGYVQERTIFFKDDGNYKTRAEVKFEGDTLVN  
RIELKGIDFKEDGNILGHKLEYNNSHNVYIMADKQKNGIKVNFKIRHNIEDGSVQLADHYQQ  
NTPIGDGPVLLPDNHYLSTQSALS KDPNEKRDHMLLEFVTAAGITLGMDELYK

## **mCherry**

MVSKGEEDNMAIIEKFMRFKVHMEGSVNGHEFEIEGEGEGRPYEGTQTAKLKVTKGGPLPF  
AWDILSPQFMYGSKAYVKHPADIPDYKLSFPEGFKWERMNFEDGGVVTVTQDSSLQDG  
EFYKVKLRGTNFPDGPVMQKKTMGWEASSERMYPEDGALKGEIKQRLKLDGGHYDAE  
VKTTYKAKKPVQLPGAYNVNIKLDITSHNEDYTIVEQYERAEGRHSTGGMDELYK

## **mCitrine**

MVSKGEELFTGVVPILVELDGDVNGHKFSVSGEGEGDATYGKLTCLKFICTTGKLPVPWPTLV  
TTFGYGLMCFARYPDHMKQHDFFKSAMPEGYVQERTIFFKDDGNYKTRAEVKFEGDTLVN  
RIELKGIDFKEDGNILGHKLEYNNSHNVYIMADKQKNGIKVNFKIRHNIEDGSVQLADHYQQ  
NTPIGDGPVLLPDNHYLSYQSKLSKDPNEKRDHMLLEFVTAAGITLGMDELYK

## **mKO2**

MVSVIKPEMKMRYMDGSVNGHEFTIEGEGTGRPYEGHQEMTLRVTMAEGGPMPFAFDL  
VSHVFCYGHRVFTKYPEEIPDYFKQAFPEGLSWERSLEFEDGGSSASVSAHISLRGNTFYHK  
SKFTGVNFPADGPIMQNSVDWEPSTEKITASDGVKGDVTMYLKLEGGGNHCKQMKT  
KAAKEILEMPGDHYIGHRLVRKTEGNITEQVEDAVAHS

## **mTagBFP2**

MVSKGEELIKENMHMKLYMEGTVDNHHFKCTSEGEGKPYEGTQTMRIKVVVEGGPLPFAFDI  
LATSFLYGSKTFINHTQGIPDFFKQSFPEGFTWERVTTYEDGGVLTATQDTSLQDGCLIYV  
KIRGVNFTSNGPVMQKKT LGWEAFTETLYPADGGLEGRNDMALKLVGGSHLIANA KTTYRS  
KKPAKNLKMPGVYVVDYRLRIKEANNETYVEQHEVAVARYCDLPSKLGHKLN

# MARC TSCHOFEN

PhD in Plant Biotechnology

## Contact

Reutegasse 5  
6900 Bregenz, Austria  
Phone +43 650 4355741  
E-Mail [marc.tschofen@gmail.com](mailto:marc.tschofen@gmail.com)  
[linkedin.com/in/marc-tschofen](https://www.linkedin.com/in/marc-tschofen)

More than 10 years of experience in expression of therapeutic proteins in plants. From the age of 15, I was dedicated to the idea of working with plants in a pharmaceutical context. Earning my PhD in April 2020, it is time for me to transfer into the plant biotech industry. I am a determined and hard worker, I learn new skills fast and I find creative solutions to challenging problems.

## EDUCATION

---

- 2015 - 2020 **PhD program Biomolecular Technology of Proteins** (BioToP) at the University of Natural Resources and Life Sciences, Vienna  
Thesis: "Recombinant zein protein bodies for the encapsulation of therapeutic proteins" under the supervision of Prof. Eva Stoger
- 2011 - 2014 Master studies in **Applied Plant Sciences** at the University of Natural Resources and Life Sciences, Vienna  
Thesis: "Expression of recombinant IgA antibodies with humanized N- and O-glycans in plants" under the supervision of Assoc. Prof. Richard Strasser  
Graduated *summa cum laude*
- 2007 - 2011 Bachelor studies in **Agricultural Sciences** at the University of Natural Resources and Life Sciences, Vienna  
Thesis: "Subcellular Localization of Recombinant Bet v 1 - the Major Birch Pollen Allergen - in Dry and Rehydrated Pollen of *Nicotiana tabacum*" under the supervision of Prof. Eva Stoger

## EXPERIENCE

---

- 2019 **iBio CDMO, Bryan, TX**  
Visiting scientist for two months developing a process for the purification of oral vaccine nanoparticles expressed in *Nicotiana benthamiana*
- 2018 **NIBIO and NMBU, Oslo, Norway**  
Visiting scientist for three months working on oral vaccine nanoparticles from *Nicotiana benthamiana* for fish in aquaculture. Labs of Jihong Clarke and Erling Koppang
- 2009 - 2014 **University of Natural Resources and Life Sciences, Vienna, Austria**  
Laboratory technician working on recombinant expression of therapeutic proteins in *Nicotiana benthamiana* and *Nicotiana tabacum*  
Assistant teacher in practical lab course *Introduction in Cell Biology and Genetics* as well as lab course *Cell Factory - Plants*

- 2012 **John Innes Centre, Norwich, UK**  
Visiting scientist for two months engineering the triterpene pathway in yeast. Metabolic biology lab of Prof. Anne Osbourn
- 2009 **Prolactal GmbH, Hartberg, Austria**  
Intern in process development in dairy industry. Developed a new, enzymatic process to produce lactose-free milk from lab to manufacturing in one month
- 2007 - 2009 **Vorarlberger Kulturhäuser Betriebsgesellschaft, Bregenz, Austria**  
Carpenter of theater stage scenery for one month and construction worker for art exhibitions for an accumulated six months

## SKILLS

---

### Laboratory skills

|                   |  |
|-------------------|--|
| Molecular Biology | Molecular cloning, PCR, agarose gel electrophoresis, transformation of <i>E. coli</i> and <i>Agrobacteria</i>  |
| Upstream          | Growth of <i>Agrobacteria</i> , manual and vacuum-assisted agroinfiltration, protein expression in <i>Nicotiana benthamiana</i> and <i>Nicotiana tabacum</i>       |
| Downstream        | Clarification of extract via centrifugation and filter press, concentration of protein and buffer exchange via tangential flow filtration, affinity chromatography |
| Protein analysis  | SDS-PAGE, Western blotting, ELISA  |
| Nanoparticles     | Laser scanning confocal microscopy, transmission electron microscopy, flow cytometry, density gradient ultracentrifugation   |

### Languages

|           |                               |
|-----------|-------------------------------|
| German    | Native language               |
| English   | Full professional proficiency |
| Hungarian | Basic skills                  |

### Other skills

|                  |   |
|------------------|---|
| PC               | MS Office, GraphPad Prism, Leica LAS X, Beckman Coulter CytExpert, Adobe Photoshop, Adobe Illustrator, Adobe InDesign, Affinity Photo, Affinity Designer, EndNote, Mendeley |
| Driver's license | European Class B (cars up to 3.5 tons)  |

## PAPERS

---

Schweska J\*, **Tschofen M**\*, et al. **2020**. Plant-derived protein bodies as delivery vehicles for recombinant proteins into mammalian cells. *Biotechnology and Bioengineering*. doi:10.1002/bit.27273 \*shared first author

Mainieri D, Marrano C, Prinsi B, Maffi D, **Tschofen M**, et al. **2018**. Maize 16-kD gamma-zein forms very unusual disulfide-bonded polymers in the endoplasmic reticulum: implications for prolamin evolution. *Journal of Experimental Botany*. doi:10.1093/jxb/ery287

**Tschofen M** et al. **2016**. Plant Molecular Farming: Much More than Medicines. *Annual review of Analytical Chemistry*. doi:10.1146/annurev-anchem-071015-041706

Hofbauer A, Melnik S, **Tschofen M**, et al. **2016**. The Encapsulation of Hemagglutinin in Protein Bodies Achieves a Stronger Immune Response in Mice than the Soluble Antigen. *Frontiers in Plant Science*. doi:10.3389/fpls.2016.00142

Dicker M, **Tschofen M**, et al. **2016**. Transient Glyco-Engineering to Produce Recombinant IgA1 with Defined N-and O-Glycans in Plants. *Frontiers in Plant Science*. doi:10.3389/fpls.2016.00018

## CONFERENCES

---

**PBVAB**: Plant-based Vaccines, Antibodies & Biologics, Albufeira, Portugal, June 5 - 7, 2017

**RPP**: 9th International Conference on Recombinant Protein Production, Dubrovnik, Croatia, April 23 - 25, 2017

## ARTICLE

# Plant-derived protein bodies as delivery vehicles for recombinant proteins into mammalian cells

Jennifer Schwestka<sup>1</sup> | Marc Tschofen<sup>1</sup> | Stefan Vogt<sup>2</sup> | Sylvain Marcel<sup>3</sup> |  
 Johannes Grillari<sup>2,4,5</sup> | Marianne Raith<sup>6</sup> | Ines Swoboda<sup>6</sup> | Eva Stoger<sup>1</sup> 

<sup>1</sup>Department of Applied Genetics and Cell Biology, University of Natural Resources and Life Sciences, Vienna, Austria

<sup>2</sup>Department of Biotechnology, Institute of Molecular Biotechnology, University of Natural Resources and Life Sciences, Vienna, Austria

<sup>3</sup>Bio CDMO, Bryan, Texas

<sup>4</sup>Christian Doppler Laboratory for Biotechnology of Skin Aging, University of Natural Resources and Life Sciences, Vienna, Austria

<sup>5</sup>Ludwig Boltzmann Institute for Experimental and Clinical Traumatology, Vienna, Austria

<sup>6</sup>Biotechnology Section, FH Campus Wien, University of Applied Sciences Campus Vienna Biocenter, Vienna, Austria

## Correspondence

Eva Stoger, Department of Applied Genetics and Cell Biology, University of Natural Resources and Life Sciences, Muthgasse 18, 1190 Vienna, Austria.  
 Email: eva.stoger@boku.ac.at

## Funding information

Austrian Science Fund, Grant/Award Number: W1224

## Abstract

The encapsulation of biopharmaceuticals into micro- or nanoparticles is a strategy frequently used to prevent degradation or to achieve the slow release of therapeutics and vaccines. Protein bodies (PBs), which occur naturally as storage organelles in seeds, can be used as such carrier vehicles. The fusion of the N-terminal sequence of the maize storage protein,  $\gamma$ -zein, to other proteins is sufficient to induce the formation of PBs, which can be used to bioencapsulate recombinant proteins directly in the plant production host. In addition, the immunostimulatory effects of zein have been reported, which are advantageous for vaccine delivery. However, little is known about the interaction between zein PBs and mammalian cells. To better understand this interaction, fluorescent PBs, resulting from the fusion of the N-terminal portion of zein to a green fluorescent protein, was produced in *Nicotiana benthamiana* leaves, recovered by a filtration-based downstream procedure, and used to investigate their internalization efficiency into mammalian cells. We show that fluorescent PBs were efficiently internalized into intestinal epithelial cells and antigen-presenting cells (APCs) at a higher rate than polystyrene beads of comparable size. Furthermore, we observed that PBs stimulated cytokine secretion by epithelial cells, a characteristic that may confer vaccine adjuvant activities through the recruitment of APCs. Taken together, these results support the use of zein fusion proteins in developing novel approaches for drug delivery based on controlled protein packaging into plant PBs.

## KEYWORDS

bioencapsulation, molecular farming, plant-made pharmaceuticals, protein bodies, recombinant proteins.

## 1 | INTRODUCTION

Oral administration of pharmaceuticals is often the desired drug delivery route for reasons such as safety, patient compliance, and socioeconomic advantages (De Smet, Allais, & Cuvelier, 2014;

Sastry, Nyshadham, & Fix, 2000). Oral vaccines, for instance, have the additional benefit of being able to elicit not only immunoglobulin G-mediated serum immunity but also immunoglobulin A (IgA)-mediated mucosal immunity, thus providing an advantage since many pathogens enter the host through mucosal surfaces (Breedveld & van Egmond, 2019). However, a major challenge for oral therapeutics is the need for them to withstand

Jennifer Schwestka and Marc Tschofen contributed equally to the study.

This is an open access article under the terms of the Creative Commons Attribution License, which permits use, distribution and reproduction in any medium, provided the original work is properly cited.

© 2020 The Authors. *Biotechnology and Bioengineering* published by Wiley Periodicals, Inc.

the harsh conditions of the gastric system, such as low pH and digestive enzymes. To ensure that the active components remain intact upon arrival at their effector site, they need to be fortified to prevent degradation. One way to achieve such robustness is by encapsulating therapeutics into micro- or nanoparticles.

Zein, a prolamin-type storage protein from maize seeds, is extensively used for encapsulation purposes because it is biocompatible and biodegradable (Luo & Wang, 2014) and was generally recognized as safe for oral use by the US Food and Drug Administration in 1985 (Zhang et al., 2015). There are several ways in which zein can be used for encapsulation purposes. Most studies have used *in vitro* methods such as phase separation, spray drying, supercritical antisolvent technique, emulsification/solvent evaporation, or chemical crosslinking techniques (Zhang et al., 2016). Most *in vitro* encapsulation studies using zein have focused on the incorporation of poorly water-soluble, nonproteinaceous compounds like curcumin (Patel, Hu, Tiwari, & Velikov, 2010), aceclofenac (Karthikeyan, Vijayalakshmi, & Korrapati, 2014), quercetin (Penalva, González-Navarro, Gamazo, Esparza, & Irache, 2017), or alpha-tocopherol (Luo, Zhang, Whent, Yu, & Wang, 2011), but these methods have also been used to encapsulate lysozyme (Zhong & Jin, 2009) and the antioxidant proteins catalase and superoxide dismutase (S. Lee, Alwahab, & Moazzam, 2013; S. Lee, Kim, & Park, 2016).

Alternatively, zein-containing protein storage organelles, so-called zein protein bodies (PBs), found in maize endosperm cells (Lending & Larkins, 1989), may offer natural bioencapsulation strategies for recombinant oral pharmaceuticals. This assumption has been substantiated by experiments with rice seeds showing that the sequestration of recombinant proteins in endogenous storage organelles containing rice prolamins confers protection from digestive proteolysis after oral administration in an animal model (Nochi et al., 2007). A faster and more versatile method for encapsulating proteins into the protective environment of zein micro/nanocarriers is to create a fusion protein in which the protein of interest is fused to a partial sequence of zein. Expression of such fusion protein results in *in vivo* bioencapsulation in various production hosts, within newly induced storage organelles. Amongst the various classes of zeins:  $\alpha$  (19 and 22 kDa),  $\beta$  (15 kDa),  $\gamma$  (16, 27, and 50 kDa),  $\delta$  (10 kDa; Woo, Hu, Larkins, & Jung, 2001)—the 27 kDa  $\gamma$ -zein was identified as the key element that induces the formation of endogenous as well as recombinant PBs. Furthermore, it was discovered that the N-terminal 93 amino acids of 27 kDa  $\gamma$ -zein (abbreviated gz93 from here on) are sufficient to produce PBs in other plants, and even in heterologous expression systems such as fungal, insect, and mammalian cells (Llop-Tous et al., 2010; Torrent et al., 2009). Various proteins with different properties in terms of molecular mass and function, including growth factors (Torrent et al., 2009), viral vaccine candidate proteins (Hofbauer et al., 2016; Mbewana, Mortimer, Pêra, Hitzeroth, & Rybicki, 2015; Whitehead et al., 2014), and enzymes (Llop-Tous, Ortiz, Torrent, & Ludevid, 2011), have been successfully incorporated into newly induced PBs in plants like *Nicotiana benthamiana* when fused to gz93. *N. benthamiana* is frequently used for the production of biopharmaceuticals because

it is well suited for the transient expression of recombinant proteins, and this method offers advantages over other expression systems in terms of speed, safety, scalability, and reduced upstream production costs. However, the cost savings in the upstream process are sometimes offset by industrial downstream processes for the purification of biopharmaceuticals, which are often quite laborious and may account for approximately 70–80% of the total manufacturing costs regardless of the expression host (Schillberg, Raven, Spiegel, Rasche, & Buntru, 2019). In the case of orally delivered plant-made products, the complexity of the downstream process could be reduced and plant tissues could be administered after minimal processing, allowing to take maximum benefit of the competitive upstream production costs offered by plants.

Previously, it was reported that zein PBs can have an adjuvant effect when administered by injection. For example, the fusion of a therapeutic HPV vaccine candidate to the Zera® peptide, a self-assembly domain very similar to gz93, enhanced the immune responses in mice (Whitehead et al., 2014). Similarly, when we fused hemagglutinin-5 (H5) to gz93, the resulting PBs were able to elicit a strong immune response that was on par with soluble H5 plus Freund's complete adjuvant, while soluble H5 without adjuvant failed to induce an immune response (Hofbauer et al., 2016). Particulate formulations of antigens generally show this immunostimulatory effect and one possible explanation is that upon internalization of a single particle, many copies of the antigen enter the cell, whereas a much higher dose must be administered to achieve comparable local concentrations surrounding the cell (Colino et al., 2009; Snapper, 2018). Alternatively, the enhanced immune response may also be due to superior antigen display and stability or other immunostimulatory signals (Smith, Simon, & Baker, 2013). In addition, gz93 harbors eight repeats of a proline-rich domain (VHLPPP)<sub>8</sub> that closely resembles the sweet arrow peptide (VRLPPP)<sub>3</sub>, which is known for having cell-penetrating properties (Sánchez-Navarro, Teixidó, & Giralt, 2017).

In the present study, we focus on the potential of PBs for oral application. We explore a downstream procedure based on two consecutive tangential flow filtrations (TFFs) as a means to enrich the zein PBs from larger amounts of leaf tissue, and we investigate the internalization efficiency of zein PBs into cells of the mucosal lining by comparing the uptake of fluorescent gz93 PBs and polystyrene beads of comparable size. We demonstrate efficient PB internalization into intestinal epithelial cells as well as antigen-presenting cells (APCs). Finally, we analyze whether the epithelial cells secrete cytokines, which are known to recruit APCs.

## 2 | MATERIALS AND METHODS

### 2.1 | Molecular cloning

The coding sequences of gz93-enhanced green fluorescent protein (eGFP) and gz93-mTagBFP2 were designed *in silico* and synthesized by GeneCust, Europe. The sequences were then cloned into the pTRA vector, a derivative of pPAM (GenBank AY027531), by restriction

cloning using *Sma*I and *Xba*I cut sites. The translated sequence starts with the N-terminus of 27 kDa  $\gamma$ -zein (GenBank accession number: AF371261) including its native signal peptide and the first 93 amino acids of the mature protein (hence gz93), followed by a short flexible (GGGG)<sub>2</sub> linker, which finally connects to the eGFP or the monomeric blue fluorescent protein (mTagBFP2; Subach, Cranfill, Davidson, & Verkhusha, 2011). gz93-eGFP is expressed under control of a 35S promoter with a duplicated transcriptional enhancer and a 35S terminator, both originating from *Cauliflower mosaic virus*. In addition, the transcribed region contains a 5'-untranslated region from *Tobacco etch virus*, which confers the increased stability of the messenger RNA. Two matrix attachment regions of tobacco Rb7 (Halweg, Thompson, & Spiker, 2005) flank the promoter and terminator up- and downstream, respectively, to suppress transgene silencing.

## 2.2 | Plant material and agroinfiltration

*N. benthamiana* plants were cultivated in the soil in a growth chamber with a 16 hr photoperiod at 70% relative humidity and day/night temperatures of 26°C and 16°C, respectively. The gz93-eGFP and gz93-mTagBFP2 plasmids were transferred into chemically competent *Agrobacterium tumefaciens* GV3101-pMP90RK. Cultures of this *Agrobacterium* strain were inoculated from glycerol cryo-stocks and cultivated in YEB medium containing 25 mg/L kanamycin, 25 mg/L rifampicin, and 50 mg/L carbenicillin. Cultures were incubated at 28°C while shaking at 200 rpm. Before infiltration, the cultures were pelleted and washed twice with infiltration medium (10 mM MES pH 5.6, 10 mM MgCl<sub>2</sub>, 100  $\mu$ M acetosyringone) and adjusted to OD<sub>600</sub> 0.2 with infiltration medium. The infiltration of *N. benthamiana* leaves was performed manually with 1 ml syringes. Leaves were harvested 8 days postinfiltration (dpi) for the production of PBs for uptake assays, while smaller samples for size determination were harvested at 4 and 12 dpi as well.

## 2.3 | PB size determination

The diameter of gz93-eGFP PBs was determined at 4, 8, and 12 dpi by analyzing the maximum projected z-stacks of confocal laser scanning microscopy (CLSM) pictures. For each sample, a 5  $\times$  5 mm section was excised from the agroinfiltrated leaves of *N. benthamiana* and mounted on a glass slide with tap water as the immersion medium. The samples were observed under a Leica SP5 Confocal Laser Scanning Microscope using a  $\times$ 63 water immersion objective (NA 1.20). The Argon laser power was set to 16% and the 488 nm laser line was set to 2% output for the excitation of eGFP. Forty-eight pictures along the z-axes were recorded at a resolution of 1,024  $\times$  1,024 pixels for each picture with a step size of 1.1  $\mu$ m (bidirectional scanning at 400 Hz, 2x line averaging). Maximum projections of z-stacks were exported from Leica Software and analyzed using Adobe Photoshop. In total, 832, 986, and 821 individual PBs from at least three samples per time point were measured for 4, 8, and 12 dpi, respectively.

## 2.4 | Processing of plant material

*N. benthamiana* leaf material expressing gz93-eGFP or gz93-mTagBFP2 was harvested at 8 dpi and stored at -20°C until processing. Leaf material, 200 g, was homogenized in a Waring-type blender with the addition of 800 ml phosphate-buffered saline (PBS) extraction buffer (137 mM NaCl, 2.7 mM KCl, 10 mM Na<sub>2</sub>HPO<sub>4</sub>, 1.8 mM KH<sub>2</sub>PO<sub>4</sub>, pH 7.4) supplemented with 2% Triton X-100. The extract was further homogenized with a disperser (IKA ULTRA-TURRAX® S 25 N-10 G) and then repeatedly pelleted by centrifugation at 15,000 rcf for 30 min at 4°C. The supernatants were discarded, and the pellets were washed twice with PBS extraction buffer including 2% Triton X-100 and twice with PBS lacking Triton X-100. The resulting suspension was then filtered through a 180  $\mu$ m nylon mesh filter utilizing a vacuum-assisted bottle-top filter holder. Small amounts of antifoam Y-30 were added when necessary. This was then subjected to the first TFF using a nylon filter cloth with a 10  $\mu$ m cut-off. Since TFF systems with this pore rating were not available, we built a prototype TFF filter holder that can be equipped with any cloth or membrane. This filter holder provided a surface area of 96 cm<sup>2</sup> and was operated by a peristaltic pump. gz93-eGFP PBs passed through the 10  $\mu$ m filter and the permeate was washed and concentrated using a second TFF with a 0.65  $\mu$ m cut-off (CO2-E65U-07-N; Spectrum Labs). Once some of the permeate had passed the first filter, both systems could be operated simultaneously. The concentrated retentate was subjected to low-speed density centrifugation over a cushion of 40% CsCl (1.4225 g/cm<sup>3</sup>) at 4,800 rcf for 30 min at 20°C. The top layer was collected and washed twice with five sample volumes PBS, to remove CsCl, by pelleting at 21,000 rcf for 5 min at 20°C.

## 2.5 | Flow cytometry of PBs

Processed samples of gz93-eGFP PBs were measured in a V-bottom 96-well plate and data were collected for 10,000 events using a flow cytometer (CytoFlex S; Beckman Coulter). eGFP signal was excited at 488 nm and emission was measured at 525 nm. Forward, side scatter, and eGFP gain was set to 40, 24, and 50, respectively. To show the reproducibility of the method, three independent measurements, each including five replicates, were performed. Flow cytometry data were analyzed with CytExpert 2.3 (Beckman Coulter).

## 2.6 | Determination of nicotine content

Nicotine extraction was performed as described (Moghbel, Ryu, & Steadman, 2015). PBs derived from 50 mg of leaves (FW) were extracted for 2 hr in a 1-ml extraction solution (40% aqueous methanol containing 0.1% 1 N hydrochloric acid). The supernatant was collected and the pellet was re-extracted twice. The supernatants were combined and evaporated to dryness (Savant Speed Vac SC-110 with cooling unit RVT-100; Savant instruments, Holbrook). For comparison, 50 mg of leaves of *N. benthamiana* were ground and extracted according to the same protocol. A nicotine

standard (N0267; Merck, Germany) was used for quantification. For high performance liquid chromatography-electrospray ionization-tandem mass spectrometry (HPLC-ESI-MS/MS) measurements, the sample was dissolved in 12  $\mu$ l of 80 mM ammonium formate buffer (pH 3.0) and 5  $\mu$ l was loaded on a BioBasic C18 column (BioBasic 18, 150  $\times$  0.32 mm, 5  $\mu$ m; Thermo Fisher Scientific, Waltham, MA) using a Dionex UltiMate 3000 system directly linked to a QTOF instrument (maXis 4G ETD; Bruker). A gradient from 99.0% to 6.2% of solvent A and 1.0–93.8% of solvent B (solvent A: 80 mM ammonium formate buffer at pH 3.0, B: 80% acetonitrile and 20% A) was applied over a 10 min interval at a flow rate of 6  $\mu$ l/min. The mass spectrometer was equipped with the standard ESI source and measurements were performed in positive ion, DDA mode (= switching to MSMS mode for eluting peaks). MS scans were recorded (range, 100–1,500  $m/z$ ) and the four highest peaks were selected for fragmentation. Instrument calibration was performed using an ESI calibration mixture (Agilent).

## 2.7 | Mammalian cell culture

Human colonic epithelial cells (HCEC-1CT, CkHT-039-0229; Evercyte GmbH, Vienna) were routinely grown at 37°C under a humidified atmosphere of 7% CO<sub>2</sub> in DMEM:199 (4:1/Biochrom, Germany) supplemented with 2% cosmic calf serum (HyClone, Logan, UT), EGF (25 ng/ml), hydrocortisone (1 g/ml), insulin (10 g/ml), transferrin (2 g/ml), and sodium selenite (5 nM; all from Sigma-Aldrich, St. Louis, MO). Differentiation of cells toward colonic epithelial cells (described by Roig et al., 2010) was induced by culturing cells for 48 hr in DMEM:199 (4:1) supplemented with 0.1% cosmic calf serum, EGF (1.25 ng/ml), hydrocortisone (1  $\mu$ g/ml), insulin (10  $\mu$ g/ml), transferrin (2  $\mu$ g/ml), sodium selenite (5 nM), and GSK-2 inhibitor IX (5  $\mu$ m; Merck).

U937 cells (ATCC CRL 1593) were cultivated in Roswell Park Memorial Institute 1640 media (Biochrom, Germany) containing 10% heat-inactivated fetal calf serum and 4 mM L-glutamine (Sigma-Aldrich). Differentiation of cells toward macrophage-like cells was induced by culturing  $7 \times 10^5$  cells/ml in medium containing 100 nM phorbol 12-myristate 13-acetate for 24 hr. The medium was changed to routine medium and cells were cultivated for further 48 hr until the cells attached to the surface showing the development of a dendritic-like morphology.

## 2.8 | PB uptake and flow cytometry of HCEC cells

For uptake studies, the medium was supplemented with 100 units/ml of penicillin, and 100  $\mu$ g/ml of streptomycin (Sigma-Aldrich) and  $2 \times 10^4$  cells/cm<sup>2</sup> were seeded and differentiated for 48 hr until confluence was reached. On the basis of the results from the quantification of PBs using a flow cytometer, cells were incubated with 150 gz93-eGFP PBs/cell at 37°C ( $n = 3$ ) for 2, 6, 12, 18, and 24 hr. Before cell detachment using 0.1%/0.02% Trypsin/EDTA for 5 min, the cells were washed thoroughly with PBS to remove the remaining particles. The uptake of fluorescent particles into the cells

was analyzed in a flow cytometer (CytoFlex S; Beckman Coulter). Yellow-green-labeled 1- $\mu$ m polystyrene microspheres (F13081; Thermo Fisher Scientific) were used for comparison. As a negative control, cells were kept for 6 hr at 4°C to prevent active particle uptake. The negative control was carried out with 150 gz93-eGFP PBs or polystyrene microspheres (PS beads) per cell, respectively, and the signal obtained was subsequently subtracted from the fluorescent signal obtained from cells incubated at 37°C.

The supernatant of cells was collected after 24 hr of incubation either with or without gz93-eGFP PBs or PS beads, centrifuged for 15 min with 500 rcf at 4°C, and stored at -80°C until analysis of the cytokine content. Cytokines (interleukin-6 [IL-6], granulocyte-macrophage colony-stimulating factor [GM-CSF]) secreted into the media by HCEC-1CT cells, were measured using the MILLIPLEX® MAP Human Cytokine/Chemokine panel (HCYTOMAG-60K; Merck Millipore, Burlington, MA). As a positive control, cells were incubated for 24 hr with 200 ng/ml tumor necrosis factor- $\alpha$  (Sigma-Aldrich) to induce cytokine secretion.

## 2.9 | Microscopy of mammalian cells

HCEC cells were seeded in eight-well microslides (Cat #80826; ibidi, Gräfelfing, Germany) and differentiated after a cell number of  $3 \times 10^4$  cells/cm<sup>2</sup> was reached. After incubation with gz93-eGFP PBs for 4 hr, cells were washed three times with PBS. To visualize the cell nuclei, cells were stained for 5 min with 2  $\mu$ g/ml Hoechst 33342 (H1399; Thermo Fisher Scientific). In addition, cells were incubated for 5 min at 37°C with 5  $\mu$ g/ml of the lipophilic cell membrane dye FM4-64 (T13320; Thermo Fisher Scientific). The cellular uptake of PBs into HCEC-1CT was confirmed by CLSM using a Leica TCS SP8 with a  $\times 63$  water immersion objective (NA 1.20; Leica Microsystems, Wetzlar, Germany; lasers: diode 405 nm, white light laser 488 nm, 565 nm; detectors: HyD 432–472 nm, PMT 503–515 nm). Z-stacks were generated with a step size of 0.7  $\mu$ m.

U937 cells were incubated for 2 hr with gz93-eGFP and gz93-mTagBFP2 PBs at 37°C. Lysosomes of cells were loaded by pulsing cells with 0.1 mg/ml Alexa Fluor 647 Dextran for 4.5 hr, and then cells were studied for 2 hr. Cellular uptake of PBs into U937 cells was confirmed by CLSM as described above.

## 3 | RESULTS

### 3.1 | Gz93-eGFP PBs produced in *N. benthamiana* leaves are enriched by a filtration-based process

For the production of fluorescent recombinant PBs, eGFP was genetically fused to the C-terminus of gz93 connected by a flexible (GGGG)<sub>2</sub> linker. The resulting construct (gz93-eGFP) was transferred to leaves of *N. benthamiana* by agroinfiltration and the formation of spherical PBs was confirmed by CLSM (Figure S1A). The size distribution of PBs was analyzed at 4, 8, and 12 dpi,

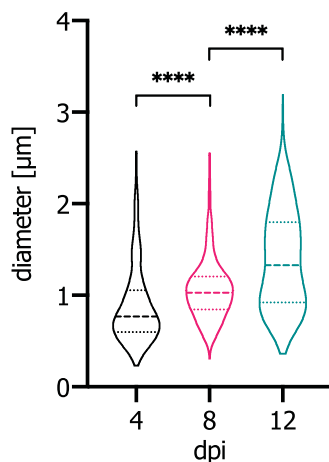


**FIGURE 1** Size determination of gz93-eGFP PBs. Samples of *Nicotiana benthamiana* were analyzed by CLSM at 4, 8, and 12 dpi. The diameter of PBs increases significantly over time as determined by one-way ANOVA with post hoc Tukey's test (\*\*\*\* $p < .0001$ ). ANOVA, analysis of variance; CLSM, confocal laser scanning microscope; dpi, days post infiltration; eGFP, enhanced green fluorescent protein; PBs, protein bodies [Color figure can be viewed at wileyonlinelibrary.com]

and median diameters of 0.77 ( $SD \pm 0.43$ ), 1.03 ( $SD \pm 0.34$ ), and 1.33 ( $SD \pm 0.55$ )  $\mu\text{m}$  were determined, respectively (Figure 1), indicating that gz93-eGFP particles keep increasing in size. We chose to harvest PBs at 8 dpi with a median diameter of 1.03  $\mu\text{m}$  for cellular uptake studies.

To obtain sufficient amounts of PBs, we developed a new downstream procedure for the enrichment of zein PBs that is based on a combination of filtration steps (Figure 2) and therefore more easily scalable than previously described processes based on ultracentrifugation (Hofbauer et al., 2016; Whitehead et al., 2014). Our procedure comprises initial washing steps with buffer containing Triton X-100 to solubilize membranes and to remove soluble host proteins and other compounds from the insoluble fraction. This was followed by coarse straining through a 180  $\mu\text{m}$  mesh and two subsequent TFFs with pore sizes of 10 and 0.65  $\mu\text{m}$ , respectively. The first TFF removes large cell debris while gz93-eGFP PBs pass through

the filter. The second TFF step was carried out to remove additional soluble host proteins and particles that are smaller than gz93-eGFP PBs. Through this procedure, it was possible to reduce the sample volume and concentrate it by a factor of 100. As a result, much more of the sample could be subjected to centrifugation over a cushion of 40% CsCl (1.4225  $\text{g}/\text{cm}^3$ ) that allows separating particles with a higher density than gz93-eGFP PBs (e.g., starch granules). In addition, this step is performed at 4,800 rcf, and this enables more of the sample to be processed compared with procedures where centrifugation is done at ultrahigh speeds (>50,000 rcf).

The resulting preparations of gz93-eGFP PBs were evaluated by flow cytometry. This method allowed us to identify two populations of particles with distinct fluorescence properties (Figure S2). In agreement with visual inspection by confocal microscopy, we concluded that the population of fluorescent particles represents gz93-eGFP PBs while the rest is probably cell debris. The mean concentration of fluorescent particles ( $n = 3$ ) was  $3.18\text{E}+06$  events/ $\mu\text{l}$  ( $SD \pm 13.2\%$ ) corresponding to  $5.12\text{E}+07$  gz93-eGFP PBs/g fresh weight of leaves.

The nicotine levels of *N. benthamiana* leaves and of the gz93-eGFP PB preparation were determined using HPLC-ESI-MS/MS (Table S1). The nicotine content in *N. benthamiana* leaves was around 47,500 ng/g, whereas the residual nicotine content in a PB sample derived from 1 g of leaves was 3.89 ng ( $SD \pm 0.2$ ), demonstrating that during the downstream procedure, nicotine was depleted by a factor of  $1.22\text{E}+04$ . The residual amount of nicotine is comparable with the nicotine content found in some vegetables. For example, the levels of nicotine in the edible parts of tomato and eggplant are 3–7 ng/g (Moldoveanu, Scott, & Lawson, 2016), and according to Andersson, Wennström, and Gry (2003), the average nicotine exposure from consumption of vegetables is approximately 1,000 ng/day.

### 3.2 | Gz93-eGFP PBs are endocytosed by human colon epithelial cells and stimulate cytokine release

To demonstrate the endocytosis of zein PBs into cells of the human intestinal barrier, we used the human colon epithelial cell line HCEC-1CT (immortalized by hTERT and CDK4), which maintains expression

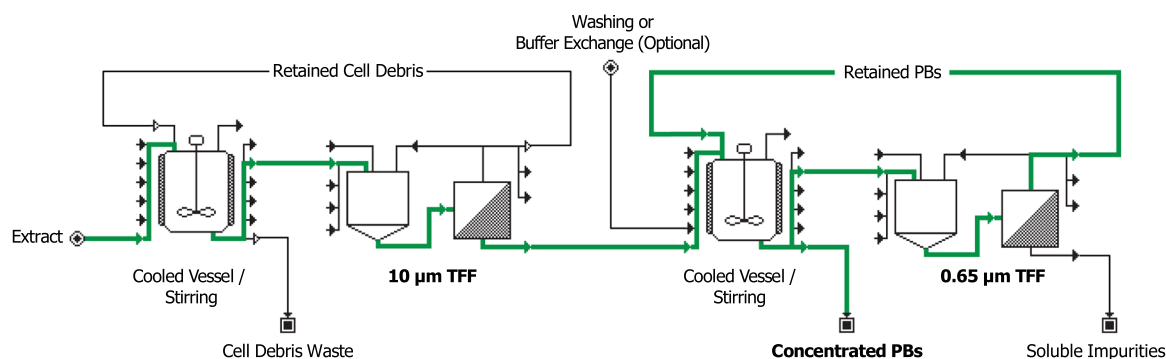


**FIGURE 2** A scalable process for the enrichment of zein PBs, based on two consecutive tangential flow filtrations. At the first step, cell debris is retained by a 10- $\mu\text{m}$  nylon filter while PBs are able to pass and the second step concentrates the PBs while allowing soluble contaminants to permeate. In this process flow chart, the path of PBs is highlighted in green. PBs, protein bodies [Color figure can be viewed at wileyonlinelibrary.com]

of cell-type-specific markers and functions of colon epithelial cells (Roig et al., 2010). The uptake of gz93-eGFP PBs into HCEC-1CT cells was demonstrated by CLSM and quantified by flow cytometry. CLSM images showed that cells are able to take up gz93-eGFP PBs within 4 hr of incubation (Figure 3a-d). The cellular internalization of a gz93-eGFP PB was confirmed by providing optical sections (xy-) with xz- and yz-projections (shown in Figure 3e), which allowed a clear differentiation between extracellular and internalized PBs. Furthermore, the internalization is proven by the overlay of the green signal, originating from the gz93-eGFP PB, and the red signal emitted by FM4-64 reported to stain endocytic membranes (Hansen, Rasmussen, Niels-Christiansen, & Danielsen, 2009).

A second experiment was carried out to quantitatively assess the uptake of PBs by flow cytometry and to compare the uptake efficiencies of PBs and PS beads. On the basis of the quantification of fluorescent events per  $\mu\text{l}$ , 150 gz93-eGFP PBs or PS beads per cell were added to in vitro cultures of HCEC-1CT cells and incubated for 2, 6, 12, 18, and 24 hr. Endocytosis of gz93-eGFP PBs occurred faster than that of PS beads, as indicated by a sharper increasing curve for the PBs, reaching a plateau after 12 hr (Figure 4). Mean values after 12 hr reached 66.5% ( $SD \pm 6.2$ ) and 43.5% ( $SD \pm 4.9$ ) for gz93-eGFP PBs and PS beads, respectively. The difference of 22.9% ( $SD \pm 4.6$ ) was significant in Student's *t* test ( $p < .01$ ). Also, after exposure for 18 and 24 hr, the overall number of fluorescent cells incubated with PS beads remained below the levels obtained with gz93-eGFP PBs (*t* test;  $p < .05$ ).

Having confirmed that human colon epithelial cells are able to endocytose gz93-eGFP PBs, we investigated whether endocytosis might lead to the secretion of cytokines that can activate the immune

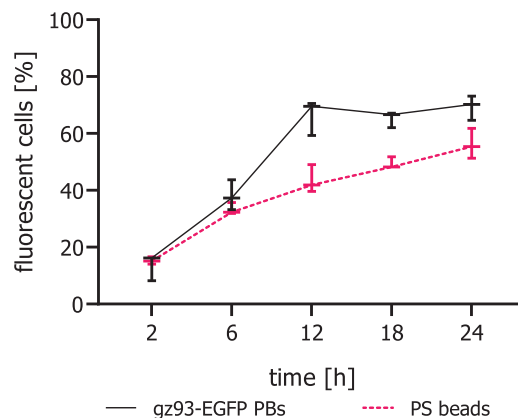


**FIGURE 4** Uptake of gz93-eGFP PBs by HCEC-1CT cells in comparison to fluorescent polystyrene beads. The relative number of fluorescent HCEC-1CT cells was determined by flow cytometry at the indicated time points. Values are shown as medians with their 95% confidence interval. eGFP, enhanced green fluorescent protein; PBs, protein bodies [Color figure can be viewed at wileyonlinelibrary.com]

system. Amongst others, the cytokine GM-CSF is known to have an activating effect on APCs, like macrophages and dendritic cells (Hamilton, 2002). We thus collected the culture medium supernatants from the uptake assays ( $n = 3$ ) and subjected them to Luminex assays. The secretion of GM-CSF was only elevated upon administration of 150 gz93-eGFP PBs per cell but not after treatment with the same amount of PS beads (Figure 5a). IL-6 levels were also significantly increased upon incubation with gz93-eGFP PBs as compared with the same dose of PS beads (Figure 5b).

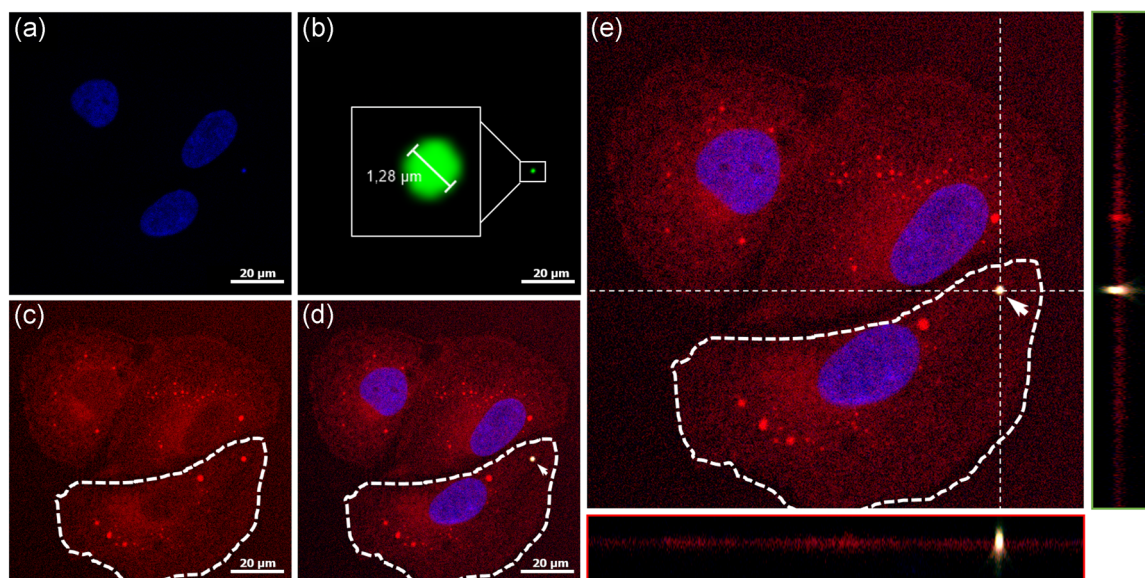


**FIGURE 3** HCEC-1CT cells have internalized gz93-eGFP PBs after 4 hr of incubation. The cell nucleus was stained with Hoechst 33342, displayed in blue (a), gz93-eGFP PBs emit green fluorescence (b), and the cell membrane and intracellular structures were stained in red with FM4-64 (c). When all channels are merged (d) an orange signal results from the overlay of the green and red fluorescence that indicates the internalization of gz93-eGFP PB into HCEC-1CT cells. The cell was imaged in 32 sections (with a step size of 0.7  $\mu\text{m}$ ), and the cell is shown in the xy-axis at  $z = 11$ . yz- (e, green panel) and xz-projections (e, red panel) clearly confirm the internalization of the analyzed PB (arrow). The bar represents 20  $\mu\text{m}$ . eGFP, enhanced green fluorescent protein; PBs, protein bodies [Color figure can be viewed at wileyonlinelibrary.com]

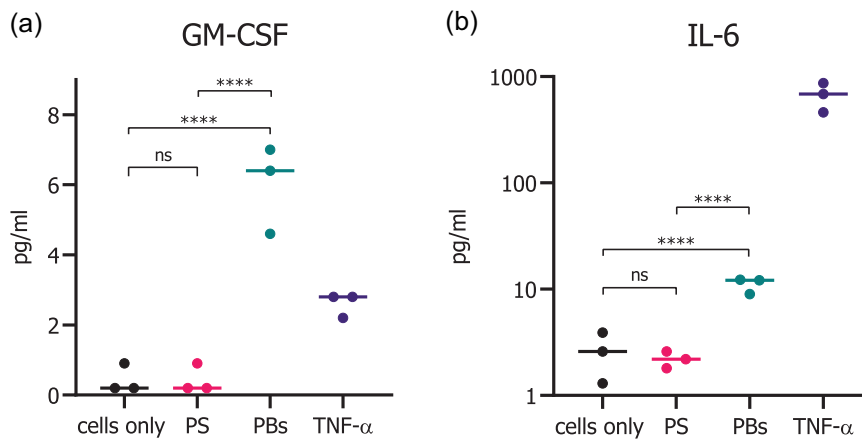


**FIGURE 5** Cytokine secretion of HCEC-1CT cells after 24 hr of incubation with gz93-eGFP PBs and PS beads. Cells incubated with gz93-eGFP PBs showed a significant increase in GM-CSF and IL-6 secretion compared with cells treated with polystyrene beads. Untreated cells (cells only) were used as a negative control and TNF- $\alpha$  treated cells as a positive control. Values for three independent experiments are shown and the median values are indicated.  $^{ns}p > .05$ ,  $^{****}p \leq .0001$ . eGFP, enhanced green fluorescent protein; GM-CSF, granulocyte-macrophage colony-stimulating factor; IL-6, interleukin-6; PBs, protein bodies; TNF- $\alpha$ , tumor necrosis factor- $\alpha$  [Color figure can be viewed at [wileyonlinelibrary.com](#)]

### 3.3 | PBs are taken up by immune cells

We then investigated the uptake of fluorescent PBs into immune cells using the human myelomonocytic cell line U937. Cells were first matured and differentiated as could be seen by decreased cell

proliferation and attachment to the surface. After 2 hr, most of the cells had taken up multiple gz93-eGFP PBs (Figure 6a,b). To obtain information about the localization of the internalized particles, we visualized the endosomal compartments of those cells with Dextran Alexa Fluor 647, which is known to be internalized in late endosomes

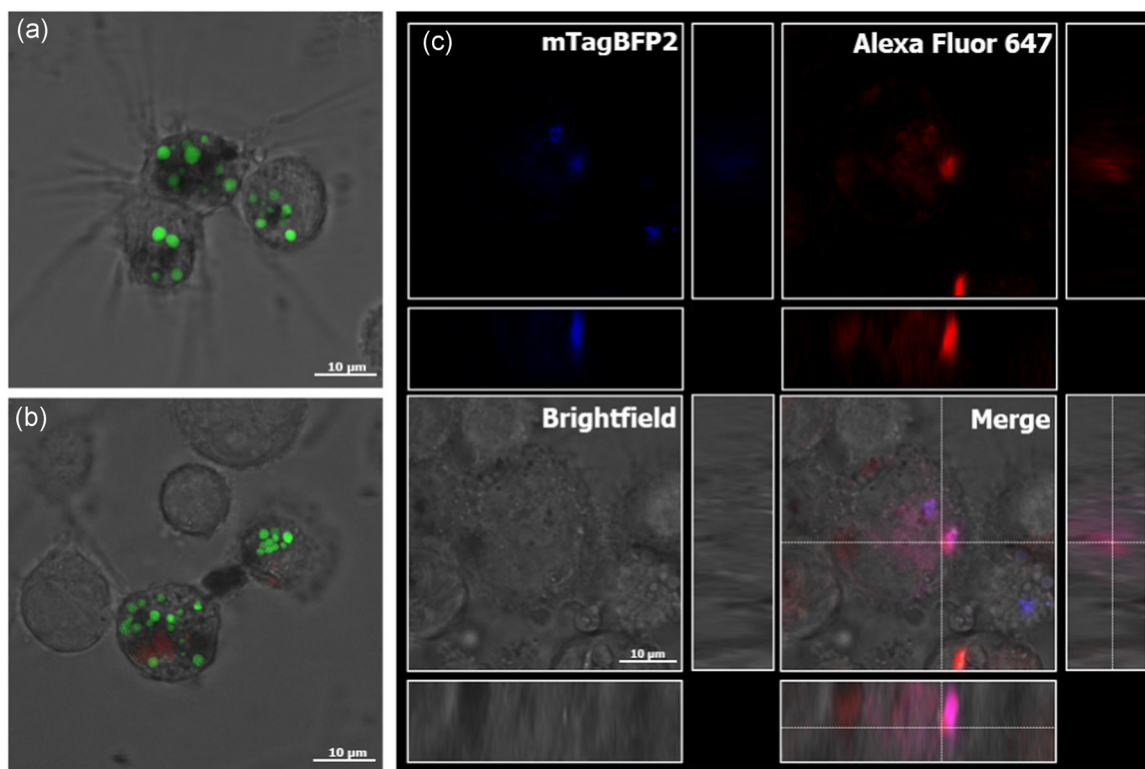


**FIGURE 6** The uptake of gz93-eGFP and gz93-mTagBFP2 PBs into U937 cells was confirmed by CLSM. Upon PMA treatment, cells attached to the vessel surface and exhibited morphological changes such as the growth of dendrite-like structures (a). Endosomal compartments were loaded and visualized with Alexa Fluor 647 Dextran (red, b). Colocalization of blue fluorescent gz93-mTagBFP2 PBs with endosomal compartments (red) results in a purple signal (c, merge). The bar represents 10  $\mu$ m. CLSM, confocal laser scanning microscope; eGFP, enhanced green fluorescent protein; PBs, protein bodies; PMA, phorbol 12-myristat-13-acetat [Color figure can be viewed at [wileyonlinelibrary.com](#)]

after endocytosis (Johnson, Ostrowski, Jaumouillé, & Grinstein, 2016). Since eGFP fluorescence is not stable in the acidic environment of late endosomes, we also used for this experiment PBs containing mTagBFP2, a blue fluorescent protein variant with a pKa of  $2.7 \pm 0.2$  (Subach et al., 2011). In the gz93-mTagBFP2 PBs, GFP was replaced with mTagBFP2, but otherwise, they were produced and recovered in the same manner as described for the gz93-eGFP PBs and had a similar appearance and size (Figure S1B). We were able to observe the colocalization of gz93-mTagBFP2 PBs in compartments stained with Dextran Alexa Fluor 647 (Figure 6c). It is, therefore, likely that the PBs are transported to the late endosomes, where usually antigen processing takes place.

## 4 | DISCUSSION

The induction of mucosal immunity by subunit vaccines is a promising prophylactic strategy, which is especially effective against enteric infections (Ghaffari Marandi, Zolfaghari, Kazemi, Motamedi, & Amani, 2019; Qadri, Svennerholm, Faruque, & Sack, 2005; Shojaei Jeshvaghani et al., 2019). However, protein-based oral vaccines require the protection of the antigen to ensure sufficient stability and transport to the intestine and the underlying immune system (Davitt & Lavelle, 2015; Kour, Rath, Sharma, & Goyal, 2018). Encapsulation of antigenic payload in nanoparticles made of chitosan or synthetic polymers like poly(DL-lactico-glycolic acid) (PLGA) provides such protection and has been used as a successful strategy to induce sIgA antibodies upon oral administration (Edelman et al., 1993; Fattal, Pecquet, Couvreur, & Andrement, 2002).

In this study, we focused on using zein PBs as alternative oral drug delivery vehicles since they combine several beneficial properties: Zein PBs have been shown to be recalcitrant against digestion by various proteases (S. H. Lee & Hamaker, 2006), have an adjuvant effect (Hofbauer et al., 2016; Whitehead et al., 2014), and they can mediate the sustained release of in vitro encapsulated small molecule drugs and even DNA (Acevedo et al., 2018; Farris, Brown, Ramer-Tait, & Pannier, 2017; Regier, Taylor, Borczyk, Yang, & Pannier, 2012; Zhang et al., 2015). In addition, the encapsulation in zein PBs can be achieved directly in the plant production host as an integral part of the upstream process.

For the induction of a mucosal immune response, uptake of an antigen at the intestinal surface is crucial. However, little is known about the ability of zein PBs to interact with mammalian cells. We have, therefore, investigated the uptake of fluorescent zein PBs into human intestinal epithelial and APCs. We could show that the PBs are internalized into intestinal epithelial cells at a higher rate than synthetic polystyrene beads. After 12 hr of incubation, the proportion of cells that had taken up fluorescent PBs reached 66.5% ( $SD \pm 6.2$ ). In contrast, after 12 hr of incubation with PS beads, only 43.5% ( $\pm 4.9$ ) of cells had internalized PS particles, and the number of fluorescent cells reached only 56.1% ( $\pm 5.3$ ) after 24 hr. This enhanced uptake efficiency of PBs might be due to the amphipathic proline-rich repeat found in the N-terminal sequence of  $\gamma$ -zein, which favors interaction with membranes (Kogan et al., 2004) and is assumed to have cell-penetrating effects that could

promote cellular uptake (Fernández-Carneado, Kogan, Castel, & Giralt, 2004).

In addition to the uptake of fluorescent PBs, we also showed an immunostimulatory effect on the cells, resulting in an increased secretion of chemoattractant molecules such as GM-CSF. GM-CSF is involved in the differentiation of granulocytes and macrophages and in the activation and proliferation of neutrophils, macrophages, and dendritic cells (Hamilton, 2002). With respect to mucosal immunization, the presence of GM-CSF was shown to increase antigen-specific antibody production (Okada et al., 1997). GM-CSF also promotes IL-6 secretion (Evans, Shultz, Dranoff, Fuller, & Kamdar, 1998), and accordingly IL-6 levels were also elevated when cells were subjected to PBs. Both chemokines play a pivotal role in the initiation of a humoral response to antigenic proteins (Tada, Hidaka, Kiyono, Kunisawa, & Aramaki, 2018), and IL-6 has been explored as a molecular adjuvant for mucosal vaccines (Rath et al., 2013; Su et al., 2008; Thompson & Staats, 2011). The observed cytokine release indicates the PB formulation's potential to enhance immunity and to exert an adjuvant effect, which is in agreement with the findings of Whitehead et al. (2014) and Hofbauer et al. (2016).

In addition to antigen uptake via intestinal epithelial cells, dendritic cells can capture antigens directly from the intestinal lumen by extending dendrites through the epithelium (Rescigno et al., 2001). Since GM-CSF is known to recruit dendritic cells to the subepithelial layer (Egea, Hirata, & Kagnoff, 2010), it is feasible that its secretion would lead to an increased number of dendrites reaching through tight junctions. Therefore, we investigated the uptake of PBs into APCs using the monocytic model cell line U937 (Altaf & Revell, 2013). APCs have the ability to internalize particles of various sizes with high efficiency. CLSM images confirmed the uptake of multiple PBs per cell. To obtain information about the subcellular localization of the internalized particles, we visualized the endosomal compartments with Dextran Alexa Fluor 647 and we used PBs containing a blue fluorescent protein that remains stable in the acidic environment found in late endosomes and lysosomes. Indeed, several particles colocalized with fluorescently labeled endosomal organelles, indicating that PBs might be processed within the endolysosomal system. From there, peptides can be loaded onto major histocompatibility complex class II molecules, which is the prerequisite for a successful immune response (Blum, Wearsch, & Cresswell, 2013; Roche & Furuta, 2015).

Particulate vaccine strategies have been reported to be effective at lower antigen doses compared to soluble formulations (De Smet et al., 2014), but oral vaccines generally require a higher dose of antigen to induce an immune response when compared to traditional parenteral immunizations (Pavot, Rochereau, Genin, Verrier, & Paul, 2012). This presents a challenge in the development of oral vaccine applications, and the corresponding production platforms need to be highly scalable. Even though plant-based production systems are very flexible with respect to upstream production, the downstream processing procedure often includes rate-limiting bottlenecks. For example, in most previous reports, the isolation of PBs from leaf material involved a density gradient ultracentrifugation step (Hofbauer et al., 2016; Joseph et al.,

2012; van Zyl, Meyers, & Rybicki, 2017). In the present study, the PBs were recovered by a newly established enrichment process based on several low-speed centrifugations and TFF steps, which can be easily adapted to kg amounts of leaf material without the need to invest in expensive large equipment for continuous ultracentrifugation. The removal of nicotine during the process was demonstrated, and the residual amount of nicotine in the sample was comparable to the nicotine content found in widely consumed vegetables (Moldoveanu et al., 2016). We have also demonstrated that fluorescent zein PBs can be analyzed and quantified by flow cytometry. It is likely that the procedure can also be adapted for nonfluorescent particles by using antigen-specific antibodies with fluorescent labels, thereby providing a general procedure for quality control of particulate formulations. It is important to note that oral vaccine formulations do not require the extensive purification and sterile conditions necessary for injected formulations, and downstream processing procedures reported for plant-made oral vaccine candidates range from simple homogenization or minimal processing of plant material to partial purification (Chan & Daniell, 2015; Loza-Rubio et al., 2012; Merlin, Pezzotti, & Avesani, 2017; Pniewski et al., 2018). The presence of plant-derived contaminants such as cell wall debris or starch particles, which cannot be completely removed by filtration and density centrifugation steps, are therefore unlikely to constitute a regulatory problem. On the contrary, biocompatible plant constituents, such as starch microparticles, have even been studied as vaccine adjuvants (Rydell & Sjöholm, 2004; Stertman, Lundgren, & Sjöholm, 2006).

In conclusion, we have shown that zein PBs produced in *N. benthamiana* leaves can be recovered by a newly developed filtration-based downstream procedure and we observed their efficient internalization into cultured cells of the intestinal epithelium as well as APCs. These results support the further development of novel approaches for in planta protein drug encapsulation and delivery, including the design of functionalized multicomponent PBs with defined structures and uptake kinetics for the bioencapsulation of pharmaceutical proteins.

## ACKNOWLEDGMENTS

The authors would like to acknowledge the financial support by the Austrian Science Fund FWF (W1224). The cytokine measurement was performed by the Institute of Immunology at the Medical University of Vienna and nicotine measurement was performed by Daniel Maresch at the BOKU Department of Chemistry. Dr. Berenice Carrillo is acknowledged for critically reading the manuscript.

## CONFLICT OF INTERESTS

The authors declare that there are no conflict of interests.

## ORCID

Eva Stoger  <http://orcid.org/0000-0002-7651-7992>

## REFERENCES

- Acevedo, F., Hermosilla, J., Sanhueza, C., Mora-Lagos, B., Fuentes, I., Rubilar, M., ... Alvarez-Lorenzo, C. (2018). Gallic acid loaded PEO-core/zein-shell nanofibers for chemopreventive action on gallbladder cancer cells. *European Journal of Pharmaceutical Sciences*, 119, 49–61. <https://doi.org/10.1016/j.ejps.2018.04.009>
- Altaf, H., & Revell, P. A. (2013). Evidence for active antigen presentation by monocyte/macrophages in response to stimulation with particles: The expression of NF $\kappa$ B transcription factors and costimulatory molecules. *Inflammopharmacology*, 21(4), 279–290. <https://doi.org/10.1007/s10787-013-0170-z>
- Andersson, C., Wennström, P., & Gry, J. (2003). *Nicotine alkaloids in Solanaceous food plants* (TemaNord 2003:531). Copenhagen, Denmark: Nordic Council of Ministers.
- Blum, J. S., Wearsch, P. A., & Cresswell, P. (2013). Pathways of antigen processing. *Annual Review of Immunology*, 31(1), 443–473. <https://doi.org/10.1146/annurev-immunol-032712-095910>
- Breedveld, A., & van Egmond, M. (2019). IgA and Fc $\alpha$ RI: Pathological roles and therapeutic opportunities. *Frontiers in Immunology*, 10, 553. <https://doi.org/10.3389/fimmu.2019.00553>
- Chan, H.-T., & Daniell, H. (2015). Plant-made oral vaccines against human infectious diseases-Are we there yet? *Plant Biotechnology Journal*, 13(8), 1056–1070. <https://doi.org/10.1111/pbi.12471>
- Colino, J., Chattopadhyay, G., Sen, G., Chen, Q., Lees, A., Canaday, D. H., ... Snapper, C. M. (2009). Parameters underlying distinct T cell-dependent polysaccharide-specific IgG responses to an intact Gram-positive bacterium versus a soluble conjugate vaccine. *Journal of Immunology*, 183(3), 1551–1559. <https://doi.org/10.4049/jimmunol.0900238>
- Davitt, C. J. H., & Lavelle, E. C. (2015). Delivery strategies to enhance oral vaccination against enteric infections. *Advanced Drug Delivery Reviews*, 91, 52–69. <https://doi.org/10.1016/j.addr.2015.03.007>
- De Smet, R., Allais, L., & Cuvelier, C. A. (2014). Recent advances in oral vaccine development. *Human Vaccines & Immunotherapeutics*, 10(5), 1309–1318. <https://doi.org/10.4161/hv.28166>
- Edelman, R., Russell, R. G., Losonsky, G., Tall, B. D., Tacket, C. O., Levine, M. M., & Lewis, D. H. (1993). Immunization of rabbits with enterotoxigenic *E. coli* colonization factor antigen (CFA/I) encapsulated in biodegradable microspheres of poly (lactide-co-glycolide). *Vaccine*, 11(2), 155–158. [https://doi.org/10.1016/0264-410X\(93\)90012-M](https://doi.org/10.1016/0264-410X(93)90012-M)
- Egea, L., Hirata, Y., & Kagnoff, M. F. (2010). GM-CSF: A role in immune and inflammatory reactions in the intestine. *Expert Review of Gastroenterology & Hepatology*, 4(6), 723–731. <https://doi.org/10.1586/egh.10.73>
- Evans, R., Shultz, L. D., Dranoff, G., Fuller, J. A., & Kamdar, S. J. (1998). CSF-1 regulation of I $\beta$  gene expression by murine macrophages: A pivotal role for GM-CSF. *Journal of Leukocyte Biology*, 64(6), 810–816. <https://doi.org/10.1002/jlb.64.6.810>
- Farris, E., Brown, D. M., Ramer-Tait, A. E., & Pannier, A. K. (2017). Chitosan-zein nano-in-microparticles capable of mediating in vivo transgene expression following oral delivery. *Journal of Controlled Release*, 249, 150–161. <https://doi.org/10.1016/j.jconrel.2017.01.035>
- Fattal, E., Pecquet, S., Couvreur, P., & Andremont, A. (2002). Biodegradable microparticles for the mucosal delivery of antibacterial and dietary antigens. *International Journal of Pharmaceutics*, 242(1–2), 15–24. [https://doi.org/10.1016/S0378-5173\(02\)00181-3](https://doi.org/10.1016/S0378-5173(02)00181-3)
- Fernández-Carneado, J., Kogan, M. J., Castel, S., & Giralte, E. (2004). Potential peptide carriers: Amphipathic proline-rich peptides derived from the N-terminal domain of  $\gamma$ -zein. *Angewandte Chemie International Edition*, 43(14), 1811–1814. <https://doi.org/10.1002/anie.200352540>

- Ghaffari Marandi, B. H., Zolfaghari, M. R., Kazemi, R., Motamedi, M. J., & Amani, J. (2019). Immunization against *Vibrio cholerae*, ETEC, and EHEC with chitosan nanoparticle containing LSC chimeric protein. *Microbial Pathogenesis*, 134, 103600. <https://doi.org/10.1016/j.micpath.2019.103600>
- Halweg, C., Thompson, W. F., & Spiker, S. (2005). The Rb7 matrix attachment region increases the likelihood and magnitude of transgene expression in tobacco cells: A flow cytometric study. *The Plant Cell*, 17(2), 418–429. <https://doi.org/10.1105/tpc.104.028100>
- Hamilton, J. A. (2002). GM-CSF in inflammation and autoimmunity. *Trends in Immunology*, 23(8), 403–408. [https://doi.org/10.1016/S1471-4906\(02\)02260-3](https://doi.org/10.1016/S1471-4906(02)02260-3)
- Hansen, G. H., Rasmussen, K., Niels-Christiansen, L.-L., & Danielsen, E. M. (2009). Endocytic trafficking from the small intestinal brush border probed with FM dye. *American Journal of Physiology: Gastrointestinal and Liver Physiology*, 297(4), G708–G715. <https://doi.org/10.1152/ajpgi.00192.2009>
- Hofbauer, A., Melnik, S., Tschofen, M., Arcalis, E., Phan, H. T., Gresch, U., ... Stoger, E. (2016). The encapsulation of hemagglutinin in protein bodies achieves a stronger immune response in mice than the soluble antigen. *Frontiers in Plant Science*, 7, 142. <https://doi.org/10.3389/fpls.2016.00142>
- Johnson, D. E., Ostrowski, P., Jaumouillé, V., & Grinstein, S. (2016). The position of lysosomes within the cell determines their luminal pH. *The Journal of Cell Biology*, 212(6), 677–692. <https://doi.org/10.1083/jcb.201507112>
- Joseph, M., Ludevid, M. D., Torrent, M., Rofidal, V., Tauzin, M., Rossignol, M., & Peltier, J.-B. (2012). Proteomic characterisation of endoplasmic reticulum-derived protein bodies in tobacco leaves. *BMC Plant Biology*, 12(1), 36. <https://doi.org/10.1186/1471-2229-12-36>
- Karthikeyan, K., Vijayalakshmi, E., & Korrapati, P. S. (2014). Selective Interactions of zein microspheres with different class of drugs: An in vitro and in silico analysis. *AAPS PharmSciTech*, 15(5), 1172–1180. <https://doi.org/10.1208/s12249-014-0151-6>
- Kogan, M. J., López, O., Cocera, M., López-Iglesias, C., De la Maza, A., & Giral, E. (2004). Exploring the interaction of the surfactant N-terminal domain of  $\gamma$ -zein with soybean phosphatidylcholine liposomes. *Biopolymers*, 73(2), 258–268. <https://doi.org/10.1002/bip.10578>
- Kour, P., Rath, G., Sharma, G., & Goyal, A. K. (2018). Recent advancement in nanocarriers for oral vaccination. *Artificial Cells, Nanomedicine, and Biotechnology*, 46(sup3), S1102–S1114. <https://doi.org/10.1080/21691401.2018.1533842>
- Lee, S., Alwahab, N. S. A., & Moazzam, Z. M. (2013). Zein-based oral drug delivery system targeting activated macrophages. *International Journal of Pharmaceutics*, 454(1), 388–393. <https://doi.org/10.1016/j.ijpharm.2013.07.026>
- Lee, S., Kim, Y.-C., & Park, J.-H. (2016). Zein-alginate based oral drug delivery systems: Protection and release of therapeutic proteins. *International Journal of Pharmaceutics*, 515(1–2), 300–306. <https://doi.org/10.1016/j.ijpharm.2016.10.023>
- Lee, S. H., & Hamaker, B. R. (2006). Cys155 of 27 kDa maize  $\gamma$ -zein is a key amino acid to improve its in vitro digestibility. *FEBS Letters*, 580(25), 5803–5806. <https://doi.org/10.1016/j.febslet.2006.09.033>
- Lending, C. R., & Larkins, B. A. (1989). Changes in the zein composition of protein bodies during maize endosperm development. *The Plant Cell*, 1(10), 1011–1023. <https://doi.org/10.1105/tpc.1.10.1011>
- Llop-Tous, I., Ortiz, M., Torrent, M., & Ludevid, M. D. (2011). The expression of a xylanase targeted to ER-protein bodies provides a simple strategy to produce active insoluble enzyme polymers in tobacco plants. *PLoS one*, 6(4):e19474. <https://doi.org/10.1371/journal.pone.0019474>
- Llop-Tous, I., Madurga, S., Giral, E., Marzabal, P., Torrent, M., & Ludevid, M. D. (2010). Relevant elements of a maize  $\gamma$ -zein domain involved in protein body biogenesis. *Journal of Biological Chemistry*, 285(46), 35633–35644. <https://doi.org/10.1074/jbc.M110.116285>
- Loza-Rubio, E., Rojas-Anaya, E., López, J., Olivera-Flores, M. T., Gómez-Lim, M., & Tapia-Pérez, G. (2012). Induction of a protective immune response to rabies virus in sheep after oral immunization with transgenic maize, expressing the rabies virus glycoprotein. *Vaccine*, 30(37), 5551–5556. <https://doi.org/10.1016/j.vaccine.2012.06.039>
- Luo, Y., Wang, Q., & Luo, Y. (2014). Zein-based micro- and nano-particles for drug and nutrient delivery: A review. *Journal of Applied Polymer Science*, 131(16), 1–12. <https://doi.org/10.1002/app.40696>
- Luo, Y., Zhang, B., Whent, M., Yu, L. L., & Wang, Q. (2011). Preparation and characterization of zein/chitosan complex for encapsulation of  $\alpha$ -tocopherol, and its in vitro controlled release study. *Colloids and Surfaces B: Biointerfaces*, 85(2), 145–152. <https://doi.org/10.1016/j.colsurfb.2011.02.020>
- Mbwana, S., Mortimer, E., Péra, F. F. P. G., Hitzeroth, I. I., & Rybicki, E. P. (2015). Production of H5N1 influenza virus matrix protein 2 ectodomain protein bodies in tobacco plants and in insect cells as a candidate universal influenza vaccine. *Frontiers in Bioengineering and Biotechnology*, 3, 197. <https://doi.org/10.3389/fbioe.2015.00197>
- Merlin, M., Pezzotti, M., & Avesani, L. (2017). Edible plants for oral delivery of biopharmaceuticals. *British Journal of Clinical Pharmacology*, 83(1), 71–81. <https://doi.org/10.1111/bcp.12949>
- Moghbel, N., Ryu, B., & Steadman, K. J. (2015). A reversed-phase HPLC-UV method developed and validated for simultaneous quantification of six alkaloids from *Nicotiana* spp. *Journal of Chromatography B*, 997, 142–145. <https://doi.org/10.1016/j.jchromb.2015.06.006>
- Moldoveanu, S. C., Scott, W. A., & Lawson, D. M. (2016). Nicotine analysis in several non-tobacco plant materials. *Beiträge Zur Tabakforschung International/Contributions to Tobacco Research*, 27(2), 54–59. <https://doi.org/10.1515/cttr-2016-0008>
- Nochi, T., Takagi, H., Yuki, Y., Yang, L., Masumura, T., Mejima, M., ... Kiyono, H. (2007). Rice-based mucosal vaccine as a global strategy for cold-chain- and needle-free vaccination. *Proceedings of the National Academy of Sciences of the United States of America*, 104(26), 10986–10991. <https://doi.org/10.1073/pnas.0703766104>
- Okada, E., Sasaki, S., Ishii, N., Aoki, I., Yasuda, T., Nishioka, K., ... Okuda, K. (1997). Intranasal immunization of a DNA vaccine with IL-12- and granulocyte-macrophage colony-stimulating factor (GM-CSF)-expressing plasmids in liposomes induces strong mucosal and cell-mediated immune responses against HIV-1 antigens. *Journal of Immunology*, 159(7), 3638–3647.
- Patel, A., Hu, Y., Tiwari, J. K., & Velikov, K. P. (2010). Synthesis and characterisation of zein-curcumin colloidal particles. *Soft Matter*, 6(24), 6192. <https://doi.org/10.1039/c0sm00800a>
- Pavot, V., Rochereau, N., Genin, C., Verrier, B., & Paul, S. (2012). New insights in mucosal vaccine development. *Vaccine*, 30(2), 142–154. <https://doi.org/10.1016/j.vaccine.2011.11.003>
- Penalva, R., González-Navarro, C. J., Gamazo, C., Esparza, I., & Irache, J. M. (2017). Zein nanoparticles for oral delivery of quercetin: Pharmacokinetic studies and preventive anti-inflammatory effects in a mouse model of endotoxemia. *Nanomedicine: Nanotechnology, Biology and Medicine*, 13(1), 103–110. <https://doi.org/10.1016/j.nano.2016.08.033>
- Pniewski, T., Milczarek, M., Wojas-Turek, J., Pajtasz-Piasecka, E., Wietrzyk, J., & Czyż, M. (2018). Plant lyophilisate carrying S-HBsAg as an oral booster vaccine against HBV. *Vaccine*, 36(41), 6070–6076. <https://doi.org/10.1016/j.vaccine.2018.09.006>
- Qadri, F., Svennerholm, A.-M., Faruque, A. S. G., & Sack, R. B. (2005). Enterotoxigenic *Escherichia coli* in developing countries: Epidemiology, microbiology, clinical features, treatment, and prevention. *Clinical Microbiology Reviews*, 18(3), 465–483. <https://doi.org/10.1128/CMR.18.3.465-483.2005>
- Rath, T., Kuo, T. T., Baker, K., Qiao, S.-W., Kobayashi, K., Yoshida, M., ... Blumberg, R. S. (2013). The immunologic functions of the neonatal Fc receptor for IgG. *Journal of Clinical Immunology*, 33(S1), 9–17. <https://doi.org/10.1007/s10875-012-9768-y>

- Regier, M. C., Taylor, J. D., Borczyk, T., Yang, Y., & Pannier, A. K. (2012). Fabrication and characterization of DNA-loaded zein nanospheres. *Journal of Nanobiotechnology*, 10, 44. <https://doi.org/10.1186/1477-3155-10-44>
- Rescigno, M., Urbano, M., Valzasina, B., Francolini, M., Rotta, G., Bonasio, R., ... Ricciardi-Castagnoli, P. (2001). Dendritic cells express tight junction proteins and penetrate gut epithelial monolayers to sample bacteria. *Nature Immunology*, 2(4), 361–367. <https://doi.org/10.1038/86373>
- Roche, P. A., & Furuta, K. (2015). The ins and outs of MHC class II-mediated antigen processing and presentation. *Nature Reviews Immunology*, 15(4), 203–216. <https://doi.org/10.1038/nri3818>
- Roig, A. I., Eskiocak, U., Hight, S. K., Kim, S. B., Delgado, O., Souza, R. F., ... Shay, J. W. (2010). Immortalized epithelial cells derived from human colon biopsies express stem cell markers and differentiate in vitro. *Gastroenterology*, 138(3), 1012–1021. <https://doi.org/10.1053/j.gastro.2009.11.052>
- Rydell, N., & Sjöholm, I. (2004). Oral vaccination against diphtheria using polyacryl starch microparticles as adjuvant. *Vaccine*, 22(9–10), 1265–1274. <https://doi.org/10.1016/j.vaccine.2003.09.034>
- Sánchez-Navarro, M., Teixido, M., & Giral, E. (2017). Jumping hurdles: Peptides able to overcome biological barriers. *Accounts of Chemical Research*, 50(8), 1847–1854. <https://doi.org/10.1021/acs.accounts.7b00204>
- Sastry, S. V., Nyshadham, J. R., & Fix, J. A. (2000). Recent technological advances in oral drug delivery—A review. *Pharmaceutical Science & Technology Today*, 3(4), 138–145. [https://doi.org/10.1016/S1461-5347\(00\)00247-9](https://doi.org/10.1016/S1461-5347(00)00247-9)
- Schillberg, S., Raven, N., Spiegel, H., Rasche, S., & Buntru, M. (2019). Critical analysis of the commercial potential of plants for the production of recombinant. *Proteins Frontiers in Plant Science*, 10, <https://doi.org/10.3389/fpls.2019.00720>
- Shojaei Jeshvaghani, F., Amani, J., Kazemi, R., Karimi Rahjerdi, A., Jafari, M., Abbasi, S., & Salமான, A. H. (2019). Oral immunization with a plant-derived chimeric protein in mice: Toward the development of a multipotent edible vaccine against *E. coli* O157: H7 and ETEC. *Immunobiology*, 224(2), 262–269. <https://doi.org/10.1016/j.imbio.2018.12.001>
- Smith, D. M., Simon, J. K., & Baker, J. R. (2013). Applications of nanotechnology for immunology. *Nature Reviews Immunology*, 13(8), 592–605. <https://doi.org/10.1038/nri3488>
- Snapper, C. M. (2018). Distinct immunologic properties of soluble versus particulate antigens. *Frontiers in Immunology*, 9(MAR), <https://doi.org/10.3389/fimmu.2018.00598>
- Stertman, L., Lundgren, E., & Sjöholm, I. (2006). Starch microparticles as a vaccine adjuvant: Only uptake in Peyer's patches decides the profile of the immune response. *Vaccine*, 24(17), 3661–3668. <https://doi.org/10.1016/j.vaccine.2005.10.059>
- Su, B., Wang, J., Wang, X., Jin, H., Zhao, G., Ding, Z., ... Wang, B. (2008). The effects of IL-6 and TNF- $\alpha$  as molecular adjuvants on immune responses to FMDV and maturation of dendritic cells by DNA vaccination. *Vaccine*, 26(40), 5111–5122. <https://doi.org/10.1016/j.vaccine.2008.03.089>
- Subach, O. M., Cranfill, P. J., Davidson, M. W., & Verkhusha, V. V. (2011). An enhanced monomeric blue fluorescent protein with the high chemical stability of the chromophore. *PLoS one*, 6(12):e28674. <https://doi.org/10.1371/journal.pone.0028674>
- Tada, R., Hidaka, A., Kiyono, H., Kunisawa, J., & Aramaki, Y. (2018). Intranasal administration of cationic liposomes enhanced granulocyte-macrophage colony-stimulating factor expression and this expression is dispensable for mucosal adjuvant activity. *BMC Research Notes*, 11(1), 472. <https://doi.org/10.1186/s13104-018-3591-3>
- Thompson, A. L., & Staats, H. F. (2011). Cytokines: The future of intranasal vaccine adjuvants. *Clinical and Developmental Immunology*, 2011, 289597. <https://doi.org/10.1155/2011/289597>
- Torrent, M., Llopart, B., Lasserre-Ramassamy, S., Llop-Tous, I., Bastida, M., Marzabal, P., ... Ludevid, M. D. (2009). Eukaryotic protein production in designed storage organelles. *BMC Biology*, 7(1), 5. <https://doi.org/10.1186/1741-7007-7-5>
- Whitehead, M., Öhlschläger, P., Almajhdī, F. N., Alloza, L., Marzábal, P., Meyers, A. E., ... Rybicki, E. P. (2014). Human papillomavirus (HPV) type 16 E7 protein bodies cause tumour regression in mice. *BMC Cancer*, 14(1), 367. <https://doi.org/10.1186/1471-2407-14-367>
- Woo, Y.-M., Hu, D. W.-N., Larkins, B. A., & Jung, R. (2001). Genomics analysis of genes expressed in maize endosperm identifies novel seed proteins and clarifies patterns of zein gene expression. *The Plant Cell*, 13(10), 2297–2317. <https://doi.org/10.2307/3871509>
- Zhang, Y., Cui, X., Che, X., Zhang, H., Shi, N., Li, C., ... Kong, W. (2015). Zein-based films and their usage for controlled delivery: Origin, classes and current landscape. *Journal of Controlled Release*, 206(2699), 206–219. <https://doi.org/10.1016/j.jconrel.2015.03.030>
- Zhang, Y., Cui, L., Li, F., Shi, N., Li, C., Yu, X., ... Kong, W. (2016). Design, fabrication and biomedical applications of zein-based nano/micro-carrier systems. *International Journal of Pharmaceutics*, 513(1–2), 191–210. <https://doi.org/10.1016/j.ijpharm.2016.09.023>
- Zhong, Q., & Jin, M. (2009). Nanoscale structures of spray-dried zein microcapsules and in vitro release kinetics of the encapsulated lysozyme as affected by formulations. *Journal of Agricultural and Food Chemistry*, 57(9), 3886–3894. <https://doi.org/10.1021/jf803951a>
- van Zyl, A. R., Meyers, A. E., & Rybicki, E. P. (2017). Development of plant-produced protein body vaccine candidates for bluetongue virus. *BMC Biotechnology*, 17(1), 47. <https://doi.org/10.1186/s12896-017-0370-5>

## SUPPORTING INFORMATION

Additional supporting information may be found online in the Supporting Information section.

**How to cite this article:** Schwestka J, Tschofen M, Vogt S, et al. Plant-derived protein bodies as delivery vehicles for recombinant proteins into mammalian cells. *Biotechnology and Bioengineering*. 2020;1–11. <https://doi.org/10.1002/bit.27273>



## RESEARCH PAPER

# Maize 16-kD $\gamma$ -zein forms very unusual disulfide-bonded polymers in the endoplasmic reticulum: implications for prolamin evolution

Davide Mainieri,<sup>1</sup> Claudia A. Marrano,<sup>1</sup> Bhakti Prinsi,<sup>2</sup> Dario Maffi,<sup>2</sup> Marc Tschofen,<sup>3</sup> Luca Espen,<sup>2</sup> Eva Stöger,<sup>3</sup> Franco Faoro,<sup>2</sup> Emanuela Pedrazzini,<sup>1,\*</sup> and Alessandro Vitale<sup>1,\*</sup>

<sup>1</sup> Istituto di Biologia e Biotecnologia Agraria, CNR, 20133 Milano, Italy

<sup>2</sup> Dipartimento di Scienze Agrarie e Ambientali, Università degli Studi di Milano, 20133 Milano, Italy

<sup>3</sup> Department of Applied Genetics and Cell Biology, University of Natural Resources and Life Sciences, Vienna, Austria

\*Correspondence: [vitale@ibba.cnr.it](mailto:vitale@ibba.cnr.it) or [pedrazzini@ibba.cnr.it](mailto:pedrazzini@ibba.cnr.it)

Received 18 May 2018; Editorial decision 25 July 2018; Accepted 25 July 2018

Editor: Chris Hawes, Oxford Brookes University, UK

## Abstract

**In the lumen of the endoplasmic reticulum (ER), prolamin storage proteins of cereal seeds form very large, ordered heteropolymers termed protein bodies (PBs), which are insoluble unless treated with alcohol or reducing agents. In maize PBs, 16-kD  $\gamma$ -zein locates at the interface between a core of alcohol-soluble  $\alpha$ -zeins and the outermost layer mainly composed of the reduced-soluble 27-kD  $\gamma$ -zein. 16-kD  $\gamma$ -zein originates from 27-kD  $\gamma$ -zein upon whole-genome duplication and is mainly characterized by deletions in the N-terminal domain that eliminate most Pro-rich repeats and part of the Cys residues involved in inter-chain bonds. 27-kD  $\gamma$ -zein also forms insoluble PBs when expressed in transgenic vegetative tissues. We show that in Arabidopsis leaves, 16-kD  $\gamma$ -zein assembles into disulfide-linked polymers that fail to efficiently become insoluble. Instead of forming PBs, these polymers accumulate as very unusual threads that markedly enlarge the ER lumen, resembling amyloid-like fibers. Domain-swapping between the two  $\gamma$ -zeins indicates that the N-terminal region of 16-kD  $\gamma$ -zein has a dominant effect in preventing full insolubilization. Therefore, a newly evolved prolamin has lost the ability to form homotypic PBs, and has acquired a new function in the assembly of natural, heteropolymeric PBs.**

**Keywords:** Cereal seeds, disulfide bonds, endoplasmic reticulum, genome-wide duplication, neofunctionalization, prolamins, protein bodies, protein evolution.

## Introduction

Prolamins are present only in the seeds of grasses, where they are usually the main proteins, and thus constitute the major global source of food protein (Shewry and Halford, 2002). Their most striking and unique cell biology feature is their accumulation within the lumen of the endoplasmic reticulum (ER) as very large heteropolymers, termed protein bodies (PBs; Shewry and Halford, 2002; Pedrazzini *et al.*, 2016). Most proteins that enter

the ER are destined to be secreted or sorted to distal locations of the endomembrane system, whereas ER residents, which are mainly folding helpers, have specific amino acid signals that allow their retention/retrieval in the ER (Gomez-Navarro and Miller, 2016). Since these signals are not present in prolamins, the question arises as to what are the molecular features that determine prolamin ER residence and ordered PB formation.

Maize (*Zea mays*) prolamins are divided into four classes:  $\alpha$ -zeins (>30 genes),  $\gamma$ -zeins (three genes), and  $\delta$ -zeins and  $\beta$ -zeins (both single genes; Woo *et al.*, 2001; Xu and Messing, 2008). 27-kD  $\gamma$ -zein and  $\beta$ -zein are the oldest maize prolamins (Xu and Messing, 2008). Whole-genome duplications (WGD), particularly common in plants (Jiao *et al.*, 2011), are followed by rearrangements that can lead to gene loss or retention. In the latter case, functional buffering or neofunctionalization can occur, and play important roles in evolution (Chapman *et al.*, 2006; Kassahn *et al.*, 2009). About 5–12 million years ago, maize underwent WGD followed by allotetraploidization (Swigoňová *et al.*, 2004). As a result,  $\gamma$ -zein, originally a single gene encoding a polypeptide of 27-kD and one of the most ancient maize prolamins, now has representatives in homologous regions of chromosome 7 (27- and 50-kD  $\gamma$ -zein; hereafter referred to as 27 $\gamma$ z and 50 $\gamma$ z) and chromosome 2 (16-kD  $\gamma$ -zein; 16 $\gamma$ z). 16 $\gamma$ z most probably originates from duplication of the 27 $\gamma$ z gene followed by deletion events (Xu and Messing, 2008).

During endosperm development,  $\gamma$ - and  $\beta$ -zeins are synthesized first, forming a PB where  $\alpha$ - and  $\delta$ -zeins will later accumulate (Lending and Larkins, 1989). In the mature PB,  $\beta$ -zein, 27 $\gamma$ z, and 50 $\gamma$ z form the outer layer in contact with the luminal face of the ER membrane, whereas  $\alpha$ - and  $\delta$ -zeins form the inner core, with 16 $\gamma$ z located at the interface between the core and the outer layer (Lending and Larkins, 1989; Yao *et al.*, 2016). Yeast two-hybrid data suggest that 16 $\gamma$ z can interact with zeins of all classes (Kim *et al.*, 2002, 2006). 27 $\gamma$ z expressed in vegetative tissues of transgenic plants forms homotypic PBs, indicating that no specific features of the maize endosperm ER are necessary to form a PB (Geli *et al.*, 1994). The primary sequence of 27 $\gamma$ z (Fig. 1) consists of the transient signal peptide for translocation into the ER (co-translationally removed), followed by a region containing eight or seven (depending on the maize variety) repeats of the hexapeptide PPPVHL and seven Cys residues involved in inter-chain bonds that make the protein insoluble in non-reducing conditions, and finally a second region homologous to 2S albumins, which are vacuolar storage proteins present in various amounts in all land plants (Vitale *et al.*, 1982; Prat *et al.*, 1985; Mainieri *et al.*, 2014). 2S albumins belong to a larger class characterized by the eight-cysteine motif, consisting of four intra-chain disulfide bonds between three helical domains (Pedrazzini *et al.*, 2016; Fig. 1). This motif is also conserved in 27 $\gamma$ z (Ems-McClung *et al.*, 2002). Progressive Cys-to-Ser mutation of the seven Cys residues of the N-terminal region lead to increased solubility and a parallel increase in the ability to leave the ER along the secretory pathway (Mainieri *et al.*, 2014). When the N-terminal region including the first six Cys residues is fused at the C-terminus of phaseolin, the vacuolar 7S storage globulin of common bean, the chimeric protein zeolin formed homotypic PBs in the ER (Mainieri *et al.*, 2004). Zeolin was instead efficiently secreted upon *in vivo* treatment with a reducing agent, or when its six Cys residues were mutated to Ser (Pompa and Vitale, 2006). Overall, these studies indicate that the N-terminal region of 27 $\gamma$ z contains key information for PB assembly and that its Cys residues are necessary for this process.

16 $\gamma$ z is mainly characterized by the loss of large part of the N-terminal, Pro-rich domain and three of its seven Cys residues (Prat *et al.*, 1987; Fig. 1). Additionally, its C-terminal region has lost one Cys residue of the eight-cysteine motif and has acquired a new one near the C-terminus, resulting in a new CysProCys sequence. This tripeptide could form an intra-chain disulfide bond (Yu *et al.*, 2012); however, it is not known whether this occurs in 16 $\gamma$ z. The changes that have generated 16 $\gamma$ z are noteworthy, since Cys residues are rarely lost once acquired during evolution (Wong *et al.*, 2011; Feyertag and Alvarez-Ponce, 2017). 16 $\gamma$ z can thus provide information on the minimal requirements for PB biogenesis and the features that allow the formation of heteropolymeric maize PBs. Here, we show that, unlike 27 $\gamma$ z, ectopically expressed 16 $\gamma$ z remains in part soluble, mainly because of the mutations in the N-terminal region. 16 $\gamma$ z is unable to form PBs, but it stably accumulates as polymers that markedly enlarge the ER lumen, giving rise to very unusual filamentous structures. These characteristics indicate neofunctionalization after WGD and cast light on the molecular basis for the specific organization of maize PBs.

## Materials and methods

### Analysis of maize PBs

Seeds from *Zea mays* inbred line W64A, collected at 25 d post-pollination and stored at  $-80^{\circ}\text{C}$ , were homogenized in a mortar using 5 ml  $\text{g}^{-1}$  ice-cold 100 mM Tris-Cl, pH 7.4, 1.0 mM EDTA (buffer H), 7% (w/w) sucrose, and cComplete™ Protease Inhibitor Cocktail (Roche). After filtration through cheesecloth, the homogenate was loaded on two layers of 35% and 60% (w/w) sucrose in buffer H and centrifuged in a swinging rotor for 90 min at  $4^{\circ}\text{C}$ , 78900  $g_{av}$  (i.e. the average  $g$  calculated at the middle length of the tube). The 7% sucrose supernatant, the interface between 7% and 35% sucrose, and the interface between 35% and 60% sucrose were collected. After denaturation in the presence of 1% SDS and 4% 2-mercaptoethanol (2-ME), proteins were analysed using 15% SDS-PAGE. As expected (Vitale *et al.*, 1982), zeins were at the interface between 35% and 60% sucrose, and hence this is termed the PB fraction. To treat PBs with different solvents, immediately after collection the PB fraction was first diluted with the same volume of buffer H and centrifuged for 10 min at  $4^{\circ}\text{C}$ , 1500  $g_{av}$ . The PB pellet was then resuspended in one of the following solvents: (i) buffer H, 1% Triton X-100, 20 min,  $4^{\circ}\text{C}$ ; (ii) buffer H, 2 mM dithiothreitol (DTT), 20 min,  $4^{\circ}\text{C}$ ; (iii) buffer H, 4% 2-ME, 20 min,  $4^{\circ}\text{C}$ ; and (iv) 70% ethanol in  $\text{H}_2\text{O}$ , 90 min,  $25^{\circ}\text{C}$ . After each treatment, samples were centrifuged for 10 min at  $4^{\circ}\text{C}$ , 1500  $g$ , the pellet and supernatant were then denatured and analysed using 15% SDS-PAGE and staining with Coomassie Brilliant Blue. Protein Molecular Weight Markers (Fermentas, Vilnius, Lithuania) were used as molecular mass markers.

### Plasmid constructions

The pDHA vector containing the coding sequence of 27-kD  $\gamma$ -zein followed by the FLAG epitope DYKDDDDK (hereafter termed 27 $\gamma$ zf) has been described previously (Mainieri *et al.*, 2014). To construct a similarly tagged 16-kD  $\gamma$ -zein (16 $\gamma$ zf), a genomic fragment of *Z. mays* W64A comprising the coding and untranslated flanking sequences of 16-kD  $\gamma$ -zein (a kind gift from Angelo Viotti, CNR), identical to GenBank sequence EU953296.1, was amplified by PCR using the following oligonucleotides: 5'-ACTCAGGTCGACATGAA GGTGCTGATCGTTGCCCTTG -3' (where the SalI restriction site is in italics and the 16-kD  $\gamma$ -zein ATG start codon is in bold) and 5'-TCGATGGCATTGCTCACTTGTCGTCGTCCTTGTAGTCG

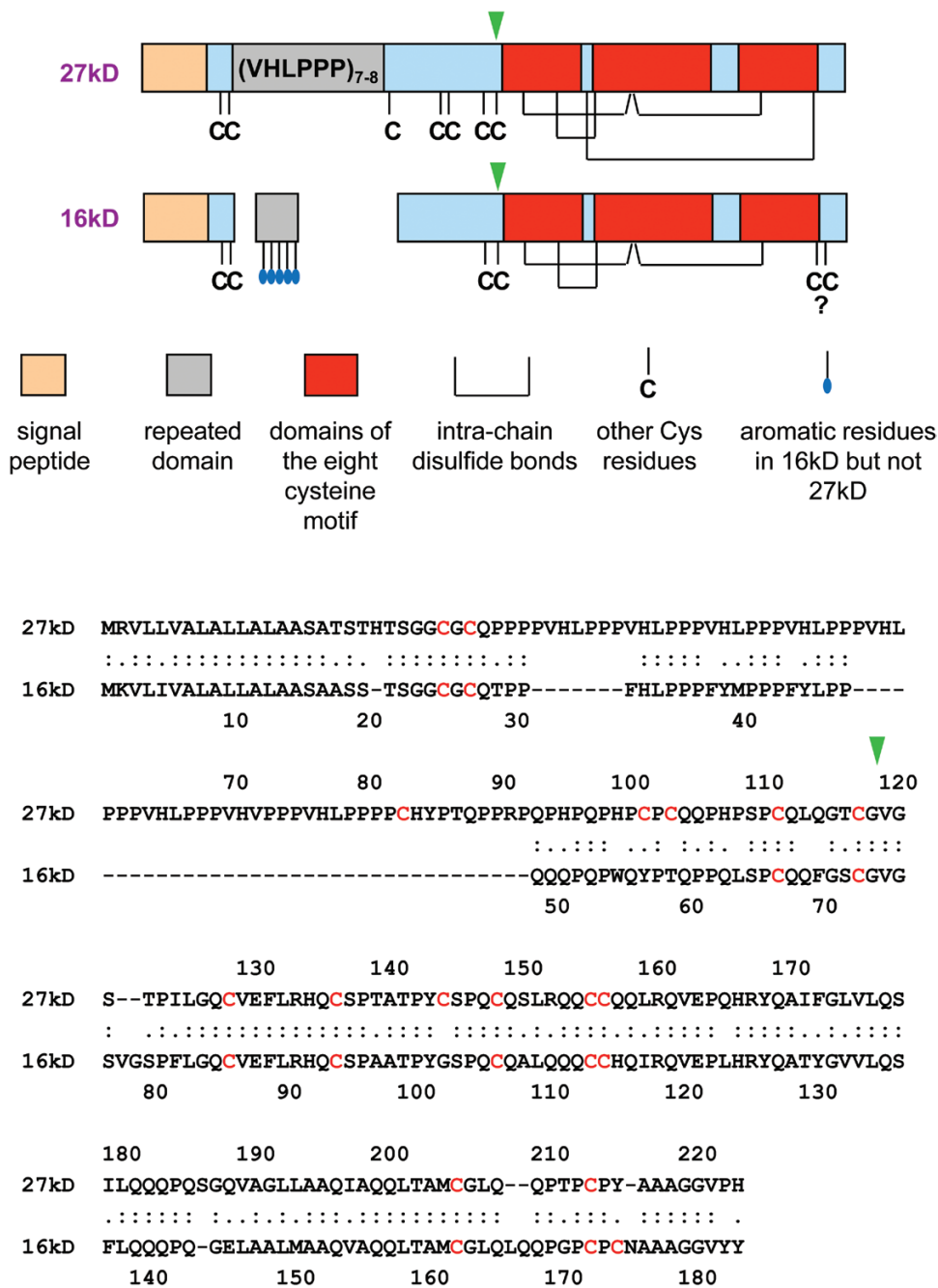


**Fig. 1.** Schematic diagram and amino acid sequence of the 27-kD and 16-kD  $\gamma$ -zein primary translation products. The question mark indicates that the linkage status of the two Cys residues towards the C-terminus of the 16-kD  $\gamma$ -zein is not known. The green arrowheads indicate the points at which the N- and C-terminal regions of the two polypeptides were exchanged, to produce constructs 27/16 and 16/27. In the amino acid sequences, Cys residues are highlighted in red.

TAGTAGACACCGCCGGCAGC -3', (where the SphI restriction site is in italics and the reverse complement of the codons encoding the FLAG epitope is underlined). The sequence was restricted with SalI and SphI and reinserted into the similarly restricted pDHA vector for transient expression.

To produce transgenic Arabidopsis, the EcoRI fragments containing the 16 $\gamma$ zf or 27 $\gamma$ zf expression cassettes were excised from pDHA and subcloned into EcoRI-linearized pGreenII0179 (John Innes Centre, Norwich, UK). The *Agrobacterium tumefaciens* strain GV3101 containing the pSoup helper plasmid was transformed with the resulting constructs.

To prepare the chimeric construct 16/27, which is formed by the N-terminal primary sequence of 16 $\gamma$ zf until Cys<sup>73</sup> followed by the C-terminal sequence of 27 $\gamma$ zf starting from Gly<sup>118</sup> (see Fig. 1), DNA was

synthesized (Integrated DNA Technologies, Leuven, Belgium) based on the two sequences and inserted into SalI/SphI restricted pDHA. To prepare the exactly reciprocal construct 27/16, the following DNA sequence was synthesized: from the Bpu10I restriction site of the sequence encoding 27 $\gamma$ zf until its Gly<sup>118</sup> codon (which corresponds to Gly<sup>74</sup> of 16 $\gamma$ zf), continuing with the 16 $\gamma$ zf sequence from Val<sup>75</sup> until its stop codon, and ending with a SphI restriction site. This sequence was used to substitute the Bpu10I/SphI fragment in pDHA encoding 27 $\gamma$ zf.

*Transient expression in tobacco protoplasts*

Transient expression was performed in protoplasts prepared from young (4–7 cm) leaves of tobacco (*Nicotiana tabacum* SR1) grown in axenic

conditions, as described previously (Mainieri *et al.*, 2014). Resuspensions of  $10^6$  protoplasts were transfected using 40  $\mu\text{g}$  per million protoplasts of plasmid or, for co-transfections, 60  $\mu\text{g}$  (25  $\mu\text{g}$  of each plasmid plus empty pDHA to a final amount of 60  $\mu\text{g}$ ). After transfection and incubation for 20 h at 25 °C, protoplasts were either homogenized for protein blot analysis or subjected to pulse-chase labelling. Extraction of intracellular and secreted proteins in reducing or oxidizing conditions and protein blot analysis with rabbit anti-FLAG antibody (1:2000 dilution, Sigma-Aldrich) and the Super-Signal West Pico Chemiluminescent Substrate (Pierce Chemical, Rockford, IL) were performed as described previously (Mainieri *et al.*, 2014). Protein Molecular Weight Markers (Fermentas, Vilnius, Lithuania) were used as molecular mass markers.

Pulse-chase labelling was performed with 100  $\mu\text{Ci ml}^{-1}$  Easytag mixture of  $^{35}\text{S}$ -labelled Met and Cys (PerkinElmer) for 1 h at 25 °C. Chase was initiated by adding unlabelled Met and Cys to 10 mM and 5 mM, respectively. After incubation at 25 °C for the desired chase time, two volumes of ice-cold W5 buffer (Mainieri *et al.*, 2014) were added to each sample, which were then centrifuged at 60  $g_{av}$  for 10 min. Collected protoplasts and supernatant (containing secreted proteins) were homogenized with two volumes of ice-cold 150 mM NaCl, 1.5 mM EDTA, 1.5% Triton X-100, 150 mM Tris-Cl pH 7.5, supplemented with cOmplete™ Protease Inhibitor Cocktail. After centrifugation at 10 000  $g_{av}$ , the pellet was resuspended in the same buffer supplemented with 4% 2-ME and centrifuged again. The soluble fractions of the first and second centrifugation were immunoselected using the anti-FLAG antibody and protein A Sepharose (GE Healthcare) and analysed using SDS-PAGE and radiography, using  $^{14}\text{C}$ -methylated proteins (Sigma-Aldrich) as molecular mass markers. Radioactive proteins were detected using the Starion FLA-9000 Phosphoimage System (Fujifilm) and quantified using TotalLab Quant (TotalLab, Newcastle upon Tyne, UK).

#### Expression in transgenic *Arabidopsis*

Transgenic *Arabidopsis thaliana* (ecotype Columbia) plants expressing 16 $\gamma\text{zf}$  or 27 $\gamma\text{zf}$  were produced by the floral dip method (Clough and Bent, 1998) with the transformed *A. tumefaciens* described above. Hygromycin-resistant T0 plants were identified and the homozygous progenies were selected. Experiments were then conducted using T2 or T3 plants. Plants were grown in soil at 23 °C under a 16/8 h light/dark cycle or in sterile conditions on half-concentrated Murashige and Skoog media (Duchefa Biochemie) supplemented with 10  $\text{g L}^{-1}$  Sucrose and 0.8% (w/v) phytoagar (Duchefa Biochemie).

Leaves at 4–6 weeks old were homogenized in leaf homogenization buffer (150 mM Tris-Cl, pH 7.5, 150 mM NaCl, 1.5 mM EDTA, 1.5% Triton X-100, cOmplete™ Protease Inhibitor Cocktail), supplemented (reducing conditions) or not (oxidizing conditions) with 4% (v/v) 2-ME. Soluble and insoluble proteins were separated by centrifugation at 1500  $g_{av}$  for 10 min at 4 °C. Samples were adjusted to 1.0% SDS, 4% 2-ME and analysed using SDS-PAGE followed by protein blotting with the anti-FLAG antibody (1:2000 dilution).

#### Subcellular fractionation

*Arabidopsis* leaves at 4–6 weeks old were homogenized in 10 mM KCl, 2 mM MgCl<sub>2</sub>, 100 mM Tris-Cl, pH 7.8 (buffer A), and 12% (w/w) sucrose at 4 °C, followed by isopycnic ultracentrifugation using linear 16–65% (w/w) sucrose gradients in buffer A as described previously (Mainieri *et al.*, 2004). Fractions of 650  $\mu\text{l}$  were collected; 40  $\mu\text{l}$  samples of each fraction were denatured and analysed by SDS-PAGE, followed by protein blotting with anti-FLAG antibody or rabbit anti-endoplasmic serum (Klein *et al.*, 2006; 1:2500 dilution).

To determine the solubility of  $\gamma$ -zeins present in the different subcellular fractions, fractions around either 1.19 or 1.29 density were frozen to break membranes and were then pooled. An equal volume of buffer A was added and the suspension was centrifuged at 1500  $g_{av}$  for 10 min, 4 °C. Supernatants (soluble proteins) were collected and denatured with SDS-PAGE denaturation buffer. Pellets were either resuspended in SDS-PAGE denaturation buffer or were further extracted with 70% ethanol in H<sub>2</sub>O for 90 min at 25 °C, and centrifuged at 1500  $g_{av}$  for 10 min, 25 °C.

The soluble fraction (ethanol-soluble) and insoluble pellet (ethanol-insoluble) were collected and denatured for SDS-PAGE.

#### Velocity sucrose-gradient ultracentrifugation

*Arabidopsis* leaves were homogenized in ice-cold leaf homogenization buffer. The homogenate was loaded on top of a linear sucrose gradient (150 mM NaCl, 1 mM EDTA, 0.1% Triton X-100, 50 mM Tris-Cl, pH 7.5, 5–25% [w/v] sucrose). After centrifugation at 200 000  $g_{av}$  for 20 h, 4 °C, equal volumes of each fraction were analysed using SDS-PAGE and protein blotting. An identical gradient loaded with molecular mass markers was run in parallel. For velocity ultracentrifugation in reducing conditions, leaf homogenization buffer was supplemented with 4% 2-ME, and the sucrose gradient buffer was supplemented with 2% DTT.

#### Electron microscopy

Tissue fragments (1–2 mm<sup>2</sup>) from fully expanded *Arabidopsis* leaves were fixed, embedded, and immunolabelled as previously described (Faoro *et al.*, 1991). Tissues were fixed in 1.2% glutaraldehyde and 3.3% paraformaldehyde in 0.1 M phosphate buffer, pH 7.4, at 4 °C for 2 h, post-fixed in 1% OsO<sub>4</sub> in the same buffer for 2 h, dehydrated in an ethanol series, and then embedded in Spurr's resin. For immunocytochemical localization, post-fixation was omitted and the embedding resin used was London Resin White. Immunolabelling was carried out on ultrathin sections mounted on nickel grids and incubated overnight at 4 °C with anti-FLAG antibody or, as a negative control, anti-Cucumber mosaic virus polyclonal antibody (DSMZ, Braunschweig, Germany), both at 1:1000 dilution. After washing, sections were incubated for 1 h at room temperature, with 15 nm gold-labelled goat anti-rabbit serum (1:20; British BioCell, Cardiff, UK) and stained with 2% uranyl acetate and lead citrate, before being examined with a 100SX TEM (Jeol, Japan) operating at 80 KV.

#### Fluorescence microscopy

Leaves from *Arabidopsis* plants grown for 2 weeks in soil were cut in half lengthwise and primary veins were removed. Staining was with 3,3'-dihexyloxycarbocyanine (DiOC6, Molecular Probes) at a concentration of 0.5  $\mu\text{g ml}^{-1}$  in PBS for 10 min, followed by washing three times in PBS. Small sections of stained leaves were placed on a microscope slide and visualized with a 63x oil immersion objective mounted on an Axiovert 200 microscope (Carl Zeiss) equipped for epifluorescence. Simultaneous visualization of DiOC6 stain (488 nm excitation/520 nm emission) and bright-field (visible lamp) was performed using the sequential scanning facility of the microscope. Images were assembled with Adobe Photoshop software 10.0.

## Results

### *A proportion of 16 $\gamma\text{z}$ present in maize PB is solubilized by alcohol*

16 $\gamma\text{z}$  can be efficiently solubilized from maize endosperm by 70% ethanol supplied with reducing agent (Kim *et al.*, 2006), but its solubility in each of these agents alone is less clear. Treatment of purified PBs with buffer containing 2 mM DTT efficiently solubilizes 27 $\gamma\text{z}$  and 50 $\gamma\text{z}$ , but not PB polypeptides with molecular mass in the 16-kD range (Vitale *et al.*, 1982). We therefore examined in more detail the solubility of 16 $\gamma\text{z}$  accumulated in maize. An endosperm PB fraction prepared using a sucrose gradient was first treated with buffer containing 4% 2-mercaptoethanol (2-ME buffer, Fig. 2A). This reducing buffer solubilizes recombinant 27 $\gamma\text{z}$  (Mainieri *et al.*, 2014). The polypeptides that are underlined in Fig. 2 were identified

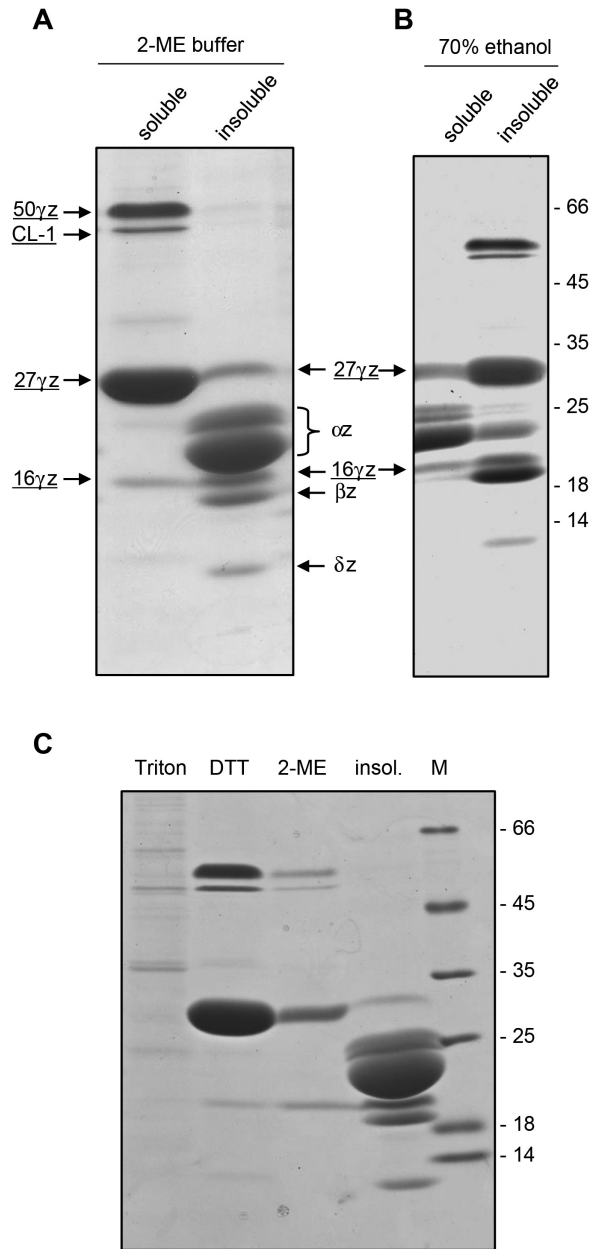


**Fig. 2.** The solubility of 16 $\gamma$ z accumulated in maize protein bodies (PBs) is intermediate between those of  $\alpha$ -zeins and the other  $\gamma$ -zeins. PBs purified from maize seeds, collected at 25d after pollination, were treated at 4 °C with buffer containing 4% 2-ME (A) or at 25 °C with 70% ethanol in H<sub>2</sub>O (B). After centrifugation, soluble and insoluble proteins were analysed using SDS-PAGE and Coomassie staining. The different zein polypeptides ( $\alpha$ z,  $\beta$ z,  $\gamma$ z,  $\delta$ z) and CL-1 are indicated. Those whose identities were confirmed by LC-ESI-MS/MS are underlined (see Supplementary Fig. S1 and Supplementary Table S1). (C) Purified PBs were sequentially extracted with buffer containing 1% Triton X-100, 2 mM DTT, and 4% 2-ME. After each step, the suspension was centrifuged and the soluble material was analysed using SDS-PAGE and Coomassie staining, together with the insoluble material of the last extraction (insol.). The positions of molecular mass markers (M, in kD) are indicated to the right in (B) and (C).

by LC-ESI-MS/MS analysis (Supplementary Fig. S1 and its associated Methods, and Supplementary Table S1; 27 $\gamma$ z and 16 $\gamma$ z identities were confirmed in both the soluble and insoluble fractions); polypeptides without underlining indicate zeins

identified solely based on their typical SDS-PAGE migration rates (notice that prolamins migrate more slowly than expected from their sequences). The 2-ME buffer very efficiently solubilized 27 $\gamma$ z and 50 $\gamma$ z (Fig. 2A), as expected (Vitale *et al.*, 1982). In contrast, solubilization of 16 $\gamma$ z was only partial, with most of the protein remaining in the insoluble precipitate, unlike the two other  $\gamma$ -zeins (Fig. 2A).  $\alpha$ -zeins, which are alcohol-soluble (Misra *et al.*, 1976), were efficiently solubilized by 70% ethanol at 25 °C (Fig. 2B). In addition, a significant proportion of 16 $\gamma$ z was solubilized by ethanol, whereas 50 $\gamma$ z and 27 $\gamma$ z remained totally or almost totally insoluble (Fig. 2B). When PBs were sequentially extracted with buffer containing non-ionic detergent, 2 mM DTT (as in Vitale *et al.*, 1982) or 4% 2-ME, the results confirmed that  $\gamma$ -zeins are insoluble unless reduced and indicated that DTT was not more efficient than 2-ME in solubilizing 16 $\gamma$ z (Fig. 2C).

Minor amounts of corn legumin-1 (CL-1), an 11S storage globulin (Woo *et al.*, 2001; Yamagata *et al.*, 2003), were extracted using non-reducing buffer containing non-ionic detergent, but most of this protein was extracted in the presence of a reducing agent (Fig. 2A–C, Supplementary Fig. S1). 11S storage proteins usually accumulate in protein storage vacuoles, but the presence of CL-1 in PBs, especially at late stages of endosperm maturation, has been observed previously (Arcalis *et al.*, 2010; Reyes *et al.*, 2011).

The solubility of 16 $\gamma$ z accumulated in maize was therefore intermediate between that of  $\alpha$ -zeins and the other  $\gamma$ -zeins, and distinct from that of CL-1, and  $\beta$ - and  $\delta$ -zeins (these two minor zeins were not efficiently solubilized by either solvent, Fig. 2), indicating that 16 $\gamma$ z may have specific polymerization properties. We verified this by comparing the destinies of 16 $\gamma$ z and 27 $\gamma$ z expressed individually in plant cells.

#### *Recombinant 16 $\gamma$ z and 27 $\gamma$ z are retained intracellularly but have different solubility*

The 16 $\gamma$ z sequence was tagged at the C-terminus with the FLAG epitope. This construct (16 $\gamma$ zf) and similarly tagged 27 $\gamma$ z (27 $\gamma$ zf; Mainieri *et al.*, 2014) were first transiently expressed in tobacco protoplasts. SDS-PAGE and protein blotting with anti-FLAG antibody performed ~20 h after transfection indicated that 16 $\gamma$ zf was recovered intracellularly, with almost no sign of secretion (Fig. 3A). In addition to the expected abundant monomers, a small proportion of 16 $\gamma$ zf was detected as what appear to be dimers and larger oligomers, not disassembled by the denaturation buffer. Both the lack of secretion and the incomplete disassembly by the SDS-PAGE denaturing/reducing buffer were also characteristic of 27 $\gamma$ zf expressed in protoplasts (Fig. 3A, and see Mainieri *et al.*, 2014) and leaves of transgenic Arabidopsis (Geli *et al.*, 1994). Sequential extraction with non-reducing buffer and then buffer supplemented with 4% 2-ME indicated that 27 $\gamma$ zf was almost completely insoluble unless reduced (Fig. 3A, S2 fraction), as previously established (Mainieri *et al.*, 2014). A significant proportion of 16 $\gamma$ zf molecules was instead also soluble in the absence of reducing agent (Fig. 3A, S1 fraction), indicating inefficient formation of insoluble polymers. 70% ethanol did not solubilize either of the two constructs (Fig. 3B, SE fraction). When 27 $\gamma$ zf

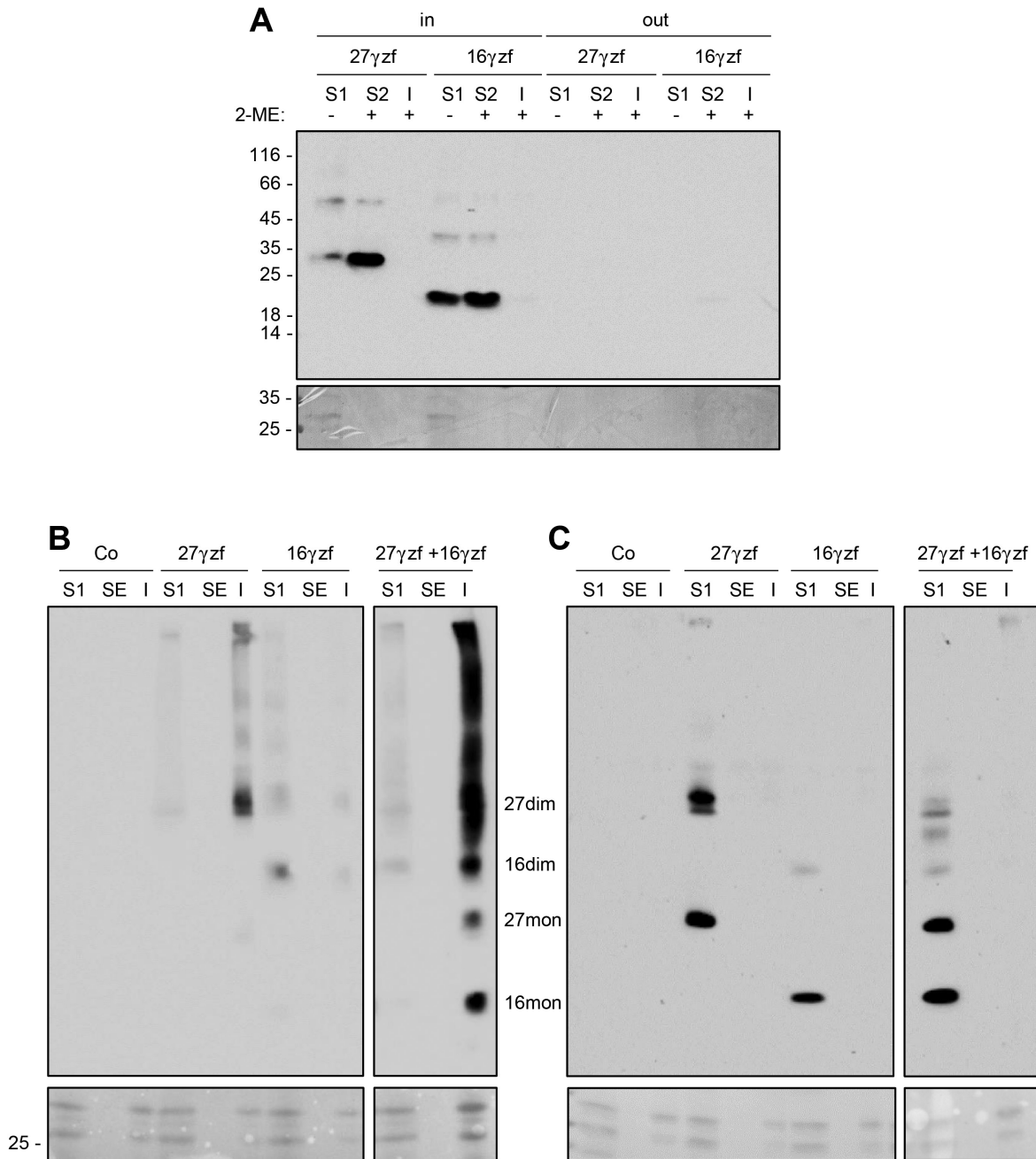


**Fig. 3.** Recombinant 16 $\gamma$ z and 27 $\gamma$ z are retained intracellularly but have different solubility. Protoplasts were isolated from tobacco leaves and transiently transformed either with plasmids encoding the indicated constructs or with the empty vector (Co) and analysed after incubation for 20 h. (A) Protoplasts (in) or incubation medium (out) were homogenized in the absence (–) of 2-ME. After centrifugation, soluble (S1) and insoluble fractions were collected. The insoluble material was resuspended in the presence (+) of 2-ME and subjected to a second centrifugation, to obtain the new soluble (S2) and insoluble (I) fractions. (B) Protoplasts were homogenized in the absence of 2-ME. After centrifugation, soluble (S1) and insoluble fractions were collected. The insoluble material was resuspended with 70% ethanol and subjected to a second centrifugation, to obtain the new soluble (SE) and insoluble (I) fractions. (C) As in (B), but the first homogenization was performed in the presence of 4% 2-ME. In (A–C), the upper images show analysis of each fraction by SDS-PAGE and protein blotting with anti-FLAG antibody, whilst the lower images show Ponceau S staining. The positions of molecular mass markers are shown to the left, in kD. In (B, C) the positions of dimers (dim) and monomers (mon) of 27 $\gamma$ zf (27) and 16 $\gamma$ zf (16) are indicated.

and 16 $\gamma$ zf were transiently co-expressed, both were almost completely insoluble in non-reducing buffer or 70% ethanol (Fig. 3B, I fraction). Therefore, the two  $\gamma$ -zeins interacted, and 27 $\gamma$ zf had a dominant effect in inhibiting 16 $\gamma$ zf solubility in the absence of reducing agent. When the first buffer of the sequential extraction was supplemented with 4% 2-ME, both individually expressed and co-expressed  $\gamma$ -zeins were fully

solubilized, confirming the role of disulfide bonds in determining insolubility (Fig. 3C, S1 fraction). These data were consistent with the insolubility of 16 $\gamma$ z when natural maize PBs were treated with non-reducing buffer (see Fig. 2C) and suggested that its partial solubility in ethanol was due to interactions with  $\alpha$ -zeins. The relative proportions of monomers and oligomers detected by SDS-PAGE varied in independent experiments,

but their different solubility in non-reducing conditions, when individually expressed, was consistently observed (compare Fig. 3A and B, and see also Supplementary Fig. S2).

*In transgenic Arabidopsis, 16 $\gamma$ zf is mostly unable to assemble into subcellular structures with the typical PB density*

To compare the long-term destinies of the two zeins, the tagged constructs were expressed in transgenic Arabidopsis under a constitutive promoter. These plants did not show visually evident phenotypes or clear alterations in growth and reproduction. For each construct, accumulation in leaves varied in different independent transgenic plants, but the electrophoretic pattern was unaffected by the level of final accumulation (Fig. 4A). 16 $\gamma$ zf showed the same electrophoretic patterns whether extracted from transgenic leaves or transiently transfected protoplasts, while most 27 $\gamma$ zf monomers were clearly of higher apparent molecular mass in transgenic leaves (around 40 kD), with only a minor proportion migrating as in transient expression (around 30 kD; compare Figs 3A and 4A). This indicated 27 $\gamma$ zf-specific post-translational modifications that were not yet detectable during the first hours after synthesis, and that did not occur in maize seeds. Hydroxylation of proline residues is the most likely explanation, as previously observed (Geli *et al.*, 1994; Mainieri *et al.*, 2014).

Subcellular localization was first investigated by isopycnic ultracentrifugation of homogenates prepared in the absence of detergent, to maintain membrane integrity. 27 $\gamma$ zf accumulated mainly in structures with density around 1.29 (Fig. 4B). This is consistent with the known ability of 27 $\gamma$ z to form homotypic PBs in the absence of the other zeins (Geli *et al.*, 1994; Coleman *et al.*, 1996) and the known high density of zein or zeolin PBs in maize or transgenic plants (Larkins and Hurkman, 1978; Geli *et al.*, 1994; Mainieri *et al.*, 2004). Much lower amounts of 27 $\gamma$ zf, probably constituted by newly synthesized molecules not yet assembled into dense PBs, were recovered in lighter subcellular fractions that contain the ER resident endoplasmic reticulum (Klein *et al.*, 2006) and have the typical ER density (Fig. 4B). 16 $\gamma$ zf was similarly present in the two distinct subcellular fractions, but most of the protein was in this case in the endoplasmic reticulum-containing ER, suggesting a poor ability to form PBs (Fig. 4C).

To determine the solubility of 16 $\gamma$ zf or 27 $\gamma$ zf present at the two positions along the gradient, fractions around 1.19 or 1.29 density were pooled, extracted with buffer without reducing agent, and centrifuged to separate soluble and insoluble proteins. Around 50% of 16 $\gamma$ zf present in the less-dense fraction was solubilized by this treatment (Fig. 4D, S1), whereas nearly 100% of 16 $\gamma$ zf or 27 $\gamma$ zf present in fractions at 1.29 density was insoluble (Fig. 4D, P1). Treatment of P1 with 70% ethanol did not solubilize 16 $\gamma$ zf or 27 $\gamma$ zf (Fig. 4D, SE and PE; note that treatment with ethanol makes the denaturation of oligomers more difficult). We concluded that the relevant proportion of 16 $\gamma$ zf that was not assembled into dense subcellular structures was in part also soluble in the absence of reducing agent, but no 16 $\gamma$ zf molecules insoluble in aqueous buffer were alcohol-soluble. This strongly suggested that 16 $\gamma$ z in maize PBs

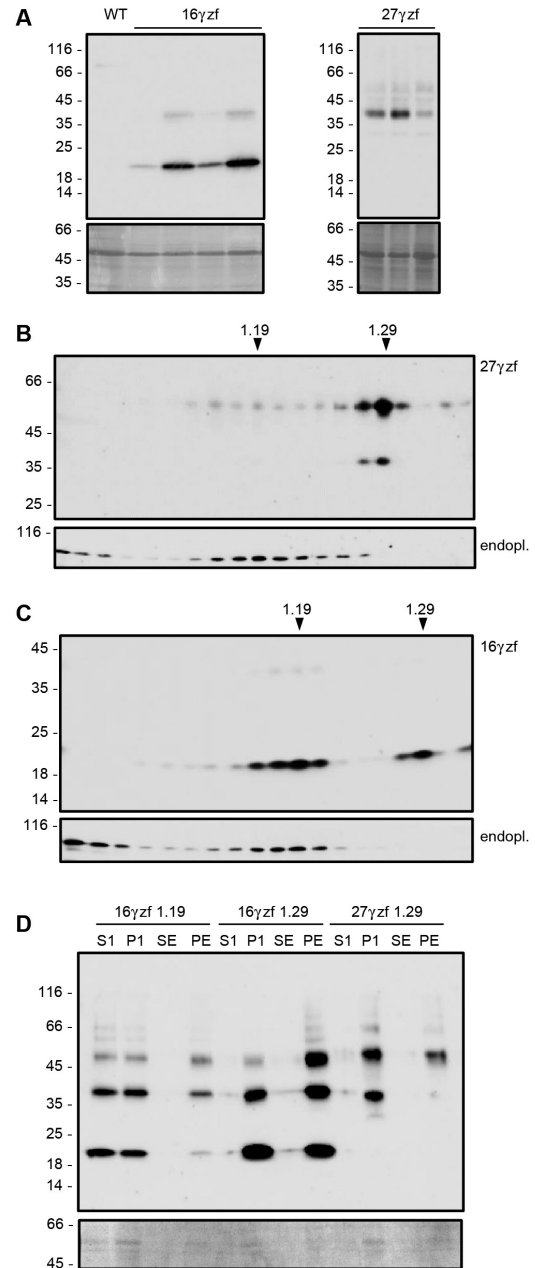


**Fig. 4.** Assembly of 16 $\gamma$ zf into dense subcellular structures is inefficient. (A) Leaves from transgenic Arabidopsis expressing 27 $\gamma$ zf or 16 $\gamma$ zf, or from wild-type plants (WT) were homogenized in the presence of 2-ME. Soluble proteins were analysed using SDS-PAGE. Each individual lane represents an independent transgenic plant. The upper images are protein blots with anti-FLAG antibody; lower images are Ponceau S staining. (B, C) Leaves from transgenic Arabidopsis expressing 27 $\gamma$ zf (B) or 16 $\gamma$ zf (C) were homogenized in the presence of 12% (w/w) sucrose and in the absence of detergent. The homogenates were fractionated by ultracentrifugation on 16–65% (w/w) isopycnic sucrose gradients. Proteins in each gradient fraction were analysed by SDS-PAGE and protein blotting, with anti-FLAG (27 $\gamma$ zf, 16 $\gamma$ zf) antibody or anti-endoplasmic reticulum (endopl.) serum. The top of gradients are at the left and the numbers at the top indicate the density ( $\text{g ml}^{-1}$ ). (D) Fractions around either 1.19 or 1.29 density from the gradients shown in (B, C) were pooled, extracted with buffer without reducing agent and centrifuged. Supernatants (S1) and pellets (P1) were collected. An aliquot of P1 was further treated with 70% ethanol and centrifuged to obtain ethanol-soluble (SE) and insoluble (PE) material. The upper image shows analysis by SDS-PAGE and protein blotting with anti-FLAG antibody; the lower image shows Ponceau S staining. In (A–D) the numbers at the left indicate the positions of molecular mass markers (kD).

is partially alcohol-soluble due to association with alcohol-soluble  $\alpha$ -zeins, as also suggested by the data in Fig. 3B.

When homogenates, prepared in non-reducing buffer supplemented with non-ionic detergent, were subjected to velocity sucrose-gradient ultracentrifugation, both 27 $\gamma$ zf and zeolin migrated at the bottom of tubes, indicating that they are large polymers (Mainieri *et al.*, 2004, 2014). Given the partial different subcellular localization and solubility of 16 $\gamma$ zf with respect of 27 $\gamma$ zf, we investigated whether 16 $\gamma$ zf also forms large polymers held together by disulfide bonds. Two plants accumulating different amounts of 16 $\gamma$ zf were analysed, to verify whether the expression levels influenced oligomerization (Fig. 5A). 16 $\gamma$ zf migrated to the bottom of the velocity ultracentrifugation tubes, independently of its level of accumulation (Fig. 5B, bottom panels). When leaf homogenization and velocity centrifugation were performed in reducing conditions, 16 $\gamma$ zf migrated in a position corresponding to monomers (Fig. 5B, top panels).

We concluded that 16 $\gamma$ zf forms extensive, disulfide-dependent polymers, in spite of its poor ability to form high-density subcellular compartments. We therefore used electron microscopy to compare the subcellular structures formed by 27 $\gamma$ zf and 16 $\gamma$ zf.

#### *16 $\gamma$ zf polymerizes into unusual reticular threads that markedly alter ER morphology*

In addition to typical ER membranes (Fig. 6A, ER, compare with wild-type tissue in 6D), 27 $\gamma$ zf leaf tissue showed electron-dense, round structures with diameters from a few hundred nanometres to more than one micron, with attached ribosomes (Fig. 6, PB). These structures, not present in wild-type plants, were labelled by anti-FLAG antibody (Fig. 6B, C), thus indicating that 27 $\gamma$ zf formed PBs. Homotypic PBs formed by recombinant 27 $\gamma$ z have been observed in Arabidopsis vegetative

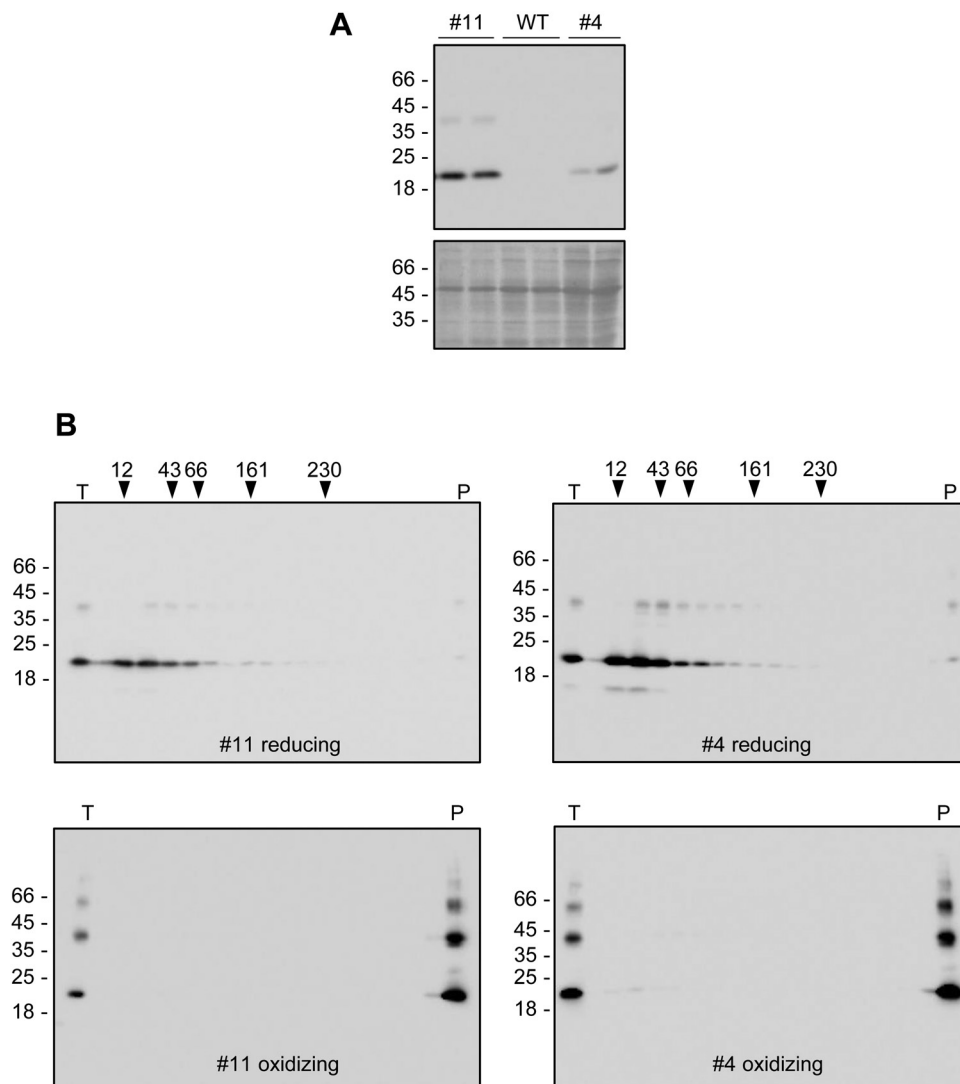


**Fig. 5.** 16 $\gamma$ zf forms large, disulfide-dependent polymers. (A) Homogenates were prepared from leaves of two independent transgenic Arabidopsis lines that accumulate different amounts of 16 $\gamma$ zf (#11 and #4, two plants for each line), and from leaves of untransformed wild-type Arabidopsis (WT), and analysed using SDS-PAGE. The upper image shows the protein blot with anti-FLAG antibody; the lower image shows Ponceau S staining. (B) Homogenates were prepared in either oxidizing or reducing buffer, and fractionated by velocity gradient ultracentrifugation. The top of each gradient is at the left. T, unfractionated total homogenate; P, pellet at the bottom of the tube after centrifugation. The numbers at the top indicate the positions where molecular mass markers migrate along the gradients. In (A, B) the numbers at the left indicate the positions of SDS-PAGE molecular mass markers (kD).

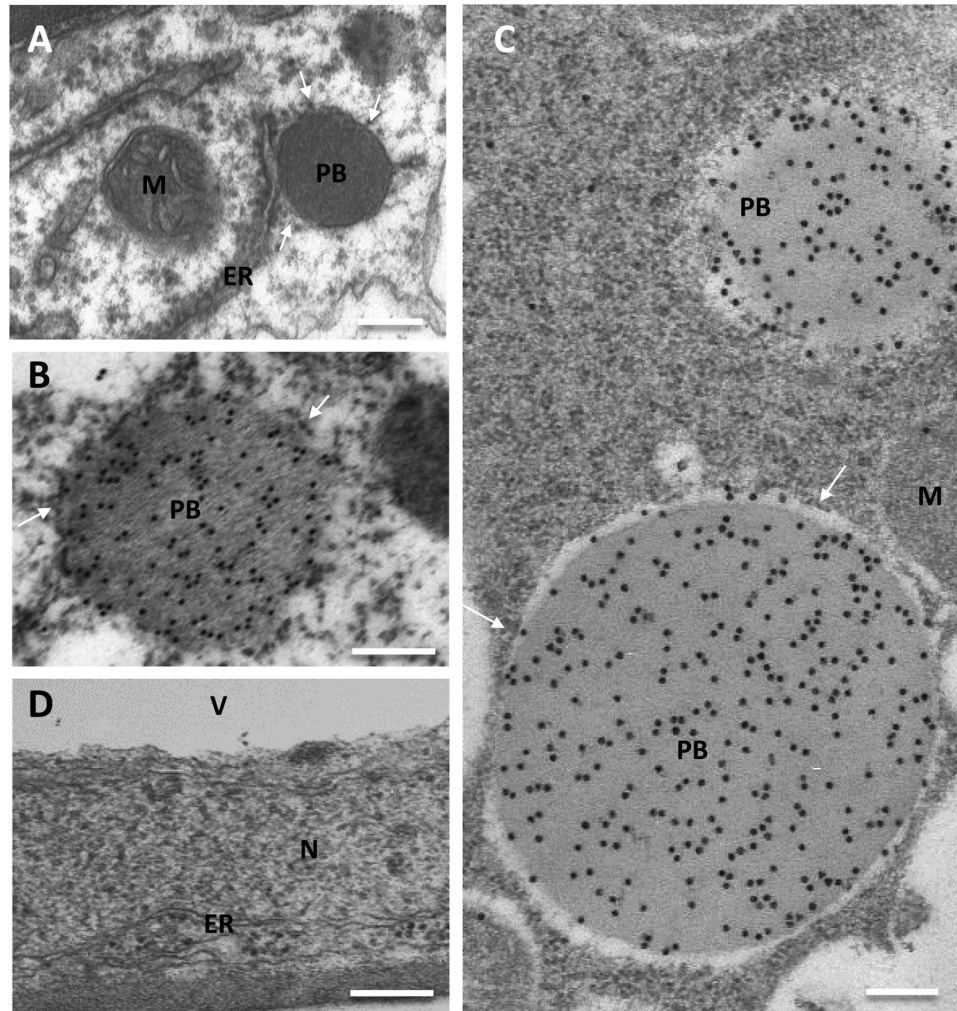


**Fig. 6.** 27 $\gamma$ zf forms protein bodies (PBs). Leaves from 6-week-old transgenic *Arabidopsis* plants expressing 27 $\gamma$ zf (A–C) or wild-type plants (D) were examined using electron microscopy. (A, D) Ultrathin sections post-fixed with osmium. (B, C) Immunolabelling with anti-FLAG antibody and secondary 15-nm gold-conjugated goat anti-rabbit serum. ER, endoplasmic reticulum; PB, protein body; M, mitochondria; N, nucleus, V, vacuole. Arrows indicate ribosomes. Note that in non-osmicated immunolabelled tissues (B, C) ER membranes are not detectable; however, numerous ribosomes are visible aligned outside the PB periphery (arrows). Scale bars are 200 nm.

tissues (Geli *et al.*, 1994) and tobacco seeds (Coleman *et al.*, 1996), although with smaller sizes than those that we observed.

Markedly different structures were formed by 16 $\gamma$ zf (Fig. 7). Large, irregular dilatations enclosed by a single membrane, often several micrometres wide, were detected (Fig. 7A; in Supplementary Fig. S3 black arrowheads mark the margins of this dilatation). The boundary membrane was surrounded by ribosomes (arrows in Fig. 7A, lower enlarged inset, and 7C, enlarged inset) and connections with tubular ER were occasionally seen (white arrowheads in Supplementary Fig. S3). The vacuole was often pressing against these dilatations, sometimes leaving space for a thin layer of cytoplasm outside the dilated ER (visible in the post-fixed sample in Fig. 7A, and more easily seen in Supplementary Fig. S3 where the ER membrane is indicated). The lumen of the ER dilatations contained very extensive electron-dense structures of two forms: very electron-opaque, osmiophilic threads of various lengths and irregular orientation (well represented in Fig. 7A, C) were mainly observed, whereas a minor proportion formed more compact irregular structures of lighter electron-density

(Fig. 7B, enlarged inset, and more evident in Fig. 7D, E). In non-osmicated tissues immunolabelled with anti-FLAG antibody, the convolutions appeared less sharp; however, gold particles were mostly aligned on them (Fig. 7B, D). No labelling occurred using an irrelevant antibody, confirming that the structures were formed by 16 $\gamma$ zf (Fig. 7E). The relative abundance of the two types of structures was variable in different ER dilatations, but when independent transgenic plants accumulating high (Fig. 7A, B, D, E) or low (Fig. 7C) amounts of 16 $\gamma$ zf were compared, no clear relationship between recombinant protein abundance and the type of 16 $\gamma$ zf structure could be established.

The ER vital lipophilic dye DiOC6 also efficiently stains PBs in developing endosperm cells in both rice and maize, probably due to its high affinity for the hydrophobic prolamin polypeptides (Muench *et al.*, 2000; Washida *et al.*, 2004). To complement the observations of electron microscopy, leaves were incubated with DiOC6 and observed under conventional fluorescence microscopy (Fig. 8). In 16 $\gamma$ zf leaves, DiOC6 highlighted enlarged structures of various sizes.

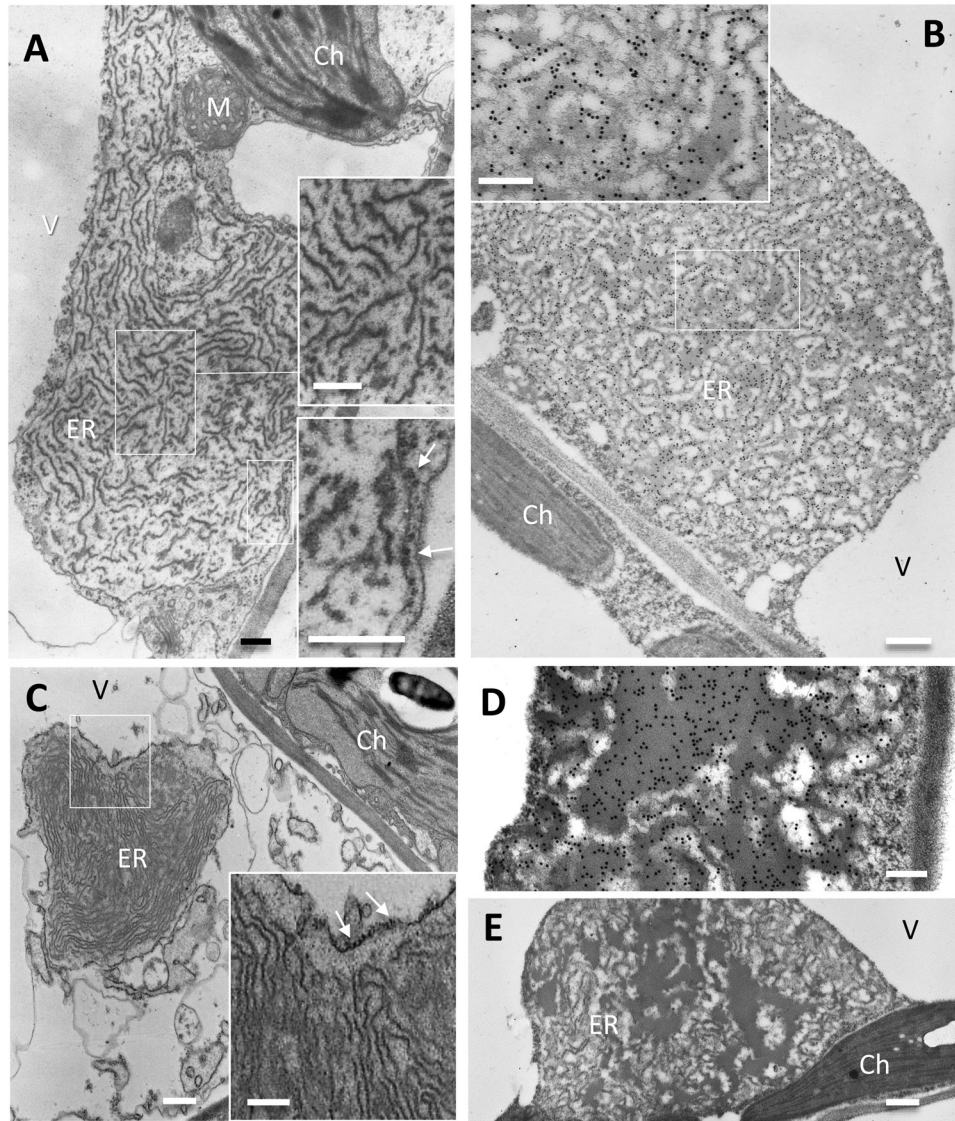


**Fig. 7.**  $16\gamma zf$  does not form protein bodies (PBs) but forms electron-dense structures in highly enlarged endoplasmic reticulum (ER) lumen. Leaves from 6-week-old transgenic *Arabidopsis* plants accumulating  $16\gamma zf$  in high (A, B, D, E) or low (C) amounts were analysed. (A, C) Ultrathin sections post-fixed with osmium. (B, D, E) Immunolabelling with anti-FLAG antibody (B, D) or irrelevant antibody as a negative control (E), and secondary 15-nm gold-conjugated goat anti-rabbit serum. The insets in (A–C) show magnifications to better illustrate the ribosomes attached on the cytosolic side of the ER membrane (arrows) and the electron-dense convoluted structures within the ER lumen. Ch, chloroplasts; M, mitochondria; V, vacuole. Scale bars in (A, D) and all insets are 200 nm; bars in (B, C, E) are 500 nm.

Higher magnification (Fig. 8A, inset, and magnification in 8D) showed that their content was not uniform, consistent with the structures observed by electron microscopy (Fig. 8D, arrow and compare with Fig. 7). In  $27\gamma zf$  leaves, more uniformly stained PBs with the classical size and round morphology were visible, as expected (Fig. 8G, and arrows in 8J). Structures similar to those in  $16\gamma zf$  and  $27\gamma zf$  were not detected in wild-type tissue, even at very high camera exposure times that highlighted the cell periphery, as expected for the ER lipophilic dye (Fig. 8M). Both the  $16\gamma zf$  structures and the  $27\gamma zf$  PBs were also detected under transmitted light (Fig. 8E, K, arrows).

We concluded that  $16\gamma zf$ , unlike  $27\gamma zf$ , is unable to form PBs and instead polymerizes into novel electron-dense structures that mostly appear as irregular threads and cause marked enlargement of the ER lumen.

#### *The N-terminal domain of $16\gamma zf$ is responsible for the inefficient formation of insoluble polymers*

To identify the structural features of  $16\gamma zf$  that did not allow efficient formation of insoluble polymers, we measured the loss of solubility during pulse-chase labelling in transiently transfected tobacco protoplasts. After pulse labelling for 1 h with a mixture of [ $^{35}$ S]Met and [ $^{35}$ S]Cys, protoplasts were subjected to chase for 0, 4, or 8 h. At each time-point, protoplasts were directly extracted in reducing conditions (thus solubilizing all molecules of each construct, to measure synthesis and stability; Fig. 9A, B) or sequentially extracted: first in non-reducing buffer and then treating the insoluble material with reducing buffer (to calculate at each time-point the percentage of molecules that are insoluble unless reduced, Fig. 9C). Each extract was immunoselected with anti-FLAG antibody and analysed using SDS-PAGE

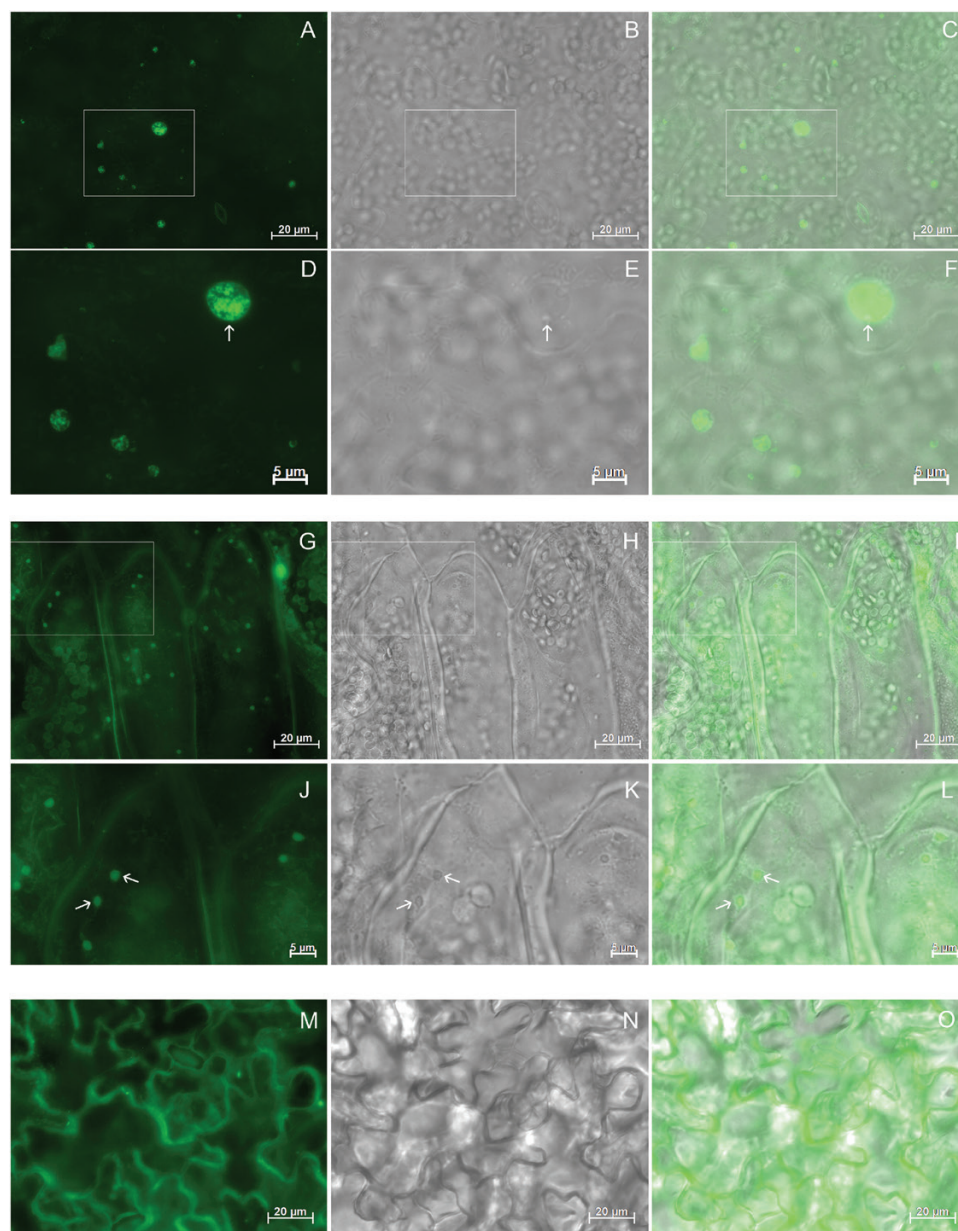


**Fig. 8.** 27 $\gamma$ zf protein bodies (PBs) and 16 $\gamma$ zf endoplasmic reticulum (ER) enlargements can be detected by fluorescence staining of the ER. Leaf tissue from 16 $\gamma$ zf (A–F), 27 $\gamma$ zf (G–L) or wild-type (M–O) *Arabidopsis* plants was stained with DiOC6 dye and examined using epifluorescence microscopy. (A, D, G, J, M): DiOC6 fluorescence (green); (B, E, H, K, N): bright-field; (C, F, I, L, O): merged images. Camera exposure time (ms): 61 (A), 502 (G), 8352 (M). Boxes in (A–C) and (G–I) indicate the regions that are shown at higher magnification in (D–F) and (J–L), respectively. Arrows indicate enlarged ER (D–F) or PBs (J–L).

and radiography. Newly synthesized 16 $\gamma$ zf and 27 $\gamma$ zf had the expected molecular mass (Fig. 9A). 16 $\gamma$ zf was slightly more stable during the chase (Fig. 9B; data are from two fully independent experiments). Already at the 0 h chase time-point, a much higher percentage of 27 $\gamma$ zf than 16 $\gamma$ zf was insoluble unless reduced (Fig. 9C). Insolubility increased during the chase, but the marked difference between the two zeins remained, as expected from the previous solubility assays (Figs 3, 4D). To map the insolubility determinant, we prepared two constructs, 27/16 and 16/27, in which the N-terminal domain of each zein was exchanged with that of the other (Fig. 1, the green arrowheads indicate the points of exchange). Since most of the molecular mass difference between the two zeins is due to their N-terminal

domain, the SDS-PAGE migrations of 27/16 and 16/27 are similar to those of 27 $\gamma$ zf and 16 $\gamma$ zf, respectively (Fig. 9A). The replacement of the natural N-terminal domain of 27 $\gamma$ zf with that of 16 $\gamma$ zf markedly inhibited insolubilization (Fig. 9C, compare 27 $\gamma$ zf and 16/27), whereas the reciprocal replacement markedly stimulated this process (Fig. 9C, compare 16 $\gamma$ zf and 27/16). This indicated that the N-terminal domain is the major determinant for the different behavior of the two zeins.

## Discussion

Mutations and insertions in the ancient seed storage proteins of the 2S albumin class were the first events in the origination of

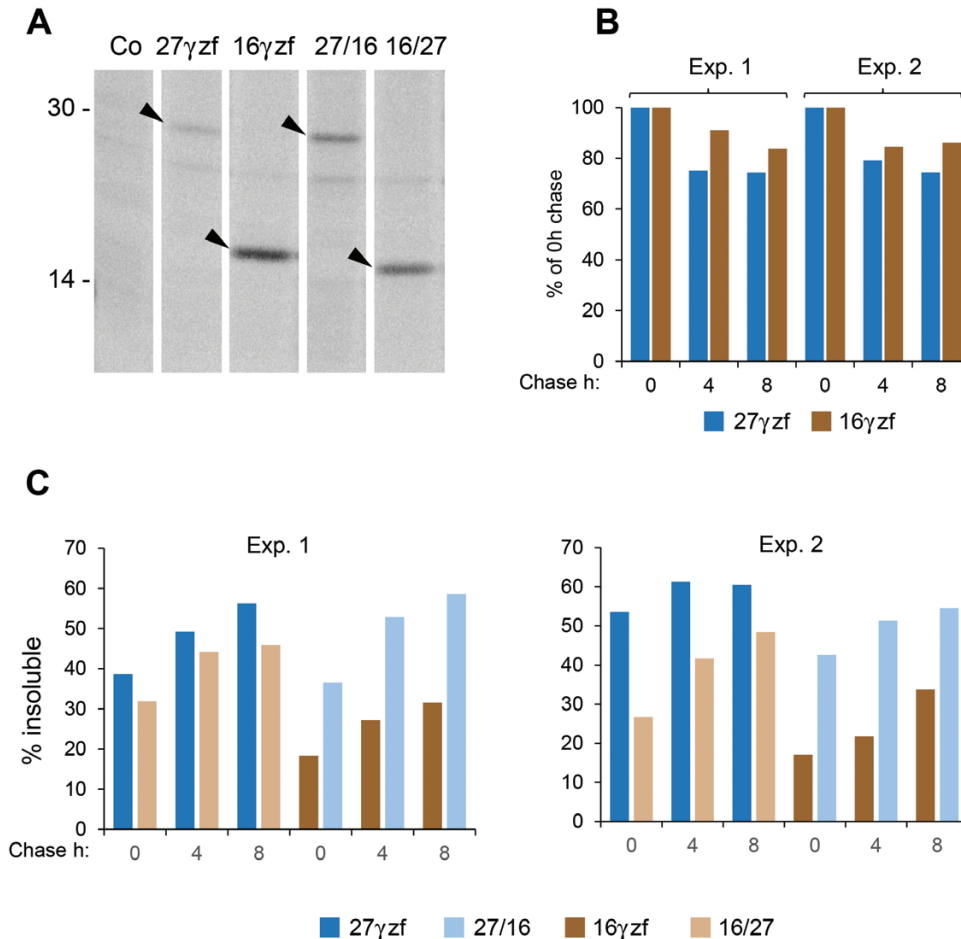


**Fig. 9.** The N-terminal domain of 16γzf has a major role in inhibiting the formation of insoluble polymers. Protoplasts prepared from tobacco leaves were transiently transfected either with plasmids encoding the indicated constructs or with empty plasmids (Co). (A) Transfected protoplasts were pulse-labelled with radioactive amino acids for 1 h before homogenization in reducing conditions. Proteins were immunoselected using anti-FLAG antibody and analysed using SDS-PAGE and radiography. The different lanes are from a single exposure of a single radiograph from which irrelevant lanes have been removed. The newly synthesized recombinant polypeptides (arrowheads) and the positions of molecular mass markers (numbers at left, kD) are indicated. (B) Protoplasts pulse-labelled as in (A) were subjected to chase for the indicated time (h), homogenized in the presence of 2-ME, immunoselected with anti-FLAG antibody, and analysed using SDS-PAGE and radiography. At each chase time-point, the densities of the relevant radioactive bands were quantified and expressed as percentage of the intensity at 0 h chase. (C) Protoplasts pulse-labelled as in (A) and chased for the indicated time (h) were then subjected to sequential homogenization steps, first in the absence 2-ME and then treating the insoluble material with 2-ME. Proteins at each step were immunoselected with anti-FLAG antibody and analysed using SDS-PAGE and radiography. At each time-point, the densities of the relevant radioactive bands were quantified and, for each construct, expressed as percentage in the second immunoprecipitation step divided by the sum of the two immunoprecipitations (% insoluble). In (B, C) values from two fully independent transient expression experiments are shown.

prolamins (Xu and Messing, 2009; Gu *et al.*, 2010; Pedrazzini *et al.*, 2016). This led to the assembly in PBs and a change in the subcellular compartment used for permanent accumulation from the vacuole to the ER, particularly in rice and panicoïd cereals such as maize, sorghum, and millet (Lending and Larkins, 1989; Shewry and Halford, 2002; Saito *et al.*, 2012).

16γz originated upon maize WGD (Xu and Messing, 2008) and it is mainly characterized by deletions in the N-terminal region of 27γz, the most ancient γ-zein. We have shown here that recombinant 16γzf ectopically expressed in vegetative tissues accumulated within the ER, forming unusual structures. These did not resemble PBs or other ER-located polymers formed by natural or recombinant proteins expressed in plants (Bagga *et al.*, 1995; Mainieri *et al.*, 2004; de Virgilio *et al.*, 2008; Conley *et al.*, 2009; Saito *et al.*, 2009; Torrent *et al.*, 2009; Llop-Tous *et al.*, 2010). 16γzf structures mainly consisted of extensive, convoluted but well-defined filamentous threads; more

rarely, the enlarged ER also contained irregular, homogeneously electron-dense sectors, which may represent the proportion of 16γzf that had become insoluble. At the onset of prolamins accumulation, initial irregular dilatations along the ER have been observed in rice, but with diameters below 1 μm (Kawagoe *et al.*, 2005). 8S globulin, a mung bean vacuolar storage protein, forms 0.2–0.6 μm ER enlargements in transgenic tobacco BY2 cells and, as a GFP fusion, in Arabidopsis vegetative tissues and young developing seeds, to be correctly deposited in Arabidopsis storage vacuoles only at later seed development (Wang *et al.*, 2013). The sizes of these ER structures are one order of magnitude smaller compared the dilatations caused by 16γzf. Wider, irregular ER enlargements are formed by the expression of the N-terminal region of 27γz in Arabidopsis, but these have homogeneous electron density, with no signs of filaments (Geli *et al.*, 1994). PBs formed by chimeric fusions containing spider elastin-like polypeptides can have a loosely

packed content, but they are round and rarely larger than 3  $\mu\text{m}$ , with no well-defined filaments (Conley *et al.*, 2009; Phan *et al.*, 2014). Thus, the unusual structures that we found formed by 16 $\gamma\text{zf}$  markedly differed from 27 $\gamma\text{zf}$  PBs and from ER enlargements formed by various other storage proteins at early stages of seed development or by protein fusions that polymerize in the ER.

However, 16 $\gamma\text{zf}$  threads strikingly resemble those formed by diabetes insipidus-inducing mutants of the antidiuretic hormone arginine vasopressin precursor (Birk *et al.*, 2009; Beuret *et al.*, 2017). These dominant mutations can be in different locations along the precursor, but they all result in abnormal inter-chain disulfide bonds leading to oligomerization and, in some cases, partial resistance to denaturation by SDS/reducing agent, whereas the normal precursor has eight intra-chain bonds. The misfolded precursors thus accumulate in the ER instead of trafficking to secretory granules and form irregularly packed electron-dense filaments, which in some cases coalesce in more uniformly electron-dense regions, similar to 16 $\gamma\text{zf}$ . Although the mutated precursors seem unable to form canonical amyloid cross- $\beta$ -sheets, their ability to form fibers resembles amyloid aggregation (Beuret *et al.*, 2017).

Our results indicated that 16 $\gamma\text{zf}$  was not a structurally defective protein rapidly degraded by ER quality control. 16 $\gamma\text{zf}$  threads were disulfide-bonded polymers that remained partially soluble in oxidizing conditions, unlike 27 $\gamma\text{zf}$  polymers. Only when the two recombinant zeins were co-expressed, 16 $\gamma\text{zf}$  become fully insoluble unless reduced, indicating direct interactions with 27 $\gamma\text{zf}$ . 16 $\gamma\text{z}$  present in natural maize PBs was in part solubilized by alcohol together with  $\alpha$ -zeins, but no alcohol-soluble 16 $\gamma\text{zf}$  was detected in transgenic Arabidopsis or upon transient co-expression with 27 $\gamma\text{zf}$ . This supports the hypothesis that, in maize, at least one of the alcohol-soluble  $\alpha$ -zeins directly interacts with 16 $\gamma\text{z}$ , consistent with the location of 16 $\gamma\text{z}$  in natural PBs (Lending and Larkins, 1989; Yao *et al.*, 2016) and the results of yeast two-hybrid assays (Kim *et al.*, 2002, 2006). A specific role of 16 $\gamma\text{z}$  in natural, heterotypic PB assembly is also supported by the characteristics of two maize mutations with opaque endosperm, *mucronate* and *opaque10*. *mucronate* is a frameshift mutation that completely changes the 16 $\gamma\text{z}$  sequence for the last 63 amino acids, abolishes its solubility in 70% ethanol supplemented with 2-ME, and markedly weakens the interaction with 22-kD  $\alpha$ -zein (Kim *et al.*, 2006). In *mucronate* seeds, the overall amount of zeins is reduced (Salamini *et al.*, 1983) and PBs have angular deformations that often interrupt the outer layer, indicating defects in the organization of the interface between  $\alpha$ - and  $\gamma$ -zeins (Zhang and Boston, 1992). *opaque10* is a frameshift mutation generating a premature stop codon in a cereal-specific protein located in PBs (Yao *et al.*, 2016). *opaque10* PBs are misshaped and often irregularly elongated. The ordered localizations of 16 $\gamma\text{z}$  and of the 22-kD  $\alpha$ -zein that is normally located next to it are disrupted, and the two zeins are dispersed in the PB (Yao *et al.*, 2016). RNAi, used to inhibit the synthesis of  $\gamma$ -zeins in maize, also causes PB misshaping and angular deformations (Wu and Messing, 2010). A specific role of 16 $\gamma\text{z}$  could not be established in this case, since the synthesis of both the 27- and 16-kD polypeptides was almost fully inhibited. However,

RNAi in which the synthesis of 16 $\gamma\text{z}$ , 50 $\gamma\text{z}$ , and  $\beta$ -zein was concomitantly suppressed indicated that these proteins are mainly involved in PB expansion, whereas 27 $\gamma$ -zein controls PB initiation and shape, consistent with our data in transgenic Arabidopsis (Guo *et al.*, 2013).

Sorghum (*Sorghum bicolor*), a very close relative of maize (Swigoňová *et al.*, 2004), has not undergone WGD and contains only two genes belonging to the same prolamin II group of  $\gamma$ -zeins, *kafirin2 $\gamma$ 27* and *kafirin2 $\gamma$ 50* (Belton *et al.*, 2006; Xu and Messing, 2009), and is therefore lacking a 16 $\gamma\text{z}$  orthologue. Similar to  $\beta$ - and  $\gamma$ -zeins,  $\beta$ - and  $\gamma$ -kafirins form the more electron-dense structures of the PB; however, these are not limited to the PB periphery and are also concentrated in the central core or form patches within the less-dense regions (Shull *et al.*, 1992). This lack of organization in layers with clear boundaries between dense and less-dense regions (the latter mainly containing  $\alpha$ -type prolamins), compared to maize PBs may thus be related to the absence of a 16 $\gamma\text{z}$ -like prolamin.

Our domain-exchange results suggested that the different behavior of the two  $\gamma$ -zeins was mainly due to their N-terminal domains. A synthetic version of the (VHLPPP)<sub>8</sub> repeated segment has an amphipathic polyproline II structure and *in vitro* affinity to liposomes that partially mimics the lipid composition of the plant ER, suggesting that the repeat may favor interaction of 27 $\gamma\text{z}$  with the inner surface of the ER membrane (Kogan *et al.*, 2004). The Zera sequence is a 27 $\gamma\text{z}$  portion almost identical to the one used to construct zeolin and, like zeolin, it determines PB formation in a Cys-dependent fashion when fused to a number of proteins (Torrent *et al.*, 2009). In a Zera-fluorescent protein fusion, progressive deletion of the Pro-rich hexapeptides leads to progressively increased secretion and reduced PB size but does not alter their spherical shape (Llop-Tous *et al.*, 2010), indicating that the peculiar structures formed by 16 $\gamma\text{z}$  are not simply due to the loss of repeats. Indeed, the N-terminal region of 16 $\gamma\text{z}$  has also lost three Cys residues and contains two degenerated Pro-rich sequences containing two new Tyr residues—aromatic amino acids inhibit the formation of polyproline II helices (Brown and Zondlo, 2012)—as well as other aromatic amino acids and a new Gln-rich short sequence (Fig. 1). In combination, these features may have abolished the ability to interact orderly with lipids and determined the formation of rod-like polymers involved in stabilizing the  $\gamma$ -zein/ $\alpha$ -zein interface.

Proteins containing disulfide bonds generally have higher evolutionary rates (Feyertag and Alvarez-Ponce, 2017). Intra-chain disulfides probably stabilize important conformations and thus have a buffering, chaperone-like effect that makes the polypeptide more tolerant to mutations; thus, once acquired, inter-chain disulfides are rarely changed (Wong *et al.*, 2011; Feyertag and Alvarez-Ponce, 2017). Unpaired Cys residues are also relatively more conserved than other amino acids (Wong *et al.*, 2011). The major deletion and the mutations generating 16 $\gamma\text{z}$  have eliminated a number of 27 $\gamma\text{z}$  cysteine residues and have altered the biochemical and polymerization properties of the prolamin, but they have not caused gross misfolding and degradation by quality control. They have instead promoted a new role of the protein and a new PB organization.

Prolamins form peculiar heteropolymers. Analysis of many prolamin polypeptides and their positioning within a PB in different grasses indicates that a high genetic variability is tolerated, probably because PB function is simply constituted by the high accumulation of reduced nitrogen in the first compartment of the secretory pathway. However, within an individual species, certain requirements for optimal PB assembly exist, as indicated by the many natural and artificial cereal mutants analysed. We have shown here that an apparently defective zein polypeptide, generated upon maize whole-genome duplication, forms very unusual structures that may explain its specific structural role at the interface between the ancient and the more recently evolved maize prolamins. The organization of 16 $\gamma$ z structures resembles abnormally disulfide-linked, amyloid-like fibers formed by pathological mutants of a human hormone precursor. It thus appears that mutations giving rise to similar abnormal structures within the ER can result in pathogenic loss of function in one case but can be exploited in a developmental process in another.

## Supplementary data

Supplementary data are available at *JXB* online.

Fig. S1. Identities of the major polypeptides present in purified maize PBs, as determined by LC-ESI-MS/MS analysis (including the protocol for protein in-gel digestion and the analysis).

Fig. S2. Variability in denaturation-resistant oligomers.

Fig. S3. Dilated ER in leaf cells of transgenic *Arabidopsis* expressing 16 $\gamma$ zf.

Table S1. Peptide identification by LC-ESI-MS/MS analysis, and protein assignment.

## Acknowledgments

This work was supported by the Project 'Risorse biologiche e tecnologie innovative per lo sviluppo sostenibile del sistema agroalimentare' and Project 'Filagro - Strategie innovative e sostenibili per la filiera agroalimentare' of the 2006 and 2012 Agreements between Regione Lombardia and CNR. (to EP and AV).

## Author Contributions

D. Mainieri, EP, ES, and AV designed the research; D. Mainieri, CAM, BP, D. Maffi, MT, LE, FF, EP, and AV performed the experiments; ES, FF, EP, and AV wrote the manuscript.

## References

- Arcalis E, Stadlmann J, Marcel S, Drakakaki G, Winter V, Rodriguez J, Fischer R, Altmann F, Stoger E. 2010. The changing fate of a secretory glycoprotein in developing maize endosperm. *Plant Physiology* **153**, 693–702.
- Bagga S, Adams H, Kemp JD, Sengupta-Gopalan C. 1995. Accumulation of 15-kilodalton zein in novel protein bodies in transgenic tobacco. *Plant Physiology* **107**, 13–23.
- Belton PS, Delgadillo I, Halford NG, Shewry PR. 2006. Kafirin structure and functionality. *Journal of Cereal Science* **44**, 272–286.
- Beuret N, Hasler F, Prescianotto-Baschong C, Birk J, Rutishauser J, Spiess M. 2017. Amyloid-like aggregation of provasopressin in diabetes insipidus and secretory granule sorting. *BMC Biology* **15**, 5.
- Birk J, Friberg MA, Prescianotto-Baschong C, Spiess M, Rutishauser J. 2009. Dominant pro-vasopressin mutants that cause diabetes insipidus form disulfide-linked fibrillar aggregates in the endoplasmic reticulum. *Journal of Cell Science* **122**, 3994–4002.
- Brown AM, Zondlo NJ. 2012. A propensity scale for type II polyproline helices (PPII): aromatic amino acids in proline-rich sequences strongly disfavor PPII due to proline–aromatic interactions. *Biochemistry* **51**, 5041–5051.
- Chapman BA, Bowers JE, Feltus FA, Paterson AH. 2006. Buffering of crucial functions by paleologous duplicated genes may contribute cyclicity to angiosperm genome duplication. *Proceedings of the National Academy of Sciences, USA* **103**, 2730–2735.
- Clough SJ, Bent AF. 1998. Floral dip: a simplified method for *Agrobacterium*-mediated transformation of *Arabidopsis thaliana*. *The Plant Journal* **16**, 735–743.
- Coleman CE, Herman EM, Takasaki K, Larkins BA. 1996. The maize gamma-zein sequesters alpha-zein and stabilizes its accumulation in protein bodies of transgenic tobacco endosperm. *The Plant Cell* **8**, 2335–2345.
- Conley AJ, Joensuu JJ, Menassa R, Brandle JE. 2009. Induction of protein body formation in plant leaves by elastin-like polypeptide fusions. *BMC Biology* **7**, 48.
- de Virgilio M, De Marchis F, Bellucci M, Mainieri D, Rossi M, Benvenuto E, Arcioni S, Vitale A. 2008. The human immunodeficiency virus antigen Nef forms protein bodies in leaves of transgenic tobacco when fused to zeolin. *Journal of Experimental Botany* **59**, 2815–2829.
- Ems-McClung SC, Benmoussa M, Hainline BE. 2002. Mutational analysis of the maize gamma zein C-terminal cysteine residues. *Plant Science* **162**, 131–141.
- Faoro F, Tornaghi R, Belli G. 1991. Localization of the Closteroviruses on grapevine thin sections and their identification by immunogold labelling. *Journal of Phytopathology* **133**, 297–306.
- Feyertag F, Alvarez-Ponce D. 2017. Disulfide bonds enable accelerated protein evolution. *Molecular Biology and Evolution* **34**, 1833–1837.
- Geli MI, Torrent M, Ludevid D. 1994. Two structural domains mediate two sequential events in [gamma]-zein targeting: protein endoplasmic reticulum retention and protein body formation. *The Plant Cell* **6**, 1911–1922.
- Gomez-Navarro N, Miller E. 2016. Protein sorting at the ER–Golgi interface. *The Journal of Cell Biology* **215**, 769–778.
- Gu YQ, Wanjugi H, Coleman-Derr D, Kong X, Anderson OD. 2010. Conserved globulin gene across eight grass genomes identify fundamental units of the loci encoding seed storage proteins. *Functional & Integrative Genomics* **10**, 111–122.
- Guo X, Yuan L, Chen H, Sato SJ, Clemente TE, Holding DR. 2013. Nonredundant function of zeins and their correct stoichiometric ratio drive protein body formation in maize endosperm. *Plant Physiology* **162**, 1359–1369.
- Jiao Y, Wickett NJ, Ayyampalayam S, *et al.* 2011. Ancestral polyploidy in seed plants and angiosperms. *Nature* **473**, 97–100.
- Kassahn KS, Dang VT, Wilkins SJ, Perkins AC, Ragan MA. 2009. Evolution of gene function and regulatory control after whole-genome duplication: comparative analyses in vertebrates. *Genome Research* **19**, 1404–1418.
- Kawagoe Y, Suzuki K, Tasaki M, Yasuda H, Akagi K, Katoh E, Nishizawa NK, Ogawa M, Takaiwa F. 2005. The critical role of disulfide bond formation in protein sorting in the endosperm of rice. *The Plant Cell* **17**, 1141–1153.
- Kim CS, Gibbon BC, Gillikin JW, Larkins BA, Boston RS, Jung R. 2006. The maize *Mucronate* mutation is a deletion in the 16-kDa  $\gamma$ -zein gene that induces the unfolded protein response. *The Plant Journal* **48**, 440–451.
- Kim CS, Woo Ym YM, Clore AM, Burnett RJ, Carneiro NP, Larkins BA. 2002. Zein protein interactions, rather than the asymmetric distribution of zein mRNAs on endoplasmic reticulum membranes, influence protein body formation in maize endosperm. *The Plant Cell* **14**, 655–672.
- Klein EM, Mascheroni L, Pompa A, Ragni L, Weimar T, Lilley KS, Dupree P, Vitale A. 2006. Plant endoplasmic reticulum supports the protein

- secretory pathway and has a role in proliferating tissues. *The Plant Journal* **48**, 657–673.
- Kogan MJ, López O, Cocera M, López-Iglesias C, De La Maza A, Giralt E.** 2004. Exploring the interaction of the surfactant N-terminal domain of  $\gamma$ -Zein with soybean phosphatidylcholine liposomes. *Biopolymers* **73**, 258–268.
- Larkins BA, Hurkman WJ.** 1978. Synthesis and deposition of zein in protein bodies of maize endosperm. *Plant Physiology* **62**, 256–263.
- Lending CR, Larkins BA.** 1989. Changes in the zein composition of protein bodies during maize endosperm development. *The Plant Cell* **1**, 1011–1023.
- Llop-Tous I, Madurga S, Giralt E, Marzabal P, Torrent M, Ludevid MD.** 2010. Relevant elements of a maize  $\gamma$ -zein domain involved in protein body biogenesis. *The Journal of Biological Chemistry* **285**, 35633–35644.
- Mainieri D, Morandini F, Maîtrejean M, Sacconi A, Pedrazzini E, Alessandro V.** 2014. Protein body formation in the endoplasmic reticulum as an evolution of storage protein sorting to vacuoles: insights from maize  $\gamma$ -zein. *Frontiers in Plant Science* **5**, 331.
- Mainieri D, Rossi M, Archinti M, Bellucci M, De Marchis F, Vavassori S, Pompa A, Arcioni S, Vitale A.** 2004. Zeolin. A new recombinant storage protein constructed using maize  $\gamma$ -zein and bean phaseolin. *Plant Physiology* **136**, 3447–3456.
- Misra PS, Mertz ET, Glover DV.** 1976. Studies on corn proteins. IX. Comparison of the amino acid composition of Landry-Moureaux and Paulis-Wall endosperm fractions. *Cereal Chemistry* **53**, 699–704.
- Muench DG, Chuong SD, Franceschi VR, Okita TW.** 2000. Developing prolamine protein bodies are associated with the cortical cytoskeleton in rice endosperm cells. *Planta* **211**, 227–238.
- Pedrazzini E, Mainieri D, Marrano CA, Vitale A.** 2016. Where do protein bodies of cereal seeds come from? *Frontiers in Plant Science* **7**, 1139.
- Phan HT, Hause B, Hause G, Arcalis E, Stoger E, Maresch D, Altmann F, Joensuu J, Conrad U.** 2014. Influence of elastin-like polypeptide and hydrophobin on recombinant hemagglutinin accumulations in transgenic tobacco plants. *PLoS ONE* **9**, e99347.
- Pompa A, Vitale A.** 2006. Retention of a bean phaseolin/maize  $\gamma$ -Zein fusion in the endoplasmic reticulum depends on disulfide bond formation. *The Plant Cell* **18**, 2608–2621.
- Prat S, Cortadas J, Puigdomènech P, Palau J.** 1985. Nucleic acid (cDNA) and amino acid sequences of the maize endosperm protein glutelin-2. *Nucleic Acids Research* **13**, 1493–1504.
- Prat S, Pérez-Grau L, Puigdomènech P.** 1987. Multiple variability in the sequence of a family of maize endosperm proteins. *Gene* **52**, 41–49.
- Reyes FC, Chung T, Holding D, Jung R, Vierstra R, Otegui MS.** 2011. Delivery of prolamins to the protein storage vacuole in maize aleurone cells. *The Plant Cell* **23**, 769–784.
- Saito Y, Kishida K, Takata K, Takahashi H, Shimada T, Tanaka K, Morita S, Satoh S, Masumura T.** 2009. A green fluorescent protein fused to rice prolamins forms protein body-like structures in transgenic rice. *Journal of Experimental Botany* **60**, 615–627.
- Saito Y, Shigemitsu T, Yamasaki R, et al.** 2012. Formation mechanism of the internal structure of type I protein bodies in rice endosperm: relationship between the localization of prolamins species and the expression of individual genes. *The Plant Journal* **70**, 1043–1055.
- Salamini F, Di Fonzo N, Fornasari E, Gentinetta E, Reggiani R, Soave C.** 1983. *Mucronate*, *Mc*, a dominant gene of maize which interacts with *opaque-2* to suppress zein synthesis. *Theoretical and Applied Genetics* **65**, 123–128.
- Shewry PR, Halford NG.** 2002. Cereal seed storage proteins: structures, properties and role in grain utilization. *Journal of Experimental Botany* **53**, 947–958.
- Shull JM, Watterson JJ, Kirleis AW.** 1992. Purification and immunocytochemical localization of kafirins in *Sorghum bicolor* (L. Moench) endosperm. *Protoplasma* **171**, 64–74.
- Swigoňová Z, Lai J, Ma J, Ramakrishna W, Llaca V, Bennetzen JL, Messing J.** 2004. Close split of sorghum and maize genome progenitors. *Genome Research* **14**, 1916–1923.
- Torrent M, Llompart B, Lasserre-Ramassamy S, Llop-Tous I, Bastida M, Marzabal P, Westerholm-Parvinen A, Saloheimo M, Heifetz PB, Ludevid MD.** 2009. Eukaryotic protein production in designed storage organelles. *BMC Biology* **7**, 5.
- Vitale A, Smaniotto E, Longhi R, Galante E.** 1982. Reduced soluble proteins associated with maize endosperm protein bodies. *Journal of Experimental Botany* **33**, 439–448.
- Wang J, Shen J, Cai Y, Robinson DG, Jiang L.** 2013. Successful transport to the vacuole of heterologously expressed mung bean 8S globulin occurs in seed but not in vegetative tissues. *Journal of Experimental Botany* **64**, 1587–1601.
- Washida H, Sugino A, Messing J, Esen A, Okita TW.** 2004. Asymmetric localization of seed storage protein RNAs to distinct subdomains of the endoplasmic reticulum in developing maize endosperm cells. *Plant & Cell Physiology* **45**, 1830–1837.
- Wong JW, Ho SY, Hogg PJ.** 2011. Disulfide bond acquisition through eukaryotic protein evolution. *Molecular Biology and Evolution* **28**, 327–334.
- Woo YM, Hu DW, Larkins BA, Jung R.** 2001. Genomics analysis of genes expressed in maize endosperm identifies novel seed proteins and clarifies patterns of zein gene expression. *The Plant Cell* **13**, 2297–2317.
- Wu Y, Messing J.** 2010. RNA interference-mediated change in protein body morphology and seed opacity through loss of different zein proteins. *Plant Physiology* **153**, 337–347.
- Xu J-H, Messing J.** 2008. Organization of the prolamins gene family provides insight into the evolution of the maize genome and gene duplications in grass species. *Proceedings of the National Academy of Sciences, USA* **105**, 14330–14335.
- Xu J-H, Messing J.** 2009. Amplification of prolamins storage protein genes in different subfamilies of the Poaceae. *Theoretical and Applied Genetics* **119**, 1397–1412.
- Yamagata T, Kato H, Kuroda S, Abe S, Davies E.** 2003. Uncleaved legumin in developing maize endosperm: identification, accumulation and putative subcellular localization. *Journal of Experimental Botany* **54**, 913–922.
- Yao D, Qi W, Li X, Yang Q, Yan S, Ling H, Wang G, Wang G, Song R.** 2016. Maize *opaque10* encodes a cereal-specific protein that is essential for the proper distribution of zeins in endosperm protein bodies. *PLoS Genetics* **12**, e1006270.
- Yu M, Lau TY, Carr SA, Krieger M.** 2012. Contributions of a disulfide bond and a reduced cysteine side chain to the intrinsic activity of the high-density lipoprotein receptor SR-BI. *Biochemistry* **51**, 10044–10055.
- Zhang F, Boston RS.** 1992. Increases in binding protein (BiP) accompany changes in protein body morphology in three high-lysine mutants of maize. *Protoplasma* **171**, 142–152.



#### ANNUAL REVIEWS **Further**

Click [here](#) to view this article's online features:

- Download figures as PPT slides
- Navigate linked references
- Download citations
- Explore related articles
- Search keywords

# Plant Molecular Farming: Much More than Medicines

Marc Tschofen,<sup>1</sup> Dietmar Knopp,<sup>2</sup> Elizabeth Hood,<sup>3</sup>  
and Eva Stöger<sup>1</sup>

<sup>1</sup>Department of Applied Genetics and Cell Biology, University of Natural Resources and Life Sciences, 1190 Vienna, Austria;  
email: [eva.stoeger@boku.ac.at](mailto:eva.stoeger@boku.ac.at)

<sup>2</sup>Institute of Hydrochemistry, Chair for Analytical Chemistry, Technische Universität München, 80333 Munich, Germany

<sup>3</sup>Arkansas State University Biosciences Institute, Jonesboro, Arkansas 72467

Annu. Rev. Anal. Chem. 2016. 9:271–94

First published online as a Review in Advance on  
March 30, 2016

The *Annual Review of Analytical Chemistry* is online  
at [anchem.annualreviews.org](http://anchem.annualreviews.org)

This article's doi:  
10.1146/annurev-anchem-071015-041706

Copyright © 2016 by Annual Reviews.  
All rights reserved

## Keywords

biofuel, papermaking, plant biotechnology, plant-made proteins,  
recombinant protein, technical enzymes

## Abstract

Plants have emerged as commercially relevant production systems for pharmaceutical and nonpharmaceutical products. Currently, the commercially available nonpharmaceutical products outnumber the medical products of plant molecular farming, reflecting the shorter development times and lower regulatory burden of the former. Nonpharmaceutical products benefit more from the low costs and greater scalability of plant production systems without incurring the high costs associated with downstream processing and purification of pharmaceuticals. In this review, we explore the areas where plant-based manufacturing can make the greatest impact, focusing on commercialized products such as antibodies, enzymes, and growth factors that are used as research-grade or diagnostic reagents, cosmetic ingredients, and biosensors or biocatalysts. An outlook is provided on high-volume, low-margin proteins such as industrial enzymes that can be applied as crude extracts or unprocessed plant tissues in the feed, biofuel, and papermaking industries.

## INTRODUCTION

Molecular farming is the production of recombinant proteins in plants with the intention to use the protein itself as the product, in purified form, crude extracts, or in planta, rather than seeking a change in phenotype, performance, or metabolism. The first examples of molecular farming involved the production of an antibody and human serum albumin in transgenic plants and plant cell suspension cultures (1, 2). This led to the rapid exploration of many different plant species as hosts for the production of recombinant pharmaceutical proteins, a field sometimes described as molecular pharming (3, 4). Many proof-of-principle studies were published in the following years, but the breakthrough to commercial success only came once a defined regulatory framework was accepted for plant-derived biologics, culminating in 2012 with the approval of taliglucerase alfa, a recombinant form of human glucocerebrosidase developed by Protalix Biotherapeutics for the treatment of the lysosomal storage disorder Gaucher's disease (5).

Although pharming applications have taken the limelight, another quieter revolution has been under way in the area of plant-derived nonpharmaceutical proteins, which were first successfully commercialized by the US biotechnology company ProdiGene, Inc., in the late 1990s (6). Other companies have since taken up this mantle, including those with a clinical development program, in the realization that nonpharmaceutical products can reach the market more quickly because of the much lower regulatory burden. The product portfolio ranges from technical enzymes and research-grade reagents to cosmetic products (3, 7). There are more nonpharmaceutical products already on the market than there are pharmaceutical proteins undergoing clinical development (**Table 1**). Veterinary products produced in plants are also gaining attention, reflecting imminent regulatory changes enforcing the reduction of antibiotic use in food and dairy animals (8–10).

The benefits of molecular farming for pharmaceutical products are often described in terms of costs, scalability, and safety. Nonpharmaceutical products also benefit from the low costs and greater scalability of plants, but the benefits are magnified because downstream processing and purification does not have to meet the strict criteria enforced for pharmaceutical good manufacturing practice (GMP). A number of molecular farming products, including cell culture components, feed/food supplements, and cosmetic ingredients, attract a premium because the manufacturers can claim animal- and endotoxin-free production. There are also products not needing to be purified, such as enzymes that conditionally digest lignocellulose, that can be used to facilitate papermaking, biofuel production, and the manufacture of animal feed by avoiding the need for expensive additives and environmentally damaging pretreatment processes.

In this review, we discuss the nonpharmaceutical products of molecular farming in more detail, focusing on commercialized products such as antibodies, enzymes, and growth factors that are used as research-grade or diagnostic reagents, cosmetic ingredients, biosensors, and biocatalysts (including the conversion of plant biomass into sugars) and to facilitate bioremediation. Most commercial nonpharmaceutical products of molecular farming are currently produced on a small to medium scale, making it possible to rely on contained growing facilities rather than field cultivation, which attracts additional regulatory scrutiny. However, for low-margin products with a large potential market, the full potential of molecular farming will only be realized if large-scale production can be achieved.

## THE BENEFITS OF PLANTS AS EXPRESSION HOSTS

The benefits offered by plants as expression hosts are highlighted in several recent reports containing favorable head-to-head comparisons with other platforms (11–13). One of the key advantages of all plant-based systems is that plants are much less expensive than mammalian cells but have

**Table 1 Commercial development of nonpharmaceutical proteins produced in plants**

| Product  | Company                        | Application   | Plant species             | Development stage | Country       | Processing degree | Advantage                   | Source  |
|--|--------------------------------|---|---------------------------|-------------------|---------------|-------------------|-----------------------------|---|
| Trypsin, avidin, endo-1,4- $\beta$ -D-glucanase      | ProdiGene/Sigma-Aldrich        | Technical reagents                                    | Maize seeds               | Commercialized    | United States | Purified          | Cost, animal-free           | <a href="http://www.sigmaaldrich.com">http://www.sigmaaldrich.com</a> |
| Cellobiohydrolase I                                  | Infinite Enzymes/Sigma-Aldrich | Technical reagent                                     | Maize seeds               | Commercialized    | United States | Purified          | Cost, integrated production | <a href="http://www.sigmaaldrich.com">http://www.sigmaaldrich.com</a> |
| Growth factors, cytokines, thioredoxin, TIMP-2       | Agrenvec                       | Research reagents                                     | Tobacco leaves, transient | Commercialized    | Spain         | Purified          | Cost, animal-free           | <a href="http://www.agrenvec.com">http://www.agrenvec.com</a>         |
| Growth factors, cytokines                            | ORF Genetics                   | Research reagent                                      | Barley seeds              | Commercialized    | Iceland       | Purified          | Cost, animal-free           | <a href="http://www.orfgenetics.com">http://www.orfgenetics.com</a>   |
| Epithelial growth factor                             | Sif Cosmetics                  | Cosmetics   | Barley seeds              | Commercialized    | Iceland       | Purified          | Cost, animal-free           | <a href="http://www.sifcosmetics.com">http://www.sifcosmetics.com</a> |
| Albumin, lactoferrin, lysozyme, transferrin, insulin | Ventria Bioscience/InVitria    | Research reagents                                     | Rice seeds                | Commercialized    | United States | Purified          | Cost, animal-free           | <a href="http://www.invitria.com">http://www.invitria.com</a>         |
| Aprotinin  | Kentucky Bio-Processing        | Research reagent                                      | Tobacco leaves, transient | Commercialized    | United States | Purified          | Cost                        | <a href="http://www.kbpllc.com">http://www.kbpllc.com</a>             |
| Collagen   | CollPlant                      | Research reagent, tissue culture, health applications | Transgenic tobacco        | Commercialized    | Israel        | Purified          | Cost, animal-free           | <a href="http://www.collplant.com">http://www.collplant.com</a>       |

(Continued)

**Table 1 (Continued)**

| Product  | Company  | Application                             | Plant species             | Development stage         | Country       | Processing degree    | Advantage   | Source  |
|--|--|---|---------------------------|---------------------------|---------------|----------------------|---|---|
| Trypsin, enterokinase, growth factors, cytokines | Natural Bio-Materials                            | Research reagents, cosmetic ingredients | Rice cell suspension      | Commercialized            | South Korea   | Purified             | Cost, animal-free                                     | <a href="http://www.nbms.co.kr">http://www.nbms.co.kr</a>               |
| Antibody   | Center for Genetic Engineering and Biotechnology | Purification of a hepatitis B vaccine   | Transgenic tobacco        | Commercial application    | Cuba          | Purified             | Cost  | <a href="http://gndp.cigb.edu.cu">http://gndp.cigb.edu.cu</a>           |
| $\alpha$ -Amylase                                | Syngenta   | Bioethanol production                   | Maize seeds               | Commercialized            | United States | Biomass extract      | Cost, integrated production                           | <a href="http://www.syngenta.com">http://www.syngenta.com</a>           |
| Phytase  | Origin Agritech                                  | Feed                                    | Maize seeds               | Commercialization pending | China         | Delivered in biomass | Increased mineral availability, integrated production | <a href="http://www.originseed.com.cn">http://www.originseed.com.cn</a> |
| Growth factors                                   | NexGen   | Tissue culture reagent                  | Tobacco leaves, transient | Commercialized            | South Korea   | Purified             | Cost, animal-free                                     | <a href="http://www.nexgen.com">http://www.nexgen.com</a>               |

a similar secretory pathway. This allows them to fold and assemble complex proteins efficiently due to the presence of chaperones and protein disulfide isomerases that catalyze the formation of disulfide bonds, a capability not shared by bacterial production systems. This has proved invaluable for the production of pharmaceuticals, particularly multimeric proteins such as antibodies but also complex technical proteins such as collagen and spider silk (14–17). The secretory pathway is also where posttranslational modifications (PTMs) are carried out, including glycosylation,  $\gamma$ -carboxylation,  $\beta$ -hydroxylation, amidation, proline hydroxylation, and sulfation (18, 19). Glycosylation has received the most attention because there are differences in N-glycan and O-glycan structures between plants and mammals, and even between different plant and mammalian species, which can affect protein structure, biological activity, and stability when the protein is injected as a drug (20, 21). The precise control of glycosylation has allowed the production of plant-derived glycoproteins with humanlike or human-compatible glycans, as well as biobetters in which the glycan profiles have been tweaked to improve efficacy or longevity, or to simplify downstream processing (5, 22, 23). Glycosylation is less relevant for nonpharmaceutical proteins, but the other forms of modification listed above are necessary for some products to assemble properly; for example, proline hydroxylation is required for the assembly of collagen, and this capability can be conferred on plants by genetic engineering of the production host (17).

## OPTIMIZING THE YIELDS OF RECOMBINANT PROTEINS IN PLANTS

As with all expression systems, the yields of any given product of molecular farming are not predictable, because this depends on a combination of the intrinsic properties of the protein, the host, and the production strategy. Standardized approaches have been developed to improve the expression construct and this can be combined with various forms of strain and process optimization to ensure the greatest synergy between the host and its environment (24, 25). Strain optimization strategies are platform-specific. Plant cell suspension cultures can be improved by high-throughput screening to identify the most productive cells and use them to produce high-yielding monoclonal cell lines (26). In contrast, the yields in whole plants can be increased by breeding and selection among the best performing primary transformants, which identifies those with stable transgenes at permissive integration sites and pairs them with the optimal genetic background (27, 28). Process optimization strategies are similarly diverse. In cell cultures, this involves medium optimization and the testing of different bioreactor designs and process parameters, which has been accelerated recently by the use of statistical experimental designs to test multiple parameters simultaneously (29). For transgenic plants and transient expression platforms, the environment of the plant can have a substantial impact; for example, differences in temperature of only 1–2°C can change the yields of a recombinant protein by up to 15% (30). The combination of good construct design, optimal genetic background, and a supportive environment has achieved extraordinary yields of up to 10.6% of the total soluble protein (TSP) for human serum albumin expressed in rice seeds (31), 30% TSP for industrial enzymes expressed in maize seeds (32), 36% TSP for a murine antibody expressed in *Arabidopsis* (33), and more than 70% TSP for proteins expressed in tobacco chloroplasts (34).

## DIFFERENT SYSTEMS FOR DIFFERENT APPLICATIONS

The biopharmaceutical industry has consolidated around a small number of microbes and mammalian cell types grown in fermenters, but there is much more diversity in molecular farming, where different platforms offer overlapping and complementary benefits. Three major strategies

## GENE TRANSFER STRATEGIES

Molecular farming involves several distinct strategies for gene transfer that may involve either stable transformation or transient expression of a nonintegrated transgene. Stable transformation usually involves the integration of exogenous DNA into the nuclear genome, achieved using either *Agrobacterium tumefaciens* or a physical delivery technique such as particle bombardment. This can be applied to plant cells in culture to generate transgenic cell lines, or to callus tissue that can regenerate into whole transgenic plants. Alternatively, cell lines can be derived from transgenic plants directly. It is also possible to introduce transgenes into the plastid genome of certain species to generate transplastomic plants (119). There are several different transient expression methods. One approach is agroinfiltration, in which *A. tumefaciens* is injected or vacuum infiltrated into leaves so that many leaf cells take up but do not integrate the T-DNA and milligrams of protein can be produced in a few weeks (120–122). Other transient expression systems are based on systemically spreading plant RNA viruses (123–128). These approaches are combined in the Magniflection and CPMV-HT (*Cowpea mosaic virus* hypertranslatable) platforms, in which deconstructed viruses that cannot spread systemically are instead delivered to many cells by agroinfiltration (129–132).

have emerged: cell suspension cultures, transgenic plants, and transient expression (7, 35) (see the sidebar Gene Transfer Strategies).

One of the consequences of this diversity is that the platform can be matched to the requirements of the product rather than the product being modified to suit the platform, the latter being the typical approach in the biopharmaceutical industry. Plant cell cultures are grown in chemically defined sterile medium in fermenters and are particularly suitable for cosmetic ingredients and research/diagnostic reagents required in small quantities. The transient expression system can produce large amounts of protein in a short time, which is ideal for products with irregular demand and unstable markets. Transgenic plants have a long development process, but ultimately they are the most scalable and can be used to produce proteins required in the largest amounts. They are also the most suitable platform for in situ products, such as enzymes for the degradation of lignocellulose. In the special case of products that need to be stockpiled in an environment with no cold chain, transgenic cereal plants are ideal because recombinant proteins expressed in seeds have been shown to remain stable and active for several years without significant degradation (36).

## PROTEIN TARGETING

Recombinant proteins can be selectively expressed in particular plant organs by using restrictive rather than constitutive promoters. This strategy is chosen for two reasons. First, restrictive promoters often achieve higher yields in their target tissues than constitutive promoters (e.g., the promoters of endogenous storage protein genes in cereals are usually more active in seeds than promoters for housekeeping genes such as those encoding actin and ubiquitin). Second, it is often beneficial to target recombinant proteins to sink tissues, where they are more stable and do not interfere with vegetative growth (37).

Proteins can also be targeted to specific cellular compartments such as the cytosol, apoplast, or plastids or the lumen of the endomembrane system, using specific peptide tags. The endoplasmic reticulum (ER) is the first part of the secretory pathway, and its oxidizing environment supports protein folding, assembly, and PTM to a much greater extent than the cytosol. Proteins are directed to the ER by including an N-terminal signal peptide (38). By default, these pass through the Golgi body and are secreted to the apoplast, but other signals can be added to retrieve proteins to the

ER or divert them to the vacuole (39–41). The secretory pathway in seeds is ideal for molecular farming because it includes specialized storage organelles that allow proteins to accumulate and become encapsulated in a protective matrix (37, 42, 43). These storage organelles can even be induced ectopically in tissues that are not adapted for storage functions and provide a simple strategy for producing active insoluble enzyme polymers (44). For pharmaceutical applications, the inclusion of additional peptide tags changes the nature of the product and attracts additional regulatory scrutiny, but this is not an issue for nonpharmaceutical products and protein targeting can therefore be exploited fully to maximize yields and to accumulate a recombinant protein in a suitable compartment (**Figure 1**).

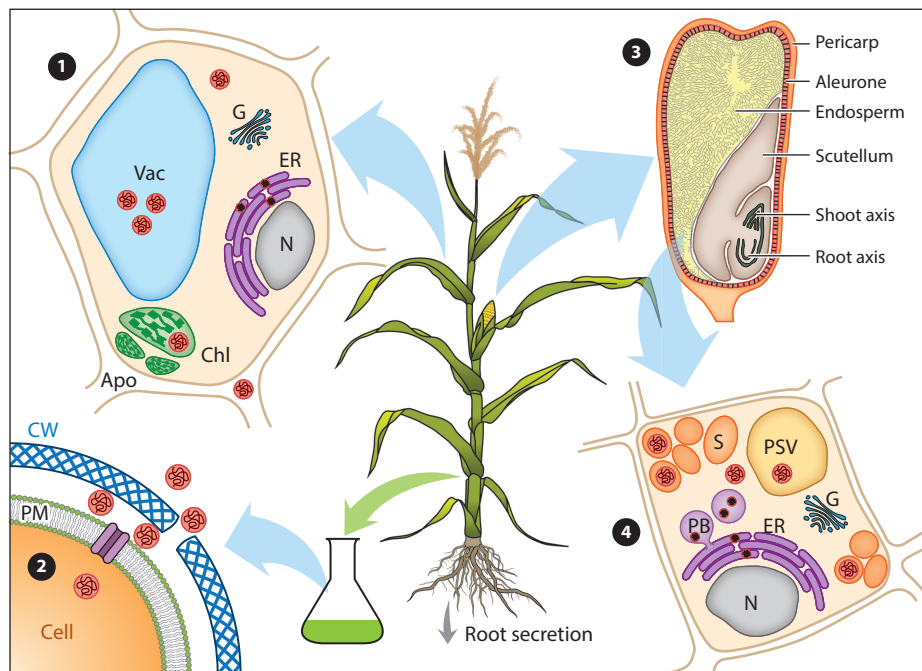


**Figure 1**

Targeting strategies for the expression of recombinant proteins. Recombinant proteins can be selectively expressed in particular plant organs such as leaves, roots, seeds or in cell cultures derived from one of these organs. Proteins can also be targeted to specific cellular compartments. In vegetative cells (**1**), proteins (red circles) can be targeted to the apoplast (Apo), the vacuole (Vac), or the cytosol, or they can be retained in the endoplasmic reticulum (ER). Recombinant proteins can also be targeted to the chloroplasts (Chl) by means of a signal peptide. Alternatively, the recombinant gene can be inserted in the chloroplast genome and expressed directly in the plastids. This approach often results in high yields of recombinant protein but does not support certain posttranslational modifications such as glycosylation. When plant cells are cultivated in a suspension culture, it is often beneficial to secrete the protein to the apoplast, because this facilitates purification from the culture medium (**2**). In some cases, digestion of the cell wall (CW) is an option to efficiently release protein trapped between the plasma membrane (PM) and the cell wall. Seeds (**3**) are a very attractive site for the accumulation of recombinant proteins due to their native storage capabilities. Within the seed, recombinant proteins may be directed to either the endosperm or the embryo. The unique storage organelles of the seed cells (**4**) include protein storage vacuoles (PSV), ER-derived protein bodies (PB), and starch granules (S), all of which have been used for protein accumulation. Finally, proteins can be produced in roots and secreted to the rhizosphere. This strategy is often preferred for phytoremediation purposes. Abbreviations: G, Golgi body; N, nucleus.

## DOWNSTREAM PROCESSING AND PURIFICATION

Downstream processing is the set of physical and chemical steps used to purify recombinant proteins from the biological starting material. Recombinant proteins produced in microbes or mammalian cells are usually secreted into the medium, and downstream processing follows a standardized procedure involving centrifugation and/or filtration to remove cells and debris, then chromatography steps tailored to each product. The diversity of molecular farming platforms means that the equivalent downstream processes for plants must cater to the different properties of each host system at least during the early steps. Whereas plant cell suspension cultures, aquatic plants, and some hydroponic whole-plant systems can secrete recombinant proteins into the medium, most products are retained within the plant tissue and must be released by disruption, which introduces numerous soluble and insoluble process-related contaminants (30).

The basic downstream process for whole-plant tissues therefore begins with extraction, which is achieved by homogenization or milling to disrupt cells and release the product into a buffer. For small-scale processes, the buffer may contain additives such as protease inhibitors to protect the target protein, but this becomes too expensive at larger scales and different strategies, such as flocculation, heat precipitation, or direct capture using robust affinity media, are required to rapidly remove impurities (30). Insoluble debris can be removed by centrifugation, but again this is difficult to scale up, so filtration is preferred when process scalability is important. Several in-line depth filters may be necessary to progressively remove coarse and fine debris, followed by a membrane filter to remove fines. Once the extract is clarified, further downstream processing is based on chromatography steps tailored to the product and is therefore similar to all other platforms.

However, a number of novel purification strategies have been developed in plants based on the use of fusion tags that encourage partitioning (see the sidebar Protein Tags for Purification). The disruption of plant tissues introduces process-related contaminants that are not found in bacteria, yeast, or mammalian cells (e.g., fibers, oils, and superabundant plant proteins such as RuBisCO) and these may require specific early processing steps to ensure removal (45–47). As discussed above, for upstream process optimization, downstream processing in molecular farming is now being addressed using statistical experimental designs and multivariate statistics to build quality into the process and ensure robust purification. Several costing studies have been reported recently using either top-down (48, 49) or bottom-up (50, 51) analytical approaches. Although plants do not produce endotoxins, downstream processing must nevertheless cater for their removal because the bacteria that colonize plants do produce endotoxins, and large amounts are produced during agroinfiltration. Similarly, plants do not support mammalian viruses but virus removal is

### PROTEIN TAGS FOR PURIFICATION

Several protein sequence tags have been used to simplify the downstream processing and purification of plant-derived recombinant proteins, including common affinity tags such as His<sub>6</sub> for immobilized metal affinity chromatography and more sophisticated tags for specialized separation processes that are less expensive and more scalable. The latter include elastin-like polypeptide tags that allow purification by temperature-dependent inverse transition cycling (133), hydrophobins that promote hydrophobic phase partitioning (134, 135), and oleosins that target proteins to the oil bodies of seeds, which can be separated in an oily phase by flotation centrifugation (136–138). Like the tags used for protein targeting, purification tags attract regulatory scrutiny for pharmaceutical products, but this is not an issue when the product is not intended for medical use.

still necessary under GMP conditions to prevent contamination with adventitious viruses during production, although the risk of contamination is acknowledged to be much lower than in mammalian systems (45). The costs of downstream processing for injectable pharmaceutical proteins are therefore similar across all platforms and can account for up to 80% of overall production costs, severely compromising any cost savings achieved by upstream production in plants. These restrictions do not apply to nonpharmaceutical products, and processing therefore represents a much smaller proportion of overall costs, even when the products are purified for use as technical reagents (52–54).

## OPPORTUNITIES FOR PURIFIED PRODUCTS

### Diagnostic and Technical Reagents

Bioanalytical methods rely on specific, high-affinity binding between a detection reagent and its target, for example, an enzyme and substrate or an antibody and antigen. Whereas enzymes are mostly used for process control and clinical diagnosis (e.g., the measurement of blood glucose), antibodies are used in a wider range of applications (see the sidebar Analytical Applications of Antibodies Produced by Molecular Farming). These include immunological assays for the detection of protein biomarkers, food allergens, toxins, chemical contaminants in food (e.g., pesticides, adulterants, and packaging derivatives), persistent organic pollutants in the environment, and pathogens for the purposes of disease monitoring and containment (55). Sensitive and cost-effective analytical methods are required for high-throughput screening when many samples need to be tested, and this approach is also useful for screening drug and catalyst libraries and for chemical reaction discovery and development (56, 57).

Antibodies were originally isolated from animals and were used as full-size molecules or enzymatic cleavage products such as Fab and F(ab)<sub>2</sub> antigen-binding fragments. The ability to produce antibodies as recombinant proteins and create libraries for screening against target antigens has enabled the development of smaller derivatives such as single-chain variable fragment(s) (scFv) and nanobodies [also known as variable heavy-chain antibody fragments (VHHs)] that facilitate screening for improved specificity, affinity, and stability (58, 59). Alternative binding scaffolds such as affibodies and anticalins can also be produced as recombinant proteins (60–62). Recombinant antibodies, fragments, and novel binders can also be produced as fusion proteins that extend their

### ANALYTICAL APPLICATIONS OF ANTIBODIES PRODUCED BY MOLECULAR FARMING

Many antibodies have been produced by molecular farming and some have already been tested for a wide range of analytical applications, including immunoaffinity solid-phase extraction and immunoextraction, which remove analytes without contaminants even when the analytes are present at low concentrations. The antibodies can be immobilized onto solid support materials like agarose, silica, polystyrene-divinylbenzene, and glass, as well as monolithic materials. Further applications include other immunoassay formats such as lateral flow devices, which are popular in food chemistry for on-site detection of allergens, pathogens, and toxins and for food authentication by key biomarkers (139, 140). More recent microfluidic platforms and bead-based methods reflect advances in nanoparticle technology and the synthesis of antibody-functionalized detection probes (141–143). In addition to the diagnostic use of antibodies in different immunoassay formats, there is an increasing interest in developing highly selective sorbents for efficient sample preparation.

functionality, for example, by combining a binding domain with a visual marker protein or with a toxin to allow the selective killing of cancer cells (58, 63).

Small antibody derivatives such as scFv are routinely produced in bacteria because they fold spontaneously and do not usually require glycosylation. In contrast, full-size antibodies contain multiple disulfide bonds and N-glycans, and although they can be produced in bacteria (64), mammalian cells are preferred. Chinese hamster ovary cells are the favored platform for pharmaceutical antibodies because they produce high titers. However, this platform is among the most expensive and is not suitable for low-margin antibodies used as technical reagents. Plants offer the necessary economy and scalability for technical reagents, so they have been widely used to produce antibody variants. The first demonstration of molecular farming was the production of a full-size IgG in tobacco (1), and many different formats and fragment types have been produced since then (65). Plants have also been used to produce a full-size secretory IgA, which normally requires two different types of mammalian cell (14) and an IgM, which is among the most complex of human proteins (15).

In a particularly innovative use of plants, Julve et al. (66) cloned an entire VHH library in deconstructed *Tobacco mosaic virus* vectors and introduced them into *Nicotiana benthamiana* leaves by agroinfiltration. Mosaic patterns of leaf cells, each infected with one particular strain of the virus (and hence one VHH coding sequence), were formed due to the phenomenon of superinfection exclusion, where two versions of the same virus cannot exist in the same cell, because one is always outcompeted. Whole-leaf extracts thus represented a polyclonal mixture of antibodies, whereas individual infection zones were monoclonal.

There are currently no plant-derived pharmaceutical antibody products on the market, although several have progressed to clinical development (45) and a tobacco-derived antibody against *Streptococcus mutans* has been approved as a medical device for the treatment of dental caries. A tobacco-derived antibody was also approved by Cuban authorities in 2006 as an affinity purification reagent for a hepatitis B vaccine produced in yeast (67). Although this antibody is not used as a pharmaceutical, it nevertheless had to meet GMP standards as part of the vaccine manufacturing process. The production of nonpharmaceutical antibodies in various formats has been demonstrated for applications in diagnostics, food processing, and quality validation, but none of these products have yet reached the market (58, 68).

Although plant-derived antibodies have not yet been marketed as diagnostics or research-grade reagents, other proteins have been produced in plants for this purpose. ProdiGene began this process by developing maize as a commercial platform for the production of enzymes and technical reagents, including avidin and  $\beta$ -glucuronidase (GUS), both of which are important molecular biology research tools (52, 53). An important principle demonstrated by these case studies was that molecular farming can be economically viable even when the natural source of a protein is abundant (e.g., egg whites for avidin and *E. coli* for GUS) and where a market is already established. The average yield of avidin in maize was 0.5% of the dry seed weight. A typical egg contains 1.5 mg of avidin, so 800 kg of eggs but only 20 kg of corn would be required to produce 20 g of avidin (69). The yield of *E. coli* GUS in maize was 80 mg/kg dry seed, and the maize product was identical in size and almost identical in functional parameters ( $pI$ ,  $K_m$ ,  $V_{max}$ , and  $K_i$ ) to its *E. coli* counterpart (53). Both GUS and avidin from maize have been distributed as research reagents by Sigma-Aldrich, and avidin is currently available.

## Biocatalysts

Trypsin is a serine protease found in the digestive system of many vertebrates and it can hydrolyze almost any protein at the C-terminal side of the basic amino acids lysine or arginine. In mammals,

pancreatic cells produce and store the inactive precursor trypsinogen and secrete it to the duodenum, where enteropeptidases as well as already-cleaved trypsin molecules activate it by cleaving off the propeptide Val-Asp-Asp-Asp-Asp-Lys (70).

The broad activity of trypsin makes it useful for many applications, ranging from food processing and leather tanning to specialized functions such as cleaving biopharmaceutical proteins and digesting proteins into peptides for proteomic analysis. Industrial trypsin is usually isolated from bovine or porcine pancreas, but these sources are deemed unsafe for pharmaceutical applications due to the risk of contamination with viruses and prions (71). However, the production of recombinant trypsin is challenging because the autoactivation of trypsinogen disrupts the host cell. In *E. coli*, this has been circumvented by periplasmic targeting or induction during the late logarithmic growth phase of a high-density, fed-batch culture, resulting in a yield of 56 mg/L (72). In yeast, cultivation can be carried out below the optimal pH range of trypsin to maintain its inactive state (73, 74). Alternatively, a mutation was introduced to prevent self-cleavage of the propeptide, resulting in yields of up to 40 mg/L, but the product must then be cleaved with a different enzyme in vitro (75).

In plants, these issues have been addressed by expressing inactive trypsinogen in maize seeds under the control of the embryo-preferred globulin-I promoter and the optimized barley  $\alpha$ -amylase signal sequence, resulting in a yield of 3.3% TSP (76). The progeny of this maize line produced 58 mg of trypsin per kilogram of seed. The trypsinogen was fully converted into active trypsin upon extraction apparently by autocatalytic processing and/or endopeptidases in the seeds. The maize-derived trypsin was functionally identical and physically similar to native bovine trypsin ( $V_{\max}$ ,  $K_m$ , pH optimum, stability, and inhibition by aprotinin and benzamidine), although unlike the native protein, it was also glycosylated (76). Further characterization revealed an unusual non-consensus N-glycosylation site at Asp77 (77). This product was marketed as TrypZean<sup>TM</sup> and has been distributed since 2002 by Sigma-Aldrich (product no. T3568, T3449) as a reagent to dissociate adherent cells from vessel surfaces. TrypZean is covered by a number of patents and patent applications (78). Recombinant bovine trypsin was also produced in rice cell suspension cultures under the control of the sucrose starvation-inducible rice  $\alpha$ -amylase 3D promoter achieving yields of 68 mg/L of medium (79). This product is currently marketed by Natural Bio-Materials, South Korea (Table 1).

Only a few manufacturers can offer recombinant animal-free trypsin at a price that is competitive with maize-derived trypsin. TrypZean usually sells at approximately \$10/mg whereas trypsin from *Escherichia coli* costs more or less the same and that from *Pichia pastoris* is twice as expensive. Despite all efforts, none of these systems achieves the economy of trypsin from bovine or porcine pancreas, which sells at approximately \$100/g (78). However, certifiable animal- and endotoxin-free products are quality attributes that are valued in the market for tissue culture components and cosmetics (Table 1).

## Biopolymers

Plants are the main source of the world's most abundant natural polymers—lignocellulose and starch—both of which offer sustainable alternatives to nonrenewable, fossil-derived fuels and materials. Molecular farming has a role to play in this context because it also allows plants to be developed as a source of fibrous animal proteins such as collagen, keratin, silk, and elastin, which have remarkable strength, toughness, elasticity, and biocompatibility and can therefore be used to produce novel and sustainable biopolymers that could replace oil-based plastics (80).

Collagens are the main structural proteins in the extracellular matrix of mammals. The most abundant form is type I collagen which is a helical heterotrimer composed of two  $\alpha 1(I)$  and

one  $\alpha 2(I)$  polypeptide chains. The heterotrimeric helix represents procollagen which then polymerizes with other helices to form fibrils and fibers of indeterminate length with elaborate three-dimensional structures (81). The Israeli biotechnology company CollPlant has developed a tobacco line producing fully functional recombinant human collagen. They achieved this by expressing procollagen  $\alpha 1(I)$  and  $\alpha 2(I)$  along with a human proline-4-hydroxylase to allow the PTM of proline residues that is required for structural stabilization, and a human lysyl hydroxylase 3 that affects fibril diameter. By targeting the protein to the vacuole, they obtained a yield of 2% TSP, which translates to 200 mg/kg leaf material (17). CollPlant now markets its recombinant human collagen as Collage<sup>TM</sup> for tissue repair and wound management applications. Conventional medical collagen is sourced from animals and human cadavers with the consequent risk of infection. These collagens also need to be processed to remove cross-links before use, whereas the plant-derived collagen is pathogen free and has no cross-links, so it can be modified to meet the demands of any given application. Collagen is also used in cell culture, cosmetics, and adhesives, as well as in the food industry in the form of gelatin.

Many insect and spider species produce silk, which is a proteinaceous fiber with two main components: the structural protein fibroin and the adhesive protein sericin. The physicochemical properties of silk proteins differ from species to species and even within a species. The strength, elasticity, and stiffness can vary depending on the amino acid sequence and arrangement of fibers. The orb web spider *Nephila clavipes* produces different kinds of silk for webs, cocoons, and draglines. The dragline silk is five times stronger by weight than steel and three times tougher than *p*-aramid (Kevlar<sup>®</sup>), one of the strongest man-made fibers (16). Silk proteins are challenging to express in microbes and mammalian cells because they are several hundred kilodaltons in size and cannot be secreted. Scheller et al. (82) were the first to produce spider silk proteins in plants, achieving yields of up to 2% TSP in tobacco leaves and potato tubers. Various strategies have been developed to ensure that recombinant silk proteins are produced at the correct native size, including dimerization by nonrepetitive C-termini, cross-linking by transglutaminase, and intein-mediated multimerization (16, 83, 84).

## PRODUCTS WITHOUT THE NEED FOR PURIFICATION

### Feed Additives

Feed additives improve the quality of animal feed by providing direct nutrition (e.g., milk proteins) or by improving the digestibility of existing components. The latter category, known as feed enzymes, is generally divided into two classes: those required to break down indigestible fibers (e.g., hemicellulases) and those required to remove antinutritional factors (e.g., phytases). Feed additives are routinely produced in microbes and then added to animal feeds as supplements. This is an expensive process and the combined market for feed enzymes is projected to reach \$727 million in 2015 (85). A more efficient and less expensive strategy would be to express these enzymes directly in the feed crops as shown in the following three examples.

Maize kernels are a good source of phosphorus, but the element is stored primarily as a complex with phytate, which cannot be digested by monogastric animals, because they lack the enzyme phytase. Phytate also sequesters other essential mineral nutrients such as iron, zinc, and calcium (86). These issues are currently addressed by supplementing animal feed with expensive recombinant phytase produced in *P. pastoris*, but the costs could be reduced by expressing phytase directly in feed crops. The endosperm-specific overexpression of *Aspergillus niger* phytase in maize produced an enzyme that was functionally equivalent to the commercial supplement, and the enzyme activity was sufficient to achieve adequate phosphorus release from normal maize by adding just 5 g

of transgenic seeds to 1 kg of the regular diet. The enzyme was also resistant to gastric digestion allowing it to act on phytate in the gut. Following successful field trials in chickens, phytase-enhanced maize was released as China's first transgenic crop in 2009, and the biosafety certificate was renewed in 2015 (87).

Like phytase, the enzymes  $\beta$ -mannanase and  $\beta$ -glucanase are often added to animal feeds to eliminate antinutritional factors. In this case, the targets are mannans and glucans, which absorb water and increase the viscosity of chyme, thus restricting access to the intestinal surface and reducing the efficiency of nutrient uptake. Maize lines expressing *Bispora* sp. MEY-1  $\beta$ -mannanase under the control of an embryo-specific promoter were tested because *Bispora* is an acidophile and the enzyme should therefore remain functional in the low-pH gastric environment. The enzyme was found to remain active under the same conditions as the commercial supplement from *P. pastoris* but was more thermotolerant during pelleting, with an activity of 10,000 U/kg (87). A feeding trial of  $\beta$ -mannanase supplements in pigs revealed that 400 U/kg feed achieved the greatest feed efficiency, so 40 g of the transgenic seeds per kilogram of conventional diet is sufficient to achieve the anticipated effects (88). The same group also expressed an acidic endo- $\beta$ -1,3-1,4-glucanase in maize embryos with an activity of 170,000 U/kg and stability over the pH range 1.0–8.0 (89).

## Biofuel

The United States is currently the largest producer of maize in the world. Historically, maize has been used primarily for animal feed with only 20% used for food, seed production, and industrial applications. More recently, the growth of the biofuel industry has seen this profile change radically, and today the proportion of maize used for feed and bioethanol production is roughly equal at 44% each, with the remainder used for food, seed, and other (90). The 13.3 billion gallons of bioethanol produced in the United States every year represent 55% of global production.

Maize as food and feed is a good source of carbohydrates, primarily in the form of starch, and this polymer is also the feedstock required for bioethanol production, resulting in competition among producers of feed, food, and bioethanol for agricultural space. However, bioethanol can also be produced from cellulose and hemicellulose, which have nutritional value only for ruminants, are much more abundant than starch and sugar, and are often found in the residue or bagasse from food/feed crops. Biofuels derived from cellulose and hemicellulose would therefore be more sustainable and would not compete with food and feed. Cell wall polymers such as lignocellulose and hemicellulose are abundant sources of fermentable sugars, but the sugars are not released as readily as they are from starch because the polymers tend to be cross-linked, structurally heterogeneous, and pseudocrystalline, making them recalcitrant to enzymatic hydrolysis without harsh and expensive pretreatments. A combination of several enzymes is then required to yield sugars from the recalcitrant biomass, and even conservative estimates suggest that up to 0.6 tons of pure enzyme would be needed to generate the 20 billion gallons of bioethanol that the United States has mandated for 2022, with an estimated infrastructure cost of nearly \$30 billion to achieve this output using microbial fermentation (91).

The expression of polymer-degrading enzymes in plants would be less expensive than in microbes, and the enzymes could be purified, used as crude extracts, or preferably expressed in the biofuel crop directly. The complete hydrolysis of cellulose to glucose requires three enzymes (an exo-1,4- $\beta$ -glucanase, an endo-1,4- $\beta$ -glucanase, and a  $\beta$ -D-glucosidase), and a second stream of fermentable pentoses can be derived from xylan using the enzymes endo-1,4- $\beta$ -D-xylanase,  $\beta$ -xylosidase, and  $\alpha$ -glucuronidase; most of these enzymes have already been successfully expressed in plants (92). Maize lines individually expressing endo- $\beta$ -1,4-glucanase and endo- $\beta$ -1,4-xylanase

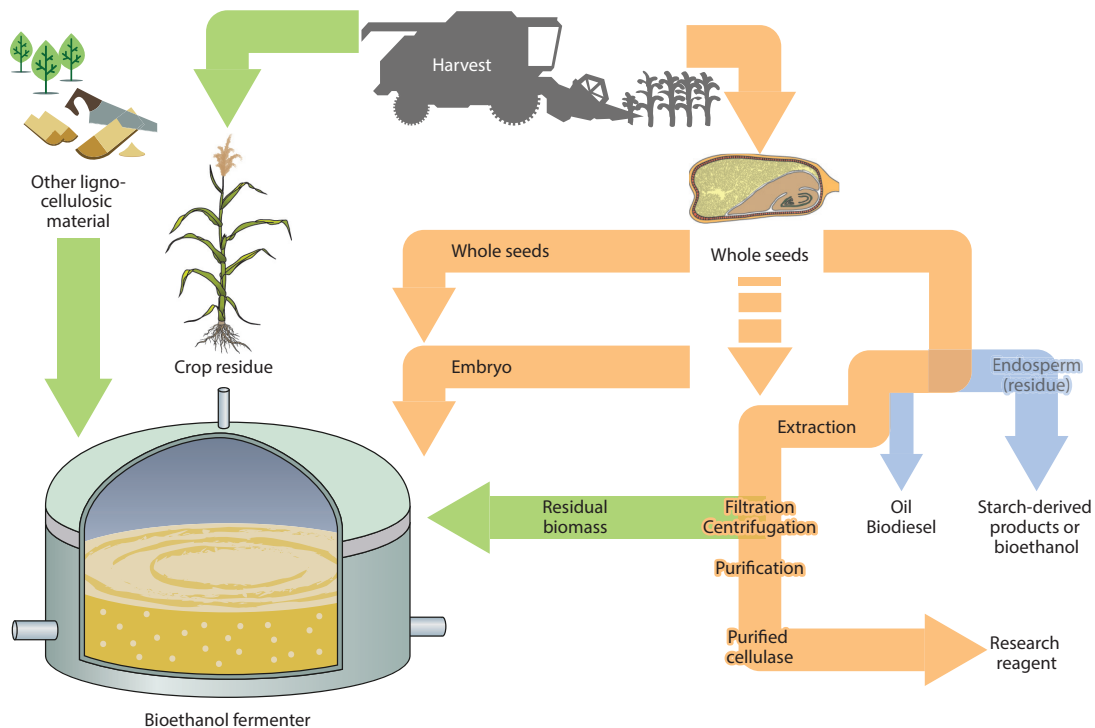


**Figure 2**

Plant-derived recombinant enzymes for biofuel production. Cellulases produced in maize seeds can be purified as research reagents or used in the bioethanol production process either as crude extract or enzyme-containing biomass. The residues arising from the processing steps provide additional biomass or valuable side products. Biomass flows are represented by green, added value product streams by blue, and cellulase-containing fractions by orange arrows. If the cellulase is produced in the embryo, then endosperm and embryo can be separated to reduce the enzyme-to-biomass ratio and the residual endosperm can be used for starch-derived products. Similarly, the embryo can be defatted to obtain oil as a valuable side product.

were produced by the US company Agrivida and were shown to increase bioethanol production from 42% to 65% theoretical ethanol yield (93). This group also engineered an improved thermostable xylanase containing a bacterial self-splicing intein that prevents autohydrolysis during growth but can be induced by heat after harvest (94).

Another company, Edenspace Systems Corporation, has patented transgenic plants expressing cellulase, hemicellulase, ligninase, or combinations thereof for improved saccharification (95). Currently, the only commercially available plant-derived hydrolase is an exo-1,4- $\beta$ -glucanase from *Trichoderma reesei* produced in maize by Infinite Enzymes, LLC as a purified protein (Sigma-Aldrich product no. E6412). The pricing includes the costs for extraction and purification making it unsuitable for large-scale applications. Even so, the enzyme is expressed under the control of the embryo-preferred globulin-1 promoter, so defatted germ formulations can be used for industrial saccharification (91) as shown in **Figure 2**. Expression levels of >6% TSP were achieved (96) corresponding to 0.5% of the dry seed weight after seven backcrosses and two generations of self-pollination (91). Assuming that expression levels can be improved to 1% of the dry seed weight and that saccharification requires 30 g of enzyme per gallon of biofuel, a cultivation area of only 64 square miles for enzyme production would be sufficient to achieve an output of 20 million gallons of biofuel.

The production of biofuels from lignocellulosic biomass will take time to establish on a global scale, and in the meantime it may be possible to optimize the production of bioethanol production from maize starch by improving the efficiency of amylases, the enzymes that digest starch into sugars. The current conversion process involves the addition of  $\alpha$ -amylase and/or  $\beta$ -amylase. Enogen<sup>®</sup> is a maize line expressing a thermostable  $\alpha$ -amylase, which was developed by Syngenta and approved by the US Department of Agriculture in 2011. If conventional maize feedstock is mixed with Enogen at a 3:1 ratio, production costs fall by \$0.04 per gallon, water usage by 7.7%, and natural gas consumption by 8.9% (97). Amylase-expressing plants could also be used for malting, baking, and the production of glucose and fructose syrup from starch (98).

## Paper Manufacturing

In the paper manufacturing industry, the raw wood pulp undergoes a delignification process to separate the lignin from the cellulose fibers and the cellulose-rich pulp is often bleached to produce white paper. Both processes require harsh physical and chemical treatments that generate environmental pollution. Laccase is a copper-containing oxidoreductase found in white rot fungi that can oxidize phenolic compounds such as lignin, and this can be incorporated into almost every part of the papermaking process to reduce the use of chemicals and energy, avoid chemical waste, and improve paper strength and quality (99). As in the other cases discussed above, the main factor that prevents the adoption of laccase-based pulping is the cost of the microbial recombinant enzyme. Similarly, molecular farming would allow the enzyme to be applied as crude extracts or to be expressed in the trees used for the raw material as long as it remained inactive prior to cropping. Laccase from the white rot fungus *Trametes versicolor* has been produced in maize and some detrimental effects were observed even when expression was controlled by an embryo-preferred promoter with subcellular targeting to the cell wall (100). The yield was 2.0% TSP or 50 ppm of seed weight in the fifth generation (101). Xylanase can also be used to process pulp (102). The sequential treatment of pulp with xylanase and laccase resulted in a 50% reduction in postcolor number, a 15.71% increase in the tear index, and lower levels of absorbable organic halogens (34%) in the bleach effluents (103). Laccase could also be used to treat textile mill effluents, remove phenolic compounds from beverages, remove sulfur from fossil fuels, and develop biosensors (104). Plants that are engineered to secrete laccase from their roots could also be used to remove pesticides and xenohormones from the soil (104–106).

## Future Products

Enzymes are advantageous for industrial processes because they yield specific products (thus reducing toxic residues) and operate at low temperatures using water as a solvent (thus reducing the need for harsh chemicals). The current industrial enzyme market is worth approximately \$8 billion with a compound annual growth rate of 7% (107). Plants are ideal for the production of enzymes because they are inexpensive and highly scalable, which means it is much less expensive to expand production capacity than would be the case for any fermenter-based system (108). Plants can also produce enzymes that are toxic to microbes and animal cells. The applications of molecular farming in the field of industrial enzymes will depend on the ability to produce cost-effective alternatives for recombinant enzymes currently produced in microbes.

Enzymatic biodiesel is one of the most lucrative new applications of biotechnology-derived enzymes because it is a nonpolluting and carbon-neutral fuel (109). Biodiesel can be manufactured from numerous oils and fats, including virgin vegetable oils and waste cooking oils and fats. Europe produces the most biodiesel in the world with the United States in second place, and the global

production volume exceeds 6 billion gallons per year (110). Recombinant enzymes for biodiesel production are generally too expensive when produced in microbes, but plants could be used for the inexpensive production of lipases and phospholipases that can be purified, used as crude extracts, or expressed in oil crops directly. Phospholipase can also be used to remove gum from vegetable oils to prevent the formation of emulsions that limit the yield of pure oils for food and biodiesel applications (111).

The biorefinery concept will also be important in future developments because this will allow the design of low-waste processes in which all raw materials are converted into useful products, for example, sugar cane processes that also process the bagasse and wood pulping processes that also utilize the tree bark (112). Xylanase and oxidation/reduction enzymes such as laccase and peroxidase are suitable for these applications because the reactions are difficult to achieve through nonenzymatic means, offering a large potential market for low-cost recombinant enzymes produced on a large scale in plants rather than microbes (114). Enzymes such as manganese peroxidase and laccase have been produced in maize seeds (100, 113). The manganese peroxidase accumulated to high levels without detrimental effects when the enzyme was targeted to the embryo cell wall, whereas laccase lignified the embryo and inhibited germination suggesting it should be produced in an inactive form to allow normal vegetative growth.

### Economic Considerations

The economic principles of molecular farming depend not only on the actual costs of the process but also the development time, which can range from 1 year for a product required in small amounts produced using a transient expression system to 7–10 years for a product required on a large scale produced in transgenic crop seeds. The scale of production provides the greatest benefit compared to fermenter-based systems because it costs much more to scale up fermenter infrastructure than to grow additional hectares of a production crop, even if the crop is grown in greenhouses rather than open fields (108). We consider here the development of transgenic maize lines expressing cellobiohydrolase (CBH1) as a case study (115–117).

The transformation and regeneration of transgenic maize lines takes approximately 1 year. When the T1 seeds are available, they are screened to identify the best-performing lines. The best T1 plants are crossed with elite inbred germplasm, backcrossed over six generations, and self-crossed for a further two generations to generate parental transgenic lines in an elite background that can be used to generate hybrids for enzyme production. This process takes 4 years if a winter nursery is used to double the generations achieved per year but is worth the effort because large increases in yield are achieved. In the case of the CBH1 lines, the production hybrids achieved a twentyfold increase in yield over the original T1 seeds (116). During the breeding process, excess grain was used to optimize extraction and purification methods for product characterization and to test downstream applications in biomass conversion (117).

The most challenging stage of the process is scaling up production to meet customer demand. The initial laboratory-scale process was suitable for the purification of approximately 1 g of enzyme per month from 2 kg of grain and could be achieved using bench-scale equipment. In contrast, a typical pulp and paper mill would require approximately 12 kg of enzyme per week. Infinite Enzymes (<http://www.infiniteenzymes.com>) is currently working with an agricultural engineer to design a process that will meet this demand by supplying 1,900 L of extract containing the enzyme at a concentration of 6 g/L. Assuming an enzyme yield of 0.5% dry seed weight, this would require the processing of 2.5 tonnes of seed per week. This is well beyond laboratory scale but far below the commercial scale of most US agricultural processing companies (e.g., ADM, which processes more than 76,000 tonnes of grain per day). The development of a processing facility is

therefore challenging because most equipment is designed for smaller laboratory scale or larger industrial scale operations. Pilot plant equipment can be used to provide standard apparatus such as mixing tanks, but more specialized equipment such as wet or dry milling units to separate germ and endosperm and continuous flow filtration units adequate for removing flour solids are more difficult to source. The cost of scale-up can approach \$500,000 to \$1 million, although one way to lower this cost is to lease the equipment.

The upstream production scale required to meet demand can be calculated by using conservative yield estimates of 1 tonne of grain per acre. Approximately 730 hectares (1,825 acres) would therefore be needed to produce enough grain to meet the annual demand of one pulp and paper mill. In the United States, this scale of production could be carried out under permit without deregulating the product as long as sufficient isolation could be achieved. Although this is possible, it is not ideal, because the cost of custom grain production is relatively high at \$1,200 per acre. Profit can be made if the sales volume is high and processing is efficient, but this clearly demonstrates why it is important to optimize the enzyme yield to maximize production per hectare. In other countries, the regulatory burden of medium- to large-scale production (118) is circumvented by growing the production crop in greenhouses, for example, ORF Genetics in Iceland.

## CONCLUSION

The plant-derived nonpharmaceutical proteins that are commercially available currently outnumber the medical products of molecular farming, reflecting the shorter development times and lower regulatory burden outside the pharmaceutical industry. Most of the nonpharmaceutical proteins are produced on a small to medium scale, which avoids the regulatory burden associated with large-scale agricultural production. However, molecular farming is increasingly being considered as an economic alternative not only for the production of pure diagnostic and technical reagents required in small amounts but also for high-volume, low-margin industrial enzymes that can be applied as crude extracts or unprocessed plant tissues in the feed, biofuel, and papermaking industries, which will require increasingly larger industrial processes.

### SUMMARY POINTS

1. Plant-based production systems are established on the market. The first product for human medical use was commercialized in 2012, but currently the nonpharmaceutical products outnumber the pharmaceutical products as they do not require clinical studies and thus generate faster returns.
2. The palette of market sectors comprises research-grade or diagnostic reagents, cosmetic ingredients, biosensors or biocatalysts but also industrial enzymes used in the feed, biofuel, and papermaking industries.
3. Key advantages of plant-derived products are animal- and endotoxin-free production and cost advantages for the raw materials and processing.
4. Large-scale use of technical reagents, antibodies, and industrial applications could become feasible, but scale-up will require some investment to install equipment for these products.

5. Plants are renewable biomass for energy production. Enzymes used in the biomass conversion process could be produced directly in the plant biomass rather than in separate microbial systems.
6. Further development and widespread success of the technology will be strongly influenced by the level of regulation and restrictions applied to genetically modified plants and products derived thereof. In order to directly benefit from the technology, Europe will have to be proactive in the regulatory process.

## DISCLOSURE STATEMENT

Infinite Enzymes, LLC is owned by E.H. and partners.

## ACKNOWLEDGMENTS

The authors acknowledge financial support by the Austrian Science Fund (I1103) and the German Research Foundation (KN348/16–1).

## LITERATURE CITED

1. Hiatt A, Cafferkey R, Bowdish K. 1989. Production of antibodies in transgenic plants. *Nature* 342:76–78
2. Sijmons PC, Dekker BM, Schrammeijer B, Verwoerd TC, van den Elzen PJ, Hoekema A. 1990. Production of correctly processed human serum albumin in transgenic plants. *Biotechnology* 8:217–21
3. Paul MJ, Teh AY, Twyman RM, Ma JK. 2013. Target product selection—Where can molecular pharming make the difference? *Curr. Pharm. Des.* 19:5478–85
4. Stöger E, Fischer R, Moloney M, Ma JK. 2014. Plant molecular pharming for the treatment of chronic and infectious diseases. *Annu. Rev. Plant Biol.* 65:743–68
5. Tekoah Y, Shulman A, Kizhner T, Ruderfer I, Fux L, et al. 2015. Large-scale production of pharmaceutical proteins in plant cell culture—the protalix experience. *Plant Biotechnol. J.* 13:1199–208
6. Hood E, Witcher D, Maddock S, Meyer T, Baszczynski C, et al. 1997. Commercial production of avidin from transgenic maize: characterization of transformant, production, processing, extraction and purification. *Mol. Breed.* 3:291–306
7. Fischer R, Schillberg S, Buyel JF, Twyman RM. 2013. Commercial aspects of pharmaceutical protein production in plants. *Curr. Pharm. Des.* 19:5471–77
8. Kolotilin I, Topp E, Cox E, Devriendt B, Conrad U, et al. 2014. Plant-based solutions for veterinary immunotherapeutics and prophylactics. *Vet. Res.* 45:117
9. MacDonald J, Doshi K, Dussault M, Hall JC, Holbrook L, et al. 2015. Bringing plant-based veterinary vaccines to market: Managing regulatory and commercial hurdles. *Biotechnol. Adv.* 33(8):1572–81
10. Clarke JL, Waheed MT, Lossl AG, Martinussen I, Daniell H. 2013. How can plant genetic engineering contribute to cost-effective fish vaccine development for promoting sustainable aquaculture? *Plant Mol. Biol.* 83:33–40
11. Avesani L, Merlin M, Gecchele E, Capaldi S, Brozzetti A, et al. 2014. Comparative analysis of different biofactories for the production of a major diabetes autoantigen. *Transgenic Res.* 23:281–91
12. Merlin M, Gecchele E, Capaldi S, Pezzotti M, Avesani L. 2014. Comparative evaluation of recombinant protein production in different biofactories: the green perspective. *Biomed. Res. Int.* 2014:136419
13. Baeshen NA, Baeshen MN, Sheikh A, Bora RS, Ahmed M, et al. 2014. Cell factories for insulin production. *Microb. Cell Fact.* 13:141
14. Ma JK, Hiatt A, Hein M, Vine ND, Wang F, et al. 1995. Generation and assembly of secretory antibodies in plants. *Science* 268:716–19

15. Loos A, Gruber C, Altmann F, Mehofer U, Hensel F, et al. 2014. Expression and glycoengineering of functionally active heteromultimeric IgM in plants. *PNAS* 111:6263–68
16. Hauptmann V, Weichert N, Rakhimova M, Conrad U. 2013. Spider silks from plants - a challenge to create native-sized spidroins. *Biotechnol. J.* 8:1183–92
17. Stein H, Wilensky M, Tsafir Y, Rosenthal M, Amir R, et al. 2009. Production of bioactive, post-translationally modified, heterotrimeric, human recombinant type-I collagen in transgenic tobacco. *Biomacromolecules* 10:2640–45
18. Komori R, Amano Y, Ogawa-Ohnishi M, Matsubayashi Y. 2009. Identification of tyrosylprotein sulfotransferase in Arabidopsis. *PNAS* 106:15067–72
19. Matsubayashi Y. 2011. Post-translational modifications in secreted peptide hormones in plants. *Plant Cell Physiol.* 52:5–13
20. Gomord V, Fitchette AC, Menu-Bouaouiche L, Saint-Jore-Dupas C, Plasson C, et al. 2010. Plant-specific glycosylation patterns in the context of therapeutic protein production. *Plant Biotechnol. J.* 8:564–87
21. Strasser R, Altmann F, Steinkellner H. 2014. Controlled glycosylation of plant-produced recombinant proteins. *Curr. Opin. Biotechnol.* 30:95–100
22. Cox KM, Sterling JD, Regan JT, Gasdaska JR, Frantz KK, et al. 2006. Glycan optimization of a human monoclonal antibody in the aquatic plant *Lemna minor*. *Nat. Biotechnol.* 24:1591–97
23. Forthall DN, Gach JS, Landucci G, Jez J, Strasser R, et al. 2010. Fc-glycosylation influences Fcγ receptor binding and cell-mediated anti-HIV activity of monoclonal antibody 2G12. *J. Immunol.* 185:6876–82
24. Ullrich KK, Hiss M, Rensing SA. 2015. Means to optimize protein expression in transgenic plants. *Curr. Opin. Biotechnol.* 32:61–67
25. Twyman RM, Schillberg S, Fischer R. 2013. Optimizing the yield of recombinant pharmaceutical proteins in plants. *Curr. Pharm. Des.* 19:5486–94
26. Kirchhoff J, Raven N, Boes A, Roberts JL, Russell S, et al. 2012. Monoclonal tobacco cell lines with enhanced recombinant protein yields can be generated from heterogeneous cell suspension cultures by flow sorting. *Plant Biotechnol. J.* 10:936–44
27. Hood EE, Devaiah SP, Fake G, Egelkroun E, Teoh KT, et al. 2012. Manipulating corn germplasm to increase recombinant protein accumulation. *Plant Biotechnol. J.* 10:20–30
28. Rademacher T, Sack M, Arcalis E, Stadlmann J, Balzer S, et al. 2008. Recombinant antibody 2G12 produced in maize endosperm efficiently neutralizes HIV-1 and contains predominantly single-GlcNAc N-glycans. *Plant Biotechnol. J.* 6:189–201
29. Fischer R, Vasilev N, Twyman RM, Schillberg S. 2015. High-value products from plants: the challenges of process optimization. *Curr. Opin. Biotechnol.* 32:156–62
30. Buyel JF. 2015. Process development strategies in plant molecular farming. *Curr. Pharm. Biotechnol.* 16:966–82
31. He Y, Ning T, Xie T, Qiu Q, Zhang L, et al. 2011. Large-scale production of functional human serum albumin from transgenic rice seeds. *PNAS* 108:19078–83
32. Devaiah SP, Requesens DV, Chang YK, Hood KR, Flory A, et al. 2013. Heterologous expression of cellobiohydrolase II (Cel6A) in maize endosperm. *Transgenic Res.* 22:477–88
33. De Jaeger G, Scheffer S, Jacobs A, Zambre M, Zobell O, et al. 2002. Boosting heterologous protein production in transgenic dicotyledonous seeds using *Phaseolus vulgaris* regulatory sequences. *Nat. Biotechnol.* 20:1265–68
34. Oey M, Lohse M, Kreikemeyer B, Bock R. 2009. Exhaustion of the chloroplast protein synthesis capacity by massive expression of a highly stable protein antibiotic. *Plant J.* 57:436–45
35. Twyman RM, Stöger E, Schillberg S, Christou P, Fischer R. 2003. Molecular farming in plants: host systems and expression technology. *Trends Biotechnol.* 21:570–78
36. Doran PM. 2006. Foreign protein degradation and instability in plants and plant tissue cultures. *Trends Biotechnol.* 24:426–32
37. Hofbauer A, Stöger E. 2013. Subcellular accumulation and modification of pharmaceutical proteins in different plant tissues. *Curr. Pharm. Des.* 19:5495–502
38. Martoglio B, Dobberstein B. 1998. Signal sequences: more than just greasy peptides. *Trends Cell Biol.* 8:410–15

39. Schouten A, Roosien J, van Engelen FA, de Jong GA, Borst-Vrenssen AW, et al. 1996. The C-terminal KDEL sequence increases the expression level of a single-chain antibody designed to be targeted to both the cytosol and the secretory pathway in transgenic tobacco. *Plant Mol. Biol.* 30:781–93
40. Neuhaus JM, Rogers JC. 1998. Sorting of proteins to vacuoles in plant cells. *Plant Mol. Biol.* 38:127–44
41. Robinson DG, Oliviusson P, Hinz G. 2005. Protein sorting to the storage vacuoles of plants: a critical appraisal. *Traffic* 6:615–25
42. Takaiwa F. 2013. Update on the use of transgenic rice seeds in oral immunotherapy. *Immunotherapy* 5:301–12
43. Hood E, Cramer C, Medrano G, Xu J. 2012. Protein targeting: strategic planning for optimizing protein products through plant biotechnology. In *Plant Biotechnology and Agriculture*, ed. A Arie, MH Paul, pp. 35–54. San Diego, CA: Academic
44. Llop-Tous I, Ortiz M, Torrent M, Ludevid MD. 2011. The expression of a xylanase targeted to ER-protein bodies provides a simple strategy to produce active insoluble enzyme polymers in tobacco plants. *PLOS ONE* 6:e19474
45. Ma JK, Drossard J, Lewis D, Altmann F, Boyle J, et al. 2015. Regulatory approval and a first-in-human phase I clinical trial of a monoclonal antibody produced in transgenic tobacco plants. *Plant Biotechnol. J.* 13:1106–20
46. Wilken LR, Nikolov ZL. 2012. Recovery and purification of plant-made recombinant proteins. *Biotechnol. Adv.* 30:419–33
47. Buyel JF, Twyman RM, Fischer R. 2015. Extraction and downstream processing of plant-derived recombinant proteins. *Biotechnol. Adv.* 33:902–13
48. Tuse D, Tu T, McDonald KA. 2014. Manufacturing economics of plant-made biologics: case studies in therapeutic and industrial enzymes. *Biomed. Res. Int.* 2014:256135
49. Ou J, Guo Z, Shi J, Wang X, Liu J, et al. 2014. Transgenic rice endosperm as a bioreactor for molecular pharming. *Plant Cell Rep.* 33:585–94
50. Walwyn DR, Huddy SM, Rybicki EP. 2014. Techno-economic analysis of horseradish peroxidase production using a transient expression system in *Nicotiana benthamiana*. *Appl. Biochem. Biotechnol.* 175:841–54
51. Buyel JF, Kaever T, Buyel JJ, Fischer R. 2013. Predictive models for the accumulation of a fluorescent marker protein in tobacco leaves according to the promoter/5'UTR combination. *Biotechnol. Bioeng.* 110:471–82
52. Hood EE, Kusnadi A, Nikolov Z, Howard JA. 1999. Molecular farming of industrial proteins from transgenic maize. *Adv. Exp. Med. Biol.* 464:127–47
53. Witcher D, Hood E, Peterson D, Bailey M, Bond D, et al. 1998. Commercial production of  $\beta$ -glucuronidase (GUS): a model system for the production of proteins in plants. *Mol. Breeding* 4:301–12
54. Howard JA, Hood E. 2005. Bioindustrial and biopharmaceutical products produced in plants. In *Advances in Agronomy*, Vol. 85, ed. D Sparks, pp. 91–124. San Diego, CA: Academic
55. Loos R, Carvalho R, Antonio DC, Comero S, Locoro G, et al. 2013. EU-wide monitoring survey on emerging polar organic contaminants in wastewater treatment plant effluents. *Water Res.* 47:6475–87
56. Creminon C, Taran F. 2015. Enzyme immunoassays as screening tools for catalysts and reaction discovery. *Cbem. Commun.* 51:7996–8009
57. Collins KD, Gensch T, Glorius F. 2014. Contemporary screening approaches to reaction discovery and development. *Nat. Chem.* 6:859–71
58. De Meyer T, Muyldermans S, Depicker A. 2014. Nanobody-based products as research and diagnostic tools. *Trends Biotechnol.* 32:263–70
59. Geering B, Fussenegger M. 2015. Synthetic immunology: modulating the human immune system. *Trends Biotechnol.* 33:65–79
60. Skerra A. 2007. Alternative non-antibody scaffolds for molecular recognition. *Curr. Opin. Biotechnol.* 18:295–304
61. Richter A, Eggenstein E, Skerra A. 2014. Anticalins: exploiting a non-Ig scaffold with hypervariable loops for the engineering of binding proteins. *FEBS Lett.* 588:213–18
62. Schiefner A, Skerra A. 2015. The menagerie of human lipocalins: a natural protein scaffold for molecular recognition of physiological compounds. *Acc. Chem. Res.* 48:976–85

63. Justino CIL, Duarte AC, Rocha-Santos TAP. 2015. Analytical applications of affibodies. *Trac-Trends Anal. Chem.* 65:73–82
64. Robinson MP, Ke N, Lobstein J, Peterson C, Szkodny A, et al. 2015. Efficient expression of full-length antibodies in the cytoplasm of engineered bacteria. *Nat. Commun.* 6:8072
65. Orzaez D, Granell A, Blazquez MA. 2009. Manufacturing antibodies in the plant cell. *Biotechnol. J.* 4:1712–24
66. Julve JM, Gandia A, Fernandez-del-Carmen A, Sarrion-Perdigones A, Castelijns B, et al. 2013. A coat-independent superinfection exclusion rapidly imposed in *Nicotiana benthamiana* cells by tobacco mosaic virus is not prevented by depletion of the movement protein. *Plant Mol. Biol.* 81:553–64
67. Pujol M, Ramirez NI, Ayala M, Gavilondo JV, Valdes R, et al. 2005. An integral approach towards a practical application for a plant-made monoclonal antibody in vaccine purification. *Vaccine* 23:1833–37
68. Ritala A, Leelavathi S, Oksman-Caldentey KM, Reddy VS, Laukkanen ML. 2014. Recombinant barley-produced antibody for detection and immunoprecipitation of the major bovine milk allergen, beta-lactoglobulin. *Transgenic Res.* 23:477–87
69. Hood E, Howard J. 2014. Commercial plant-produced recombinant avidin. In *Commercial Plant-Produced Recombinant Protein Products: Case Studies*, ed. JA Howard, EE Hood, pp. 15–25. Berlin: Springer
70. Neurath H, Walsh KA. 1976. Role of proteolytic enzymes in biological regulation (a review). *PNAS* 73:3825–32
71. Merten OW. 2002. Virus contaminations of cell cultures—biotechnological view. *Cytotechnology* 39:91–116
72. Yee L, Blanch HW. 1993. Recombinant trypsin production in high cell density fed-batch cultures in *Escherichia coli*. *Biotechnol. Bioeng.* 41:781–90
73. Mattanovich D, Katinger H, Hohenblum H, Naschberger S, Weik R. 2008. Method for the manufacture of recombinant trypsin. US Patent No. 20030157634 A1
74. Muller R, Glaser S, Geipel F, Thalhofer JP, Rexer B, et al. 2010. Method for producing recombinant trypsin. US Patent No. 20080064084 A1
75. Hanquier J, Sorlet Y, Desplancq D, Baroche L, Ebtinger M, et al. 2003. A single mutation in the activation site of bovine trypsinogen enhances its accumulation in the fermentation broth of the yeast *Pichia pastoris*. *Appl. Environ. Microbiol.* 69:1108–13
76. Woodard SL, Mayor JM, Bailey MR, Barker DK, Love RT, et al. 2003. Maize (*Zea mays*)-derived bovine trypsin: characterization of the first large-scale, commercial protein product from transgenic plants. *Biotechnol. Appl. Biochem.* 38:123–30
77. Zhang H, Huang RY, Jalili PR, Irungu JW, Nicol GR, et al. 2010. Improved mass spectrometric characterization of protein glycosylation reveals unusual glycosylation of maize-derived bovine trypsin. *Anal. Chem.* 82:10095–101
78. Krishnan A, Woodard S. 2014. TryZean™: an animal-free alternative to bovine trypsin. See Ref. 69, pp. 43–63
79. Kim NS, Yu HY, Chung ND, Kwon TH, Yang MS. 2014. High-level production of recombinant trypsin in transgenic rice cell culture through utilization of an alternative carbon source and recycling system. *Enzyme Microb. Technol.* 63:21–27
80. Bornke F, Broer I. 2010. Tailoring plant metabolism for the production of novel polymers and platform chemicals. *Curr. Opin. Plant Biol.* 13:354–62
81. Canty EG, Kadler KE. 2005. Procollagen trafficking, processing and fibrillogenesis. *J. Cell Sci.* 118:1341–53
82. Scheller J, Guhrs KH, Grosse F, Conrad U. 2001. Production of spider silk proteins in tobacco and potato. *Nat. Biotechnol.* 19:573–77
83. Hauptmann V, Menzel M, Weichert N, Reimers K, Spohn U, Conrad U. 2015. In planta production of ELPylated spider silk-based proteins results in non-cytotoxic biopolymers. *BMC Biotechnol.* 15:9
84. Weichert N, Hauptmann V, Menzel M, Schallau K, Gunkel P, et al. 2014. Transglutamination allows production and characterization of native-sized ELPylated spider silk proteins from transgenic plants. *Plant Biotechnol. J.* 12:265–75
85. Bhavsar K, Khire JM. 2014. Current research and future perspectives of phytase bioprocessing. *RSC Adv.* 4:26677–91

86. Gupta RK, Gangoliya SS, Singh NK. 2015. Reduction of phytic acid and enhancement of bioavailable micronutrients in food grains. *J. Food Sci. Technol.* 52:676–84
87. Xu X, Zhang Y, Meng Q, Meng K, Zhang W, et al. 2013. Overexpression of a fungal beta-mannanase from *Bispora* sp. MEY-1 in maize seeds and enzyme characterization. *PLOS ONE* 8:e56146
88. Lv JN, Chen YQ, Guo XJ, Piao XS, Cao YH, Dong B. 2013. Effects of supplementation of beta-mannanase in corn-soybean meal diets on performance and nutrient digestibility in growing pigs. *Asian-Australas. J. Anim. Sci.* 26:579–87
89. Zhang Y, Xu X, Zhou X, Chen R, Yang P, et al. 2013. Overexpression of an acidic endo-beta-1,3-1,4-glucanase in transgenic maize seed for direct utilization in animal feed. *PLOS ONE* 8:e81993
90. Ranum P, Pena-Rosas JP, Garcia-Casal MN. 2014. Global maize production, utilization, and consumption. *Ann. N. Y. Acad. Sci.* 1312:105–12
91. Hood E, Requesens D. 2014. Commercial plant-produced recombinant cellulases for biomass conversion. See Ref. 69, pp. 231–46
92. Li Q, Song J, Peng S, Wang JP, Qu GZ, et al. 2014. Plant biotechnology for lignocellulosic biofuel production. *Plant Biotechnol. J.* 12:1174–92
93. Zhang D, VanFossen A, Pagano R, Johnson J, Parker M, et al. 2011. Consolidated pretreatment and hydrolysis of plant biomass expressing cell wall degrading enzymes. *BioEnergy Res.* 4:276–86
94. Shen B, Sun X, Zuo X, Shilling T, Appgar J, et al. 2012. Engineering a thermoregulated intein-modified xylanase into maize for consolidated lignocellulosic biomass processing. *Nat. Biotechnol.* 30:1131–36
95. Blaylock MJ, Ferguson BW, Lee DA. 2012. Energy crops for improved biofuel feedstocks. US Patent No. 20070250961 A1
96. Hood EE, Love R, Lane J, Bray J, Clough R, et al. 2007. Subcellular targeting is a key condition for high-level accumulation of cellulase protein in transgenic maize seed. *Plant Biotechnol. J.* 5:709–19
97. Urbanchuk JM, Kowalski DJ, Dale B, Kim S. 2009. Corn amylase: improving the efficiency and environmental footprint of corn to ethanol through plant biotechnology. *AgBioForum* 12:149–54
98. van der Maarel MJ, van der Veen B, Uitdehaag JC, Leemhuis H, Dijkhuizen L. 2002. Properties and applications of starch-converting enzymes of the alpha-amylase family. *J. Biotechnol.* 94:137–55
99. Widsten P, Kandelbauer A. 2008. Laccase applications in the forest products industry: a review. *Enzyme Microb. Technol.* 42:293–307
100. Hood EE, Bailey MR, Beifuss K, Magallanes-Lundback M, Horn ME, et al. 2003. Criteria for high-level expression of a fungal laccase gene in transgenic maize. *Plant Biotechnol. J.* 1:129–40
101. Bailey MR, Woodard SL, Callaway E, Beifuss K, Magallanes-Lundback M, et al. 2004. Improved recovery of active recombinant laccase from maize seed. *Appl. Microbiol. Biotechnol.* 63:390–97
102. Juturu V, Wu JC. 2012. Microbial xylanases: engineering, production and industrial applications. *Biotechnol. Adv.* 30:1219–27
103. Sharma A, Thakur VV, Shrivastava A, Jain RK, Mathur RM, et al. 2014. Xylanase and laccase based enzymatic kraft pulp bleaching reduces adsorbable organic halogen (AOX) in bleach effluents: a pilot scale study. *Bioresour. Technol.* 169:96–102
104. Singh Arora D, Kumar Sharma R. 2010. Ligninolytic fungal laccases and their biotechnological applications. *Appl. Biochem. Biotechnol.* 160:1760–88
105. Wang GD, Li QJ, Luo B, Chen XY. 2004. *Ex planta* phytoremediation of trichlorophenol and phenolic allelochemicals via an engineered secretory laccase. *Nat. Biotechnol.* 22:893–97
106. Singh R, Cabrera ML, Radcliffe DE, Zhang H, Huang Q. 2015. Laccase mediated transformation of 17beta-estradiol in soil. *Environ. Pollut.* 197:28–35
107. Li S, Yang X, Yang S, Zhu M, Wang X. 2012. Technology prospecting on enzymes: Application, marketing and engineering. *Comput. Struct. Biotechnol. J.* 2:1–11
108. Howard J, Nikolov Z, Hood E. 2011. Enzyme production systems for biomass conversion. In *Plant Biomass Conversion*, ed. E Hood, P Nelson, R Powell, pp. 227–53. Hoboken, NJ: Wiley-Blackwell
109. Ranganathan SV, Narasimhan SL, Muthukumar K. 2008. An overview of enzymatic production of biodiesel. *Bioresour. Technol.* 99:3975–81
110. Du W, Li W, Sun T, Chen X, Liu D. 2008. Perspectives for biotechnological production of biodiesel and impacts. *Appl. Microbiol. Biotechnol.* 79:331–37

111. Yang B, Wang Y-H, Yang J-G. 2006. Optimization of enzymatic degumming process for rapeseed oil. *J. Am. Oil Chem. Soc.* 83:653–58
112. Bussamra BC, Freitas S, Costa AC. 2015. Improvement on sugar cane bagasse hydrolysis using enzymatic mixture designed cocktail. *Bioresour. Technol.* 187:173–81
113. Clough RC, Pappu K, Thompson K, Beifuss K, Lane J, et al. 2006. Manganese peroxidase from the white-rot fungus *Phanerochaete chrysosporium* is enzymatically active and accumulates to high levels in transgenic maize seed. *Plant Biotechnol. J.* 4:53–62
114. Hayes TL, Zimmerman N, Hackle A. 2014. *World enzymes: industry study with forecasts for 2011 & 2016*. Rep. 2229, Freedonia Group, Cleveland, OH
115. Hood EE, Love R, Lane J, Bray J, Clough R, et al. 2007. Subcellular targeting is a key condition for high-level accumulation of cellulase protein in transgenic maize seed. *Plant Biotechnol. J.* 5:709–19
116. Hood EE, Devaiah SP, Fake G, Egelkrout E, Teoh K, et al. 2012. Manipulating corn germplasm to increase recombinant protein accumulation. *Plant Biotechnol. J.* 10:20–30
117. Hood NC, Hood KR, Woodard SL, Devaiah SP, Jeoh T, et al. 2014. Purification and characterization of recombinant cel7a from maize seed. *Appl. Biochem. Biotechnol.* 174:2864–74
118. Sparrow P, Broer I, Hood EE, Eversole K, Hartung F, Schiemann J. 2013. Risk assessment and regulation of molecular farming—a comparison between Europe and US. *Curr. Pharm. Des.* 19:5513–30
119. Bock R. 2015. Engineering plastid genomes: methods, tools, and applications in basic research and biotechnology. *Annu. Rev. Plant Biol.* 66:211–41
120. Whaley KJ, Hiatt A, Zeitlin L. 2011. Emerging antibody products and *Nicotiana* manufacturing. *Hum. Vaccines* 7:349–56
121. D’Aoust MA, Couture MM, Charland N, Trepanier S, Landry N, et al. 2010. The production of hemagglutinin-based virus-like particles in plants: a rapid, efficient and safe response to pandemic influenza. *Plant Biotechnol. J.* 8:607–19
122. Vezina LP, Faye L, Lerouge P, D’Aoust MA, Marquet-Blouin E, et al. 2009. Transient co-expression for fast and high-yield production of antibodies with human-like N-glycans in plants. *Plant Biotechnol. J.* 7:442–55
123. Yusibov V, Rabindran S, Commandeur U, Twyman RM, Fischer R. 2006. The potential of plant virus vectors for vaccine production. *Drugs Res. Dev.* 7:203–17
124. Yusibov V, Rabindran S. 2008. Recent progress in the development of plant derived vaccines. *Expert Rev. Vaccines* 7:1173–83
125. Yusibov V, Streatfield SJ, Kushnir N, Roy G, Padmanaban A. 2013. Hybrid viral vectors for vaccine and antibody production in plants. *Curr. Pharm. Des.* 19:5574–86
126. Canizares MC, Lomonosoff GP, Nicholson L. 2005. Development of cowpea mosaic virus-based vectors for the production of vaccines in plants. *Expert Rev. Vaccines* 4:687–97
127. Lico C, Chen Q, Santi L. 2008. Viral vectors for production of recombinant proteins in plants. *J. Cell Physiol.* 216:366–77
128. Sainsbury F, Lavoie PO, D’Aoust MA, Vezina LP, Lomonosoff GP. 2008. Expression of multiple proteins using full-length and deleted versions of cowpea mosaic virus RNA-2. *Plant Biotechnol. J.* 6:82–92
129. Marillonnet S, Thoeringer C, Kandzia R, Klimyuk V, Gleba Y. 2005. Systemic Agrobacterium tumefaciens-mediated transfection of viral replicons for efficient transient expression in plants. *Nat. Biotechnol.* 23:718–23
130. Gleba Y, Klimyuk V, Marillonnet S. 2005. Magniffection—a new platform for expressing recombinant vaccines in plants. *Vaccine* 23:2042–48
131. Gleba Y, Klimyuk V, Marillonnet S. 2007. Viral vectors for the expression of proteins in plants. *Curr. Opin. Biotechnol.* 18:134–41
132. Sainsbury F, Lomonosoff GP. 2008. Extremely high-level and rapid transient protein production in plants without the use of viral replication. *Plant Physiol.* 148:1212–18
133. Phan HT, Hause B, Hause G, Arcalis E, Stöger E, et al. 2014. Influence of elastin-like polypeptide and hydrophobin on recombinant hemagglutinin accumulations in transgenic tobacco plants. *PLOS ONE* 9:e99347

134. Reuter LJ, Bailey MJ, Joensuu JJ, Ritala A. 2014. Scale-up of hydrophobin-assisted recombinant protein production in tobacco BY-2 suspension cells. *Plant Biotechnol. J.* 12:402–10
135. Gutierrez SP, Saberianfar R, Kohalmi SE, Menassa R. 2013. Protein body formation in stable transgenic tobacco expressing elastin-like polypeptide and hydrophobin fusion proteins. *BMC Biotechnol.* 13:40
136. van Rooijen GJ, Moloney MM. 1995. Plant seed oil-bodies as carriers for foreign proteins. *Biotechnology* 13:72–77
137. Nykiforuk CL, Boothe JG, Murray EW, Keon RG, Goren HJ, et al. 2006. Transgenic expression and recovery of biologically active recombinant human insulin from *Arabidopsis thaliana* seeds. *Plant Biotechnol. J.* 4:77–85
138. Nykiforuk CL, Boothe JG. 2012. Transgenic expression of therapeutic proteins in *Arabidopsis thaliana* seed. *Methods Mol. Biol.* 899:239–64
139. Anfossi L, Baggiani C, Giovannoli C, D'Arco G, Giraudi G. 2013. Lateral-flow immunoassays for mycotoxins and phycotoxins: a review. *Anal. Bioanal. Chem.* 405:467–80
140. Taranova NA, Berlina AN, Zherdev AV, Dzantiev BB. 2015. 'Traffic light' immunochromatographic test based on multicolor quantum dots for the simultaneous detection of several antibiotics in milk. *Biosens. Bioelectron.* 63:255–61
141. Cho IH, Radadia AD, Farrokhzad K, Ximenes E, Bae E, et al. 2014. Nano/micro and spectroscopic approaches to food pathogen detection. *Annu. Rev. Anal. Chem.* 7:65–88
142. Warriner K, Reddy SM, Namvar A, Neethirajan S. 2014. Developments in nanoparticles for use in biosensors to assess food safety and quality. *Trends Food Sci. Technol.* 40:183–99
143. Knopp D, Tang D, Niessner R. 2009. Review: bioanalytical applications of biomolecule-functionalized nanometer-sized doped silica particles. *Anal. Chim. Acta* 647:14–30



# Contents

|  |     |
|--|-----|
| Applications of Optical Microcavity Resonators in Analytical Chemistry<br><i>James H. Wade and Ryan C. Bailey</i> .....  | 1   |
| Molecular Plasmonics<br><i>Andrew J. Wilson and Katherine A. Willets</i> .....   | 27  |
| Advances in Mid-Infrared Spectroscopy for Chemical Analysis<br><i>Julian Haas and Boris Mizaikoff</i> .....  | 45  |
| In Situ and In Vivo Molecular Analysis by Coherent Raman Scattering Microscopy<br><i>Chien-Sheng Liao and Ji-Xin Cheng</i> .....   | 69  |
| Advances in Magnetic Resonance Imaging Contrast Agents for Biomarker Detection<br><i>Sanbita Sinbaray and Mark D. Pagel</i> .....  | 95  |
| Progress in the Analysis of Complex Atmospheric Particles<br><i>Alexander Laskin, Mary K. Gilles, Daniel A. Knopf, Bingbing Wang, and Swarup China</i> .....   | 117 |
| Electroanalytical Ventures at Nanoscale Interfaces Between Immiscible Liquids<br><i>Damien W.M. Arrigan and Yang Liu</i> .....   | 145 |
| Reagentless, Structure-Switching, Electrochemical Aptamer-Based Sensors<br><i>Lauren R. Schoukroun-Barnes, Florika C. Macazo, Brenda Gutierrez, Justine Lottermoser, Juan Liu, and Ryan J. White</i> .....       | 163 |
| New Functionalities for Paper-Based Sensors Lead to Simplified User Operation, Lower Limits of Detection, and New Applications<br><i>Josephine C. Cunningham, Paul R. DeGregory, and Richard M. Crooks</i> ..... | 183 |
| Fabrication and Operation of Paper-Based Analytical Devices<br><i>Xiao Jiang and Z. Hugh Fan</i> .....   | 203 |

|  |     |
|--|-----|
| Glycan Arrays: From Basic Biochemical Research to Bioanalytical<br>and Biomedical Applications<br><i>Andreas Geissner and Peter H. Seeberger</i> .....   | 223 |
| Microfluidic Devices for the Measurement of Cellular Secretion<br><i>Adrian M. Schrell, Nikita Mukhitov, Lian Yi, Xue Wang, and Michael G. Roper</i> ....  | 249 |
| Plant Molecular Farming: Much More than Medicines<br><i>Marc Tschofen, Dietmar Knopp, Elizabeth Hood, and Eva Stöger</i> .....   | 271 |
| Methods for the Analysis of Protein Phosphorylation–Mediated<br>Cellular Signaling Networks<br><i>Forest M. White and Alejandro Wolf-Yadlin</i> .....  | 295 |
| Recent Progress in Monolithic Silica Columns for High-Speed<br>and High-Selectivity Separations<br><i>Tobru Ikegami and Nobuo Tanaka</i> .....   | 317 |
| Mass-Selective Chiral Analysis<br><i>Ulrich Boesl and Aras Kartouzian</i> .....  | 343 |
| The Coupled Chemical and Physical Dynamics Model of MALDI<br><i>Richard Knochenmuss</i> .....  | 365 |
| Advanced Multidimensional Separations in Mass Spectrometry:<br>Navigating the Big Data Deluge<br><i>Jody C. May and John A. McLean</i> .....   | 387 |
| Development and Applications of Liquid Sample Desorption<br>Electrospray Ionization Mass Spectrometry<br><i>Qiuling Zheng and Hao Chen</i> .....   | 411 |
| Mass Spectrometry Applied to Bottom-Up Proteomics: Entering<br>the High-Throughput Era for Hypothesis Testing<br><i>Ludovic C. Gillet, Alexander Leitner, and Ruedi Aebersold</i> .....  | 449 |
| Mass Spectrometry as a Preparative Tool for the Surface Science<br>of Large Molecules<br><i>Stephan Rauschenbach, Markus Ternes, Ludger Harnau, and Klaus Kern</i> .....   | 473 |
| Progress in Top-Down Proteomics and the Analysis of Proteoforms<br><i>Timothy K. Toby, Luca Fornelli, and Neil L. Kelleher</i> .....   | 499 |
| Proteogenomics: Integrating Next-Generation Sequencing and Mass<br>Spectrometry to Characterize Human Proteomic Variation<br><i>Gloria M. Sheynkman, Michael R. Shortreed, Anthony J. Cesnik,<br/>and Lloyd M. Smith</i> ..... | 521 |



# The Encapsulation of Hemagglutinin in Protein Bodies Achieves a Stronger Immune Response in Mice than the Soluble Antigen

Anna Hofbauer<sup>1</sup>, Stanislav Melnik<sup>1</sup>, Marc Tschofen<sup>1</sup>, Elsa Arcalis<sup>1</sup>, Hoang T. Phan<sup>2</sup>, Ulrike Gresch<sup>2</sup>, Johannes Lampel<sup>1</sup>, Udo Conrad<sup>2</sup> and Eva Stoger<sup>1\*</sup>

<sup>1</sup> Department of Applied Genetics and Cell Biology, University of Natural Resources and Life Sciences, Vienna, Austria,

<sup>2</sup> Department of Molecular Genetics, Leibniz Institute of Plant Genetics and Crop Plant Research, Gatersleben, Germany

## OPEN ACCESS

### Edited by:

Domenico De Martinis,  
ENEA Italian National Agency for New  
Technologies, Energy and Sustainable  
Economic Development, Italy

### Reviewed by:

Arun Kumar,  
GlaxoSmithKline Vaccines, Italy  
Florian Krammer,  
Mount Sinai Hospital, USA

### \*Correspondence:

Eva Stoger  
eva.stoger@boku.ac.at

### Specialty section:

This article was submitted to  
Plant Biotechnology,  
a section of the journal  
Frontiers in Plant Science

**Received:** 15 November 2015

**Accepted:** 27 January 2016

**Published:** 16 February 2016

### Citation:

Hofbauer A, Melnik S, Tschofen M,  
Arcalis E, Phan HT, Gresch U,  
Lampel J, Conrad U and Stoger E  
(2016) The Encapsulation  
of Hemagglutinin in Protein Bodies  
Achieves a Stronger Immune  
Response in Mice than the Soluble  
Antigen. *Front. Plant Sci.* 7:142.  
doi: 10.3389/fpls.2016.00142

Zein is a water-insoluble polymer from maize seeds that has been widely used to produce carrier particles for the delivery of therapeutic molecules. We encapsulated a recombinant model vaccine antigen in newly formed zein bodies *in planta* by generating a fusion construct comprising the ectodomain of hemagglutinin subtype 5 and the N-terminal part of  $\gamma$ -zein. The chimeric protein was transiently produced in tobacco leaves, and H5-containing protein bodies (PBs) were used to immunize mice. An immune response was achieved in all mice treated with H5-zein, even at low doses. The fusion to zein markedly enhanced the IgG response compared the soluble H5 control, and the effect was similar to a commercial adjuvant. The co-administration of adjuvants with the H5-zein bodies did not enhance the immune response any further, suggesting that the zein portion itself mediates an adjuvant effect. While the zein portion used to induce protein body formation was only weakly immunogenic, our results indicate that zein-induced PBs are promising production and delivery vehicles for subunit vaccines.

**Keywords:** protein bodies, molecular farming, subcellular targeting, recombinant protein, recombinant vaccine

## INTRODUCTION

Polymers are widely used as carrier biomaterials for the delivery of therapeutic molecules (Petros and DeSimone, 2010). In particular, biopolymer-based nanoparticles have proven suitable for clinical applications due to their biocompatibility and biodegradability (Panyam and Labhasetwar, 2003; Nitta and Numata, 2013). A variety of materials and preparation methods have been developed for application-specific properties in terms of particle shape, surface charge, and surface features (Petros and DeSimone, 2010). Among the protein-based biopolymers, those derived from natural proteins such as silk, collagen, elastin, and fibronectin have been studied in detail (Ruszczak and Friess, 2003; Daamen et al., 2007; Lammel et al., 2010; Nitta and Numata, 2013).

Zein, a protein-based polymer found in maize seeds, has been widely used as a carrier because of favorable properties such as biocompatibility, insolubility and low water uptake, mechanical and chemical stability, and its propensity to form coatings and microparticles (Liu et al., 2005; Lai and Guo, 2011; Wang et al., 2011; Lau et al., 2013). Zein is also generally regarded as safe (GRAS) for food use and resists digestion, making it particularly suitable as an encapsulation polymer for oral drugs (Hurtado-Lopez and Murdan, 2006b; Gong et al., 2011; Lau et al., 2013; Zou and Gu, 2013;

Ahmed et al., 2015). The intravenous delivery of drug-loaded zein-based microparticles has also been investigated as a means to achieve long-acting effects such as the slow and sustained release of pharmaceutical compounds (Lai and Guo, 2011) and more efficient drug delivery to cancer cells (Lin et al., 2011; Podaralla et al., 2012; Lohcharoenkal et al., 2014). Zein-based microspheres may also provide adjuvant effects when used as vaccine carriers (Hurtado-Lopez and Murdan, 2006a).

The *in vitro* loading of zein-based microparticles with drugs usually involves spray or freeze drying or liquid-liquid dispersion methods (Zhong and Jin, 2009; Podaralla and Perumal, 2010; Podaralla et al., 2012; Zou and Gu, 2013). These technical processes are expensive and can affect the activity of the encapsulated agent, e.g., the high temperatures required for spray drying are incompatible with many pharmaceutical proteins.

It is therefore appealing to use plants to achieve microencapsulation *in vivo* by directly incorporating recombinant proteins into naturally occurring protein storage organelles such as zein bodies (Hofbauer and Stoger, 2013). Endogenous protein storage organelles are usually found in plant seeds, and zein-like prolamins are characteristic features of cereal endosperm cells. In production systems based on cereal seeds, the recombinant protein is often targeted to accumulate in prolamins-containing storage organelles that provide a protective environment, even offering some resistance against proteolytic digestion in simulated gastric fluids (Takaiwa et al., 2015).

Instead of using the natural prolamins that are formed in rice, wheat, maize or barley endosperm, it is also possible to fuse the recombinant protein to assembly sequences that induce analogous structures in tissues such as leaves, which usually lack protein storage organelles. This ectopic protein body technology bypasses the longer generation time required to produce cereal seeds while still offering the advantages of natural bioencapsulation. Sequences that share the ability to trigger the formation of ectopic protein bodies (PBs) include those derived from cereal prolamins, synthetic elastin-like peptides (ELPs) and fungal hydrophobins (Floss et al., 2008; Conley et al., 2009; Torrent et al., 2009b; Gutierrez et al., 2013; Shigemitsu et al., 2013).

One of the most widely used assembly sequences comprises the N-terminal part of the mature 27 kD  $\gamma$ -zein protein, a member of the major prolamins-type storage protein family in maize (Shewry and Halford, 2002). Unlike other assembly sequences, it not only induces the formation of PBs but also acts as a retention sequence that stops fusion proteins from leaving the endoplasmic reticulum (ER). Consequently, the induced PBs bud from the ER as distinct round structures, underscoring the intrinsic compartment-forming properties of the zein sequence in the absence of tissue-specific factors (Mainieri et al., 2004; Llop-Tous et al., 2010). The N-terminal sequence of the 27 kD  $\gamma$ -zein protein comprises two cysteine residues downstream of the signal peptide, a repeated proline-rich domain forming an amphipathic helix, and a third section that includes four additional cysteine residues (Geli et al., 1994). Several reports have confirmed that zein-derived sequences induce ectopic PBs when appended to either the N-terminus or the C-terminus

of diverse recombinant proteins, including phaseolin (Mainieri et al., 2004), enhanced cyan fluorescent protein (Llop-Tous et al., 2010), xylanase (Llop-Tous et al., 2011), DsRed (Joseph et al., 2012), and the *Human papillomavirus* E7 protein (Whitehead et al., 2014). Moreover, the ability to induce PBs appears to be almost entirely intrinsic and independent of other host-specific factors, thus allowing the formation of ectopic PBs in fungal, insect and mammalian cells (Torrent et al., 2009a), and the budding of PBs from ectopic membranes such as the plastid envelope, when combined with alternative subcellular targeting strategies (Hofbauer et al., 2014).

Hemagglutinin is an abundant type I integral membrane glycoprotein found on the envelope of influenza viruses and it has been widely used in influenza vaccine development and as a model antigen. The precursor protein HA0 yields two chains, i.e., HA1 (~36 kDa) and HA2 (~28 kDa), following cleavage at the motif Q/E-X-R. Infectivity requires both chains to be glycosylated, and also relies on the cleavage of hemagglutinin by a protease at multiple arginine residues. (Klenk and Garten, 1994; Hulse et al., 2004). The cleavage products are then covalently linked by a disulfide bond and these HA1/HA2 units form non-covalent homotrimers (Wiley et al., 1977).

A transmembrane domain is found near the C-terminus of HA2. The three-dimensional structure of hemagglutinin reveals two domains: a stem, responsible for membrane anchoring (part of HA1 and all of HA2), and a globular head (only HA1), bearing the sialic acid receptor binding domains (RBDs) (Wilson et al., 1981). In this study we generated a fusion construct comprising the ectodomain of hemagglutinin subtype 5 and the N-terminal part of  $\gamma$ -zein (amino acids 4–93) in order to induce the storage of the recombinant fusion protein inside newly formed PBs. The chimeric protein was transiently produced in tobacco leaves and H5-containing PBs were used to immunize mice. The resulting immune response was compared to that of control groups administered with the soluble H5 antigen, with or without adjuvant.

## MATERIALS AND METHODS

### Vector Constructs

All cloning steps were carried out using the binary vector pTRA, a derivative of pPAM (GenBank AY027531). The sequence corresponding to the H5 ectodomain (amino acids 17–520) of hemagglutinin from the A/Hatay/2004/(H5N1) influenza strain (GenBank Q5QQ29) was amplified as described (Phan et al., 2014) and a plant codon-optimized signal peptide sequence derived from a murine antibody was added to the N-terminus to direct the protein into the secretory pathway (Vaquero et al., 1999). Amino acids 4–93 of the mature 27 kD  $\gamma$ -zein protein (lacking the signal peptide) were joined to the C-terminus via a (GGGS)<sub>2</sub> linker as previously described for the phaseolin fusion construct zeolin (Mainieri et al., 2004). A His<sub>6</sub>-tag was added to the C-terminus for detection. The final expression vector “H5-Zein” was produced by transferring this coding sequence to the pTRA vector between the *Tobacco etch virus* (TEV) 5'-untranslated region and the *Cauliflower*

*mosaic virus* (CaMV) 35S terminator. The expression construct was thus placed under the control of the CaMV 35S promoter with a duplicated transcriptional enhancer. An analogous construct comprising only the H5 ectodomain, a His<sub>6</sub>-tag and a C-terminal KDEL sequence was used to produce the soluble H5 antigen.

## Plant Material

Tobacco (*Nicotiana benthamiana*) plants were cultivated in soil in a growth chamber with a 16-h photoperiod, 26/16°C day/night temperatures and 70% relative humidity for 2 months.

## Agroinfiltration of Tobacco Leaves

The expression constructs were transferred by electroporation into competent *Agrobacterium tumefaciens* (GV3101) cells. The bacteria were kept as a glycerol stock and used to inoculate 5-ml aliquots of YEB medium containing 25 mg/l kanamycin, 25 mg/l rifampicin, and 50 mg/l carbenicillin. The cultures were incubated for 2 days at 28°C, shaking at 180 rpm. Each culture was mixed 1:1 with a culture containing a silencing inhibitor (HcPro) before adjusting with 2x infiltration medium (100 g/l sucrose, 3.6 g/l glucose, 8.6 g/l MS salts, pH 5.6) to an OD<sub>600</sub> of ~1.0. After adding 200 μM acetosyringone, *N. benthamiana* leaves were infiltrated using a syringe (for small-scale expression) or vacuum (for large-scale expression). Young plants were completely submerged in the suspension and vacuum was applied for 2 min. The infiltrated leaves were harvested 7 days post-infiltration (DPI).

## Protein Purification

### Soluble H5: Immobilized Metal Affinity Chromatography (IMAC)

Frozen leaf powder was mixed at a ratio of 1:2 (w/w) with cold lysis buffer (50 mM sodium phosphate buffer, pH 8.0, 300 mM NaCl, 5 mM imidazole, 0.5 mM PMSF) and sonicated briefly to induce further cell lysis. After 2 h, the suspension was centrifuged at 9000 rpm for 20 min and the supernatant was passed through a 1-μm filter. The pH was re-adjusted to 8.0 and the suspension was centrifuged as above. The supernatant was passed through a 0.45-μm filter before mixing with Ni-IDA IMAC resin (BioRad, Munich, Germany). Approximately 2 ml of 50% resin suspension was added per 50 ml supernatant. After incubation for 1 h, the resin was loaded onto a column and washed with eight volumes of wash buffer (50 mM sodium phosphate buffer, pH 8.0, 300 mM NaCl, 10 mM imidazole). The protein was eluted with elution buffer (50 mM sodium phosphate buffer, pH 8.0, 300 mM NaCl, 250 mM imidazole). The amount of protein in each fraction was determined using the Bradford assay before immunoblot analysis.

### Protein Bodies (Density Gradient Centrifugation)

The frozen leaf powder was mixed 1:1 (w/v) with extraction buffer (10 mM Tris-HCl, 0.4 M sucrose, pH 7.5) and incubated overnight at 4°C with constant shaking. The homogenate was passed through two layers of miracloth to remove solid debris and then loaded on a discontinuous sucrose gradient (3, 2.5, 2, 1.5, and 1 M in 10 mM Tris-HCl, pH 7.5). This preparation

was centrifuged at 30,000 rpm and 4°C for 3 h in a Beckman ultracentrifuge (SW 41Ti or SW32TI rotor). After separation, 500-μl fractions were collected for analysis by SDS-PAGE and immunoblotting.

## Protein PAGE and Immunoblot Analysis

Infiltrated leaves (7 DPI) were harvested and ground in liquid nitrogen to a fine powder. We then extracted 60 mg of leaf powder in 200 μl buffer K (62.5 mM Tris, pH 7.4, 10% glycine, 5% 2-mercaptoethanol, 2% SDS, 8 M urea). Ten microliter of the extract were mixed with loading buffer and boiled for 10 min before loading. Samples collected from the density gradient and IMAC procedures were mixed with 5x loading buffer, boiled at 100°C for 10 min and separated by reducing SDS-PAGE (12% polyacrylamide gel, 200 V for 90 min). Gels were stained with Coomassie Blue or transferred to a nitrocellulose membrane. The membrane was blocked with 5% (w/v) skimmed milk in phosphate buffered saline (PBS) for 1 h and then incubated with a mouse anti-poly-histidine antibody (Sigma-Aldrich Chemie GmbH, Germany) at room temperature for 2 h, diluted 1:10000. The blot was washed three times in PBS plus 0.05% Tween-20 (PBST) and then incubated for 1 h with the secondary anti-mouse alkaline phosphatase-conjugated antibody (diluted 1:5000). The membrane was washed another three times with PBST and the signal was detected using the NBT/BCIP system. For quantitation, the samples were compared to serial dilutions of a His<sub>6</sub>-tagged standard protein, and the images were analyzed using BioRad Image Lab v5.1.

## Fluorescence Microscopy

Infiltrated leaves were cut into small pieces with a razor blade and fixed in 4% (w/v) paraformaldehyde plus 0.5% (v/v) glutaraldehyde in 0.1 M phosphate buffer (pH 7.4) at 4°C overnight. For immunolocalization by confocal microscopy, vibratome sections were mounted on a glass slide, blocked with 5% (w/v) bovine serum albumin (BSA) in 0.1 M phosphate buffer (pH 7.4) and incubated with a polyclonal antibody against 27 kD γ-zein. The samples were then incubated with an AlexaFluor®488-conjugated secondary antibody and observed under a Leica SP5 confocal laser scanning microscope (CLSM).

## Immunization of Mice

Male BL6 C57/BaCl6J mice (6–8 weeks old) obtained from Charles River Laboratories, Research Models and Services were assigned to seven groups ( $n = 10$ ). Immunization was carried out by the subcutaneous injection of 150 or 300 ng of H5-zein either with or without Freund's adjuvant (1:1) (Difco Laboratories, Detroit, Michigan). For the primary immunization, complete Freund's adjuvant was used where indicated. Booster immunizations consisted of two additional injections of the same antigen (with or without incomplete Freund's adjuvant). As controls, one group received PBS with Freund's adjuvant only, and two groups were injected three times with soluble H5 (15 μg), with or without adjuvant. After the third immunization, the mice were retro-orbitally

bled and serum samples were collected for individual testing. A second set of blood samples was taken 8 weeks after the primary immunization and the mice were sacrificed immediately afterward.

The animal experiments were approved by the Landesverwaltungsamt Sachsen-Anhalt, Halle/Saale, Referat Verbraucherschutz, Veterinärangelegenheiten and by the Landkreis Harz, Amt für Veterinärwesen und Lebensmittelüberwachung, Halberstadt. All animals received humane care according to the requirements of the German Animal Welfare Act, §8 Abs. 1.

## IgG Quantitation by ELISA

The wells of a flat-bottom microtiter plate were coated with 0.2 µg per well of the antigen (purified recombinant H5 or zein (Sigma–Aldrich Chemie GmbH, Germany)). Then 100 µl of diluted serum (1:250 in PBS with 3% BSA) was added to each well and incubated at room temperature for 1.5 h. Rabbit anti-mouse IgG alkaline phosphatase-conjugated antibody (diluted 1:2000 in PBST) was used for detection. The IgG titer was determined by adding immune serum samples as serial dilutions starting at 1:1000. Curve fitting by five-parameter logistic regression was used to calculate the endpoint titer for each mouse. End-point titers were determined as the reciprocal highest serum dilutions that produced mean optical density values two-fold greater than the geometric mean of those from the negative control (injected with PBS) sera. The statistical significance was determined using Student's *t*-test (\*\**p* < 0.01; \**p* < 0.1).

Selected ELISA experiments were carried out using recombinant H5 purified via an additional size exclusion chromatography step. The same results were obtained, indicating that the H5 preparation purified via IMAC was sufficiently pure for coating, and did not contain significant amounts of immunoreactive impurities.

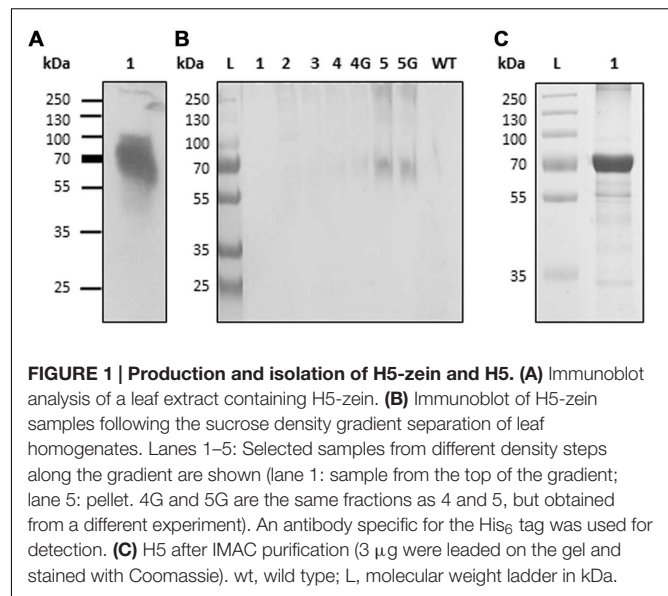
## Hemagglutination Inhibition (HI) Test

HI tests were carried out as described by Phan et al. (2013). Briefly, a 25-µl aliquot of murine serum was mixed with 25 µl PBS and added to the first well of a V-bottom microtiter plate. Twofold serial dilutions were prepared across the row of 12 wells. Aliquots (25 µl) containing 4HAU of inactivated virus [A/swan/Germany/R65/2006(H5N1)] were added to each well and incubated for 30 min at room temperature. We then pipetted 25 µl of a 1% red blood cells (RBCs) suspension into each well and the plate was again incubated for 30 min at room temperature. The HI titer was defined as the reciprocal of the highest serum dilution that achieved the complete inhibition of hemagglutination.

## RESULTS

### Hemagglutinin-Zein Fusions form PBs in *N. benthamiana* Leaves

Expression vector “H5-Zein” containing the sequence corresponding to the H5 ectodomain of hemagglutinin,



fused to amino acids 4–93 of the mature 27 kD  $\gamma$ -zein protein, was introduced into *N. benthamiana* leaves by agroinfiltration. Immunoblot analysis of extracts from the infiltrated leaves 7 DPI revealed the presence of a band corresponding to the fusion protein (Figure 1A). The higher than predicted molecular mass probably reflected the glycosylation of H5, as previously reported (Phan et al., 2014). The fusion of H5 to zein resulted in the formation of PBs, whose presence was confirmed by immunofluorescence microscopy. All labeling was concentrated in the PBs, whereas no signal was detected in the ER lumen or in the apoplast (Figure 2). This result was confirmed by the density step gradient centrifugation of leaf homogenates (Figure 1B). The gradient fractions were collected and tested by immunoblot analysis. No recombinant fusion protein was found in fractions from the top of the gradient, a small amount was present in the highest density fractions, and the majority of the fusion protein was found in the pellet (Figure 1B), similar to results reported with another zein fusion protein that forms PBs (Whitehead et al., 2014). Sucrose was removed by pooling the selected fractions and resuspending them in 10 mM Tris (pH 7.5) before centrifuging them under the same conditions as above. The supernatant was removed and the pellet was re-suspended in sterile PBS. The protein suspension was stored at  $-20^{\circ}\text{C}$  prior to the immunization experiments. A total of  $\sim 120$  µg H5-zein was recovered from 300 g of fresh infiltrated leaves. Soluble H5 lacking the zein fusion was expressed as a control and purified by IMAC as previously described (Phan et al., 2013). We recovered 1 mg of H5 from 500 g of fresh infiltrated leaves, and this was used as a positive control for immunization (Figure 1C).

### H5-Zein PBs Elicit an Immune Response in Mice

The H5-zein protein body suspension and the soluble H5 antigen were each used to immunize mice (Figure 3). The

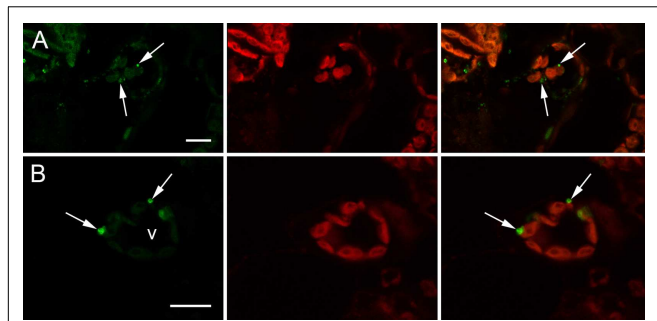


**FIGURE 2 | Immunolocalization of H5-zein in *N. benthamiana* leaves by confocal microscopy. (A)** Abundant H5-zein protein bodies (PBs) can be observed in mesophyll cells (arrows). **(B)** H5-zein PBs are 1–2 μm in diameter and can be found in the cytoplasm between the chloroplasts (arrows). The left panel shows the detection of the fusion protein. The middle panel shows autofluorescence of the chloroplasts. The right panel shows the overlay pictures. Abbreviations: v, vacuole. Bars = 10 μm.

mice were allocated to seven groups (*n* = 10 per group) and immunization was carried out by the subcutaneous injection of 150 or 300 ng of H5-zein either with or without Freund’s adjuvant. This low dosage of H5-zein bodies was chosen to confirm the hypothesis that particulate antigens are effective in small amounts. As controls, two groups were injected three times with soluble H5 (15 μg, a dose previously confirmed to provoke

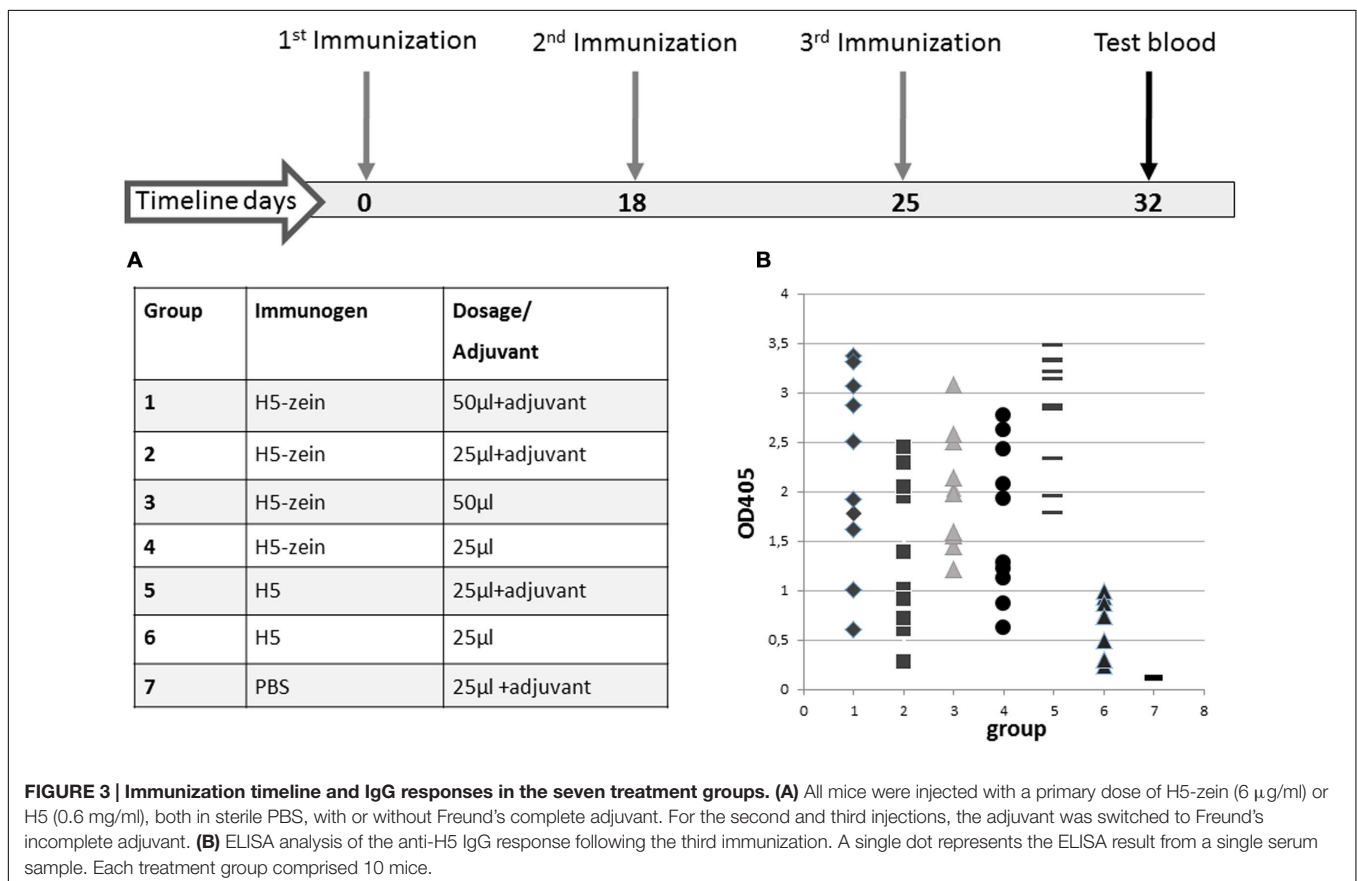
a strong humoral immune response), one with and one without adjuvant.

The plant-derived H5-zein protein body suspension was shown to elicit an IgG response in 100% of the animals, even at low doses. Interestingly, the addition of an adjuvant to the H5-zein bodies did not cause a significantly stronger immune response (Figure 3, groups 1 vs. 3 and 2 vs. 4), whereas the adjuvant had a significant impact in the control groups receiving soluble H5 (Figure 3, groups 5 vs. 6).

### The Zein Fusion Component is Only Weakly Immunogenic but has a Significant Adjuvant Activity

To confirm the observations summarized above, we carried out an in-depth comparison of IgG titers of groups 3, 5, and 6. The IgG response elicited by H5-zein without adjuvant (group 3) was comparable to that achieved by injecting soluble H5 combined with an adjuvant (group 5). In contrast, the administration of soluble H5 without adjuvant elicited a minimal IgG response (Figure 4A). This suggested that the zein component and/or the particulate nature of the protein body act as an adjuvant.

To determine whether the zein portion fused to H5 has intrinsic immunogenic properties, we investigated the IgG response directed against zein by comparing the IgG response in groups 1 (H5-zein with adjuvant), 3 (H5-zein without



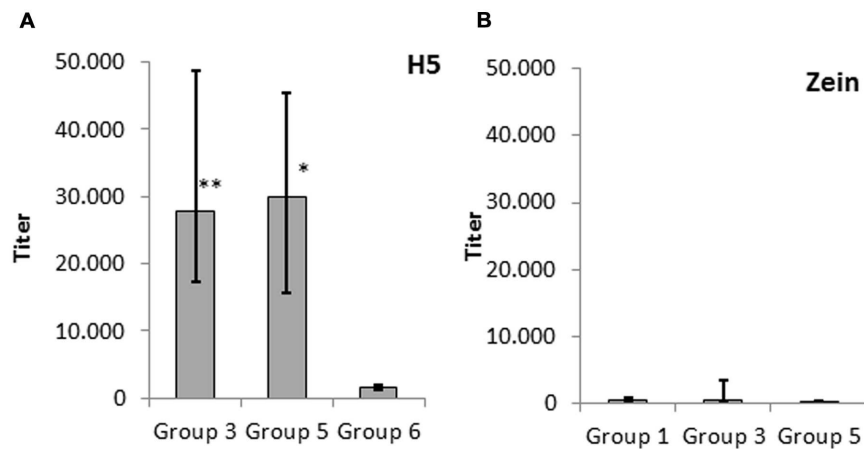


**FIGURE 4 | Serum IgG response against (A) H5 and (B) zein.** Data represent the median endpoint titer per group, whereas the lower and upper ends of the error bars represent the first and third quartiles, respectively. **(A)** Statistical analysis to compare group 3 (H5-zein without adjuvant) and group 5 (H5 with adjuvant) vs. group 6 (H5 without adjuvant). **(B)** Statistical analysis to compare group 1 (H5-zein with adjuvant) and group 3 (H5-zein without adjuvant) vs. group 5 (H5 with adjuvant). Each treatment group comprised 10 mice. Statistical significance was determined by Student's *t*-test (\*\* $p < 0.01$ ; \* $p < 0.1$ ; no asterisk indicates  $p > 0.1$ ).

adjuvant), and 5 (soluble H5 with adjuvant). Although we generally detected low IgG titers, 30% of the animals in groups 1 and 3 showed a clearly detectable IgG response against zein (Figure 4B). Overall the immune response in the treatment groups was not significantly different to that of the control group ( $p > 0.1$ ).

### HI Antibody Titers are Insignificant

All mice vaccinated with H5-zein PBs showed an immunological response so we carried out HI tests on the serum from each mouse to determine whether the induced antibodies were potentially capable of neutralizing the virus. Because of the unavailability of the A/Hatay/2004(H5N1) virus in an inactivated form, the heterologous inactivated virus strain A/swan/Germany/R65/2006(H5N1) was used for the HI assay. The deduced hemagglutinin amino acid sequence similarity of both strains is 96%, and it was previously shown that HI titres against inactivated virus A/swan/Germany/R65/2006 (H5N1) could be measured in sera from mice vaccinated with trimeric HA derived from the HA sequence corresponding to the A/Hatay/2004(H5N1) virus (Phan et al., 2013). The HI assay results indicated that the HI antibody titers were either below or marginally above the detection limit in all treatment groups (Table 1).

**TABLE 1 | HI titers against inactivated virus [A/swan/Germany/R65/2006(H5N1)].**

| Treatment group        | Geometric mean titer |
|------------------------|----------------------|
| 1 (H5-zein + adjuvant) | 6,06                 |
| 3 (H5-zein)            | 4,29                 |
| 6 (H5)                 | 3,4                  |
| 7 (PBS)                | 7,46                 |

### DISCUSSION

The expression of recombinant proteins in plants is an attractive strategy reflecting the versatility, safety, scalability, and economy of plant-based production platforms (Rybicki et al., 2013; Stoger et al., 2014). Plants also offer the possibility to accumulate recombinant pharmaceutical proteins within endogenous or ectopic protein storage organelles, which can either be derived directly from the ER or represent protein storage vacuoles (Khan et al., 2012). Here, we successfully induced the formation of ectopic PBs by fusing the H5 ectodomain of hemagglutinin to the N-terminal sequence of  $\gamma$ -zein. Previous studies have shown that the biogenesis of PBs by zein is influenced by the fusion partner, and that not all fusion proteins support the efficient formation of PBs. For example, phaseolin induces the efficient formation of zeolin PBs when fused to the N-terminal sequence of  $\gamma$ -zein (Mainieri et al., 2004). However, PBs were not formed when the *Human immunodeficiency virus* Nef antigen was fused to the same  $\gamma$ -zein sequence, but protein body formation was possible again when Nef was fused to the entire chimeric protein zeolin (de Virgilio et al., 2008).

The induction of H5-containing protein aggregates in plants has also been achieved by fusing the antigen to hydrophobin and ELPs (Phan et al., 2014). The H5-ELP PBs were approximately 800 nm in diameter whereas the H5-hydrophobin PBs were substantially smaller, with an average diameter of 250 nm. The H5-zein PBs reported herein were larger, with a diameter of 1–2  $\mu$ m, which is similar to the average size of endogenous zein bodies found in maize endosperm (Lending and Larkins, 1989). In contrast to the H5-ELP and H5-hydrophobin PBs, H5-zein formed high density structures that were insoluble in non-reducing buffers, whereas H5-ELP and H5-hydrophobin fusion proteins could be extracted in 50 mM Tris, pH 8.0 (Phan et al., 2014).

The H5-zein bodies described herein were used as a delivery vehicle for a model vaccine antigen. IgG responses were elicited in all mice immunized with H5-zein but HI assays indicated the absence of neutralizing antibodies. Our results agree with previous parenteral immunization studies using monomeric hemagglutinin fused to ELP, which, in contrast to trimeric hemagglutinin, also did not induce neutralizing antibodies (Phan et al., 2013). Although the formation of PBs involves multiple cross-linking via intermolecular disulfide bonds, this type of multimerization may not be sufficient to support the specific oligomerization state that appears to be required for the formation of specific native epitopes that may confer a seroprotective immune response. Proper trimerization may be required to complete the folding of hemagglutinin monomers and to induce conformational effects necessary for full antigenicity and the induction of neutralizing antibodies (Magadan et al., 2013). The introduction of a trimerization signal in addition to the assembly sequence may therefore be beneficial, as reported for H5-ELP fusions (Phan et al., 2013).

One remarkable outcome of our experiments was that a comparable immune response was elicited in all mice despite the H5-zein concentration being 100 times lower than the concentration of soluble H5 in the control group, which was administered with a strong adjuvant. Interestingly, the administration of an adjuvant together with the H5-zein bodies did not promote a stronger immune response, suggesting that the addition of the zein portion itself mediates an adjuvant effect. This agrees with Whitehead et al. (Whitehead et al., 2014), who recently reported that the immunogenicity of a recombinant antigen was increased in the presence of Zera<sup>®</sup>, an assembly sequence that is very similar to the N-terminal part of  $\gamma$ -zein (Torrent et al., 2009b), and the immunogenicity of the fusion protein could not be enhanced further by the inclusion of Freund's adjuvant. Similarly, the injection of synthetic zein microspheres that were loaded with ovalbumin resulted in higher IgG responses than the 'free' soluble protein (Hurtado-Lopez and Murdan, 2006a). This strongly supports the hypothesis that the zein N-terminal portion possesses intrinsic adjuvant activity, although we cannot exclude the possibility that the observed adjuvant effect was mediated by another component of the PBs. Joseph et al. reported that zein-induced PBs isolated from leaves contain additional proteins that are trapped during biogenesis (Joseph et al., 2012).

An adjuvant effect conferred by a polymer-forming protein domain is not unexpected, given its similarity to the strategy of attaching a carrier protein such as albumin or keyhole limpet hemocyanin to antigens with poor immunogenicity (Harris and Markl, 1999). By definition, an adjuvant is characterized by its ability to enhance the immunogenic efficacy of antigens in the same formulation. This can be achieved by increasing the half-life of an antigen, improving antigen delivery to its effector sites, or providing immunostimulatory signals to enhance the immune response. The observed adjuvant effect of zein particles may reflect one or more of several relevant properties. First, hydrophobic synthetic block copolymers have been shown to confer stronger adjuvant properties than hydrophilic

polymers (Newman et al., 1998; Hunter, 2002). Accordingly, the N-terminal part of  $\gamma$ -zein is partially hydrophobic, favoring intermolecular and membrane interactions (Kogan et al., 2002). It has also been reported that particulate antigens are transported more efficiently to murine splenic follicular dendritic cells *in vivo* in the absence of prior immunity, making them more immunogenic than soluble antigens (Link et al., 2012). This may also be reflected by the superior immunogenicity of hemagglutinin-containing virus-like particles compared to soluble hemagglutinin, even in the absence of an adjuvant (Shoji et al., 2015). Also, repetitive antigen display, structural, or molecular mimicry of the virus, particle-size dependent tissue penetration and trafficking to lymphatics and Toll-like receptor activation are possible mechanisms. In repetitive antigen display the spatial organization of the antigens on the particle surface facilitates B-cell receptor (antibody) co-aggregation, triggering and activation. This can support the production of long-lived high-affinity neutralizing antibodies (Smith et al., 2013). Plant-derived PBs might also provide a specific spatial antigen organization favoring a successful repetitive antigen display. Alternatively, increased half life and stability of the zein fusions in the serum *in vivo* might be responsible for the enhanced immune response. The half-life of the antigen is likely to be extended due to encapsulation in the protein body. Indeed, pharmaceutical preparations encapsulated in zein particles *in vitro* remained in the blood for at least 24 h following intravenous delivery (Lai and Guo, 2011). Interestingly, the fusion of hemagglutinin to ELP repeats did not seem to increase immunogenicity although the propensity to form protein aggregates was confirmed *in planta* (Phan et al., 2013, 2014).

Zein has several favorable general characteristics as an adjuvant, i.e., it is stable at ambient temperatures and yet it is biodegradable, encouraging its use as a biopolymer for the coating and encapsulation of recombinant proteins such as erythropoietin (Bernstein et al., 1993). However, the potential immunogenic properties of zein must be taken into account (Hurtado-Lopez and Murdan, 2006a; Whitehead et al., 2014). We detected an immune response directed against  $\gamma$ -zein although the response was much weaker than that directed against H5, and when compared to the control group administered with H5 alone, the difference between the groups was not statistically significant. However, 30% of the mice injected with H5-zein showed an immune response above background levels. A significant immune response against the zein-like sequence Zera has been reported by (Whitehead et al., 2014), warranting further studies to assess the suitability of zein bodies as drug delivery vehicles for parenteral administration. Animal studies involving the injection of zein-coated erythropoietin (Bernstein et al., 1993) and ivermectin (Gong et al., 2011) did not indicate any adverse effects. Other storage proteins, including the wheat storage protein gliadin, have also been used as coatings to prepare various proteins and pharmaceuticals *in vitro*. GliSODin<sup>®</sup> for example is an oral treatment for oxidative stress, in which superoxide dismutase (SOD) is coated with gliadin (Cloarec et al., 2007). Although gliadin protects SOD from digestion, this storage protein is also linked to the autoimmune disorder celiac disease

(Chaptal, 1957). Even so, this product has received market approval for human use.

## CONCLUSION

Zein and similar plant storage proteins have long been investigated as carriers for pharmaceuticals including recombinant proteins. The direct encapsulation of pharmaceutical proteins in the production host is a simple approach that is less expensive than the production of synthetic microparticles. Our case study using a model vaccine antigen indicates that zein-induced PBs can be used as vaccine delivery vehicles that benefit from a value-added adjuvant effect, whereas the intrinsic immunogenicity of the zein component is low. The insertion of a trimerization signal fused to H5 will be tested to determine whether this leads to the assembly of structures that can elicit neutralizing antibodies against H5. It will also be of value to develop the *in planta* protein body encapsulation strategy for the production and delivery

of further antigens, including candidates intended for oral application.

## AUTHOR CONTRIBUTIONS

AH designed and carried out experiments, analyzed data, and wrote the manuscript. SM designed and carried out experiments and analyzed data. MT and EA carried out experiments, analyzed data, and contributed to the manuscript. HP, UG, and JL carried out experiments and analyzed data. UC and ES designed the study, analyzed data, and wrote the manuscript.

## ACKNOWLEDGMENTS

The authors would like to acknowledge financial support by the Austrian Science Fund FWF (W1224 and I1461-B16). We are grateful to Dr. Jutta Veits, Friedrich-Loeffler-Institut, Greifswald-Insel Riems for providing the inactivated virus.

## REFERENCES

- Ahmed, O. A., Hosny, K. M., Al-Sawahli, M. M., and Fahmy, U. A. (2015). Optimization of caseinate-coated simvastatin-zein nanoparticles: improved bioavailability and modified release characteristics. *Drug Des. Dev. Ther.* 9, 655–662. doi: 10.2147/DDDT.S76194
- Bernstein, H., Mathiowitz, E., Morrel, E., Brickner, A., and Pabst, P. (1993). *Erythropoietin Drug Delivery System* (WO 1993025221).
- Chaptal, J. (1957). Celiac disease caused by intolerance to gliadin from wheat, oats & milk products. *Pädiatrie* 12, 737–747.
- Cloarec, M., Caillard, P., Provost, J. C., Dever, J. M., Elbeze, Y., and Zamaria, N. (2007). GliSODin, a vegetal sod with gliadin, as preventative agent vs. atherosclerosis, as confirmed with carotid ultrasound-B imaging. *Eur. Ann. Allergy Clin. Immunol.* 39, 45–50.
- Conley, A. J., Joensuu, J. J., Menassa, R., and Brandle, J. E. (2009). Induction of protein body formation in plant leaves by elastin-like polypeptide fusions. *BMC Biol.* 7:48. doi: 10.1186/1741-7007-7-48
- Daamen, W. F., Veerkamp, J. H., Van Hest, J. C., and Van Kuppevelt, T. H. (2007). Elastin as a biomaterial for tissue engineering. *Biomaterials* 28, 4378–4398. doi: 10.1016/j.biomaterials.2007.06.025
- de Virgilio, M., De Marchis, F., Bellucci, M., Mainieri, D., Rossi, M., Benvenuto, E., et al. (2008). The human immunodeficiency virus antigen Nef forms protein bodies in leaves of transgenic tobacco when fused to zeolin. *J. Exp. Bot.* 59, 2815–2829. doi: 10.1093/jxb/ern143
- Floss, D. M., Sack, M., Stadlmann, J., Rademacher, T., Scheller, J., Stoger, E., et al. (2008). Biochemical and functional characterization of anti-HIV antibody-ELP fusion proteins from transgenic plants. *Plant Biotechnol. J.* 6, 379–391. doi: 10.1111/j.1467-7652.2008.00326.x
- Geli, M. I., Torrent, M., and Ludevid, D. (1994). Two structural domains mediate two sequential events in [gamma]-zein targeting: protein endoplasmic reticulum retention and protein body formation. *Plant Cell* 6, 1911–1922. doi: 10.1105/tpc.6.12.1911
- Gong, S. J., Sun, S. X., Sun, Q. S., Wang, J. Y., Liu, X. M., and Liu, G. Y. (2011). Tablets based on compressed zein microspheres for sustained oral administration: design, pharmacokinetics, and clinical study. *J. Biomater. Appl.* 26, 195–208. doi: 10.1177/0885328210363504
- Gutierrez, S. P., Saberianfar, R., Kohalmi, S. E., and Menassa, R. (2013). Protein body formation in stable transgenic tobacco expressing elastin-like polypeptide and hydrophobin fusion proteins. *BMC Biotechnol.* 13:40. doi: 10.1186/1472-6750-13-40
- Harris, J. R., and Markl, J. (1999). Keyhole limpet hemocyanin (KLH): a biomedical review. *Micron* 30, 597–623. doi: 10.1016/S0968-4328(99)00036-0
- Hofbauer, A., Peters, J., Arcalis, E., Rademacher, T., Lampel, J., Eudes, F., et al. (2014). The induction of recombinant protein bodies in different subcellular compartments reveals a cryptic plastid-targeting signal in the 27-kDa gamma-zein sequence. *Front. Bioeng. Biotechnol.* 2:67. doi: 10.3389/fbioe.2014.00067
- Hofbauer, A., and Stoger, E. (2013). Subcellular accumulation and modification of pharmaceutical proteins in different plant tissues. *Curr. Pharm. Des.* 19, 5495–5502. doi: 10.2174/1381612811319310005
- Hulse, D. J., Webster, R. G., Russell, R. J., and Perez, D. R. (2004). Molecular determinants within the surface proteins involved in the pathogenicity of H5N1 influenza viruses in chickens. *J. Virol.* 78, 9954–9964. doi: 10.1128/JVI.78.18.9954-9964.2004
- Hunter, R. L. (2002). Overview of vaccine adjuvants: present and future. *Vaccine* 20(Suppl. 3), S7–S12. doi: 10.1016/S0264-410X(02)00164-0
- Hurtado-Lopez, P., and Murdan, S. (2006a). An investigation into the adjuvanticity and immunogenicity of zein microspheres being researched as drug and vaccine carriers. *J. Pharm. Pharmacol.* 58, 769–774. doi: 10.1211/jpp.58.6.0007
- Hurtado-Lopez, P., and Murdan, S. (2006b). Zein microspheres as drug/antigen carriers: a study of their degradation and erosion, in the presence and absence of enzymes. *J. Microencapsul.* 23, 303–314. doi: 10.1080/02652040500444149
- Joseph, M., Ludevid, M. D., Torrent, M., Rofidal, V., Tauzin, M., Rossignol, M., et al. (2012). Proteomic characterisation of endoplasmic reticulum-derived protein bodies in tobacco leaves. *BMC Plant Biol.* 12:36. doi: 10.1186/1471-2229-12-36
- Khan, I., Twyman, R. M., Arcalis, E., and Stoger, E. (2012). Using storage organelles for the accumulation and encapsulation of recombinant proteins. *Biotechnol. J.* 7, 1099–1108. doi: 10.1002/biot.201100089
- Klenk, H. D., and Garten, W. (1994). Host cell proteases controlling virus pathogenicity. *Trends Microbiol.* 2, 39–43. doi: 10.1016/0966-842X(94)90123-6
- Kogan, M. J., Dalcol, I., Gorostiza, P., Lopez-Iglesias, C., Pons, R., Pons, M., et al. (2002). Supramolecular properties of the proline-rich gamma-Zein N-terminal domain. *Biophys. J.* 83, 1194–1204. doi: 10.1016/S0006-3495(02)75243-0
- Lai, L. F., and Guo, H. X. (2011). Preparation of new 5-fluorouracil-loaded zein nanoparticles for liver targeting. *Int. J. Pharm.* 404, 317–323. doi: 10.1016/j.ijpharm.2010.11.025
- Lammel, A. S., Hu, X., Park, S. H., Kaplan, D. L., and Scheibel, T. R. (2010). Controlling silk fibroin particle features for drug delivery. *Biomaterials* 31, 4583–4591. doi: 10.1016/j.biomaterials.2010.02.024
- Lau, E. T., Giddings, S. J., Mohammed, S. G., Dubois, P., Johnson, S. K., Stanley, R. A., et al. (2013). Encapsulation of hydrocortisone and mesalazine in zein microparticles. *Pharmaceutics* 5, 277–293. doi: 10.3390/pharmaceutics5020277

- Lending, C. R., and Larkins, B. A. (1989). Changes in the zein composition of protein bodies during maize endosperm development. *Plant Cell* 1, 1011–1023. doi: 10.2307/3869002
- Lin, T., Lu, C., Zhu, L., and Lu, T. (2011). The biodegradation of zein in vitro and in vivo and its application in implants. *AAPS PharmSciTech* 12, 172–176. doi: 10.1208/s12249-010-9565-y
- Link, A., Zabel, F., Schnetzler, Y., Titz, A., Brombacher, F., and Bachmann, M. F. (2012). Innate immunity mediates follicular transport of particulate but not soluble protein antigen. *J. Immunol.* 188, 3724–3733. doi: 10.4049/jimmunol.1103312
- Liu, X., Sun, Q., Wang, H., Zhang, L., and Wang, J. Y. (2005). Microspheres of corn protein, zein, for an ivermectin drug delivery system. *Biomaterials* 26, 109–115. doi: 10.1016/j.biomaterials.2004.02.013
- Llop-Tous, I., Madurga, S., Giralt, E., Marzabal, P., Torrent, M., and Ludevid, M. D. (2010). Relevant elements of a maize gamma-zein domain involved in protein body biogenesis. *J. Biol. Chem.* 285, 35633–35644. doi: 10.1074/jbc.M110.116285
- Llop-Tous, I., Ortiz, M., Torrent, M., and Ludevid, M. D. (2011). The expression of a xylanase targeted to ER-protein bodies provides a simple strategy to produce active insoluble enzyme polymers in tobacco plants. *PLoS ONE* 6:e19474. doi: 10.1371/journal.pone.0019474
- Lohcharoenkai, W., Wang, L., Chen, Y. C., and Rojanasakul, Y. (2014). Protein nanoparticles as drug delivery carriers for cancer therapy. *Biomed Res. Int.* 2014, 180549. doi: 10.1155/2014/180549
- Magadan, J. G., Khurana, S., Das, S. R., Frank, G. M., Stevens, J., Golding, H., et al. (2013). Influenza A virus hemagglutinin trimerization completes monomer folding and antigenicity. *J. Virol.* 87, 9742–9753. doi: 10.1128/JVI.00471-13
- Mainieri, D., Rossi, M., Archinti, M., Bellucci, M., De Marchis, F., Vavassori, S., et al. (2004). Zeolin. A new recombinant storage protein constructed using maize  $\gamma$ -zein and bean phaseolin. *Plant Physiol.* 136, 3447–3456.
- Newman, M. J., Todd, C. W., and Balusubramanian, M. (1998). Design and development of adjuvant-active nonionic block copolymers. *J. Pharm. Sci.* 87, 1357–1362. doi: 10.1021/js980072c
- Nitta, S. K., and Numata, K. (2013). Biopolymer-based nanoparticles for drug/gene delivery and tissue engineering. *Int. J. Mol. Sci.* 14, 1629–1654. doi: 10.3390/ijms14011629
- Panyam, J., and Labhasetwar, V. (2003). Biodegradable nanoparticles for drug and gene delivery to cells and tissue. *Adv. Drug Deliv. Rev.* 55, 329–347. doi: 10.1016/S0169-409X(02)00228-4
- Petros, R. A., and DeSimone, J. M. (2010). Strategies in the design of nanoparticles for therapeutic applications. *Nat. Rev. Drug Discov.* 9, 615–627. doi: 10.1038/nrd2591
- Phan, H. T., Hause, B., Hause, G., Arcalis, E., Stoger, E., Maresch, D., et al. (2014). Influence of elastin-like polypeptide and hydrophobin on recombinant hemagglutinin accumulations in transgenic tobacco plants. *PLoS ONE* 9:e99347. doi: 10.1371/journal.pone.0099347
- Phan, H. T., Pohl, J., Floss, D. M., Rabenstein, F., Veits, J., Le, B. T., et al. (2013). ELPylated haemagglutinins produced in tobacco plants induce potentially neutralizing antibodies against H5N1 viruses in mice. *Plant Biotechnol. J.* 11, 582–593. doi: 10.1111/pbi.12049
- Podaralla, S., Averinini, R., Alqahtani, M., and Perumal, O. (2012). Synthesis of novel biodegradable methoxy poly(ethylene glycol)-zein micelles for effective delivery of curcumin. *Mol. Pharm.* 9, 2778–2786. doi: 10.1021/mp2006455
- Podaralla, S., and Perumal, O. (2010). Preparation of zein nanoparticles by pH controlled nanoprecipitation. *J. Biomed. Nanotechnol.* 6, 312–317. doi: 10.1166/jbn.2010.1137
- Ruszczak, Z., and Friess, W. (2003). Collagen as a carrier for on-site delivery of antibacterial drugs. *Adv. Drug Deliv. Rev.* 55, 1679–1698. doi: 10.1016/j.addr.2003.08.007
- Rybicki, E. P., Hitzeroth, II, Meyers, A., Dus Santos, M. J., and Wigdorovitz, A. (2013). Developing country applications of molecular farming: case studies in South Africa and Argentina. *Curr. Pharm. Des.* 19, 5612–5621. doi: 10.2174/1381612811319310015
- Shewry, P. R., and Halford, N. G. (2002). Cereal seed storage proteins: structures, properties and role in grain utilization. *J. Exp. Bot.* 53, 947–958. doi: 10.1093/jxbbot/53.370.947
- Shigemitsu, T., Masumura, T., Morita, S., and Satoh, S. (2013). Accumulation of rice prolamin-GFP fusion proteins induces ER-derived protein bodies in transgenic rice calli. *Plant Cell Rep.* 32, 389–399. doi: 10.1007/s00299-012-1372-2
- Shoji, Y., Prokhnevsky, A., Leffert, B., Vetter, N., Tottey, S., Satinover, S., et al. (2015). Immunogenicity of H1N1 influenza virus-like particles produced in *Nicotiana benthamiana*. *Hum. Vaccin. Immunother.* 11, 118–123. doi: 10.4161/hv.34365
- Smith, D. M., Simon, J. K., and Baker, J. R. Jr. (2013). Applications of nanotechnology for immunology. *Nat. Rev. Immunol.* 13, 592–605. doi: 10.1038/nri3488
- Stoger, E., Fischer, R., Moloney, M., and Ma, J. K. (2014). Plant molecular pharming for the treatment of chronic and infectious diseases. *Annu. Rev. Plant Biol.* 65, 743–768. doi: 10.1146/annurev-arplant-050213-035850
- Takaiwa, F., Wakasa, Y., Takagi, H., and Hiroi, T. (2015). Rice seed for delivery of vaccines to gut mucosal immune tissues. *Plant Biotechnol. J.* 13, 1041–1055. doi: 10.1111/pbi.12423
- Torrent, M., Llompard, B., Lasserre-Ramassamy, S., Llop-Tous, I., Bastida, M., Marzabal, P., et al. (2009a). Eukaryotic protein production in designed storage organelles. *BMC Biol.* 7:5. doi: 10.1186/1741-7007-7-5
- Torrent, M., Llop-Tous, I., and Ludevid, M. D. (2009b). Protein body induction: a new tool to produce and recover recombinant proteins in plants. *Methods Mol. Biol.* 483, 193–208. doi: 10.1007/978-1-59745-407-0\_11
- Vaquero, C., Sack, M., Chandler, J., Drossard, J., Schuster, F., Monecke, M., et al. (1999). Transient expression of a tumor-specific single-chain fragment and a chimeric antibody in tobacco leaves. *Proc. Natl. Acad. Sci. U.S.A.* 96, 11128–11133. doi: 10.1073/pnas.96.20.11128
- Wang, R., Tian, Z., and Chen, L. (2011). Nano-encapsulations liberated from barley protein microcapsules for oral delivery of bioactive compounds. *Int. J. Pharm.* 406, 153–162. doi: 10.1016/j.ijpharm.2010.12.039
- Whitehead, M., Ohlschlager, P., Almajhdi, F. N., Alloza, L., Marzabal, P., Meyers, A. E., et al. (2014). Human papillomavirus (HPV) type 16 E7 protein bodies cause tumour regression in mice. *BMC Cancer* 14:367. doi: 10.1186/1471-2407-14-367
- Wiley, D. C., Skehel, J. J., and Waterfield, M. (1977). Evidence from studies with a cross-linking reagent that the haemagglutinin of influenza virus is a trimer. *Virology* 79, 446–448. doi: 10.1016/0042-6822(77)90371-3
- Wilson, I. A., Skehel, J. J., and Wiley, D. C. (1981). Structure of the haemagglutinin membrane glycoprotein of influenza virus at 3 Å resolution. *Nature* 289, 366–373. doi: 10.1038/289366a0
- Zhong, Q., and Jin, M. (2009). Nanoscale structures of spray-dried zein microcapsules and in vitro release kinetics of the encapsulated lysozyme as affected by formulations. *J. Agric. Food Chem.* 57, 3886–3894. doi: 10.1021/jf803951a
- Zou, T., and Gu, L. (2013). TPGS emulsified zein nanoparticles enhanced oral bioavailability of daidzin: in vitro characteristics and in vivo performance. *Mol. Pharm.* 10, 2062–2070. doi: 10.1021/mp400086n

**Conflict of Interest Statement:** The authors declare that the research was conducted in the absence of any commercial or financial relationships that could be construed as a potential conflict of interest.

Copyright © 2016 Hofbauer, Melnik, Tschofen, Arcalis, Phan, Gresch, Lampel, Conrad and Stoger. This is an open-access article distributed under the terms of the Creative Commons Attribution License (CC BY). The use, distribution or reproduction in other forums is permitted, provided the original author(s) or licensor are credited and that the original publication in this journal is cited, in accordance with accepted academic practice. No use, distribution or reproduction is permitted which does not comply with these terms.

## Eidesstattliche Erklärung

Ich erkläre eidesstattlich, dass ich die Arbeit selbständig angefertigt habe. Es wurden keine anderen als die angegebenen Hilfsmittel benutzt. Die aus fremden Quellen direkt oder indirekt übernommenen Formulierungen und Gedanken sind als solche kenntlich gemacht. Diese schriftliche Arbeit wurde noch an keiner Stelle vorgelegt.

Wien, den 2. März 2020

A handwritten signature in blue ink that reads "Tschofen Marc". The signature is written in a cursive style.

Tschofen Marc